Of dots and lines: Characterising the development of the adrenal gland in *Xenopus laevis*

A thesis submitted for the degree of

Doctor of Philosophy

University of East Anglia
School of Biological Sciences
Norwich

By

Amy Jessica MacLeod Kerr

July 2024

Word Count: 64 223

Supervised by : **Prof. Grant N. Wheeler**

Statement of Orginiality

This copy of the thesis has been supplied on condition that anyone who consults it is understood to recognise that its copyright rests with the author and that use of any information derived therefrom must be in accordance with current UK Copyright Law. In addition, any quotation or extract must include full attribution.

Acknowledgements

Summarizing four years of hard work and expressing gratitude to all the amazing people who have supported me is no easy task. I am deeply thankful to everyone who has contributed to this journey. First, I would like to thank my supervisor Prof. Grant Wheeler, for giving me this opportunity and allowing me to explore this project freely. For the always calm demeanour and the inevitable 'C'est la vie' replies to failed experiments and for always having an open door. I would also like to thank my second supervisor, Prof. Andrea Münsterberg for her continuous support and suggestions as well as Dr. Geoff Mok for taking care of the ordering, creating some mischief here and there with sprinkles of solid advice.

I would like to thank my lab colleagues in the Wheeler, Münsterberg, Grocott and Mok lab for keeping me going, especially the people working in 'banter bay'. Of course, there must be some individual shout outs: Emily, your unwavering spirit and helping hand have held the lab together and created a great work environment. Shahrzad, although joining at the end of my stay, I enjoyed your warm presence, amazing food and the wittiest thesis presentation of the beaker brigade – big thanks to all members of this group as well. To my office bestie, trauma bonding, cat-enthusiast and lab buddy Magda, I would not have gotten through this without you. Your expertise and enthusiasm in everything science, the daily cat videos, and shelter searches and of course being able to complain in German/Austrian from time to time have been my daily highlights these past years. Our office was my safe space and fun bubble because of you. To my Vienna mentor Marilena, your talent and expertise in the lab and skilful teaching have been invaluable to me. I particularly loved rocking out with you at concerts and long conference evenings.

Next, I would like to thank a special group of friends, the 'Fellowship of the Indie'. We started our Ph.D journeys (or work and master's for some) together during a bloody pandemic. You have made Norwich my home and become my UK family. I will miss our boardgame brunches, pizza nights and everything in-between. We have 'snailed' up that impossible winding staircase and are finishing together. Sadly, that means going our separate ways, ending a wonderful era in Norwich. I know we will manage to organise get togethers no matter where we all end up.

I also want to thank my two favourite places in Norwich, The Garnet and Bricks Pizza. They provided me with (surprise surprise) Pizza and Beer after many late working hours in the lab and have been a weekly meet up spot to catch up with friends and air out any frustrations.

Of course, I need to thank my funding body, Horizon 2020 and my training network the 'NEUcrest' for providing me with a multifaceted learning and working opportunity, and for introducing me to a brilliant cohort of students to share this experience with. Lots of fun times

were had across Europe. A special thanks to William for being the most fun to work and explore new places with. To Irina, for trying to introduce me to Bioinformatics and teaching me to tackle life at your own pace. Your cake and coffee time is legendary, as is your sense of style. To Anna, I am beyond grateful to have met you and have you by my side throughout this project. For all scientific advice and discussions, surviving never-ending meetings and hosting me in London countless times, spoiling me rotten. This thesis would have never been finished without your incredible help and support.

To my housemate, colleague and partner Marco, this project has been a team effort, and I could have never done it without you by my side, always. For being there through all the failed experiments and looong working hours. You have been, as the late Queen herself once said (though not about you) "my strength and stay". I am beyond grateful to the 'NEUcrest' project, not just because of the huge opportunity it provided but because it led me to you.

Above all, I would like to thank my family. I am fortunate to have not just two, but three parents that have supported and believed in me, all my life. Papa, thank you for instilling my interest in science, even though you always hoped for me to work in Immunology, I loved all our discussions and your quirky wisdoms. Didi, I could not imagine life without you. You have been my number one supporter and always tried your hardest to understand what the hell I am doing. You are the first person I call when I need help dealing with everyday life – no matter the things we face, we are facing them together! Mum, I do not know how to express in words how grateful I am to you. You are quite literally a lioness, and the person I look up to the most in the whole world. You have always put me first and your unconditional love, support and fierce believe in me have shaped me into the person I am today. I love you all.

Finally, I would like to give a special thanks to all my froggies and the sacrifices they had to make- I seriously apologize.

Abstract

The adrenal glands (AGs) are vital endocrine organs, performing as key hormonal regulators of physiological processes such as maintaining homeostasis, immune system regulation, sex hormone production, and the "fight-or-flight" response. In mammals, the AGs sit on top of the kidneys and are composed of the mesoderm-derived outer adrenal cortex (AC), producing steroids, and the inner adrenal medulla (AM) containing neuroendocrine chromaffin cells (CCs). CCs produce and secrete catecholamines adrenaline and noradrenaline directly into the bloodstream, essentially functioning as a specialized sympathetic neuron. Despite the AGs crucial role in our physiology, their development remains poorly understood. Only recently it was shown that most CCs are in fact derived from Schwann Cell Precursors (SCPs), nerve associated glial progenitor cells derived from the neural crest (NC). The NC is a unique cell population in vertebrate embryos, giving rise to a remarkable variety of tissues in the body such as pigment cells, craniofacial cartilage and bone, the peripheral nervous system and more. Abnormal NC development can cause many syndromes (termed Neurocristopathies) some of which include tumours forming from the AM or near the AGs, like neuroblastoma. Although performing the same function across vertebrate species, the structure of AGs can differ greatly between different model species. Currently, little is known about AG development during embryogenesis in the model organism *Xenopus*. The cellular origin and biological processes governing CC development of the AM have remained particularly elusive.

In this project, marker genes were identified to create a temporal and spatial map of *Xenopus* AG development to help define the molecular landscape underlying specific functions of this organ. This information will provide fundamental knowledge to establish and utilise *Xenopus laevis* as a research model for exploring aspects of AG development and disease. Chromaffin-like cells were found interspersed across the anterior embryonic body, first appearing at the anteroventral side of the embryo. During embryogenesis, chromaffin-like cells were not found in close association with the developing pronephric kidney and marker genes for the AM and AC cells did not overlap, suggesting that the AM does not fully form during embryogenesis. NC knockdown experiments showed a significant decrease in chromaffin-like cells, indicating their NC origin and raising an interesting question on how far the NC migrates during early *Xenopus* embryogenesis.

Access Condition and Agreement

Each deposit in UEA Digital Repository is protected by copyright and other intellectual property rights, and duplication or sale of all or part of any of the Data Collections is not permitted, except that material may be duplicated by you for your research use or for educational purposes in electronic or print form. You must obtain permission from the copyright holder, usually the author, for any other use. Exceptions only apply where a deposit may be explicitly provided under a stated licence, such as a Creative Commons licence or Open Government licence.

Electronic or print copies may not be offered, whether for sale or otherwise to anyone, unless explicitly stated under a Creative Commons or Open Government license. Unauthorised reproduction, editing or reformatting for resale purposes is explicitly prohibited (except where approved by the copyright holder themselves) and UEA reserves the right to take immediate 'take down' action on behalf of the copyright and/or rights holder if this Access condition of the UEA Digital Repository is breached. Any material in this database has been supplied on the understanding that it is copyright material and that no quotation from the material may be published without proper acknowledgement.

Table of content

Acknowledgements **3**

Abstract **5**

Table of content **6**

List of Figures **11**

List of Tables **15**

Abbreviations **16**

1 Chapter I: General Intoduction **21**

1.1 Xenopus as a (disease) model system **22**

1.2 *Xenopus* development **23**

1.3 Welcome to the neural crest – A historic discovery **25**

1.4 Neural crest specification and regulation **27**

1.5 Neural crest epithelial-to-mesenchymal transition **29**

1.6 Neural crest migration and differentiation into multiple lineages **31**

1.7 Neurocristopathies **34**

1.7.1 Neurocristopathies of the adrenal glands 36

1.8 The adrenal gland – A small organ with big responsibility **39**

1.9 The adrenal cortex **39**

1.10 The adrenal medulla **42**

1.11 Tracing the origin of chromaffin cells **44**

1.12 Vertebrate adrenal gland differences and similarities **50**

1.13 The NEUcrest ITN project **53**

1.14 Aims of the thesis **54**

2 Chapter II: Materials and Methods **55**

2.1 *Xenopus* husbandry and egg collection **56**

2.2 Fertilisation of *Xenopus* eggs **56**

2.3 Fixing and storage of *Xenopus* embryos **57**

2.3.1 For WISH 57

2.3.2 For HCR 57

2.4 Dissection of Xenopus kidneys from stage 52 to stage 66 58

2.5 Cloning for *in situ* probes using pGEM®-T-Easy Vector 58

2.5.1 Primer design 58

2.5.2 RNA extraction and cDNA synthesis 59

2.5.2 Amplification of gene of interest by polymerase chain reaction (PCR) 60

2.5.3 Cloning into pGEM®-T-Easy Vector 61

2.5.4 Transformation and Colony PCR 63

2.5.5 Mini and MIDI extraction of plasmid DNA 64

2.6 Wholemount In *Situ* Hybridisation (WISH) probe synthesis 64

2.6.1 By Plasmid linearisation 64

2.6.2 By PCR reaction 67

2.7 Wholemount In *situ* Hybridisation 68

2.7.1 Bleaching embryos 69

2.7.2 Imaging 70

2.8 Hybridisation Chain Reaction (HCR) 70

2.8.1 HCR protocol adapted for Xenopus 70

2.8.2 Clearing 72

2.8.3 Visualisation 73

2.9 Cryosectioning 73

2.10 Dichromate staining 74

2.11 Immunofluorescence with anti-adrenaline on sectioned kidneys 74

2.12 Morpholino knockdown 74

2.13 Search for Potential Sympathoadrenal Cells in the Single Cell Atlas of Larval Xenopus 76

3 Chapter III: Characterisation of the development of the adrenal medulla (chromaffin cells) during Xenopus development by WISH 78

3.1 Identifying a list of candidate genes to characterise the development of the adrenal medulla in *Xenopus laevis* 79

3.1.1 Introduction: What is already known about adrenal gland development in *Xenopus* 79

3.1.2 Specification of markers involved in chromaffin cell development.....84
3.1.3 Cross-referencing pre-selected AM markers with a new tool.....85
3.2 Expression profiles of key marker genes identified for both adrenal medulla and adrenal cortex development.....90
3.3 Characterisation of AM markers during embryogenesis by Wholemount in *in situ* hybridisation.....92
3.3.1 Reptin (*ruvbl2*) marks nephrostomes and not adrenal medulla in *Xenopus*.....95
3.3.2 Phox2a.....100
3.3.3 Phox2b.....105
3.3.4 *Insm1*.....109
3.4 Characterisation of chromaffin cell markers during *Xenopus* development by WISH 113
3.4.1 Chga.....113
3.4.2 Dbh.....116
3.4.3 Pnmt.....119
3.4.4 Th.....123
3.5 Direct staining of catecholamine-producing cells in *Xenopus laevis*.....125
3.6 Expression in the developing enteric nervous system?.....128
3.7 Discussion.....133
3.7.1 Reviewing existing markers.....133
3.7.2 The noradrenergic neurons - Sympathoadrenal lineage specifiers?.134
3.7.3 NA neurons expressing CCs specific markers.....138
3.8 Are the characterized noradrenergic neurons neural crest derived?.....143
4 Chapter IV: Characterisation of adrenal cortex markers during Xenopus development by WISH.....145
4.1 Introduction.....146
***4.2 Nr5a1*.....148**
4.2.1 *Nr5a1* RNA sequencing data.....149
4.2.2 *Nr5a1* in WISH.....151
***4.3 Star*.....153**

4.3.1 *Star* RNA sequencing data 153
4.3.2 *Star* in WISH 154
4.4 Pgat **.....155**
4.4.1 *Pgat* in WISH 157
4.5 Discussion 159
4.5.1 Expression of AC markers during *X. laevis* development is in the anticipated area of the embryonic kidney 159
4.5.2 Distinguishing the adrenal cortex from the developing gonads.....162
4.5.3 Identifying the hindbrain expression pattern – locus coeruleus? 164
4.6 Summary of Chapter III and IV 168
5 Chapter V: Performing Hybridisation Chain Reaction to multiplex genes showing presumptive CCs and the AC 171
5.1 Introduction 172
5.1.1 Hybridisation Chain Reaction – HCR™ RNA-FISH 173
5.2 HCR RNA-FISH testing, targeting *phox2b* and *pax8*.....175
5.3 HCR co-expression analysis targeting *phox2a* and *dbh*.....178
5.4 HCR co-expression analysis of *phox2a* and *chga* 180
5.5 HCR co-expression analysis targeting *chga* and *dbh*.....183
5.6 Discussion of CC marker genes co-expression analysis by HCR RNA-FISH ..186
5.7 Performing Hybridisation Chain Reaction to multiplex genes to separate presumptive adrenal cortex and primordial germ cells.....191
5.7.1 HCR RNA-FISH targeting *pax8* and *pgat*.....192
5.7.2 HCR RNA-FISH targeting *nr5a1* and *pgat* 194
5.7.3 HCR RNA-FISH targeting *star* and *pgat* 195
5.8 Discussion 196
6 Chapter VI: Morpholino knockdown of the NC 199
6.1 Introduction 200
6.2 Foxd3 MO KD effect on NA neurons/putative Chromaffin cells 204
6.3 *Sox10* MO KD effect on NA neurons/Chromaffin cells.....212
6.4 Discussion and Conclusion 216

7 Chapter VII: General Discussion.....218

7.1 Summary.....219

7.2 Terminology and cell definition - Sympathetic neuron, noradrenergic neuron or chromaffin cell?.....222

7.3 Do chromaffin cells in *X. laevis* develop after embryogenesis? 226

7.4 Lineage tracing could aid in identifying time points of CCs development and association with the kidney 229

7.5 *Xenopus* AG structure may be more closely related to the Sea lamprey....231

7.6 Chromaffin-like cells are NC derived.....233

7.7 AC vs gonads.....236

7.8 Concluding Remark.....237

8 References 238

9 Appendix.....255

***9.1* Validating candidate gene markers of chromaffin cell development in *Xenopus laevis* in *Xenopus tropicalis*.....255**

9.2 Additional Figures.....259

List of Figures

Figure 1: The developmental life cycle of Xenopus laevis from fertilized egg to an adult frog. 25

Figure 2: Schematic outline of NC development and the vertebrate pan-NC-GRN regulating this process. 28

Figure 3: NCCs EMT process varies across different vertebrate species and at different axial levels. 30

Figure 4: Schematic showing NC subpopulations along the anteroposterior axis in the chick and typical NC migration pathways. 33

Figure 5: Schematic of various Neurocristopathies and the NC-lineages they derive from....38

Figure 6: Adrenal gland structure and hormones produced. 42

Figure 7: The catecholamine biosynthesis pathway in a chromaffin cell of the adrenal medulla. 44

Figure 8: Schematic depicting the developmental pathways of sympathoadrenal lineage and adrenal chromaffin cells in the mouse model. 47

Figure 9: Schematic description of genes governing the development of chromaffin cell in mammals (mouse model) and proteins that are transiently expressed during this process. .49

Figure 10: Comparison of different structures of vertebrate adrenal glands.....52

Figure 11: pGEM T Easy Vector backbone and vector information. 63

Figure 12: Schematic of the distribution of the interrenal cells in cranio-caudal directionality along the median surface of the kidney together with their corresponding sections at NF stage 63.....80

Figure 13: Schematic drawing showing the relationships between the steroidogenic tissue (gray), the chromaffin tissue (black), and the kidney in lower vertebrates.....81

Figure 14: Schematic drawing of AG shape and position among Anura species.....82

Figure 15: Developmental tree of transcriptomic analysis of NC, SCP and their downstream lineages created by and taken from (Kastriti et al., 2022). 87

Figure 16:UMAPs (gene-based embedding) showing the expression level of markers of interest within each of the cells of the different anatomical clusters in mouse model.....89

Figure 17: Expression of adrenal gland markers, both for chromaffin and steroidogenic cells, during developmental stages of X. laevis.....91

Figure 18: Schematic of pronephric kidney development in Xenopus. 93

Figure 19:Spatiotemporal expression map of control marker pax8, involved in the development of the pronephric kidney during X. laevis embryogenesis. 94

Figure 20: Whole-mount in situ hybridization analysis of Xreptin (J–Q) from Etard et al. (2000). 96

Figure 21: Wholemount in situ hybridisation analysis of reptin and pax8 during late tailbud development in X. laevis. 97

Figure 22: Schematic of Xenopus pronephric kidney at NF stage 35/36 99

Figure 23: Wholemount In Situ Hybridisation of pronephric tubule marker Cldn19 99

Figure 24: RNA sequencing data of phox2a.S 101

Figure 25: Screenshot of Xenopus laevis Chromosome 2L showing the position of the phox2a.S gene....103

Figure 26: The spatial and temporal expression pattern of phox2a during Xenopus laevis embryogenesis. 105

Figure 27: RNA sequencing data of phox2b....107

Figure 28: Spatial and temporal expression map of SA marker gene phox2b during X. laevis embryogenesis. 109

Figure 29: RNA expression analysis of insm1 chromosome variant L and S from to late tailbud NF stage 40 taken from Xenbase (Session et al., 2016). 111

Figure 30: Temporal and Spatial expression analysis of insm1 during X. laevis embryogenesis by WISH. 113

Figure 31: Spatial-temporal expression of chga mRNA by WISH from late Neurula (A) to tadpole (F). 116

Figure 32: Expression analysis of dbh RNA sequencing data during Xenopus laevis embryogenesis taken from Xenbase (Session et al., 2016). 118

Figure 33: Spatial and temporal expression of dbh mRNA in X. laevis by WISH from late neurula to tadpole....119

Figure 34: Expression analysis of pnmt RNA in Xenopus laevis during embryogenesis taken from Xenbase (Session et al., 2016)....121

Figure 35: Spatial-temporal expression of pnmt mRNA during X. laevis embryonic development by WISH. 122

Figure 36: Expression analysis of th RNA in Xenopus laevis during embryogenesis taken from Xenbase (Session et al., 2016)....124

Figure 37: Characterization of th expression during embryogenesis in X. laevis using WISH. 125

Figure 38: Dichromium staining on wholemount X. laevis embryos to identify mature chromaffin cells....126

Figure 39: Phox2a ENS development expression analysis during late tailbud NF stages 36 to 40....131

Figure 40: Phox2b ENS development expression analysis during late tailbud NF stages 36 to 40....132

Figure 41: WISH of NC marker gene hand2 showing its expression during X. laevis tailbud development....136

Figure 42: Comparison of spatial-temporal expression of key markers of chromaffin cell development during embryogenesis in X. laevis from developmental stage NF 19/20 – NF 30. 142

Figure 43: Comparison of spatial-temporal expression of key markers of chromaffin cell development during embryogenesis in X. laevis from developmental stage NF 33 – NF 45.143

Figure 44: RNA sequencing data of nr5a1 in Xenopus laevis during embryogenesis taken from Xenbase (Session et al., 2016).....150

Figure 45: Spatial and temporal expression atlas of nr5a1 during X. laevis embryogenesis by WISH.....152

Figure 46: Xenopus laevis RNA-sequencing data for Star taken from Xenbase (Session et al., 2016). 154

Figure 47: Spatial and temporal expression map of steroidogenic marker star during X. laevis embryogenesis.....155

Figure 48: Schematic of gonadal structure and morphology in X. laevis.....157

Figure 49: Spatiotemporal expression of primordial germ cell marker pgat during tailbud development of X. laevis.....158

Figure 50: Expression comparison of markers for the AC to the expression of pronephric kidney marker pax8. 161

Figure 51: Comparison of expression of adrenal cortex markers star and nr5a1 to gonadal primordial germ cell marker pgat during tailbud developmental stages in X. laevis.....164

Figure 52: Summary of marker genes that show expression in a hindbrain structure, likely the locus coeruleus (lc) in X. laevis at NF stage 40.....167

Figure 53: Summary of expression patterns identified and described throughout the process of characterizing the developing adrenal gland in Xenopus laevis.....170

Figure 54: Schematic of a two stage, multiplexed in situ hybridisation chain reaction (HCR). 174

Figure 55: HCR expression of SA specifier marker phox2b and control gene pax8 in Xenopus laevis embryo NF stage 40. 177

Figure 56: Co-expression of SA fate specifier gene phox2a with catecholamine biosynthetic enzymes dbh in Xenopus laevis. 179

Figure 57: Co-expression analysis of phox2a and dbh at NF stage 30. 180

Figure 58: Co-expression of SA specifier gene phox2a and neuroendocrine secretory protein chga in Xenopus laevis embryo.....182

Figure 59: Coexpression analysis of phox2a and chga in indicated cells at NF stage 30. 183

Figure 60: Co-expression of neuroendocrine secretory protein chga and catecholamine biosynthesis enzyme dbh at NF stage 30.....185

Figure 61: Co-expression analysis of chga and dbh in indicated cells at NF stage 30.....186

Figure 62: New discovery demonstrates the presence of sympathetic neurons in lamprey that co-express catecholamie biosynthesis enzymes th and dbh. 188

Figure 63: HCR detection of pronephric kidney marker pax8 and PGCs marker pgat at NF stage 40.....193

Figure 64: Expression of steroidogenic marker nr5a1 and PGCs marker pgat at NF stage 40. 195

Figure 65: Expression of steroidogenic marker star and PGCs marker pgat at NF stage 40. .196

Figure 66: Overview of neural crest migration in Xenopus embryos from late Neurula to early tailbud development.....201

Figure 67: Expression profile of NC marker Sox10 during early Xenopus embryogenesis by WISH. 202

Figure 68: Schematic showing the process of the Morpholino Knockdown experiments to inhibit NC development. 205

Figure 69: Dose response experiment of foxd3 Morpholino injected on one side (left) of a two-cell stage X. laevis embryo. 206

Figure 70: Example of phenotype categorization/scoring following foxd3 KD on one side of a two-cell stage embryo with insm1 mRNA expression. 206

Figure 71: The effect of NC inhibition by foxd3 MO knockdown in X. laevis. 209

Figure 72: KD of NC marker foxd3 inhibits the expression of CCs/NA neuron markers in the anteroventral region of X. laevis embryos. 211

Figure 73: The effect of NC inhibition by sox10 MO KD in X. laevis.....214

Figure 74: Inhibition of NC development by sox10 KD reduces the number of cells expressing CCs markers on the injected side compared to the uninjected side in X. laevis embryos. ...215

Figure 75: Search for potential SA cells in the single cell atlas of larval Xenopus created by (Liao et al., 2022). 231

Figure 76: Blastomeres with major contribution to the NC (red).....235

List of Tables

Table 1: List of primers used for cloning genes of interest 59
Table 2: PCR composition for 1 reaction (amplifying gene of interest) 60
Table 3: Thermocycler settings for gene amplification 61
Table 4: Restriction reaction 65
Table 5: List of WISH probes made by linearisation.....66
Table 6: PCR reaction steps 67
Table 7: Proteinase K time table 69
Table 8: List of HCR probes.....71
Table 9: Morpholino Oligo Properties.....75
Table 10: List of Solutions.....77
Table 11: Blast results showing percentage identity of genes of interest between Xenopus laevis and different species.....85

Abbreviations

AC	Adrenal Cortex
ACTH	Adrenocorticotropic Hormone
AG	Adrenal Gland
AGP	Adrenal-Gonadal Primordium
AM	Adrenal Medulla
ASCL1	Achaete-Scute Family BHLH Transcription Factor 1
AU	Arbitrary Units
AP	Anteroposterior
B	Branchial
CART	Cocaine- and Amphetamine -Regulated Transcript
CC	Chromaffin Cell
CHGA	Chromogranin A
CNCC	Cephalic/Cranial Neural Crest Cell
CNS	Central Nervous System
CT	Connecting Tubule
DA	Dorsal Aorta
DBH	Dopamine Beta Hydroxylase
DIG	Digoxigenin

DISH	Double In Situ Hybridization
DRG	Dorsal Root Ganglion/Dorsal Root Ganglia
DT	Distal Tubule
DPF	Days Post-Fertilization
E	Embryonic
EN	Enteric Neurons
ENS	Enteric Nervous System
FISH	Fluorescence In Situ Hybridization
FITC	Fluorescein
FOXD3	Forkhead Box D3
GI	Gastro- Intestinal
GR	Glucocorticoid Receptor
GRN	Gene Regulatory Network
H	Hyoid
HAND2	Heart and Neural Crest Derivatives Expressed 2
HB	Hindbrain
HCR	Hybridization Chain Reaction
HPA	Hypothalamic- Pituitary- Adrenal
IF	Immunofluorescence

IHC	Immunohistochemistry
IM	Intermediate Mesoderm
INSM1	Insulinoma Associated 1
IT	Intermediate Tubule
KD	Knockdown
LC	Locus Coeruleus
L-DOPA	Dihydroxyphenylalanine
M	Mandibular
MI	Molecular Instruments
MO	Morpholino Oligonucleotides
MRNA	Messenger RNA
NA	Noradrenergic
NB	Neural Border
NC	Neural Crest
NCC	Neural Crest Cell
NF	Nieuwkoop and Faber
NG	Neural Groove
NPB	Neural Plate Border
NS	Nephrostomes

NT	Neural Tube
OCT	Optimal Cutting Temperature
OP	Otic Placode
OV	Otic Vesicle
P	Pronephros
PBS	Phosphate-Buffered Saline
PD	Pronephric Duct
PGC	Primordial Germ Cell
PHOX2	Paired Like Homeobox 2
PI	Pineal Gland
PK	Proteinase K
PLP	Proteolipid Protein
PM	Pronephric mesenchyme
PNMT	Phenyl-ethanolamine N-methyltransferase
PNS	Peripheral Nervous System
PSNS	Peripheral Sympathetic Nervous System
PT	Proximal Tubule
RAAS	Renin-Angiotensin-Aldosterone System
RT-PCR	Reverse Transcription- Polymerase Chain Reaction

RUVBL2	RuvB like AAA ATPase 2
SA	Sympathoadrenal
SCG	Superior Cervical Ganglion
SCP	Schwann Cell Precursor
SNAI2	Snail Family Transcriptional Repressor 2
SNS	Sympathetic Nervous System
SOX10	SRY-Box 10
T	Tahara
TF	Transcription Factor
TH	Tyrosine Hydroxylase
TNCC	Trunk Neural Crest Cell
TPM	Transcripts Per Million
VN	Vagus Nerve
WISH	Whole-Mount In Situ Hybridization
WT	Wild Type
X.Laevis	Xenopus Laevis
X.Tropicalis	Xenopus Tropicalis

1 Chapter I: General Intoduction

1.1 Xenopus as a (disease) model system

The model organism *Xenopus laevis* (*X. laevis*), an aquatic species of African clawed frogs, has been used extensively in research in the last 100 years to examine fundamental developmental and cellular biological processes (Lasser et al., 2019). Initially used for rapid pregnancy testing from the 1930s, this model species has emerged as an ideal system for investigating human genetic disorders. *X. laevis* studies complement fundamental research also done in other model systems such as the mouse and zebrafish (Blum and Ott, 2019; Griffin et al., 2020). Development and morphology of most organs is well conserved between *X. laevis* and the mammalian systems, and a detailed temporal staging atlas together with the embryos relative transparency, enables easy fate mapping of cell lineages from various embryonic blastomeres and tissue regions (Desanlis et al., 2018; Tandon et al., 2017).

Compared to other vertebrate embryos, *X. laevis* embryos are large and develop rapidly and externally, allowing for easy microdissection and manipulation of specific tissues even at the earliest stages of development (Mimoto and Christian, 2011). Additionally, their ability to produce large clutches of eggs on demand by simple hormone injection gives them a great advantage over any other mammalian system. Further, *X. laevis* upkeeping is more cost efficient compared to mice housing and maintenance, while also producing a smaller litter size (Tandon et al., 2017; Blum and Ott, 2018). Developmental speed of *X. laevis* embryos can also be easily manipulated and controlled by changing the incubation temperature. While zebrafish shares several traits with *X. laevis* as predictive animal models of human disease, like producing large numbers of transparent embryos in a short amount of time while also being easy to house and maintain, they lack certain organs like the lungs, limbs or digits and are less evolutionary similar to mammals than *X. laevis* (Wheeler and Brändli, 2009). For instance, the heart in zebrafish is two-chambered while the heart in *X. laevis* is three-chambered, and therefore more similar to the mammalian heart (Wheeler and Brändli, 2009). This limits their use in research for many human congenital syndromes (Blum and Ott, 2018). *X. laevis*, like zebrafish, have also proven to be a convenient animal model for high-throughput chemical screening in drug discovery. Here, compounds can easily be added to the bathing media, and embryos screened in 96-well plates (Wheeler and Brändli, 2009).

One of the main disadvantages of *X. laevis* as a model system was its poor genetic tractability. *X. laevis* is allotetraploid, with the whole genome being duplicated, resulting in having two different copies of each gene, which are located in homologous chromosomes (Schmitt et al., 2014). These chromosomes are named according to their relative length, one short variant (S) and a long variant (L). However, this disadvantage has been overcome with the establishment of the closely related *Xenopus tropicalis* (*X. tropicalis*) as an additional model species (Blum and Ott, 2018; Hwang, Marquez and Khokha, 2019). Compared to the allotetraploid *X. laevis*, *X. tropicalis* is diploid, making it easier to perform genomic manipulation, and offers most of the embryological benefits of *X. laevis*. Additionally, they have an even faster generation time (Tandon et al., 2017). Together, these two *Xenopus* species allow rapid investigation of candidate gene function in human disease (Blum and Ott, 2018; Griffin, Liu and Sempou, 2020).

1.2 *Xenopus* development

In contrast to other vertebrate tables for normal development measured in hours and days post-fertilization, the staging system in *Xenopus* has been based on external morphology (landmarks) and internal features at stable temperatures by Nieuwkoop and Faber (Nieuwkoop and Faber, 1994; Zahn et al., 2022). Therefore, the *Xenopus* development staging system is labelled 'NF' after the authors last names, and can be applied to both *X. laevis* and *X. tropicalis* (Zahn et al., 2022*)*. Key internal and external milestones in *Xenopus* development include early cell division (NF stages 2-6), gastrulation onset (NF stage 10), neurulation (NF stages 13-21), heart beat (NF stages 33-34), gut coiling (NF stages 41-46) and limb development (NF stages 48-58) (Fig. 1). Key aspects of internal organogenesis takes place between NF stages 29-38, and includes the formation of the embryonic heart, central nervous system (CNS) patterning, and pronephric kidney formation, which begins blood filtration and osmoregulation by NF stages 37-38 (Zahn et al., 2022). At NF stages 40-46, the embryos have developed to free-swimming tadpoles, and major milestones include morphogenesis of the digestive and respiratory systems until pre-metamorphosis (Zahn et al., 2022)

Although *Xenopus* is an aquatic species and does not transition to land like other frog species, it still undergoes the post-embryonic transition of metamorphosis, a drastic process that changes most aspects of the tadpole. Metamorphosis takes place between NF stages 55-66, transforming from a tadpole to a fully adult frog. Amphibians, like *Xenopus*, highlight the evolutionary transition from aquatic to terrestrial life and represent an intermediate taxon that links mammals to vertebrates of more ancient origin (Liao et al., 2022). Metamorphosis includes gain of limbs and the absorption of the tail, as well as the loss of gills, culminating in air-breathing. Internally, it involves a switch of liver metabolism and remodelling of cranial cartilages, intestine, and skin (Buchholz, 2017). Hormones produced by the anterior pituitary gland and the so-called interrenal glands (mammalian adrenal gland) regulate the rate of metamorphosis by controlling the production and action of thyroid hormones and glucocorticoids (Denver, 2013).

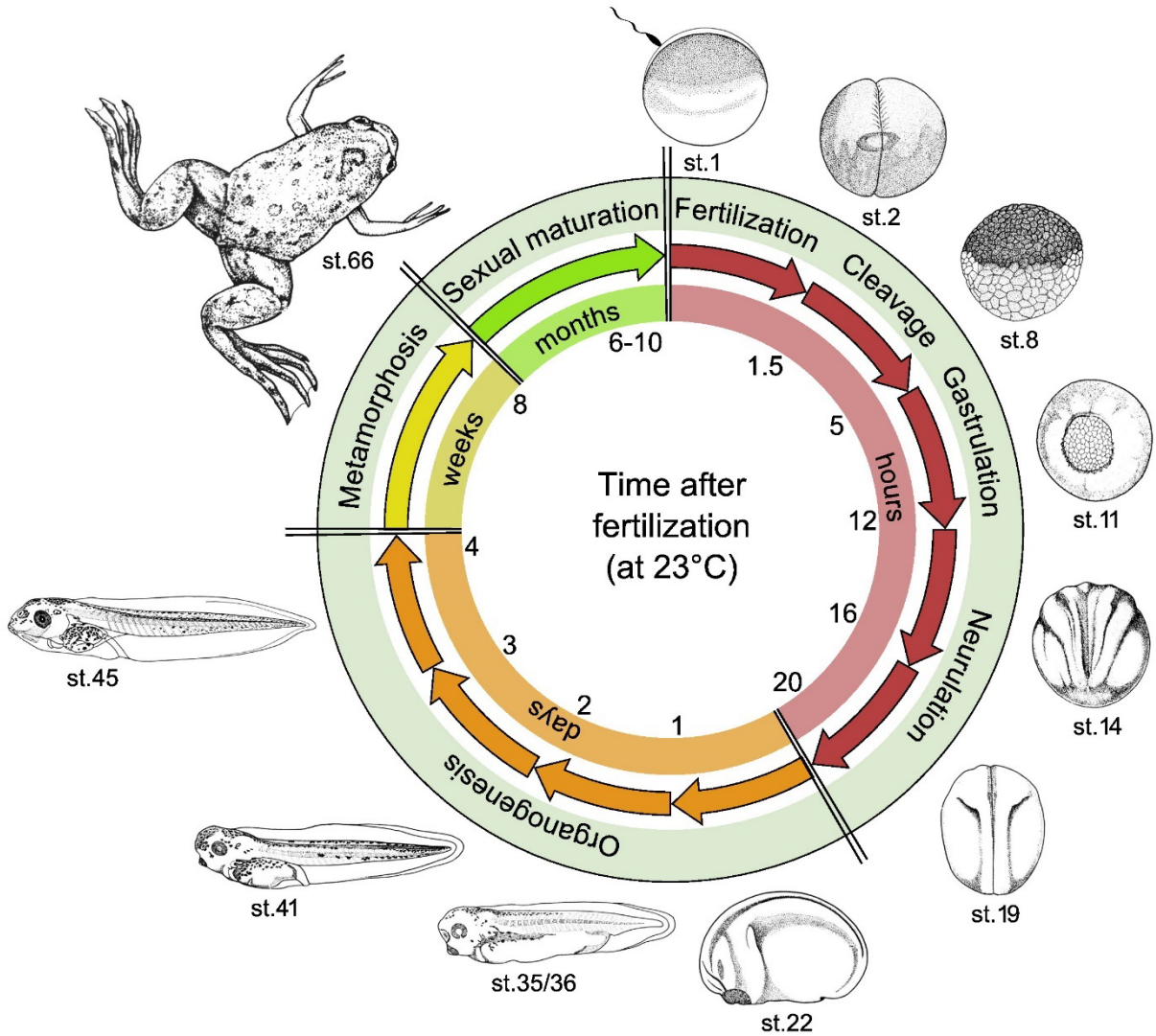

Figure 1: The developmental life cycle of Xenopus laevis from fertilized egg to an adult frog. *Embryos are staged according to (Nieuwkoop and Faber, 1994) normal staging table, based on sublte morphological changes. The figure was created by and taken from (Schmitt et al., 2014).*

1.3 Welcome to the neural crest – A historic discovery

The neural crest (NC) is a multipotent embryonic stem cell population, specific to vertebrates, giving rise to a vast spectrum of cell types. The discovery and research on neural crest cells (NCCs) has significantly advanced our understanding of vertebrate development and evolution. The NC was first identified and described by Wilhelm His in 1868, when he detected a group of cells located between the developing neural tube and the future epidermal

ectoderm (His, 1868). He discovered these cells to be the source of the dorsal and coronial ganglia in chick embryos, naming these cells 'Zwischenstrang' (intermediate chord) (Pakhomova et al., 2023). In the late 19th century, work by Julia Platt first demonstrated the migratory nature of these cells by discovering their role in the formation of the craniofacial and pharyngal cartilages (Pakhomova et al., 2023). In the mid-20th century, Nicole Le Douarin further expanded on the multipotency and extensive migratory capabilities of NCCs. Le Douarin's groundbreaking quail-chick chimera experiments were particularly influential, providing definitive evidence of the NCs contribution to various tissues and organs, including the peripheral nervous system (PNS), melanocytes, and endocrine cells of the adrenal medulla (AM) (Le Dourarin et al., 1980; Pakhomova et al., 2023). Research during the last few decades have deepened our understanding on signalling pathways and gene regulatory networks (GRN) governing NC development, as well as focussing on understanding and identifying human diseases associated with defects of NC development, which are globally called Neurocristopathies (NCPs).

The NC is first induced during late gastrulation/early neurulation, and is initially located at the neural plate border (NPB) territory, at the lateral edges of the central nervous system (CNS) (Simoes-Costa and Bronner, 2015) (Fig. 2A). During neurulation in *X. laevis*, NCCs delaminate from the NPB, undergo epithelial-to-mesenchymal (EMT) transition, and migrate extensively along several specific routes throughout the embryonic body. The diverse range of derivatives includes neurons and glia of the peripheral and enteric nervous system (ENS), endocrine cells of the AM, pigment cells (melanocytes) of the skin, and cartilage and bone cells of the craniofacial skeleton. Due to their ability to give rise to numerous derivatives, the NC has often been referred to as the 4th germ cell layer and can be divided into four main subpopulations of NCCs along the anteroposterior axis of jawed vertebrates: Cranial, Vagal, Trunk and Sacral NC (Hall, 2000; Hoppler and Wheeler, 2015; Martik and Bronner, 2017; Rothstein et al., 2018).

Although NC have been studied for over 150 years, the broad array of its derivates still leads to new discoveries and has left many unsolved questions. Researchers are still investigating fundamental aspects of NC biology, from how they arise, migrate, and differentiate during embryonic development. This includes questions as to how these cells first emerge and integrate into the vertebrate body, and why they do not become part of the CNS despite their

initial location of appearance (Bronner and Simões-Costa, 2016). The NC contribution to critical developmental processes makes it a continuous intriguing subject for scientific research and provides a plethora of questions left for embryologist to investigate.

1.4 Neural crest specification and regulation

An intricate network of various genes controls the formation and progression of NC development that has been mainly elucidated by using molecular disruption approaches, such as morpholinos or double negative constructs in *Xenopus*, zebrafish and chick (Bronner and Simões-Costa, 2016). These factors are part of a vertebrate NC-GRN, arranged in distinct hierarchical modules of signalling molecules that correspond to different stages of NC formation (Fig. 2B) (Bronner and Simões-Costa, 2016).

The NC is induced during mid-to late gastrulation stages (dependant on the organism) at the NPB, which sits at the interface between the neural and non-neural ectoderm, and between the epidermis and mesoderm (Barriga and Theveneau, 2020).

Induction of the NC and the neural border (NB) is initiated by a combination of Wnt, bone morphogenic protein (BMP) and fibroblast growth factor (FGF) signalling pathways, from neighbouring tissues, that refine the border between the forming neural and non-neural ectoderm (Martik and Bronner, 2021; Simoes-Costa and Bronner, 2015). The combination of their intersecting signalling activates a set of TFs called 'NB specifiers', including *Zic1*, *Msx2*, *Tfap2a*, *Dlx5/6*, and *Pax3/7* (Simoes-Costa and Bronner, 2015). In turn, these NB specifiers, along with extracellular signalling inputs activated during the time of specification, trigger the expression of downstream 'NC specifier' genes (Simoes-Costa and Bronner, 2015). NC specifier genes mark bona fide NC precursors, which initiate in the closing neural tube prior to emigration, and include genes like *Foxd3*, *SoxE* genes (*Sox8/9/10*), *Snai1/2*, and *Tfap2* (Bronner and Simões-Costa, 2016; Martik and Bronner, 2021). Following NC specification, NC specifier genes regulate downstream factors necessary for cells to undergo an EMT. This allows NC de-adhesion of the NPB and exit from the forming CNS (Bronner and Simões-Costa, 2016; Martik and Bronner, 2021). After delamination, NCCs activate a migratory module of

the GRN to migrate extensively throughout the embryo, and give rise to numerous distinct derivatives, once reaching the appropriate location (Martik and Bronner, 2021).

The current knowledge of the complex NC-GRN has emerged over many years, using numerous organisms and cell types. Some species-specific differences have been shown, although in small variations, with an overall relatively uniform and conserved regulatory mechanism (Martik and Bronner, 2021; Sauka-Spengler and Bronner-Fraser, 2008).

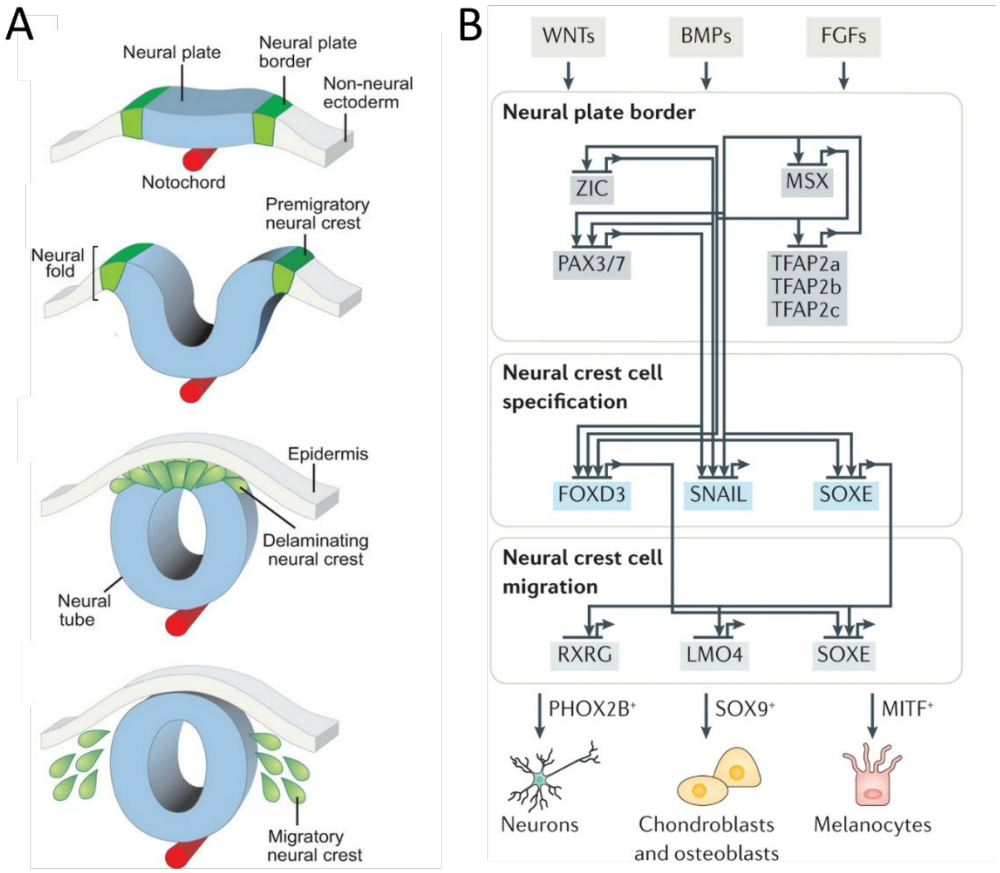

Figure 2: Schematic outline of NC development and the vertebrate pan-NC-GRN regulating this process.
A*: Progression of NC development which begins around gastrulation with the formation and specification of the NPB between the neural and non-neural ectoderm. When the neural tube begins to close, NC progenitors are specified. The NC then undergoes EMT and delaminates from the forming neural tube, migrating throughout the embryonic body to give rise to numerous derivatives.* ***B****: The vertebrate pan-NC-GRN is organized in hierarchical modules of signalling molecules and transcription factors for each step of development. Migratory NCCs express regulators that enable migration and the ability to initiate various differentiation programs. Figures created by and taken from (Simoes-Costa and Bronner, 2015) and (Martik and Bronner, 2021)*

1.5 Neural crest epithelial-to-mesenchymal transition

To acquire motility to migrate throughout the embryonic body, NCCs need to undergo an epithelial-to-mesenchymal transition. During EMT, cells undergo transcriptional and morphological changes to delaminate from the neural tube (Dongre and Weinberg, 2019; Lamouille et al., 2014; Nieto et al., 2016). Changes during EMT include the loss of cell-cell adhesion, the acquisition of a front-rear polarity, and the upregulation of various mesenchymal markers. Together, this leads to a loss of their epithelial characteristics, becoming less adhesive. Through further remodelling of their cytoskeleton, cells gain a mesenchymal phenotype, increasing cell motility (Lamouille et al., 2014; Szabó and Mayor, 2018).

Such a complex process is tightly controlled by numerous transcription factors that are present hours before NC migration is initiated (Barriga and Theveneau, 2020). EMT is induced by the expression of EMT transcription factors (EMT-TFs), including *Snail*, *Twist*, *Zeb* and *Prrx* families, which repress the expression of cell-cell adhesion proteins and activate mesenchymal programmes, through switching of their cadherins (Bronner and Simões-Costa, 2016; Nieto et al., 2016).

In *Xenopus*, the NC has been described as going through a partial EMT process, which allows cells to migrate collectively by retaining some epithelial properties, with frequent transient physical contacts through functional adherens junctions (Barriga and Theveneau, 2020). Generally, the timing of NC-EMT varies across species and according to region: cranial neural crest cells (CNCCs) delaminate simultaneously, whereas trunk neural crest cells (TNCCs) delaminate progressively from anterior to posterior (Szabó and Mayor, 2018). Onset of delamination of the NC correlates with either neural fold fusion or the formation of the somites (Szabó and Mayor, 2018). In *Xenopus* and zebrafish, NCCs delaminate prior to neural tube closure, which is followed by EMT to migrate laterally (Leathers and Rogers, 2022) (Fig.3). In rodents, delamination is independent of neural fold closure. Here, NCCs first undego EMT, delaminate and migrate before the neural tube has closed (Leathers and Rogers, 2022; Szabó and Mayor, 2018). In contrast, avian NCCs undergo EMT after neural tube closure, followed by

migration (Fig. 3) (Leathers and Rogers, 2022; Szabó and Mayor, 2018). Human NCC delamination and migration is more similar to that of rodents (Leathers and Rogers, 2022).

Following EMT and delamination from the neural tube, NCCs begin the expression of transcription factors (TFs), which is vital for cell migration and for initiating the differentiation programs leading to their distinct derivatives (Simoes-Costa and Bronner, 2015).

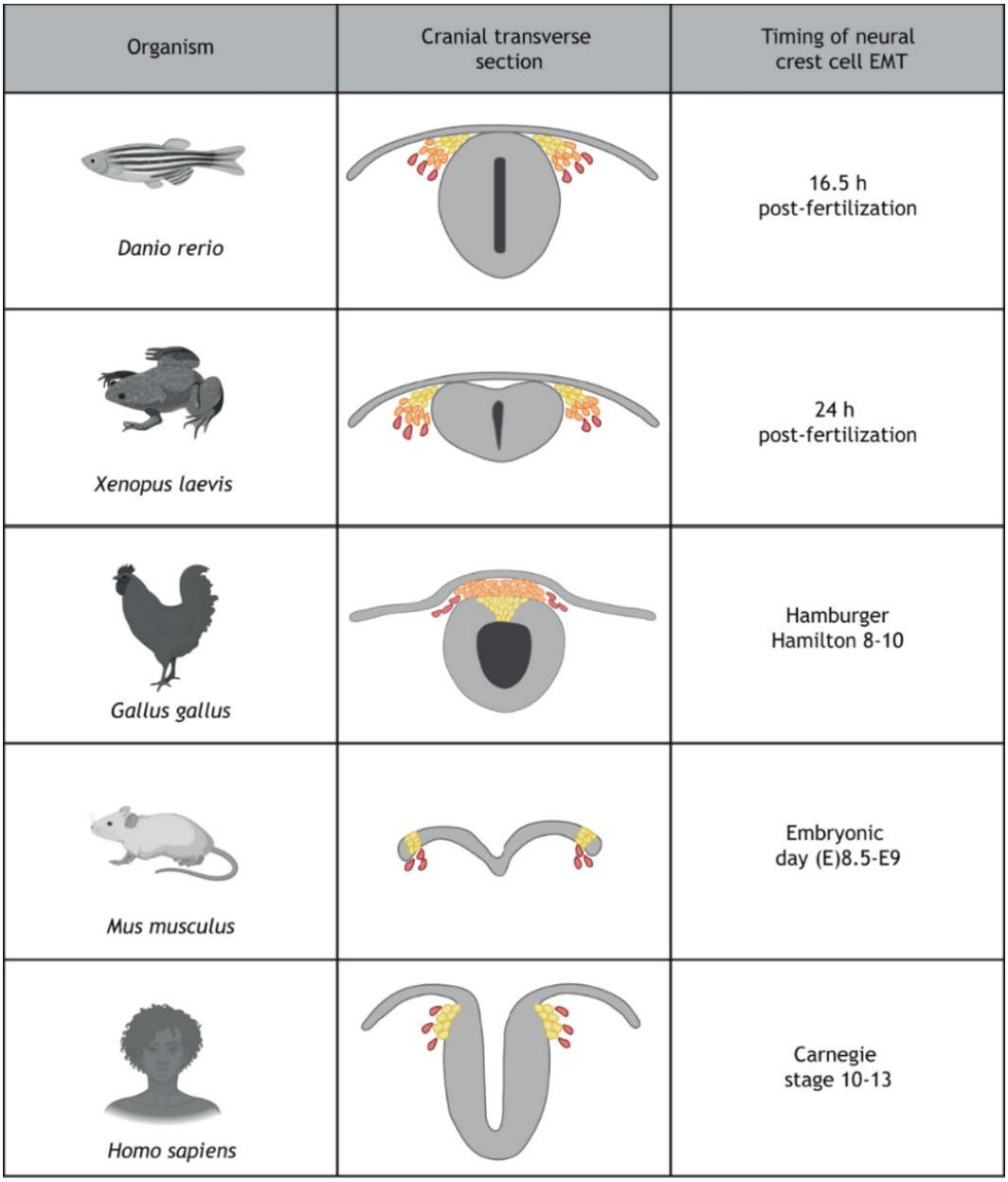

Figure 3: NCCs EMT process varies across different vertebrate species and at different axial levels.

Pre-migratory NCCs are in yellow, collective NCC migration is orange, and fully mesenchymalized NCCs are shown in red. In zebrafish and frog, NCCs arise adjacent to the neural tube, undergo rapid EMT and emigrate laterally and swiftly. In Xenopus*, NCCs undergo a staged EMT marked by temporal expression of EMT regulators and gradual loss of epithelial characteristics. NCCs of avian species must delaminate from the neural tube first before emigrating. Rodent NCCs delaminate independently of neural fold closure and begin migration prior to this event). Human NCC migration is more similar to that of rodents and avians, with similar regulatory mechanisms and developmental timelines. Image created by and taken from (Leathers and Rogers, 2022).*

1.6 Neural crest migration and differentiation into multiple lineages

Following delamination, NC progenitors undergo some of the most extensive migrations of any embryonic cell type and differentiate into an enormous variety of derivatives, using distinct pathways (Martik and Bronner, 2017; Rothstein et al., 2018). These pathways are tightly regulated by a combination of signalling molecules, extracellular matrix components and cell-cell interactions, crucial for guiding the NCCs to their specific destinations. NCCs are classified into four distinct subpopulations, based on their anatomical position, differences in migratory patterns, developmental potential and the genes expressed (Rothstein et al., 2018). These include the cranial, vagal, trunk and sacral NC (Fig. 4A).

For example, cranial and trunk NCCs exhibit differences in their routes and modes of migration, partly due to differences in their local environments and their axial level of origins (Rocha et al., 2020; Rothstein et al., 2018).

The CNCCs arise from the anterior CNS, from the forebrain to hindbrain. From here, they migrate in a continuous wave-like pattern away from the neuroepithelium to invade the tight spaces between the epidermal and mesodermal layers splitting into large, distinct streams (Rothstein et al., 2018; Szabó and Mayor, 2018; Theveneau and Mayor, 2012). The anteroposterior (AP) position of the cranial NC streams correlates with molecular markers of the neural tube, such as Hox factors, ephrins and their receptors (Szabó and Mayor, 2018). The pattern of dorsolateral CNCCs migration shows little variation between species. CNCCs give rise to the majority of the craniofacial skeleton, melanocytes and neurons of the cranial ganglia (Rothstein et al., 2018).

In contrast, TNCCs delaminate progressively after neural tube closure/formation and form a constant stream, using either the ventromedial pathway along the neural tube and notochord, or the dorsolateral pathway between the dorsal ectoderm and dermomyotome (Fig. 4B) (Rothstein et al., 2018; Theveneau and Mayor, 2012). TNCCs migrating dorsolateral give rise to melanocytes, whereas cells migrating ventromedial, also known as ventral, will form the sympathetic ganglia, neurons and glia of the dorsal root ganglia (DRG). The first wave of ventral migration is followed by a second migration wave, ventrolateral, which gives rise to Schwann cells, neurons of the enteric nervous system (ENS), and chromaffin cells (CCs) of the AM (Furlan et al. 2017, Tsubota and Kadomatsu, 2018). This will be further discussed and analysed in section 1.11. Trunk NC migration varies among species, with the ventromedial and dorsolateral paths starting simultaneously in mice, but with a delay in the dorsomedial path in chick and zebrafish (Szabó and Mayor, 2018). While the migratory pathways are distinct and separate in most species, in zebrafish and *Xenopus* some TNCCs from the ventromedial path migrate between the somites toward the dorsolateral NCCs to contribute to mesenchymal and pigment cells (Szabó and Mayor, 2018).

Interestingly, very recently it was discovered that the jawless vertebrate lamprey does form sympathetic ganglia derived of the TNCCs, which were long thought to be absent in the species, albeit much later during developmental stages than in humans (Edens et al., 2024). This demonstrates a perfect example of the need for ongoing research in this field and underscores the complexity of the lineage, opening new avenues for investigating the mechanisms underlying NCCs differentiation and migration. Additionally, enteric ganglia of the ENS are derived from TNCCs, whereas in jawed vertebrates they are derived of the vagal crest lineage (Green et al., 2017)

Vagal and sacral NCCs migrate from regions adjacent to the developing gastrointestinal (GI) tract and contribute to the ENS, which regulates gut motility. Vagal Crest is positioned between the cranial NC and trunk NC, just behind the hindbrain, while the sacral crest is found posterior to the trunk NC. These cells follow pathways rich in GDNF (glial cell line-derived neurotrophic factor) and endothelin-3, which are critical for their migration and differentiation into enteric neurons and glia (Heanue and Pachnis, 2007). The anterior vagal crest follows a dorsolateral pathway and gives rise to the cardiac NC, contributing to the

septation of the outflow tract of the heart, and great vessels and pharyngal arches 3-6, differentiating into smooth muscle cells. Additionally, the VC contributes to the formation of the ENS of the foregut and stomach by migrating ventrally along the vagus nerve, while another population of late migrating vagal crest contribute to the DRG of the peripeheral nervous system and melanocytes (Rothstein et al., 2018).

Sacral NC also contributes to enteric neurons and glial cells of the ENS but forming in the distal hindgut. Hereby, sacral NCCs migrate ventrally and colonize the gut after the vagal crest. Although the sacral NC can populate the gut in the absence of VC, it cannot replace vagal derivatives and therefore suggests differences in the molecular regulation (Burns et al., 2000; Rothstein et al., 2018). Sacral NC has only been identified in amniotes (reptiles, birds and mammals), meaning that in zebrafish and *Xenopus*, the ENS is largely derived from vagal NCCs.

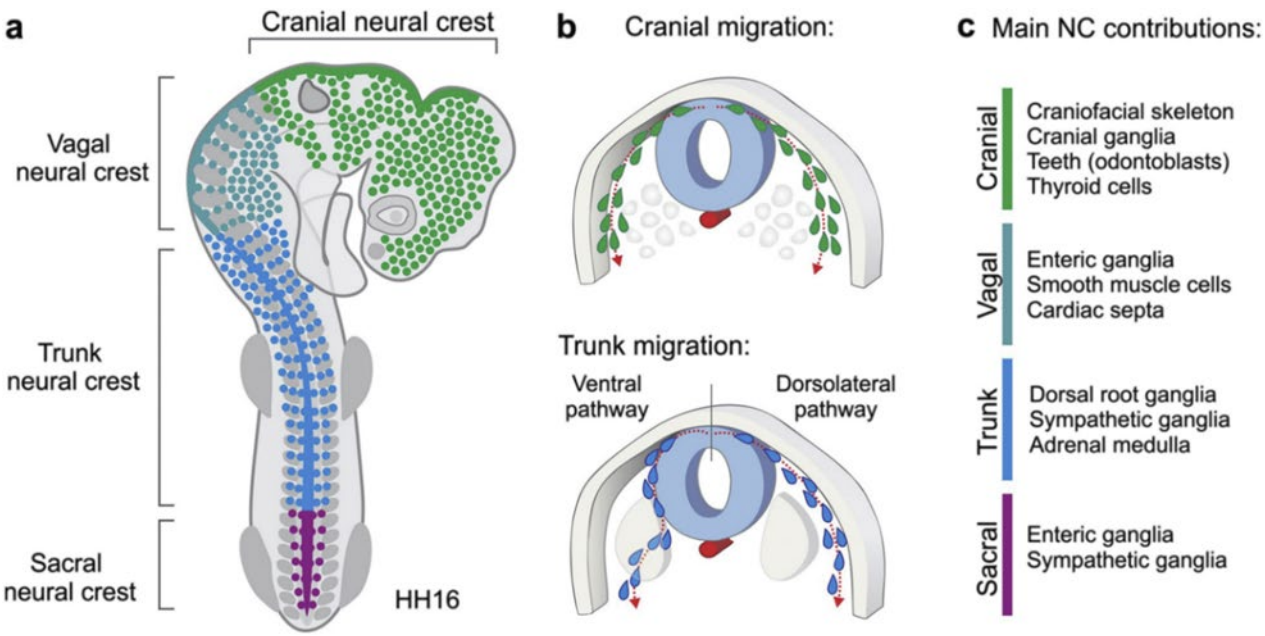

Figure 4: Schematic showing NC subpopulations along the anteroposterior axis in the chick and typical NC migration pathways.
A: The NC can be divided into four different subpopulations along the anteroposterior axis, well demonstrated in the chick embryo. B: Migration patterns differ between NC populations. CNCCs migrate dorsolateral, while TNCCs use either the dorsolateral or ventral pathway of migration, giving rise to different derivatives. C: The NC subpopulations give rise to a multitude of cells and tissues, with the main derivatives listed such as the craniofacial skeleton from

CNCCs, Enteric neurons and ganglia from vagal and sacral NC and chromaffin cells of the adrenal medulla derived from TNCCs. Image created by and taken from (Rothstein et al., 2018).

1.7 Neurocristopathies

The highly migratory and invasive nature of NCCs means the NC have a widespread contribution to a multitude of cell types and organs (Sato et al., 2019; Szabó and Mayor, 2018). However, improper NC development, typically relating to the formation, migration or differentiation of the NC, can give rise to a diverse array of syndromes termed, neurocristopathies (NCP) (Bolande, 1974; Sato et al., 2019). As our understanding of NC development has advanced in recent years, the number and variety of NCP have significantly increased to encompass more than 50 diseases (Sato et al., 2019). NCPs can be categorized into three main groups, according to the stage of NC development affected at the onset of the disease: NCP arising from defects in NC induction and specification, like Treacher Collins syndrome; NCPs arising from migration defects such as CHARGE and DiGeorge syndrome; and NCPs from differentiation defects, like Craniosynostosis, Hirschsprung's disease and Waardenburg syndrome (Medina-Cuadra and Monsoro-Burq, 2021; Vega-Lopez et al., 2018) (Fig. 5). Additionally, NCPs also encompass cancers Neuroblastoma and Melanoma. Both NCCs and cancer cells share many characteristics, cellular behaviours, numerous signalling pathways and transcription factors, implying that some tumours might reactivate part of their embryonic NC developmental programs in a dysregulated manner (Maguire et al., 2015; Theveneau and Mayor, 2012; White et al., 2011).

In the following, we will briefly introduce some of the most well-known NCPs, presenting the broad spectrum of diseases with a special focus on tumours deriving from the sympathoadrenal domain.

Treacher Collins Syndrome is a congenital craniofacial disorder causing craniofacial abnormalities, such as underdeveloped facial bones due to abnormal development of the first and second pharyngal arches, cleft palate, and hearing loss, among others (Dixon et al., 2007; Sato et al., 2019). The syndrome results from mutations in genes essential for ribosome biogenesis and NC development such as the *TCOF1*, *POLR1C,* or *POLR1D* (Dixon et al., 2007).

CHARGE Syndrome is defined by multiple congenital abnormalities including coloboma of the eye, heart defects, choanal atresia, retarded growth and development, urogenital and ear abnormalities (caused by a malformation of the cranial nerve VIII and ossicles) and cleft palate (Hale et al., 2016; Vega-Lopez et al., 2018). The syndrome is caused by mutations in the *CHD7* gene, crucial for chromatin remodelling and proper organisation of NC-derived craniofacial cartilage. This mutation affects both cranial and vagal NC (Sato et al., 2019; Vega-Lopez et al., 2018). In *Xenopus*, *chd7* is crucial for the activation of the NC transcriptional network, including *sox9*, *twist* and *slug* (Vega-Lopez et al., 2017).

Craniosynostosis involves the premature fusion of cranial sutures, leading to abnormal skull shape and potential neurological impairment (Twigg and Wilkie, 2015; Wilkie et al., 2017). This can be caused by mutations in *FGFR1, GFR2*, *FGFR3*, *TWIST1*, or *EFNB1* (Wilkie et al., 2017). The *Xenopus* model has been a useful model system to study cranial ossification and suture patterning, providing insights into human craniofacial anomalies (Vega-Lopez et al., 2018).

Waardenburg Syndrome is characterized by congenital sensorineural hearing loss, mild craniofacial anomalies and pigmentation defects in the skin, hair and eyes (Medina-Cuadra and Monsoro-Burq, 2021; Pingault et al., 2010). Waardenburg Syndrome results from mutations in *PAX3*, *MITF*, and *SOX10*, impacting the development of CNCCs and TNCCs (Pingault et al., 2010).

Hirschsprung's Disease is caused by mutations in several different genes such as *RET, EDNRB*, *EDN3*, *PHOX2B* and *SOX10*, affecting the migration and differentiation of vagal and sacral NCCs. This results in a failure of the enteric NCCs to colonize portions of the distal intestine (Heanue and Pachnis, 2007; Vega-Lopez et al., 2017). The consequential lack of enteric ganglia in parts of the colon leads to severe constipation and intestinal obstruction (Heanue and Pachnis, 2007).

Melanoma is a highly aggressive form of skin cancer, originating from malignant transformations of melanocytes, pigment producing NC derived cells. Melanoma cells have been shown to exploit an uncontrolled reactivation of EMT in adults, allowing phenotypic

switching. This enhances their migratory and invasive capabilities and contributing to tumour progression in distant regions of the body (Hoek et al., 2006; Medina-Cuadra and Monsoro-Burq, 2021). Melanoma development is driven by environmental factors like ultraviolet radiation exposure that provoke genetic mutations in genes such as *BRAF*, *NRAS*, or *PTEN* (Hoek et al., 2006; Müller et al., 2014).

Xenopus has been a valuable model in the study of the NC and its related pathologies, the NCPs. Its genome shares nearly 80% of genes known to cause human diseases, and the model has made important contributions to the better understanding of human pathologies (Medina-Cuadra and Monsoro-Burq, 2021). A comprehensive summary of research on NCPs using the *Xenopus* model has been put together by our NEUcrest partners, ranging from defects during migration (types of Waardenburg syndrome) and differentiation (Craniosynostosis) to tumourgenesis (melanoma and neuroblastoma) (Medina-Cuadra and Monsoro-Burq, 2021) (Fig.5).

1.7.1 Neurocristopathies of the adrenal glands

In humans, transformed cells of the sympathoadrenal domain give rise to tumours found in a spectrum of clinical diseases (Huber et al., 2018; Maguire et al., 2015). Tumours of the AM and paraganglia include catecholamine-secreting tumours pheochromocytomas (PCC) and paragangliomas (PGC), as well as the paediatric tumour neuroblastoma (Maguire et al., 2015). Finding the cell of origin and the mechanism driving tumorigenesis neuroblastoma and paraganglioma/pheochromocytoma is a major focus of research to this day.

Neuroblastoma is a paediatric neuroendocrine tumour of embryonic NCC origin and the most common extra-cranial solid tumour in children (Huber et al., 2018; Veschi et al., 2019). Neuroblastoma results from sporatic or somatic mutations of developmentally regulated genes including amplification of *MYCN*, mutations in *anaplastic lymphoma kinase (ALK)*, and segmental chromosomal alterations (Vega-Lopez et al., 2018). The first neuroblastoma predisposition gene discovered was *paired-like homeobox 2B* (*PHOX2B*), identified in a familial case of neuroblastoma (Trochet et al., 2004; Wulf et al., 2021). *PHOX2B* encodes a TF crucial

for the development of the autonomic nervous system and sympathoadrenal specification, underscoring that neuroblastoma likely arises from developmental issues in this NC-derived lineage (Trochet et al., 2004; Wulf et al., 2021). Missense variants in *PHOX2B* are also implicated in other NC-related diseases, like congenital central hypoventilation syndrome and Hirschsprung disease (Wulf et al., 2021). However, familial cases of neuroblastoma are rare, accounting for only 1–2% of all cases, with *PHOX2B* mutations responsible for approximately 6–10% of these familial cases (Trochet et al., 2004; Wulf et al., 2021). The recent discovery that CCs of the AM are derived from SCPs during murine embryo development, raises new questions about the cellular origin of neuroblastoma (Furlan and Adameyko, 2018; Huber et al., 2018). As the underlying mechanism, as well as the origin of neuroblastoma, remains elusive, these findings implicate SCPs besides NC progenitor cells and sympathetic neuroblasts as another possible cell of origin (Tsubota and Kadomatsu, 2017).

Paragangliomas and pheochromocytomas are rare, highly vascularized tumours, mostly present in adults which are determined based on their location, with tumours arising either from chromaffin cells in the paraxial autonomic ganglia such as Paragangliomas (PGLs), or from CCs of the AM, pheochromocytomas (PCCs) (Kastriti et al., 2020; Turchini et al., 2018). PCCs and truncal PGLs derive from the sympathoadrenal lineage secrete catecholamines, leading to tachycardia, hypertension and a high risk for stroke (Maguire et al., 2015). Both tumours can occur sporadically or within familial syndromes such as familial PCC/PGL syndrome and the Von Hippel Lindau syndrome (Vega-Lopez et al., 2018). The genetic basis of sporadically occurring PCCs includes gene alteractions of the *RET*, *NF1*, *VHL*, *SDHA-D*, and *RAS* family members and is similar to hereditary syndromes of NC tumours, like neurofibromatosis type I and multiple endocrine neoplasia (Maguire et al., 2015).

Van Hippel-Lindau (VHL) Syndrome is a rare familial multi-tumour syndrome characterised by the frequent development of tumours of the vascular system (hemangioblastomas) of the CNS, renal clear cell carcinomas, and neuroendocrine tumours (Därr et al., 2020). The disease is caused by germline mutations in the tumour suppressor, VHL, on chromosome 3p25(222) and can occur with (type 2) or without (type 1) PCC (Maguire et al., 2015; Vega-Lopez et al., 2018). Up to 30% of patients with VHL disease are found to have PCC or PGL, depending on the underlying mutations (Därr et al., 2020).

To investigate human congenital disorders of certain organs, it is vital to understand its normal function and development. Despite their importance in regulating key physiological processes in the body, the normal development of the mammalian adrenal glands (AGs), particularly the CCs of the AM are not well understood.

No research on the embryology of the *Xenopus* AG has been undertaken to support research on basic function and human disease development, and there is no information on the formation and location of the NC-derived CCs.

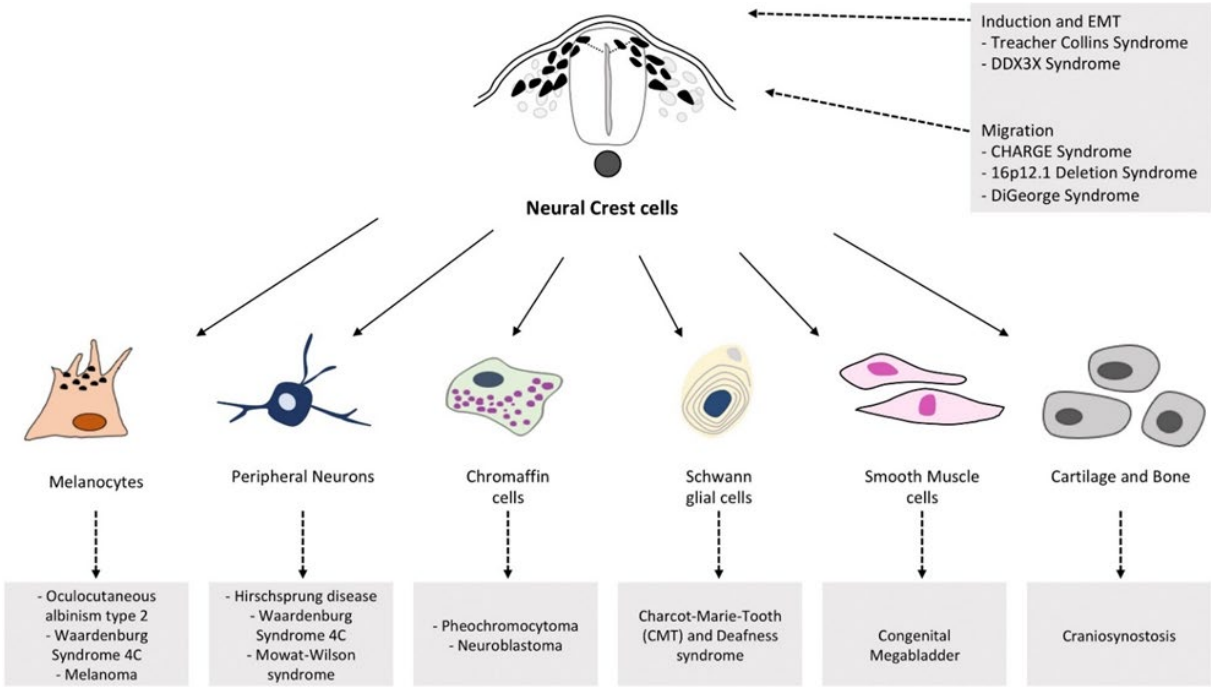

Figure 5: Schematic of various Neurocristopathies and the NC-lineages they derive from. *NCCs undergo EMT, delaminate from the neuroepithelium and migrate extensively throughout the embryonic body to differentiate into a multitude of different cell types. Defects in molecules and signals involved in NC induction, EMT, migration or differentiation can lead to a plethora of developmental diseases and syndromes called Neurocristopathies of which some are listed here. Figure taken from and created by (Medina-Cuadra and Monsoro-Burq, 2021).*

1.8 The adrenal gland – A small organ with big responsibility

Although small in size, the adrenal gland (AG) governs major physiological processes such as fluid homeostasis, secondary sexual development and, as part of the hypothalamic-pituitary-adrenal (HPA) axis, adaptation to stress. The mammalian AGs sit on top of the kidneys and, histologically, is composed of two embryonically distinct endocrine tissues: The outer steroidogenic adrenocortical tissue, which encapsulates the inner adrenal medulla (AM), containing neuroendocrine chromaffin cells (CCs) (Berger et al., 2019; Lalli and Figueiredo, 2015) (Fig. 6). The adrenal cortex (AC) produces a complex array of steroid hormones, through the process of steroidogenesis, and is a crucial component of the HPA axis. CCs of the AM are part of the sympathetic nervous system, producing catecholamines. The AM is innervated by preganglionic sympathetic neurons, which release acetylcholine and neuropeptides to stimulate CCs (Litwack, 2024). In turn, CCs produce and secrete catecholamines, nor-adrenaline and adrenaline into the bloodstream during acute stress as part of the "fight-or-flight"response (Kempná and Flück, 2008). Additionally, chromaffin vesicles contain numerous transmitters, neuropeptides, and proteins, which are released together with the catecholamines (Ehrhart-Bornstein and Bornstein, 2008).

1.9 The adrenal cortex

The adrenal cortex (AC), which comprises 80–90% of the AG, originates from mesodermal tissue and is organized into three histologically distinct layers in humans: the outer zona glomerulosa, the middle zona fasciculata, and the inner zona reticularis (Litwack, 2024) (Fig. 6). The outer zona glomerulosa produces mineralocorticoids, mainly aldosterone, which aid in the regulation of blood pressure and electrolyte balance by stimulating the reabsorption of sodium, and thus water (Bechmann et al., 2021; Litwack, 2024). Glucocorticoids, primarily cortisol, are synthesized in the zona fasciculata and are involved in the regulation of metabolism and immune system suppression. Additionally, glucocorticoids also mediate the peripheral stress response and influence catecholamine release (Lockett et al., 2024; Whirledge and Cidlowski, 2010). This interaction between cortex and medulla is crucial for the

body's ability to manage and respond to stress by increasing glucose availability, modulating immune responses, and enhancing the cardiovascular effects of catecholamines (Miller and Auchus, 2011; Whirledge and Cidlowski, 2010).

Finally, the innermost cortex layer, in close contact to the AM, the zona reticularis, develops several years after birth in humans and produces androgens. Androgens are then further converted to fully functional sex hormones in the gonads (Bechmann et al., 2021; Litwack, 2024).

Adrenal steroidogenesis is regulated by two endocrine feedback circuits: the hypothalamic-pituitary-adrenal (HPA) axis and the renin-angiotensin-aldosterone system (RAAS). The HPA axis comprises of the neurons of the hypothalamic paraventricular nucleus, corticotrope cells of the anterior pituitary, and the AC cells. Together, the HPA axis controls cortisol secretion and the stress response through a tightly controlled negative feedback mechanism, which ensures balanced hormone levels and prevents overactivation of the stress response (Lockett et al., 2024). Briefly, upon encountering stress, including physiological, psychological or environmental acute stress, the hypothalamus releases corticotropin-releasing hormone, which stimulates the anterior pituitary to secrete adrenocorticotropic hormone (ACTH) (Lockett et al., 2024; William Tank and Lee Wong, 2011). ACTH then prompts the AC to produce glucocorticoids, primarily cortisol, through a series of enzymatic modifications of cholesterol and downstream steroidogenic precursors, which lead to an increase in blood sugar levels, suppression of the immune system, and can also influence memory and mood (Lockett et al., 2024).

The RAAS is responsible for blood pressure and fluid homeostasis, and is initiated when the kidneys release renin in response to low blood pressure and low sodium levels or sympathetic nervous system activation. Renin biosynthesizes angiotensin II, a crucial vasoconstrictor, in turn stimulates the AC to release the hormone aldosterone to increase sodium and water reabsorption, stabilizing and raising blood pressure (Patel et al., 2017).

Steroidogenic cells of the AC originate from the intermediate mesoderm, appearing as a thickening of a specialized region of coelomic epithelium, known as the urogenital ridge,

forming the adrenogonadal primordium (AGP). The urogenital ridge also gives rise to the kidneys and haematopoietic progenitors (Pihlajoki et al., 2015). The AGP is in close proximity to the developing kidneys and gives rise to both the AG and the gonads (ovaries and testes), hence the name. The AC first arises at approximately four weeks post-conception in humans and at embryonic day (E) 9.5 in mice (Pignatti and Flück, 2021). The arisal of the AGP is marked by the expression of steroidogenic factor 1 (*Sf1*, also called *Nr5a1*, and will be further referred to as such), a pivotal factor for adrenal development and steroidogenesis (Pihlajoki et al., 2015). When the nuclear receptor NR5A1 is absent, the AG does not form (Xing et al., 2015). Alongside *Nr5a1*, cells of the AGP also co-express the TFs Wilms tumour suppressor-1 (Wt1), and GATA-binding protein (Gata4) (Pihlajoki et al., 2015).

As development progresses, coelomic epithelial cells in the AGP delaminate and migrate in a dorsomedial direction into the underlying mesenchyme. They upregulate expression of *Nr5a1,* while downregulating *Wt1* and *Gata4* expression, forming the adrenal primordium (Pihlajoki et al., 2015; Xing et al., 2015). Contrary to the adrenal progenitors, the gonadal progenitors in the AGP maintain expression of all three transcription factors, migrating dorsolaterally and combining with primordial germ cells (PGCs) to form the bipotential gonad (Pihlajoki et al., 2015).

At around 6 weeks of gestation in human (E12.5 in mice), the adrenal primordium is innervated by CC precursors and the AM is formed (Pignatti and Flück, 2021). Hereby, the adrenal precursors combine with NC-derived sympathoblasts, which are precursors of some of the CCs in the medulla to form the adrenal anlagen (Pihlajoki et al., 2015). However, recent discoveries have demonstrated that the majority of chromaffin cells are in fact derived of Schwann cell precursors (SCPs), challenging the previous models of adrenal medulla formation (Furlan et al., 2017). This leaves us with some open questions on how the CCs combine and integrate with the cortex derived cells and the cues facilitating their integration.

Due to species-specific differences in adrenal structure and function, many aspects of the proper adrenal development and diseases, affecting formation and functionality in humans, remain elusive. Most studies on understanding embryonic adrenal development have been done in mouse models, which deviates slightly from the structure to the human AGs (Yates et

al., 2013). In mice, the cortex of young male mice or female mice before their first pregnancy have an additional zone, the X-zone, which disappears later in life. In contrast, the human AC possesses an additional zone, the zona reticularis (Kastriti et al., 2020; Yates et al., 2013).

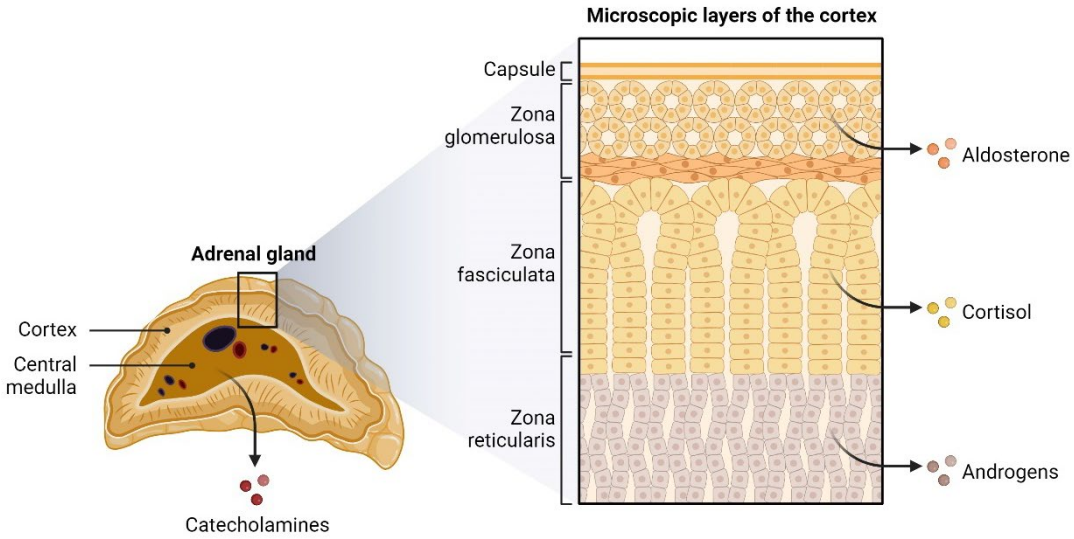

Figure 6: Adrenal gland structure and hormones produced.
Histologically, in mammals, the AG is divided into an outer cortex , producing steroids, and the inner medulla containing CCs that produce catecholamines. Figure created with BioRender.com by Linda Merrill.

1.10 The adrenal medulla

The adrenal medulla contains the NC-derived chromaffin cells. The term 'chromaffin cell' originates from histologist Alfred Kohn's 1902 observation that these cells exhibit a distinctive dark staining when treated with chromium salts. This staining results from their large cytoplasmic granules, which store catecholamines like adrenaline and noradrenaline, reacting with the chromium salts to produce a yellow-brown colour. (Hockman et al., 2018; Huber et al., 2009). CCs are adrenergic post-ganglionic sympathetic neurons, modified to secrete their vesicle contents (adrenaline, noradrenaline and dopamine) directly into the bloodstream

instead of having to innervate target organs by developing axons and dendrites like typical post-ganglionic sympathetic neurons (Shtukmaster et al., 2013; Zeineldin et al., 2022).

CCs synthesize, store and release catecholamines and can be classified into two functional subpopulations: noradrenergic cells and adrenergic cells. Noradrenergic cells express dopamine beta (β) hydroxylase (Dbh) and tyrosine hydroxylase (Th), but are only capable of synthesizing noradrenaline (Akkuratova et al., 2022). The adrenergic cells, also express *Dbh* and *Th* but, due to the additional expression of the enzyme phenyl ethanolamine N methyltransferase (PNMT), are able to produce adrenaline. Here, PNMT expression is dependant on glucocorticoid signalling from the AC (Akkuratova et al., 2022; Unsicker et al., 2013).

Adrenaline and noradrenaline are released from CCs in response to fear, exercise, or high stress situations, acting on adrenergic receptors throughout the body, resulting in increased heart rate and blood pressure (Bechmann *et al.*, 2021). Besides their role in the stress response, CCs of the AM also act as a sensory organ, monitoring the levels of plasma glucose, carbon dioxide and oxygen levels in the body (Bechmann *et al.*, 2021). As part of the hypoxia-sensing pathway, they release catecholamines to influence the breathing pattern in response to hypoxia and to adjust blood glucose levels in response to hypoglyceaemia (Cryer and Polonsky, 2008; Kastriti et al., 2019; Murtazina and Adameyko, 2023). Other than in the AM, CCs can also be found in the organ of Zuckerkandl, a cluster of CCs along the abdominal aorta, near the origin of the mesenteric artery, which regulates blood pressure during the foetal period and birth and is primarily a feature of mammals (Kastriti et al., 2019).

In rodents, CCs of the AM mainly produce adrenaline (over 95%) and produce only a small percentage of total circulating noradrenaline, which is mostly derived from overflow of the neurotransmitter dopamine from sympathetic nerve endings (Berends et al., 2019; Verhofstad et al., 1985).

Catecholamine synthesis in CCs begins with the amino acid tyrosine, which is converted into Dihydroxyphenylalanine (L-DOPA) by TH, the rate-limiting enzyme in this pathway. L-DOPA is then decarboxylated to dopamine by aromatic L-amino acid decarboxylase (Fig.7). Dopamine

is transported into chromaffin granules, where it is hydroxylated to noradrenaline by DBH. In adrenaline producing cells, noradrenaline is further methylated to adrenaline by PNMT, an enzyme induced by cortisol from the adrenal cortex (Purves, 2019; Verhofstad et al., 1985).

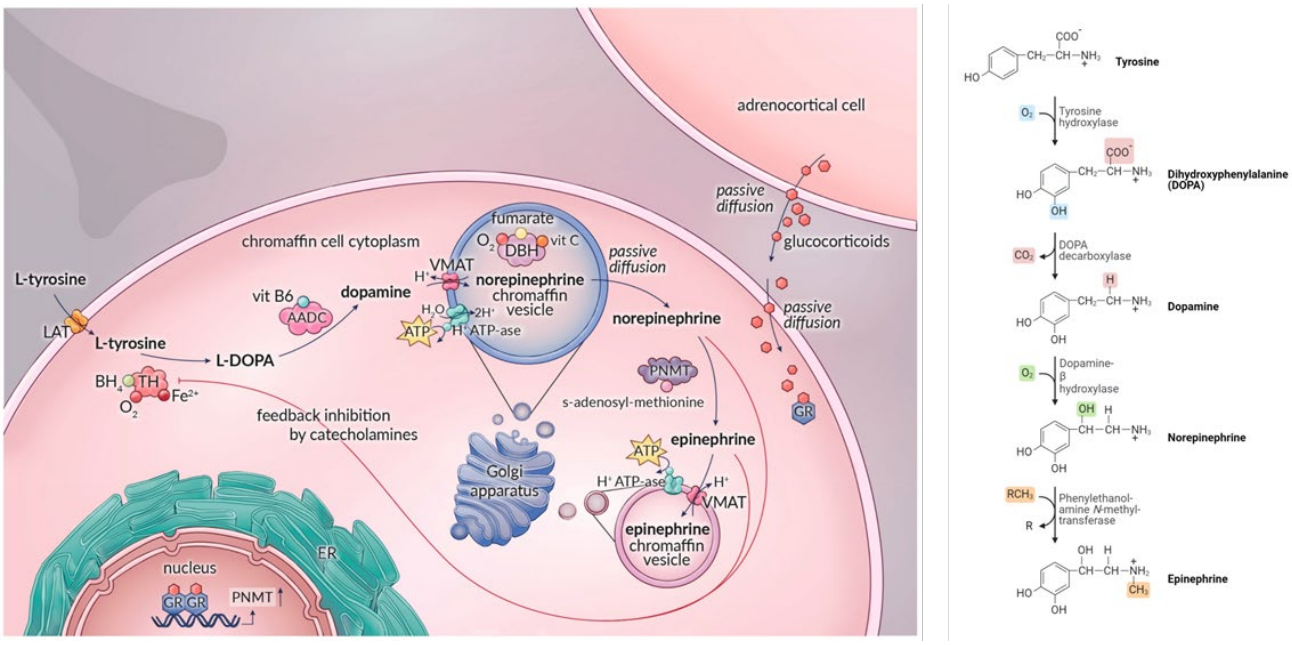

Figure 7: The catecholamine biosynthesis pathway in a chromaffin cell of the adrenal medulla.
Catecholamine synthesis starts with the uptake of the amino acid L-tyrosine into the cytoplasm of the CCs. Th fascilitates the hydroxylation of L-tryosine, producing L-dihydroxyphenylalaline (L-DOPA). L-DOPA is converted to dopamine by dopa decarboxylase. Dopamine is then hydroxylated by DBH to form noradrenaline (norepinephrine), which can be further methylated by phenylethanolamine N-methyltransferase (PNMT) to create adrenaline (epinephrine). Figure on the left was created by and taken from (Berends et al., 2019). The figure on the right was taken from and created with Biorender.com by (Purves, 2019).

1.11 Tracing the origin of chromaffin cells

Despite the CCs' central role in maintaining organ and bodily homeostasis as well as controlling the body's fight-or flight response to stressful stimuli, their origin and development are not well understood (Furlan et al., 2017). A challenge in research on differentiation and migration of NCCs into the AM is a lack of specific markers to trace developmental pathways and temporal changes of the NCCs as they transform into CCs. (Furlan et al., 2017; Unsicker et al., 2013). CCs were long thought to be directly derived from migrating TNCCs. However,

research in recent years by Furlan and Colleagues revealed that the vast majority of CCs of the AM, both in mice and zebrafish, are derived from nerve-associated glial progenitor cells, named Schwann cell precursors (SCPs) (Furlan et al., 2017).

SCPs cover embryonic peripheral nerves and use them as navigation routes to spread throughout the developing embryo (Akkuratova et al., 2022; Furlan and Adameyko, 2018). Once they have reached their destination, they detach from the nerve and differentiate towards several cell types including melanocytes, parasympathetic and sympathetic neurons, enteric neurons and specific mesenchymal cells. This multipotency of SCPs has been retained from their maternal population, the migratory NC (Kastriti and Adameyko, 2017; Kastriti et al., 2022).

Trunk NCCs in mice show two migration waves (Fig. 8). During ventral migration, cells migrate towards the DA in a chemoattrachtent manner (Tsubota and Kadomatsu, 2018). These cells will then differentiate into the sympathoadrenal (SA) lineage and form the sympathetic chain, paraganglia (including the suprarenal ganglion) and, possibly, a few CCs that inhabit the adrenal anlagen (Bechmann et al., 2021; Furlan et al., 2017). This SA fate-progression is driven by a network of specific TF genes, which include bHLH factor Mash 1 (Ascl1), the homeodomain factors Phox2a and Phox2b, and the downstream bHLH factors Hand2 and Gata2/3 and Insm1 (Bechmann et al., 2021; Kastriti et al., 2020). Their upregulation is driven by paracrine bone morphogenetic proteins (BMPs) secreted from the walls of the DA (Kastriti et al., 2020; Saito et al., 2012; Shtukmaster et al., 2013). Exposure to BMP 2/4/7 initiates the upregulation of this set of interacting TFs (Parlier *et al.*, 2008; Shtukmaster *et al.*, 2013; Kastriti, Kameneva and Adameyko, 2020).

Although directly migrating NCCs potentially contribute a small portion of CCs to developing AGs, the majority of CCs (over 70%) arise from SCPs (Furlan et al., 2017; Kastriti et al., 2019). SCPs originate from late NCCs moving towards the dorsal root ganglion (DRG), attaching to preganglionic sympathetic axons that innervate the developing AGs (Fig. 8)(Furlan et al., 2017; Kastriti et al., 2022). Such axons of the preganglionic neurons of the spinal cord extend towards developing internal organs and are guided by class 3 SEMPAPHORINS (SEMA3s) and their receptors NEUROPILIN-1 (NRP1) and NEUROPILIN-2 (NRP2) as soon as they are in close

contact to the SA primordium (Lumb et al., 2018). Once in the vicinity of the SA primordium, the SCPs detach from the preganglionic axons and differentiate into CCs and intermedullary sympathetic neurons, through a transitory 'bridge' transcriptional stage representing a progenitor cell type with its own unique transcriptional program (Furlan et al., 2017; Kastriti et al., 2022). These 'bridge' cells are immediate progenitors of CCs and are marked by the expression of *Htr3a* (5-hydroxytriptamine receptor 3A)(Fig. 9) (Furlan et al., 2017; Kameneva et al., 2022). Expression of myelin protein 0 (P0/MPZ) and brain fatty acid binding protein (FABP7), causes NCCs to give rise to the nerve-associated SCPs, which require FOXD3 and SOX10 for their further differentiation and development (Bechmann et al., 2021). The transcriptional network that underlies the multistep process of mammalian adrenomedullary cell development remains under investigation.

After a short period of differentiation, all CCs express TH and DBH, necessary for both adrenaline and noradrenaline synthesis (Kastriti et al., 2020). However, only some of these CCs can produce adrenaline, which are distinguished by the expression of PNMT (Fig. 9) (Bechmann et al., 2021).

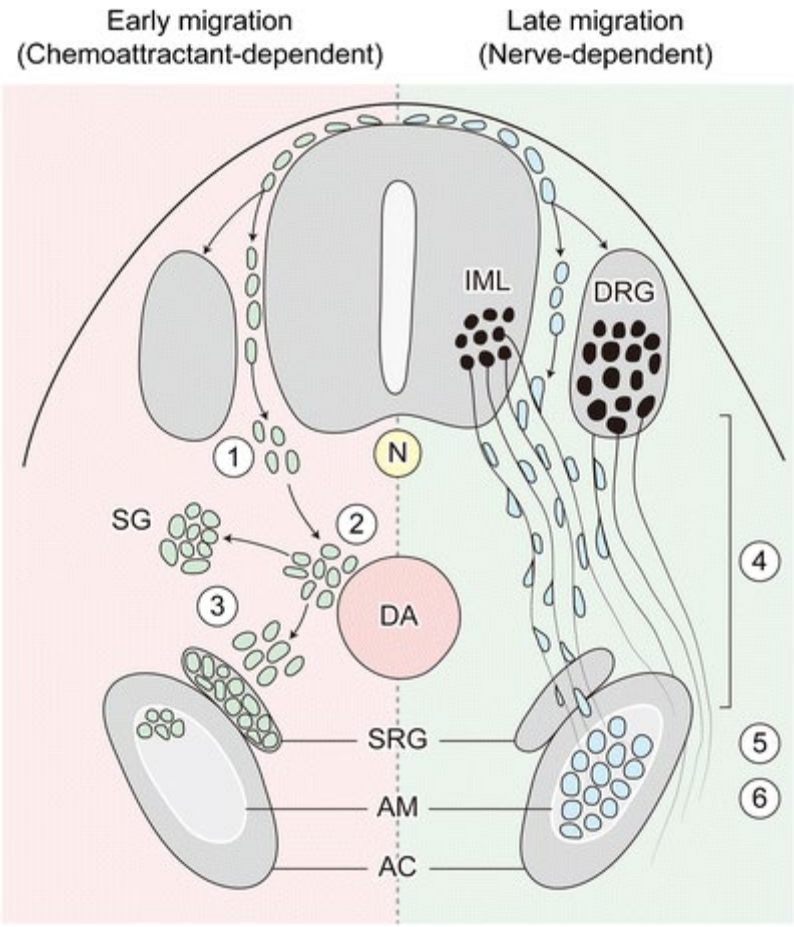

Figure 8: Schematic depicting the developmental pathways of sympathoadrenal lineage and adrenal chromaffin cells in the mouse model.

The left panel depicts how the SA lineage is derived of early migrating NCCs. 1. Early migrating NCCs move ventrolateral towards the DA in response to chemoattractants. 2. These Sox10^{+} cells then commit to the SA lineage upon reaching the DA, expressing the lineage-specifying transcription factor gene Phox2b following BMP signalling from the DA. This is a transient state where cells express both Phox2b and Sox10, typically observed in mice around E10.5. 3. These SA progenitors then lose Sox10 expression, segregate, and migrate to form either the sympathetic ganglia or the AM and suprarenal sympathetic ganglia. BMPs from the dorsal aorta are crucial for the migration of this lineage, with a small population contributing to CCs in the AM. The right panel shows that most adrenal CCs derive from late-migrating NCCs, known as Schwann cell precursors (SCPs), which migrate along preganglionic nerves from the intermediolateral cell column innervating the adrenal gland. 4. SCPs migrate ventrolateral along the axons of preganglionic neurons toward the AM. 5. SCPs commit to becoming adrenal CCs through a transitional state, expressing genes specific to this stage, including Ascl1 and Htr3a. (6) These cells then start to express lineage-specific genes, such as Phox2b and Th, facilitating their differentiation into adrenal CCs. The figure was created by and taken from (Tsubota and Kadomatsu, 2018). Figure is based on research by (Furlan et al., 2017). AC, adrenal cortex;, AM, adrenal medulla; DA, dorsal aorta; DRG, dorsal root ganglion; IML, intermediolateral cell column; N, neural tube; SG, sympathetic ganglion; SRG, suprarenal sympathetic ganglion.

The differentiation of CCs from SCPs involves a gradual downregulation of SCP genes *Sox10* and *Foxd3*, and an upregulation of adrenergic specification genes including *Phox2b*, *Ascl1* and *Th* (Furlan et al., 2017; Zeineldin et al., 2022).

The homeodomain TF Phox2b has been identified as a SA master regulator in human and mouse, essential for the initial development of both sympathetic neurons and CCs, and initiates the expression of a large set of other downstream TFs (El Faitwri and Huber, 2018; Huber, 2015). SA progenitors lacking PHOX2B can still migrate to the adrenal anlage but fail to form a centrally localized medulla (El Faitwri and Huber, 2018; Huber, 2015). Additionally, developing CCs in these progenitors do not express the enzymes necessary for catecholamine production, such as DBH and TH (Huber et al., 2005; Pattyn et al., 1999). Meanwhile, *Ascl1* (Mash1) and the *insulinoma-associated 1* (*Insm1*) gene has been shown to control sympathetic neuroblast and CCs differentiation and proliferation in mice (Huber et al., 2002; Wildner et al., 2008). *Ascl1* further activates *Phox2a*, which in turn activates genes required for catecholamine biosynthesis (Zeineldin et al., 2022). Absence of *Ascl1* in mice, strongly impairs CCs differentiation and leads to a lack of typical chromaffin vesicles and catecholamine phenotype (Huber et al., 2002). Insm1-deficient mice show a delay in CCs development and proliferation, that later proves to be lethal in foetal mice (Huber, 2015). Furthermore, CCs deficient in INSM show a reduced expression of TH, DBH and PNMT, as well as a lack of chromogranin A and B, which are components of secretory granules within the CCs. (Wildner et al., 2008). During *X.laevis* embryogenesis, *insm1* expression has been shown to be regulated by TFs *phox2* and *hand2*, and is likely recruited by *ascl1* to support endocrine differentiation of CCs (Huber, 2015; Parlier et al., 2008).

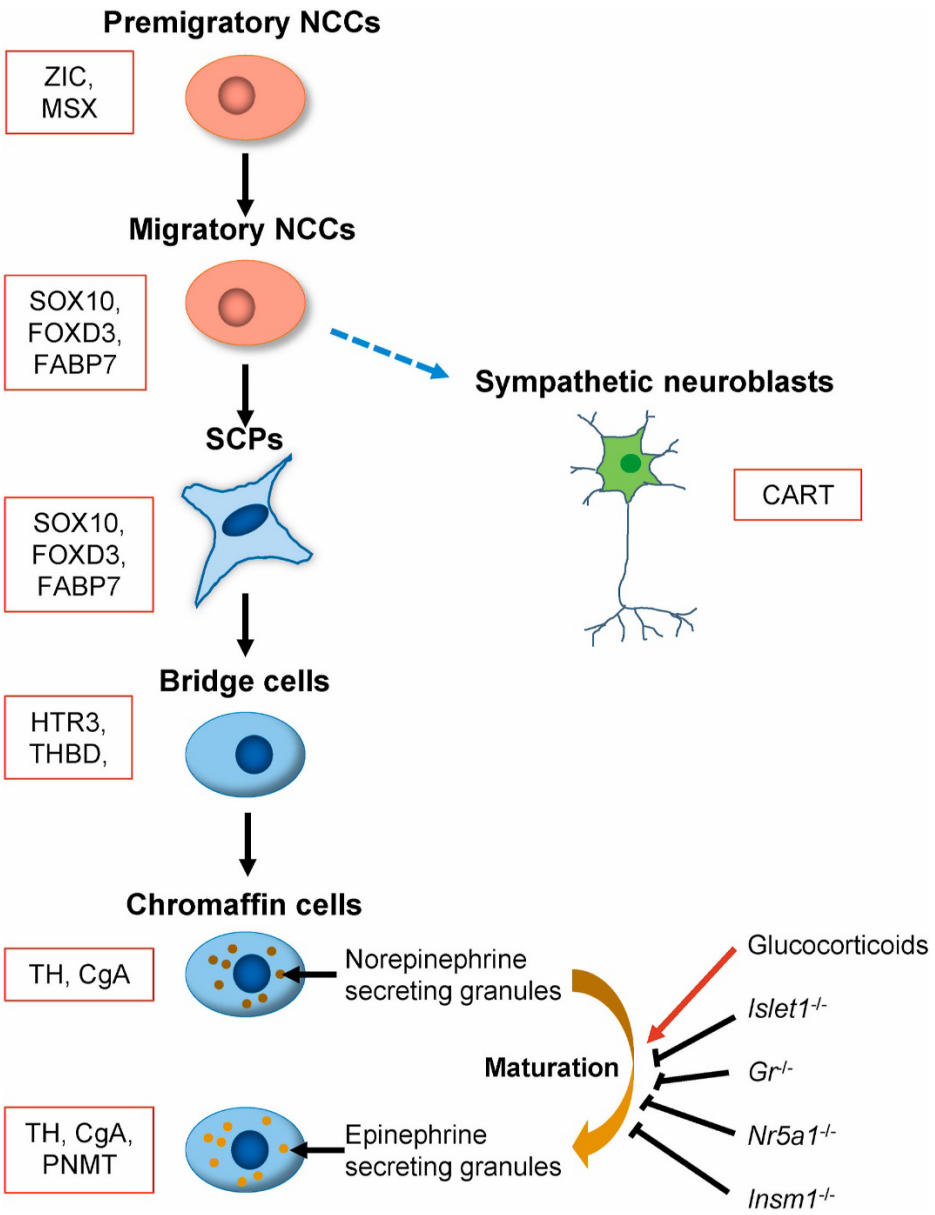

Figure 9: Schematic description of genes governing the development of chromaffin cell in mammals (mouse model) and proteins that are transiently expressed during this process. *Pre-migratory NCCs express NPB genes such as Zic and Msx, which are progressively downregulated as differentiation proceeds. Following delamination, early NCCs move towards the dorsal aorta (DA), late NCCs associate with nerve trunks at the dorsal root ganglion and gain Schwann cell precursor (SCP) properties. Both SOX10 and FOXD3 are essential for Schwann cell development and differentiation. Absence of Foxd3 causes NCCs to differentiate to neuronal or melanocyte lines. Once in the vicinity of the adrenal primordium, SCPs undergo a transcriptional 'bridge' transitory state, to differentiate to CCs, with bridge cells expressing Htr3a and Thbd. Differentiated CCs can be distinguished between noradrenaline (Th, Cga) and adrenaline- producing cells (Th, Cga, Pnmt), characterized by the expression of PNMT. Mice deficient in glucocorticoid receptor (GR), Nr5a1, or Islet-1, notably don't express Pnmt, as its expression is dependent on glucocorticoids of the AC. Figure created by and taken from (Bechmann et al., 2021).*

1.12 Vertebrate adrenal gland differences and similarities

Comparative studies of adrenal gland (AG) development across vertebrate species provide insights into the evolutionary adaptations of these organs. An important evolutionary trend in vertebrates is the gradual progression from chromaffin cells (CCs) being dispersed in various tissues and intermixed with other cell types to the formation of distinct endocrine glands (Perry and Capaldo, 2011). The structure and organisation of AGs vary significantly in vertebrates (Fig. 10) and the developmental trend from interspersed cells to distinct gland is well described when looking at AG organisation in bony fish, amphibians, reptiles, and mammals. All vertebrates possess chromaffin tissue producing catecholamines, and steroidogenic tissue, producing steroids. In most species, steroidogenic and chromaffin tissues are in close association, however, they can be dispersed from one another in fishes (Youson, 2007). Typically, the AG is divided into two main regions: the cortex and the medulla, as has been described above and is the case for mammals (Bechmann et al., 2021).

While the avian AGs possess a distinct cortical and medullary region, these are not as clearly separated as in mammals. Additionally, birds have two types of corticosteroid-producing cells: Interrenal cells and CCs. Interrenal cells are scattered within the gland, mixed with blood vessels. CC groups are without clear zonation as seen in mammals (Perry and Capaldo, 2011). This is similar to reptilian AGs, which are positioned along the kidneys, with interrenal and CCs intermixed instead of being strictly compartmentalized (Fig. 10) (Capaldo, 2023; Perry and Capaldo, 2011).

In teleosts and amphibians, the AGs are less complex and often referred to as interrenal tissues, reflecting their simpler endocrine functions and a less well-defined AG structure (Perry and Capaldo, 2011). Fish lack a distinct cortex and medulla and instead possess intermingled steroidogenic and CCs within the head kidney (Fig. 10) (Capaldo, 2023).

The organisation of steroidogenic and chromaffin tissue among amphibians differs between urodeles and anurans. In urodeles, the steroidogenic tissue forms numerous islets that sporadically contain CCs (Capaldo, 2023). These islets are scattered along the ventral surface of the mesonephric kidney, near its medial margin, and are separated from one another

(Capaldo, 2023). The degree of association between chromaffin and steroidogenic cells varies. For instance, in the families *Salamandridae* and *Plethodontidae*, the two cell types are intermixed (Capaldo, 2023). In anurans, the steroidogenic tissue on the ventral surface of the kidneys forms continuous strands with clusters of CCs (Accordi, 1991; Capaldo, 2023). In both urodeles and anurans, the compactness of the gland and the aggregation of steroidogenic and chromaffin cells vary, generally increasing as one moves from basal to more advanced families (Accordi, 1991; Capaldo, 2023). In *Xenopus*, the structure of the AG is most closely related to that described in urodeles rather than to other anuran species (Milano and Accordi, 1983).

Recently, it was discovered that even the jawless vertebrates sea lamprey seem to possess sympathetic neurons (associated with the fight-or-flight response) (Edens et al., 2024). This finding concludes that the sympathetic nervous system is a pan-vertebrate feature essential for survival (Edens et al., 2024). The developmental transition from NC-derived progenitor cells to differentiated neurons, including CCs, is complex and not yet fully understood. In mice and birds, this process is rapid, with initial noradrenergic and neuronal differentiation occurring within one day of embryonic development (Ernsberger and Rohrer, 2024). However, in sea lampreys, the process is surprisingly slow and resembles the delayed and asynchronous differentiation of the trunk sympathetic ganglia seen in zebrafish (Edens et al., 2024; Ernsberger and Rohrer, 2024).

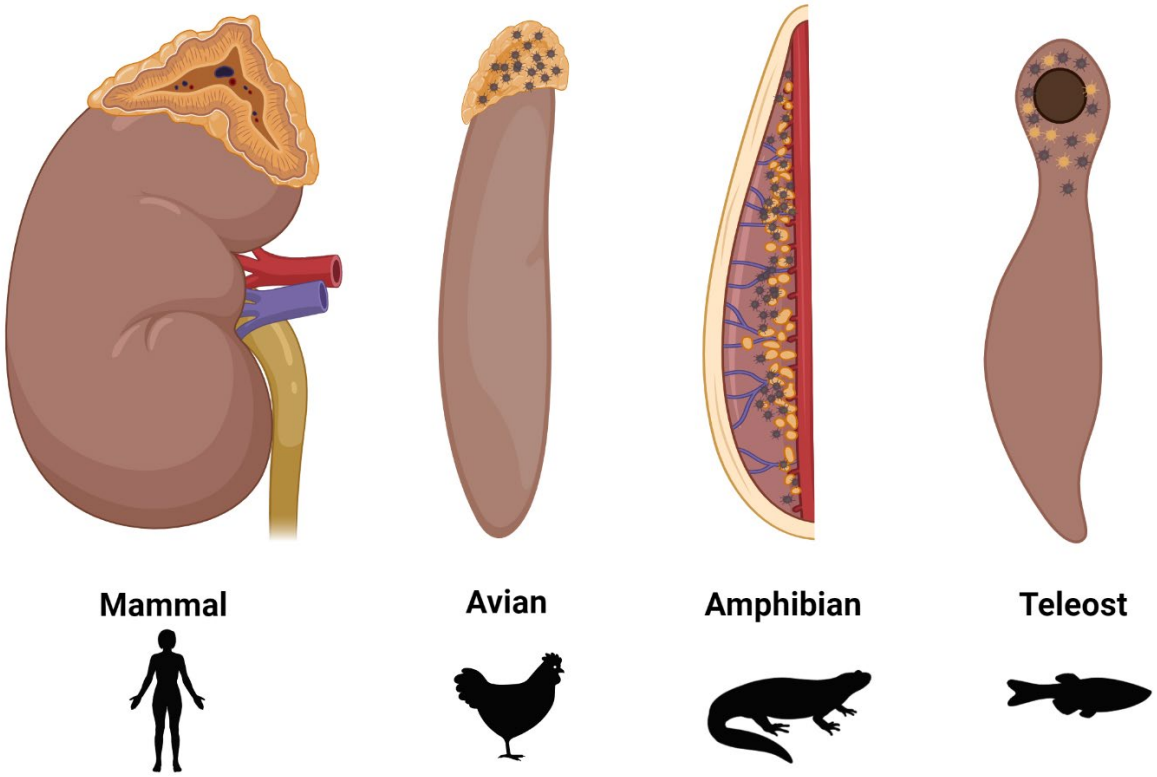

Figure 10: Comparison of different structures of vertebrate adrenal glands.
Not all adrenal tissue is the same among different vertebrate species and the arrangement of chromaffin cells and steroidogenic cells varies, although performing the same function. The avian AG sits on top of the kidney but has no definite cortex and medulla but both tissues intermingled. The AG in mammals sits on top of the kidney, with a distinct outer cortex (yellow) surrounding the inner medulla containing CCs. The AGs of amphibians lie on the ventral surface of the mesonephric kidney and have intermingled CCs (yellow) and steroidogenic cells (black) along the entire organ. However, the arrangement of CCs differs between anurans and urodeles. Anurans typically show continuous strands of steroidogenic cells containing clusters of chromaffin cells. In urodeles, the structure is not always the same but mostly presents as steroidogenic tissue as small clusters embedded in the ventral surface of the kidney, with intermingled CCs. In teleosts, both the steroidogenic and CCs are intrarenal and are intermingled within the head kidney. This figure was created with Biorender.com, based on (Di Lorenzo et al., 2020) and (Perry and Capaldo, 2011).

1.13 The NEUcrest ITN project

This project is part of the broader "NEUcrest" initiative, an EU-funded research network under the MSCA EU Horizon 2020 program (https://neucrest.curie.fr/index.php). Launched in 2019, NEUcrest unites eleven academic and industrial partners to explore various aspects of NC biology, combining the expertise and knowledge of all partners across Europe. Together with 14 other PhD students, the NEUcrest project aims at further elucidating the genetic, molecular, and epigenetic regulation of NC tissues across different model organisms, also including human induced pluripotent stem cells (hiPSCs). The overarching aim is to further unravel the mechanisms underlying Neurocristopathies (NCPs), which are as numerous as the NC derivatives themselves, and can seriously affect the quality of life for affected individuals living with such conditions. Among our cohort, research on NCPs include the study of melanoma, waardenburg syndrome, craniosynostosis and neuroblastoma. This interconnected approach will hopefully further the understanding of NC biology and drive forward both basic science and translational applications within the field.

Within this collaborative framework, my project focuses on elucidating the development of NC-derived CCs in *Xenopus laevis*, where not much is known about the embryology of the AG. To assess underlying mechanisms involved in the onset of disorders caused by the AG, it is vital to fully characterize the organs development. Once this is established, this animal model could potentially be used to identify novel disease variants and perform chemical drug-screenings to discover potential new drug treatments for human adrenal diseases.

1.14 Aims of the thesis

The adrenal gland (AG) of the well-established research model *Xenopus laevis* is a poorly studied organ, with no research on how the gland develops during embryogenesis.

Therefore, this project aims to elucidate the development of the AG, particularly the development of the NC-derived chromaffin cells of the AM in *Xenopus*, and to determine if the organ develops separate, intact or within the pronephric kidney. The goal is hereby to determine if the development of the AG of the *Xenopus* is similar to that of other animal model species such as mouse or zebrafish, and if *Xenopus* could be a good animal model to study human diseases related to this organ, such as neuroblastoma and pheochromocytoma.

To gain a basic understanding of AG development in *Xenopus*, and to provide a detailed map of AG developmental dynamics, the overarching aim of this project is to characterise genes and proteins that identify an intact AGs. To do so, this thesis was subdivided into three specific aims:

1. Identify candidate marker genes for CC development of the AM, and create a spatio-temporal map of the chosen candidate genes using Whole-mount In situ Hybridisation (WISH) and Hybridisation Chain Reaction (HCR) across *Xenopus* embryonic stages of development

2. Identify candidate marker genes for steroidogenic tissue development of the adrenal cortex (AC), and create a spatio-temporal map of the chosen candidate genes using WISH and HCR during *Xenopus* embryogenesis. Thereby, establishing the location and interaction during development between the two different tissue types making up the AG.

3. Assess the neural crests contribution to the development of the CCs of the AM in *Xenopus laevis*. This will be done by performing morpholino knockdown of NC markers Foxd3 and Sox10 and investigating the NC knockdown effect on the expression of our previously identified CC candidate gene markers.

2 Chapter II: Materials and Methods

2.1 *Xenopus* husbandry and egg collection

To be able to conduct research on *Xenopus* in the U.K at the University of East Anglia, a Personal Licence had to be obtained from the Home Office. The obtained licence enables the performance of regulated procedures on *Xenopus* in categories A (Minor/minimally invasive procedures not requiring sedation, analgesia, or general anaesthesia) and B (Minor/minimally invasive procedures involving sedation, analgesia, or brief general anaesthesia. Plus, surgical procedures conducted under brief non-recovery general anaesthesia). The practical and theoretical personal licence module training was conducted throughout November and December 2020 and the licence was obtained in February 2021. All procedures carried out were performed under the approval of the local ethics committee and according to the UK home office regulation.

Adult male and female *Xenopus laevis* were obtained from the European Xenopus Resource Centre (EXRC) based at the University of Portsmouth. Prior to embryo harvesting, female *X. laevis* were primed by injecting 100 unit of Pregnant Mare Serum Gonadotrophin (PMSG, Intervet, 1,000U/mL) into one dorsal lymph sac, 5 to 7 days in advance. The day before embryo collection, the primed females were induced with a further two injections into both dorsal lymph sacs containing human Chorionic Gonadotrophin (hCG, Chorulon, Intervet, 1,000 U/mL). To collect the eggs, gentle pressure was applied to the female's abdomen with the thumb and forefinger, encouraging release of the egg clutch into a petri dish. This procedure was performed up to 4 times a day, with a minimum 2-hour break in between.

2.2 Fertilisation of *Xenopus* eggs

Embryos were obtained by in vitro fertilisation. A male *Xenopus* was euthanised (Schedule 1) with 1g of Ethyl 3-aminobenzoate methane sulfonate salt (MS-222, Sigma-Aldrich, A 5040), dissolved in 300ml of water for 1h. Euthanasia is confirmed by severing the spinal cord and destruction and/or removal of the heart. The testes were removed and stored in testes buffer composed of 80% foetal bovine calf serum (FBS) and 20% 1X Marc's Modified Ringers (MMR: 100mM NaCl, 2mM KCl, 1mM $MgCl_2$ 2mM CaCl2, 5mM HEPES pH 7.5) and gentamycin 1U/ml.

A piece of testis was then homogenized in 1mL of 1xMMR and crushed with a pestle to release the sperm before being pipetted over the clutch of eggs and left for 10min at room temperature (RT). Fertilisation was carried out at a low salt-concentration, with eggs being engulfed in 0.1 X MMR (10 mM NaCl, 2mM KCl, 1mM MgCl, 2 mM CaCl2, 5mM HEPES p.H 7.5) and left for 20 -30mins at RT. To remove the gelatinous material surrounding the eggs/embryos, they were placed in a 2% L-cysteine solution (Sigma-Aldrich, C7352) in 1XMMR for 7min at RT under constant, careful movement. Finally, embryos were washed twice with each 1 X MMR and 0.1 X MMR before being plated on Bovine Serum Albumin (Fisher Scientific, BP9703-100) pre-coated dishes and incubated at an appropriate temperature in 0.1 XMMR.

2.3 Fixing and storage of *Xenopus* embryos

2.3.1 For WISH

Fertilised embryos were left to develop at 16-21°C (X. *laevis*) or 26°C (X. tropicalis), with speed of development increasing with higher temperatures. Once embryos had reached the desired stage, they were collected and fixed in MEMFA (3.7% formaldehyde, 1 X MEM salts, DEPC-$H_2$0 at a ratio of 1:1:8, MEM Salts) for 2h at RT, or O/N at 4°C with gentle rocking. MEMFA was removed and embryos washed twice with PBST (1 X PBS, 0.1 % Tween20) , followed by three washes with 100% Ethanol and stored in final wash at -20°C for up to 6 months.

2.3.2 For HCR

Embryos that reached desired stage were collected and fixed with 4 % paraformaldehyde (PFA). Aliquots of 4% PFA were thawed from -20 °C and cooled to 4°C. This prevents increased autofluorescence. Depending on their developmental stage, embryos were fixed from 1h – 4h (~1h/1mm tissue) at 4°C with gentle rocking . To stop fixation, embryos were washed 3 x 5 min with 1X phosphatase-buffered saline (PBS) and dehydrated and permeabilized in a series of methanol washes, with 2x 10 min 100% Methanol and a final wash in 100% Methanol for 40 min before being stored at – 20 ° C O/N or until use.

2.4 Dissection of Xenopus kidneys from stage 52 to stage 66

Xenopus laevis tadpoles and froglets were euthanised (Schedule 1) with 1g of Ethyl 3-aminobenzoate methane sulfonate salt (MS-222, Sigma-Aldrich, A 5040), dissolved in 300ml of water for 1h. To confirm euthanasia, the absence of a heartbeat was checked under the microscope for at least a minute, as well as the absence of a response to external stimuli (pinch test). Tadpoles/Froglets were then pinned down on a piece of Styrofoam and the abdomen was opened with a scalpel. Kidneys were located, once the gut was removed and an incision made upstream and downstream of the kidneys, then carefully removed with a pair of tweezers and placed in a 2 mL Eppendorf tube. Kidneys for HCR and Whole mount Immunofluorescence (IF) were fixed for 1h to 3h in 4 % PFA, again depending on developmental stage and thickness of tissue.

2.5 Cloning for *in situ* probes using pGEM®-T-Easy Vector

2.5.1 Primer design

Primers for amplifying the fragment of a mRNA of interest, were designed using https://www.xenbase.org/entry/ and searching for the gene of interest.

First, to check at which stages the gene is expressed and which chromosomal variant is more highly expressed (L. or S, X. *laevis*) the point "*Expression*" of the gene was compared, and the chromosomal variant decided. Under point "*Summary*" the CDS of gene of interest was copied (*X. tropicalis, X. laevis L.* or *X. laevis S.*) and pasted on the following website to design primers: https://www.ncbi.nlm.nih.gov/tools/primer-blast/ . The CDS was pasted on "*Enter accession, gi, or FASTA sequence*" and the following parameters were used : PCR product size was ideally set between 500 and 1000bp, primer melting temperature from: Min – 59.0°C; Opt – 60.0°C; Max – 61.0°C and depending on the organism either *X. tropicalis* or *X. laevis*.

Primer pairs were selected according to the number of possible non-specific subproducts or favourite length of the product. Primers designed and used for cloning genes of interest is listed in Table 1.

Table 1: List of primers used for cloning genes of interest

Primer Name	Sequence
Pnmt Fw	ATGAGTAACATAGAGAGTGTGGCACAG
Pnmt Rv	TTATTGTGAGTCCTGTTTTTGGGCC
Phox2b Fw	TGGAATATTCTTACCTCAATTCCTCCGC
Phox2b Rv	TCAGAACATGCTCTTGACTAGAGTGG
Dbh Fw	GGACTCGTCCGGTATTCGAC
Dbh Rv	TTGGAGGTTGTGCTGTCCTT
Nr5a1 Fw	ATGCTTTCCAAAGTGGAGCTGG
Nr5a1 Rv	TTCCCCGCTAAGGTGCTTATG
Star Fw	ATGCTGCCTGCCACCTTC
Star Rv	GTTGCTTGAAGAAGTCATTCTGCTTCG
Cyp17a1 Fw	CCGTACTGAAATGGGCCGTA
Cyp17a1 Rv	TGGGAGGGGGTGTAGAGATG
Th Fw	GAGCACCCTAATGAGCTCCG
Th Rv	GCATCGCTACCTCCTCTGG
Ruvbl2 Fw	GGAGGGCAGCAGGAGTTATT
Ruvbl2 Rv	AGGAATTCCATGGGGACTCTG

2.5.2 RNA extraction and cDNA synthesis

To create a pooled cDNA sample with the most important developmental stages (for X.*laevis*), 3-4 tadpoles at stages NF13, NF27, NF30, NF33, NF37, NF42 and NF45 each, were collected in a 1.5mL Eppendorf. Tadpoles were then snap-frozen in liquid nitrogen for ~30sec. (tadpoles above NF37 were anesthetized with MS-222 prior to snap-freezing). Snap frozen embryos

were immediately processed for RNA extraction using the Qiagen 'RNeasy Micro Kit' , according to manufacturer's instructions. RNA extracted was quantified by Nanodrop and RNA was stored at -80 °C until further processing. To make cDNA, separate for each stage, the 'SuperScript™ IV Reverse Transcriptase (10 000 U)' from Invitrogen was used, following manufacturer protocol. All cDNA from different stages were pooled together and stored at -20 °C until required.

2.5.2 Amplification of gene of interest by polymerase chain reaction (PCR)

The PCR reaction for amplifying the gene of interest with the designed primers was as follows:

Table 2: PCR composition for 1 reaction (amplifying gene of interest)

Reagent	**Reaction 1x**
2x TaqBiomix	12.5 µL
cDNA (pooled)	1 µL
Primer Forward	1 µL
Primer Reverse	1 µL
Nuclease-free water	9.5 µL
Total Volume	25 µL

The thermocycler was set up as seen in Table 3.

Table 3: Thermocycler settings for gene amplification

Step	Cycle	Temperature	Time (min:sec)
1	1	95°C	05:00
2	37	95°C	00:30
		*	00:30
		72°C	**
3	1	72°C	07:00
4	1	10°C	∞

Some settings differed between specific primer pairs and are marked here:

* The annealing temperature is set to the specific pair of primers designed and ranged anywhere from 59 °C to 63 °C.

**As the Taq polymerase can process ~1000bp/min, the elongation time was calculated accordingly.

To see if the correct DNA insert was amplified, 10 µL of the PCR reaction was run on a 1.5 % Agarose gel for 40 min at 90V and imaged using a UV trans-illuminator (BIO-RAD) to visualize the band size.

The rest of the PCR reaction was then purified using the 'QIAquick PCR purification kit' (Quiagen) according to the manufacturer protocol. The purified fragment was quantified on the Nanodrop by spectrophotometry.

2.5.3 Cloning into pGEM®-T-Easy Vector

The purified fragment of the gene of interest was cloned into the pGEM-T Easy vector (Fig 1)(Promega). This is a high-efficiency, linearized TA Vector that has a single 3'-terminal

thymidine on both ends. Having T-overhangs at the insertion site prevents recircularization of the vector, thereby helping to improve the efficiency of ligation of PCR products. As the Taq DNA polymerase (Bioline) leaves 'A' overhangs, there was no need to add A residues on the 3' to 5' ends of the PCR products. Ligation reactions were carried out according to the ratio of vector and insert which was calculated as follows:

$$\frac{(ng\ of\ vector)x(kb\ size\ of\ insert)}{(kb\ size\ of\ vector)} x\ molar\ ratio\ \frac{insert}{vector} = ng\ of\ insert$$

Ligation reactions were carried out at either a ratio of 3:1 or 1:1 condition. The vector size of pGEM-T is about 3kb. The typical concentration of vector used was 25ng. The reaction was set up as follows: x amount of calculated PCR product required, 0.5 µL of pGEM-T Easy Vector (25ng), 5 µL of 2X ligase buffer (Promega), 1 µL of Ligase T4 DNA (3U/ µL, Promega) made up to 10 µL with RNAse free H_20. The reaction was incubated for either 2h at RT or O/N at 4°C. Afterwards, the ligation reaction was transformed into competent bacteria as outlined in section 2.5.4.

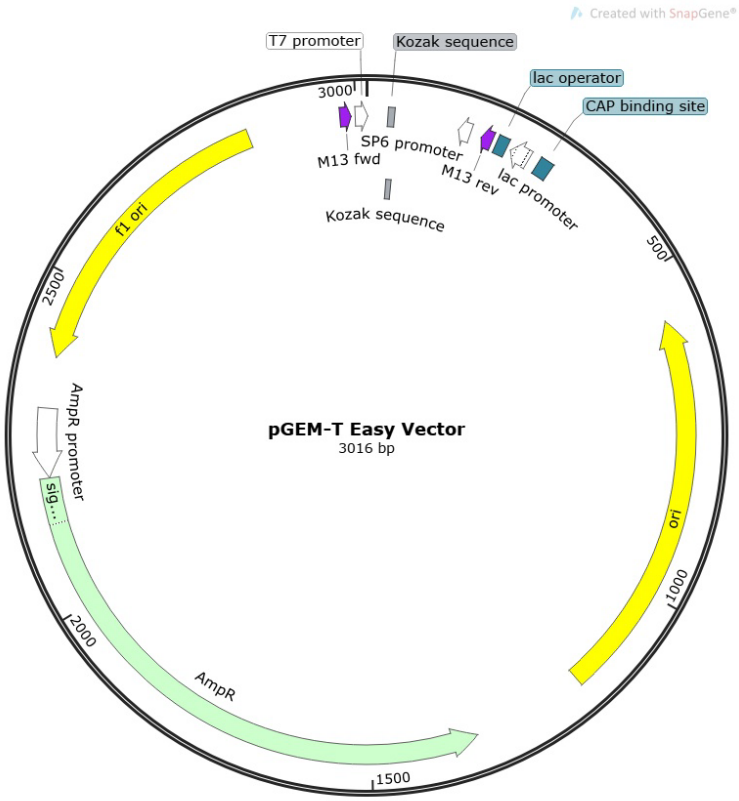

Figure 11: pGEM T Easy Vector backbone and vector information.

2.5.4 Transformation and Colony PCR

LB -Agar plates were prepared with the specific antibody (mostly Ampicillin). In case of pGEM-T Easy cloning, plates were coated with 50 µL X-gal to enable blue/white colony selection. 100 µL of DH5 alpha competent E-coli bacteria were added to 5 µL of plasmid DNA and left on ice for 30 minutes. The reaction was then heat shocked for 90 sec and 42 °C which opens the cells. After the 90 sec, cells were returned to ice for a further incubation of 5 minutes. Next, 900 µL of Lysogeny Broth (LB) media (antibody free) was added. Cells were incubated for 1h at 37°C under continuous shaking (250rpm) on the heat shaker to allow growth. The bacteria were then centrifuged for 5 min, 90% of the supernatant was removed and the last 10% used to resuspend the bacterial pellet with the pipette. 100 µL of the culture was then plated on LB-Agar plates (containing the appropriate antibiotic) and incubated O/N at 37°C.

In the case of pGEM-T Easy Vector Cloning, positive colonies, containing the gene of interest within the vector, were identified by Colony PCR. Therefore, 5 different colonies were picked (white colonies), and colony PCR, using specific primers that were used initially to amplify the gene of interest. After mini prep (see section 2.5.5), the sequence of the gene of interest was confirmed by sequencing with M13 Fw and Rv primers (Sanger Sequencing Service, Source BioScience).

2.5.5 Mini and MIDI extraction of plasmid DNA

Single colonies of bacteria were picked and used to inoculate 5mL of LB/antibiotic liquid media (ampicillin/carbenicillin) for mini preparation. When performing MIDI preparation, a single colony was inoculated with 100mL of LB/antibiotic liquid media. Cultures were grown overnight at 37°C under continuous shaking (200rpm). If colonies grew, media turned cloudy, and plasmid DNA was isolated using Plasmid Mini Kit (resource) and Nucleobond® Xtra Midi Kit (MACHEREY-NAGEL) following the manufacturers protocol.

2.6 Wholemount In *Situ* Hybridisation (WISH) probe synthesis

2.6.1 By Plasmid linearisation

The plasmid containing a gene of interest was linearized by a restriction enzyme digest upstream/downstream of the sense/antisense probe respectively.

The restriction digests were set as follows and left O/N at 37°C :

Table 4: Restriction reaction

Reagent	**Reaction 1x**
Plasmid	2.5 µg
10 X Restriction Buffer (specific to Plasmid)	2.5 µL
Restriction Enzyme (specific to Plasmid)	2.5 µL
Nuclease-free water	To 25 µL
Total Volume	25 µL

Successful digest was tested by running 100ng (1 µL) of linearised product on a 1% agarose gel. Undigested (circular) plasmid was run along as control. The linearised plasmid was purified using 'Qioquick PCR purification kit' (Quiagen) following manufacturer instructions. The concentration of the purified product was determined by spectrophotometry (Nanodrop). The list of plasmids and their appropriate restriction enzymes used to obtain antisense probes can be found in Table 5.

Table 5: List of WISH probes made by linearisation

Plasmid Name	Antisense Linearisation	Transcribing polymerase	Plasmid source	Relevance to AG development
Sox10	EcoRI	Sp6	Wheeler plasmid bank (JP. Saint-Jeannett)	Marker of Neural Crest, used as control and to visualize trunk NC development
Snai2	EcoRI	Sp6	Wheeler plasmid bank (EXRC)	Marker of Neural Crest, used as control
FoxD3	BamHI	T7	Wheeler plasmid bank (Y.Sasai)	Marker of Neural Crest development used as control
Ascl1/Mash1	BamHI or SpeI	T7	Gift from Eric Bellefroid	Chromaffin cell differentiation
Ia1/Insm1	SacII	T7	Wheeler plasmid bank (Eric Bellefroid)	Chromaffin cell differentiation
Phox2a	NotI	T7	Gift from Eric Bellefroid	Drives NC differentiation towards adrenergic specification
Th	NotI	T7	Gift from Eric Bellefroid	Rate limiting enzyme in adrenaline synthesis, expressed by all chromaffin cells
Chga	XhoI	Sp6	Gift from Marko Horb	Neuroendocrine secretory protein present in all chromaffin cells
Pax8	EcoRI	T7	Wheeler plasmid bank (I.Desanlis)	Expressed in the developing pronephric kidney, control marker
Ruvbl2/Reptin	HindIII	Sp6	Wheeler plasmid bank (D.Wiedlich)	Potential marker of AM in *Xenopus* embryos

2.6.2 By PCR reaction

Probe synthesis could also be achieved by PCR reaction. Using the appropriate plasmid, the PCR reaction was set as shown in the following: 12.5µl TaqBiomix 2X, 1µl of appropriate primers (usually M13 Fw and M13 Rv) 10µM, 100ng of plasmid, made up with nuclease-free water to a volume of 25µl.

Table 6: PCR reaction steps

Step	Cycle	Temperature	Time (min:sec)
1	1	95°C	05:00
2	35	95°C	00:30
		59°C	00:30
		72°C	1:30
3	1	72°C	07:00
4	1	10°C	∞

Amplified products were visualized via gel electrophoresis on a 1.5% (w/v) agarose gel (TBE 1X: 45nM Tris Borate, 1mM EDTA, pH 8.0) containing 0.0001% (v/v) of 10mg/ml ethidium bromide and visualized under UV light using a UV trans-illuminator (BIO-RAD). If the PCR product was visible and of a correct size, the product was purified using QIAquick PCR purification kit following the manufacturers instruction. Purified samples were quantified by Nanodrop (performed twice using 1 µl of purification and calculating the average).

Probes were then synthesized with a promotor specific RNA polymerase Riboprobe synthesis was set up as follows: 100ng of PCR template, 4 µl of 5X transcription buffer (Promega), 2 µl dithiothreitol (DTT, Promega), 2 µl (40 U) RNA polymerase (either T7 or Sp6, Promega), 2 µl Digoxigenin (DIG, Promega), 1 µl RNase inhibitor (Promega) made up to a final volume of 20 µl with RNase free H20. The reaction was incubated as follows:

When using T7 polymerase, incubated ON at 37°C.

When using SP6 polymerase, incubated 4h at 40°C.

Any remaining DNA template was removed by adding 1 µl of DNase I (Roche) and incubating again at 37°C for a further 15 min. To check if the reaction was successful, 1 µl of the reaction was run again on a 1.5% agarose gel and visualized. Riboprobes were purified using G50 Purification Columns (Illustra, ProbeQuant G-50 Micro Columns-GE Healthcare) according to the manufacturers protocol.

Purified riboprobes were quantified again on the Nanodrop and diluted in Hybridisation Buffer to a concentration of 1 µg/ml and stored at -20°C until used for in *situ* hybridisation.

2.7 Wholemount In *situ* Hybridisation

All steps were carried out under gentle rocking, unless otherwise specified. Fixed and dehydrated embryos were rehydrated in graded ethanol washes for 5 min each, starting from 100% Ethanol, to 75% Ethanol/DEPC-PBST (1X DEPC-PBS, 0.1 % Tween20), 50% Ethanol/50% DEPC-PBST, and 25% Ethanol/DEPC-PBST, followed by two washes in DEPC-PBST. Next, embryos were treated with Proteinase K (PK) (final concentration 20 µg/ml in DEPC-PBST) for 2 – 20min, according to developmental stages (See Table 7) Embryos were washed twice for 5 min with DEPC-PBST and re-fixed in 3.7 % formaldehyde for 20 min at RT. Fixation solution was again rinsed off with 2x 5 min washes in DEPC-PBST followed by a wash in hybridisation buffer (50% formamide, 5 x SSC, 1 mg/mL Torula RNA, 100 µg/ml heparin, 1 x Denhardt's solution, 0.1 % Tween20, 0.1 % CHAPS, 10mM EDTA) until the embryos sink to the bottom of the vial. Hybridisation buffer was replaced with fresh, pre-warmed hybridisation buffer at 60°C and incubated for at least 1h at 60°C. Finally, probe hybridisation was started when hybridisation buffer is replaced with the riboprobe and incubated O/N at 60 °C.

The next day, probe was removed and saved for re-use, while embryos underwent a series of 2 X SSC washes at 60 °C. Next, embryos were RNase treated (RNase A/T1-Thermo Scientific, EN0551, 2mg/mL of 2X SSC) for 30 min at 37°C. RNase is washed away with a series of 0.2X SSC, followed by one wash in 1X Maleic acid buffer (MAB:100mM Maleic acid, 150mM NaCl,

pH7.5) all at RT before blocking (MAB with 2% BMB) for at least 1h. Blocking solution was then replaced with anti-DIG antibody solution (1:3000, 2%BMB, 20% Goat serum in 1X MAB) and incubated O/N at 4°C.

Day 3 was a pure wash step, where antibody solution is thoroughly removed by washing embryos at least 6 times for 1h each with 1X MAB at RT before being placed in 1X MAB O/N at 4°C.

Embryos were washed twice with Alkaline phosphatase treatment (NTMT: 100mM Tris pH9.5, 50mM $MgCl_2$, 1mM NaCl, 0.1%Tween20, 2mM levamisole) at RT before colour development. Probe detection was achieved by using nitro-blue tetrazolium chloride (NBT:75mg/mL in 70% dimethylformamide) and 5-bromo-4-chloro-3'-indolyphosphate p-toluidine salt (BCIP: 50mg/mL in 100% dimethylformamide) in NTMT at RT.

Colour reaction was stopped with PBST, and embryos were fixed again prior to bleaching to allow more effective observing of in *situ* staining.

Imaging of embryos was carried out on a 2% agarose plate (2 g agarose in 100 mL distilled water, 25 mL per plate). Light microscopy images were captured using Zeiss Axiovert Stemi SV 11, Jenoptik ProgRes C5 camera (Germany), ProgRes software version 2.7.6.

Table 7: Proteinase K time table

Stage (NF)	13-16	17-20	21-25	26-30	31-33	34-36	37-40	41-45
Time (min)	2	3	4	5	6	8	18	20

2.7.1 Bleaching embryos

After finishing the WISH protocol, embryos were placed in bleaching solution (44.75mL DEPC-H2O, 1. 25 mL 20X SSC pH7, 1.5 mL 30% hydrogen peroxide (H202),2.5mL formamide) for 1h at RT on a lightbox, or until all pigmentation was sufficiently removed, and turned every 30 min to achieve even bleach. After bleaching, the embryos were washed three more times in DepC-PBST and then imaged. Alternatively, for embryos undergoing HCR, 30% Peroxide

(H2H2) was added to embryos in 100% methanol (1:3). Embryos were placed on lightbox at RT again until pigmentation was again sufficiently removed (usually around 2-3h).

2.7.2 Imaging

Images of whole mount embryos were acquired using the Zeiss Axiovert Stemi SV II Light Microscope with a Jenoptic ProgRes C5 Camera attached and using ProgRes CapturePro 2.10.0.1 software (Jenoptic Optical Systems GmbH). Embryos were kept on a 2% agarose plate in dH20 during imaging.

2.8 Hybridisation Chain Reaction (HCR)

2.8.1 HCR protocol adapted for Xenopus

Hybridisation probe sets are designed and generated by Molecular Instruments Inc. A list of probes ordered is found in Table 8.

Table 8: List of HCR probes

Organism	Gene Name	Accession Number	Probe Set Size	B number
Xenopus *laevis*	*Phox2a*	NM_001090916	13	B1
Xenopus *laevis*	*Phox2b*	NM_001090914.1	10	B1
Xenopus *laevis*	*Chga*	NM_001094724	20	B3
Xenopus *laevis*	*Dbh*	XM_018232566	20	B2
Xenopus *laevis*	*Th*	XM_041591108.1	20	B2
Xenopus *laevis*	*Pax8*	NM_001088472	19	B4
Xenopus *laevis*	*Nr5a1*	NM_001097969.1	20	B4
Xenopus *laevis*	*Star*	NM_001174031.1	20	B4
Xenopus *laevis*	*Pgat*	NM_001087463	20	B2

HCR was performed with some adaptations from the HCR v.3.0 protocol for whole-mount zebrafish embryo and larvae by the manufacturer. Unless specified, all steps were carried out under rocking. Fixed and dehydrated embryos of desired developmental stage were rehydrated in a series of 5 min washes in Methanol/DEPC-PBST starting with 75% methanol/ 25% DEPC-PBST, then 50% methanol/50% DEPC-PBST and 25% Methanol/75% DEPC-PBST followed by 2 more washes in in 100% DEPC-PBST. Embryos were then permeabilized with Proteinase K (final concentration 20 µg/ml in DEPC-PBST) according to their developmental stage following the WISH protocol timetable by (Monsoro-Burq, 2007) without rocking. (See Table 7). Proteinase K is removed with 2 x 5 min washes with PBST, and embryos were postfixed in 4 % PFA for 20min at RT. PFA is washed off with 5 x 5 min washes of PBST. Embryos were pre-hybridized with 500 µl of pre-heated probe hybridization buffer (Molecular

Instruments Inc.) at 37 °C for 30 min. The hybridization buffer is replaced with 500 µl of probe solution, made up of probe hybridization buffer containing diluted probe stock of each specific marker that was tested in the experiment at a final concentration of 6nM per probe. Embryos are incubated at 37 °C O/N.

The following day, embryos were washed 4 x 15 minutes with probe wash buffer (Molecular Instruments Inc.) again at 37°C, followed by 2 x 5 min washes with 5X SCCT (5 x sodium chloride sodium citrate (SSC), 0.1% Tween20) at RT. Next, embryos were pre-amplified with amplification buffer (Molecular Instruments Inc.) for 30 minutes at RT (equilibrated to RT before use). In the meantime, the hairpin solution for amplification is prepared. For this, fluorescently tagged hairpin pairs (h1 and h2 hairpins of either Alexa Fluor 647,Alexa Fluor 594, Alexa Fluor 546 or Alexa Fluor 488) (Molecular Instruments Inc.) corresponding to the designed probes were prepared by snap cooling 10 µL of 3 µM stock: Hairpin pairs were heated to 95°C in a thermoblock for 90 sec and then left in a dark drawer at RT for 30 min to cool.

Hairpin solution was finalised by adding snap-cooled h1 and h2 hairpins to 500 µl of amplification buffer at a final concentration of 48nM. Preamplification buffer was removed from embryos and replaced with hairpin solution and left O/N at RT in the dark. The next day, hairpin solution was removed, and embryos washed in 5XSSCT for 2x5min, followed by 2x30 min. and finally 1x5min. Embryos were stored in 5XSCCT at 4°C until visualisation.

Embryos were bleached either following the protocol mentioned in chapter 2.7.1. after rehydration step, or one part 30% peroxide (H_20_2) was added to 2 parts 100% Methanol and embryos were left for about 2h prior to start of experiment.

2.8.2 Clearing

Embryos were cleared with Murrey's Clear/BABB (See Table 10). First, embryos were washed twice with PBST for 5 min each followed by a 5 min wash in 50% Methanol/PBS at RT with rotation. Next, embryos were washed 3x20 min in 100% Methanol before the first wash with

BABB for 5 min. Embryos were then cleared in BABB until going completely transparent (about an 1h), depending on stage of development, at RT with rotation.

2.8.3 Visualisation

Fluorescently labelled embryos were captured with the ZEISS Lattice SIM 3 light microscope, using the ZEN end-to-end microscopy software. Embryos cleared with BABB were left in a droplet of BABB on a slide and a coverslip was placed on top of the embryos.

2.9 Cryosectioning

Embryos were rehydrated after fixation in 75%, 50% and 25% methanol/1x PBST, PBST and incubated in 30% Sucrose solution O/N at 4 °C or until embryos have sunk to bottom of vial containing the sucrose. Embryos were then washed 3 x 5 min each in optimal cutting temperature compound (OCT, Cellpath OCT Embedding Matrix, ThermoFisher cat no. 15212776), before transferring them to cryomolds (TAAB Laboratory cat no. C094) containing OCT at RT. After sinking to the bottom of the OCT filled cryomold, embryos were positioned properly, the position and orientation marked, and then incubated on dry ice for 30min and left at -20°C until needed. Embryos were sectioned on a Cryostat and sections were transferred onto Superfrost Plus microscope slides (Thermo Scientific cat no. J1800AMNZ) O/N at -20°C. Slides were carefully washed 3 x 5 min in PBST and dried on the bench. Slides were mounted using mounting with a few drops of hydromount(pre-warmed to 37 C before use), or mounting media containing DAPI (Abcam) was added, and a coverslip placed on top. Slides were imaged with a ZEISS Lattice SIM 3 light microscope, using the ZEN end-to-end microscopy software in brightfield.

2.10 Dichromate staining

To investigate CCs in wholemount embryos, dichromium staining was performed following the protocol by (Qiu et al., 2013) with minor adaptations. Potassium dichromate was purchased from Merck (Cat. No. 207802). Xenopus embryos (NF stage 33 and 42) were first treated with PK according to Table 7 and washed with 1 X PBS three times before being fixed in dichromate solution (potassium dichromate 3 g, 40 % formaldehyde 10 ml and distilled water 90 ml) for 3 days. The solution was changed every day. Tissue samples were transferred to a 5% dichromate solution up to one week. Following dichromate staining, embryos were washed with 1X PBS multiple times before being imaged.

2.11 Immunofluorescence with anti-adrenaline on sectioned kidneys

Following cryosectioning (section 2.9.), slides were removed from the -20°C and allowed to dry at RT for at least an hour before proceeding. Slides were washed three times, 5 mins each with 1X PBST. Primary antibody (anti-adrenaline, 1:500) was applied diluted in 1 X PBST and incubated over night at 4°C. The anti-adrenaline AB was obtained from LSBio (Polyclonal Rabbit anti -all species Adrenaline, Cat. No: LS-C295834-100). Slides were washed again three times 5 min each in 1X PBST. Secondary antibody was applied diluted in PBST (ThermoFisher, Donkey anti-rabbit, Alexa Flour 555 1:1000) and incubated for 2 hours. Slides were washed again three times 5 min each in 1X PBST and slides mounted with mounting media containing DAPI (Abcam).

2.12 Morpholino knockdown

Morpholino Oligos (MO) were purchased from GeneTools, LLC and stocks were kept at RT. Prior to use, aliquots were heated up to 65 °C for 10 min and then kept on ice until use. Sequences of MO's are listed in Table 9. Embryos for microinjection were placed in 3% Ficoll (6 g Ficoll GE Healthcare PM400, 60 mL 1 X MMR, 140 mL dH_2O) and then left to develop in 3

% Ficoll at 18°C for at least 30 min after injection. After this time, Ficoll was replaced with 0.1 X MMR and embryos left to develop to desired stage. The optimal concentration for morpholino injection at 30nL for Foxd3 morpholino at 2-cell stage, and 16nL for Sox10 morpholino at the same stage, was defined by a dose-response experiment comparing 20nL, 40nL and 60nL injections and defining a midground injection requirement for both morpholinos. Embryos were injected at 2-cell stage on one side, with 20ng/10nL of MO together with 5nL of GFP capped RNA for tracing placement and quality of injection. Needles for injection were calibrated to inject 10nL prior to experiment, using the microscope graticule eyepiece .

Injections were performed on a Harvard apparatus injector (Medical Systems Research), set to the parameters P_{out}t= = 80, $P_{balance}$ = 0.6 and P_{inject} = 16 for X.*laevis*.

Table 9: Morpholino Oligo Properties

Morpholino Name	Sequence	MW	Weight
FoxD3 MO1	5'-CACTGCCGCTGCCTGACAGGGTCAT-3'	8421.04	2.53
Foxd3 Control	5'-CAGTGACGCTGCGTGACAGCGTGAT-3'	8525.12	2.56
Sox10 MO1	5'-AGCTTTGGTCATCACTCATGGTGCC-3'	8426.05	2.53

2.13 Search for Potential Sympathoadrenal Cells in the Single Cell Atlas of Larval Xenopus

To search for developmental time-points of chromaffin cell (CC) presence during *Xenopus* development, we used the single-cell atlas of larval *Xenopus* in an h5ad format, originally published in [https://doi.org/10.1038/s41467-022-31949-2] by (Liao et al., 2022). This dataset contains 188020 cells with approximately 750 genes per cell on average. We utilized the normalized and scaled gene counts, cluster and stage annotations, and calculated tSNE embedding provided by the original research paper. To search for candidate cells of sympathoadrenal nature, we used the Python package Scanpy v1.9.1 (Wolf et al., 2018). The signature expressions were calculated using the Scanpy function sc.tl.score_genes(). Cells were labeled as chromaffin-like if the expression of the corresponding signature was higher than 1.6, and as sympathoblast-like if the expression of the corresponding signature was higher than 1.2. For visualization, the Python packages Matplotlib v3.6.2 (Hunter, 2007) and Scvelo v0.2.5 (Bergen et al., 2020) were additionally used.

Table 10: List of Solutions

BABB:	one part benzyl alcohol, two parts benzyl benzoate
Bleaching solution	0.5X SSC, 5% H_2O_2, 5% Formamide in dH_2O.
BSA coating solution	4% Bovine Serum Albumin in dH_2O.
Cysteine	2% L-Cysteine, pH 7.6 in 0.1X MMR (laevis)
DEPC-solution:	200µl DEPC every liter of solution.
***Ficoll*:**	3% Ficoll in 0.1X MMR (laevis)
***Hybridisation buffer*:**	50% Formamide, 5X SSC, 1mg/ml Torula RNA, 100µg/ml Heparin, 1X Denharts, 0.1% Tween-20, 0.1% CHAPS, 5mM EDTA (pH 8.0) in dH_2O.
LB – LB agar:	10g NaCl, 5g Yeast Extract, 10g Tryptone in 1l of dH_2O (1.5% Agar for LB-Agar).
***LB ampicillin – LB agar ampicillin*:**	1:1000 Ampicillin from the 50mg/ml stock solution in LB or LB-agar.
Lysis buffer	50mM Tris HCl pH 8.5, 1mM EDTA (pH 8.0), 0.5% Tween-20, 100µg/ml Proteinase K-to add fresh every time in dH_2O.
10X MAB	1M Maleic Acid, 1.5M NaCl, 40g NaOH, pH 7.5 in dH_2O.
10X MEM salts	1M MOPS, 20mM EGTA (pH 8.0), 10mM $MgSO_4$-H_20, pH 7.4 in dH_2O.
MEMFA	1X MEM salts, 3.7% formaldehyde in DEPC-H_2O.
10X MMR	1M NaCl, 20mM KCl, 10mM $MgCl_2$, 20mM $CaCl_2$, 50mM HEPES, pH 7.5 in dH_2O.
NTMT	100mM Tris-HCl pH 9.5, 100mM NaCl, 50mM $MgCl_2$, 1% Tween20 in dH_2O.
PBS(T)	10 PBS tablets in 1l of dH_2O (or DEPC-H_2O), 0.1% Tween-20.
20X SSC	3M NaCl, 0.3M Sodium Citrate, pH 7 in dH_2O.
50X TAE	2M Tris Base, 1M Glacial Acetic Acid, 50mM EDTA (pH 8.0) in dH_2O.

3 Chapter III: Characterisation of the development of the adrenal medulla (chromaffin cells) during Xenopus development by WISH

3.1 Identifying a list of candidate genes to characterise the development of the adrenal medulla in *Xenopus laevis*

3.1.1 Introduction: What is already known about adrenal gland development in *Xenopus*

Despite being a widely studied model organism, popular particularly for studying embryogenesis, organogenesis, and human disease mechanisms, among developmental biologists, the development of the adrenal gland (AG) in *Xenopus laevis* is hardly documented.

The formation of the AG in *Xenopus laevis* was first described by a group of German scientists in 1968, in German. Here the AG was initially described as interrenal gland, a homolog to the AC in mammals (Leist et al., 1968). The development of the interrenal gland was measured starting at the beginning of pro-metamorphosis (NF stage 55) until post-metamorphosis (NF stage 59). The interrenal differentiation was categorized in four zones, each describing different phases of interrenal cell development (Fig.12). Interrenal cells exhibited a caudal to cranial migration along the kidney, during which they cross different zones of development. These cells start at the zone of blastema and move to the zone of the newly formed interrenal organ. This is followed by the zone of differentiation and finally the zone of various functional stages during which interrenal cells become 'active' (Leist et al., 1968). Cell activity was determined by the activity of the steroid dehydrogenase enzyme, which is involved in corticosteroid synthesis. Histochemical analysis of steroid dehydrogenase activity was performed on frozen sections of the interrenal gland by determining the Formazan reaction, which measures the rate of formazan formation resulting from the base-catalysed reduction of blue tetrazolium by certain steroids (Guttman, 1966; Leist et al., 1968). However, there is no real mention of CCs or their potential role in catecholamine activity or a structure related to the adrenal medulla (AM).

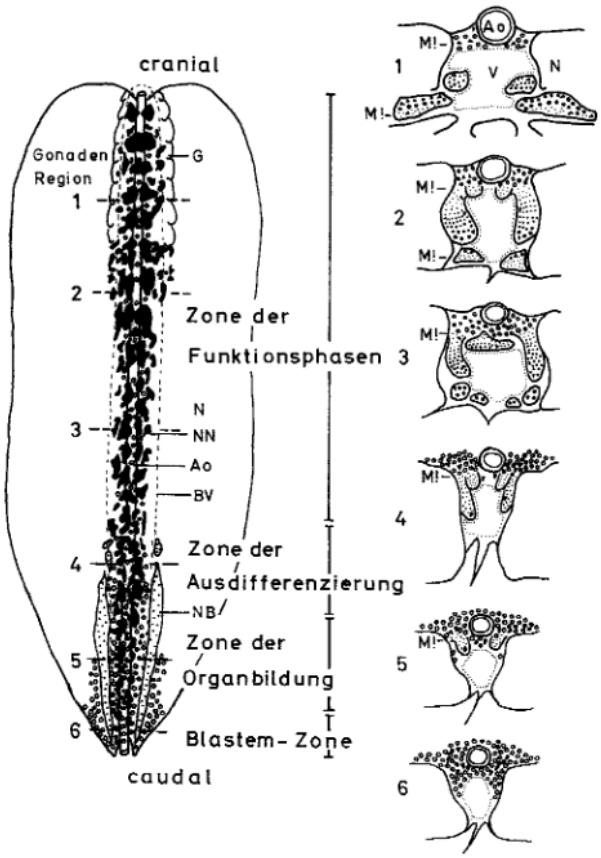

Figure 12: Schematic of the distribution of the interrenal cells in cranio-caudal directionality along the median surface of the kidney together with their corresponding sections at NF stage 63.

Interrenal cells undergo a transition from blastema cells to fully differentiated interrenal cells characterized by steroid dehydrogenase activity. First, cells show characteristics of blastema cells, with little cytoplasm and tightly packed nuclei and no activity (Blastem Zone, 6). Adjacent to this zone in cranial direction, the zone of organ formation (Zone der Organbildung, 5) contains interrenal cells characterized by more cytoplasm and less densely compacted nuclei. Cells then continue to differentiate (Zone der Ausdifferenzierung, 4) to functional interrenal cells, with larger nuclei and low activity of steroid dehydrogenase. Interrenal cells are now fully functional and can be distinguished by different levels of activity (low or high stimulated cells) and lie more ventromedial on the kidneys surface (Zone der Funktionsphase,3). Figure taken from (Leist et al., 1968).

Subsequent studies in the late 70s further expanded on the structure of adrenal islets and adrenocortical secretions in amphibians, noting similarities between *Xenopus laevis* and *Urodela* in islet arrangement, where the islets are found in patches along the midline of the kidney. This is in contrast to other anurans (frogs and toads), where islets form somewhat compact strands along the ventral surface (Hanke, 1978). Overall, CCs in amphibians were

found to be located in close association with steroidogenic cells (Hanke, 1978). In urodeles (salamander and newts), CCs were found as interspersed groups among small bodies of steroidogenic tissue, partially embedded along the ventral surface of the kidney (Fig.13) (Perry and Capaldo, 2011). This arrangement also differs amongst different branching urodeles, with some having CCs formed as isolated groups, mostly separated from the interrenal cells. This can be seen in *Sirenidae* or grouped and intermingled like in *Salamandridae* (Perry and Capaldo, 2011). In teleost fish, CCs are found in the 'head' kidney either in clusters or singly, however the composition of CCs and steroidogenic cells varies among fish in general as well as among teleost fish (Perry and Capaldo, 2011).

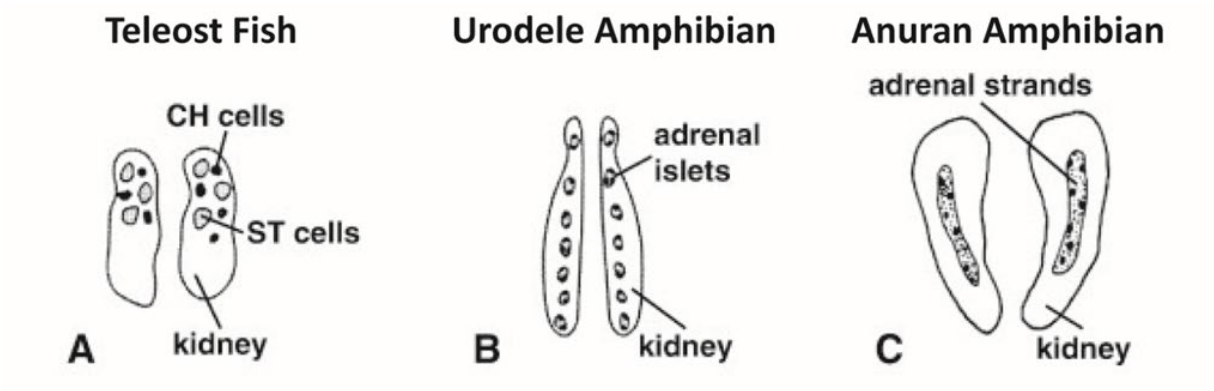

Figure 13: Schematic drawing showing the relationships between the steroidogenic tissue (gray), the chromaffin tissue (black), and the kidney in lower vertebrates.
In teleost's (A), CCs are mostly found in the anterior region of the kidney and CCs are either single or in small clusters. B and C show the clear difference of CC arrangement between Anurans and Urodeles. In Urodeles (B), CCs (black) are found interspersed along the small bodies of steroidogenic tissue (grey) whereas CCs of Anurans are clustered within continuous adrenal strands. This figure was taken from and adapted from (Perry and Capaldo, 2011). A: teleost fish; B: urodele amphibian; C: anuran amphibian.

Positional and structural comparisons among twelve species of Anura confirmed a more medial positioning of the AG in *Xenopus* along the whole length of the kidney (Fig. 14). This shows a closer relation to the shape and function of urodeles, compared to a more short and ventral positioning of the AG as seen in *Rana*, *Bufo,* or *Hyla* (Milano and Accordi, 1983). Both *Anurans* and *Urodeles*, were found to possess adrenaline and noradrenaline secreting CCs, usually intermingled, showing no preferential distribution (Accordi, 1991; Perry and Capaldo, 2011). However, it was observed that CCs formed smaller groups in *Xenopus,* and had infrequent nerve terminals on them (Milano and Accordi, 1983). In all these studies, no

information was presented as on how the AG develops during embryonic and larval stages. Overall, it can be concluded that this organ has not been thoroughly studied; the development of the AM in *Xenopus laevis* seems to be even less well-documented compared to the development of the AC, and no significant new information has been obtained in decades.

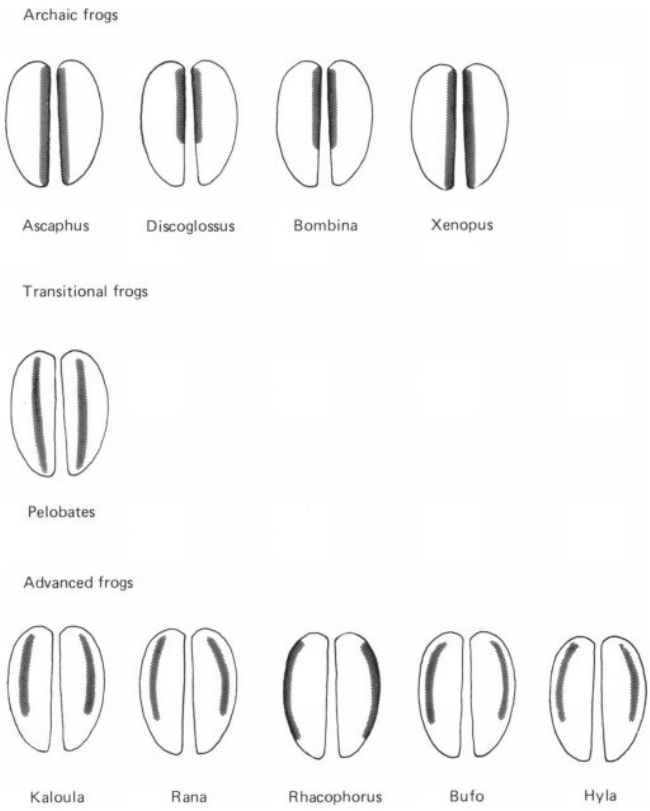

Figure 14: Schematic drawing of AG shape and position among Anura species
Xenopus is categorized in the group of archaic frogs, where the adrenal gland shows a medial position rather than lying along the ventral surface of the kidney observed in anuran genera such as Rana, Bufo and Hyla.Figure taken from and created by Milano EG, Accordi FI. 1983.

With respect to the CCs, the presence of catecholamines (adrenaline, noradrenaline and dopamine) in the blood at varying levels throughout *X. laevis* development have been shown. All three catecholamines were present from NF stage 40 onwards, but not found at earlier stages, with a first peak for adrenaline and noradrenaline, but not dopamine (Kloas et al., 1997). Both adrenaline and noradrenaline were present, and gradually increased over the first two month of the juvenile period, whereas dopamine was low throughout development but showed a dramatic elevation between the metamorphic period from NF stages 62 - 66 (Kloas

et al., 1997). Additionally, the presence of CCs was shown at NF stage 45 through immunocytochemistry, using the main catecholamine synthesizing enzymes th, dbh and pnmt. Coincidentally, a drastic increase in th-immunoreactive cells was found, with the increase of dopamine concentrations during the end of metamorphosis, implying a significance for dopamine for juveniles (Kloas et al., 1997). However, no further elaborations can be found in the literature on these cells.

In 2000, Etard et al. speculated to have found an AG marker in *Xenopus*, xReptin (Ruvbl2) (Etard et al., 2000). Here, expression was shown in the 'adrenomedullary cells' of the AG in *Xenopus*. However, this was solely determined by the position of *ruvbl2* expression in the embryo but was not explored further (Etard et al., 2000).

Another marker was described to be expressed in the AM of *Xenopus* embryos. Expression of TF *insulinoma associated 1 (insm1*) was found in neural plate primary neurons, as well as in a population of uncharacterized cells. These cells formed at the anteroventral side of the embryo, just in front of the cement gland at early tailbud stage of embryogenesis in *X. laevis* (Parlier et al., 2008). Based on the expression of *th*, these cells were identified as noradrenergic. Further, these cells are regulated by TFs *phox2a* and *hand2*, making them likely to be able to produce noradrenaline (Parlier et al., 2008). Due to the local expression dorsally to the pronephros at NF stage 24, *insm1* is suggested to mark the AM, which the authors based on the description of marker *ruvbl2* showing adrenal medullary cells in the same location (Parlier et al., 2008).

As of the start of this project, *ruvbl2* and *insm1* were the only described marker genes for development of the AM in this species.

During this chapter, I aim to define putative marker genes for CC development and differentiation in *Xenopus laevis*, and define their expression during embryonic development through qualitative analysis using Wholemount In situ hybridisation (WISH)

3.1.2 Specification of markers involved in chromaffin cell development

To be able to create a spatial-temporal map of AG development in *Xenopus*, a candidate list of genes was created to narrow down the best possible markers to use. Candidate genes were identified by scanning the literature for AM development in human, rodents, zebrafish and frog models. Additionally, genes were added based on their gene ontology (GO) term such as 'adrenal gland development' and 'chromaffin cell differentiation'. Genes were also chosen by looking at expression atlases on the EMBL website and at studies performing single cell sequencing on human foetal and mouse embryo AGs. Candidate genes were then prioritised based on species homology on BLAST (Table 11). A list of genes was then compiled, and the plasmids containing genes of interest that were already in the Wheeler laboratory were used to create riboprobes directly, while some plasmids containing genes of interest were requested from other laboratories, if found on Xenbase. Most riboprobes for candidate genes were created by designing primers and cloning the gene of interest as described in the section 2.6.

Table 11: Blast results showing percentage identity of genes of interest between Xenopus laevis and different species.

	% Identity		
Gene of Interest	***Homo sapiens***	***Mus musculus***	***Dario rerio***
Phox2a	66.90%	67.84%	75.43%
Phox2b	94.12%	97.12%	83.11%
Ascl1.S	93.51%	92.80%	83.15%
Insm1	51.46%	51.04%	55.23%
Ruvbl2	93.95%	94.38%	88.72%
Chga	56.78%	64.44%	55.32%
Chgb	36.21%	33.49%	31.34%
Th	71.17%	72.89%	69.86%
Dbh	64.11%	61.72%	58.44%
Pnmt	61.24%	59.90%	53.21%
Nr5a1	68.72%	64.26%	66.46%
Star	68.77%	65.26%	68.95%
Cyp17a1	50.31%	47.93%	69.21%

3.1.3 Cross-referencing pre-selected AM markers with a new tool

In the summer of 2022, a single cell RNA sequencing atlas of the entire neural crest cell (NCC) lineage was generated by the Adameyko lab (Kastriti et al., 2022). This atlas is publicly available online (https://www.embopress.org/doi/epdf/10.15252/embj.2021108780?src=getftr) and allows the user to identify populations of cells within the NC lineages that express a gene of interest.

This atlas was generated by using single-cell transcriptomic profiling of genetically labelled NC and schwann cell precursor (SCP) lineage cells of tissues between embryonic stage E9.5 to E18.5 in mouse embryos. With this analysis, the authors defined SCPs as a multipotent source of NC-like cells, with late NCCs and early SCPs sharing a multipotent 'hub' state that contain differentially biased cells (Kastriti et al., 2022). The resulting tree-like atlas of transcriptional events showed that the NCCs converge into a common transcriptional state, which was defined as the 'hub' state. This 'hub' state is characterized by the expression of markers *Sox8*, *Itga4* and *Serpine2*. This state represents cells that were already nerve-associated and found to contain multipotency, which it inherited from the converging NC. These 'hub' state nerve-associated cells were found to contain transcriptional programs characterized by multiple biases towards downstream fates that include the CCs and sympathetic neurons of the SA lineage, enteric glia and ganglia of the enteric nervous system lineage, melanocytes and differentiated schwann cells (Fig. 15B). To define each lineage group, cells were assigned to the defined cell types using previously published markers, indicated for each lineage (Fig, 15B). Sampled tissues were taken from a range of different stages of mouse embryonic development and some post-natal stages, and their locations within the map are indicated by different colours (Fig. 15C). The colours also correspond to the different time-points these samples were extracted from (Fig. 15A). We can see that, for the sympathoadrenal (SA) lineage, tissue samples were taken from E12.5 up until E18.5, at post-natal day 2(P2) and from adult mice.

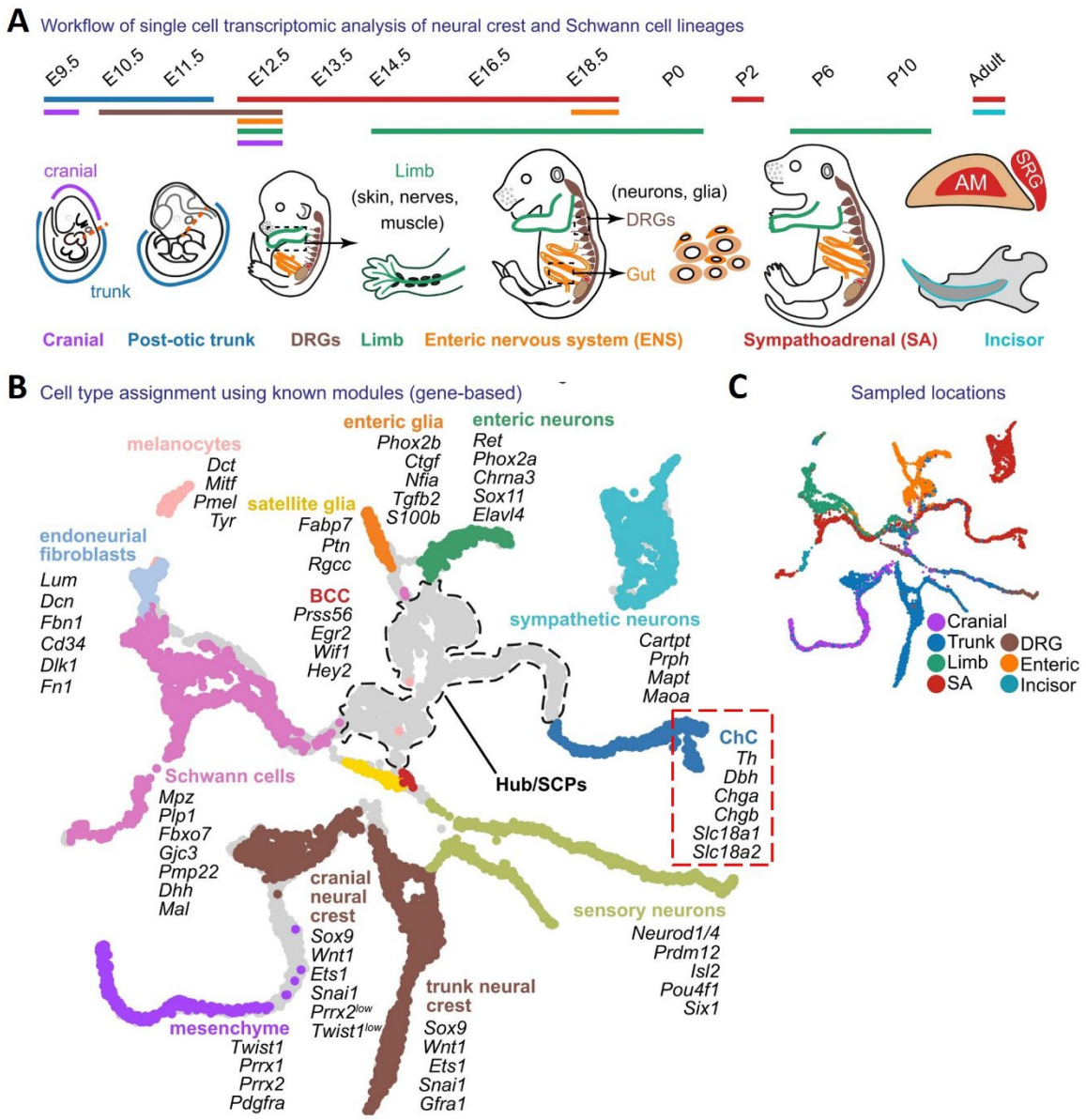

Figure 15: Developmental tree of transcriptomic analysis of NC, SCP and their downstream lineages created by and taken from (Kastriti et al., 2022).

Single cell samples for transcriptomic analysis of NC and Schwann Cell lineages were taken from genetically labelled mice between E9.5 to adult stages (A). Dissected samples of analysed lineages and their corresponding locations within the UMAP are labelled by different colours, the red shows the sympathoadrenal lineage including both sympathetic neurons and chromaffin cells of the AM (B,C). Samples were taken from mouse AM and the suprarenal ganglion (A). Red dotted lines show the genes used to identify cell identity of CCs (B). DRG, dorsal root ganglia; SA, Sympathoadrenal; SRG,suprarenal ganglion; ChC, Chromaffin cells, AM, Adrenal medulla; SCPs, Schwann cell precursor.

This atlas was used to further confirm the previous analysis, carried out to select marker genes for identifying the location of the AM. Further, it is a useful aid for having a global overview for the expression of selected genes within the NC-derived cells. When using the online pagoda2 web application, we were able to identify the expression level of each of our genes of interest within the tree-like expression. When searching for the SA lineage differentiation markers *Phox2a*, *Phox2b* and *Insm1*, we can see that they are all expressed in the branch of differentiated CCs, however in different manners (Fig. 16). *Phox2a* is found to be strongly expressed along the whole length of the CC branch (Fig. 16 A), whereas *Phox2b* and *Insm1* are both expressed mostly still within the 'hub' area that is biased towards the CC branch (Fig.16 B and C). *Insm1* expression is also found along most of the differentiated CC branch (Fig. 16 B), whereas *Phox2b* expression along the differentiated branch is low (Fig. 16 C). We also see varying levels of expression of all three markers in the sympathetic neurons assigned cell cluster. Additionally, *Phox2a* and *Phox2b* expression is in the enteric neuron branch (Fig. 16 A and B), while *Phox2b* expression is also located in the branch of the enteric glia as well as in the 'hub' state biased towards these two clusters (Fig. 16 B). We also observe expression of *Insm1* in these two clusters, however in fewer cells, and more towards the early biased cells of these two cell types (Fig. 16 C).

For CC markers *Dbh* and *Chga*, expression is high within the CC branch (Fig. 16 D and E). *Dbh* was also found to be highly expressed in the sympathetic neurons cluster (Fig. 16 E). In contrast, expression of *Ruvbl2*, the previously assigned gene marker for *X.laevis* adrenomedullary cells, is not found in the CC branch. Here, *Ruvbl2* is mostly located in mesenchyme and cranial NC branches (Fig. 16 F). Finally, the marker *Pnmt*, specific to adrenaline producing CCs, is found in very few cells in the CC branch (Fig. 16 G).

However, it is important to mention that these data sets were generated from mice. This is especially important as there are considerable evolutionary differences between the anuran and mammals. Yet, after searching the expression of our pre-selected genes of interest (Table 11) in the UMAP, we observed that all pre-selected markers for the AM are expressed in the CCs lineage, which indicates a good literature-based selection.

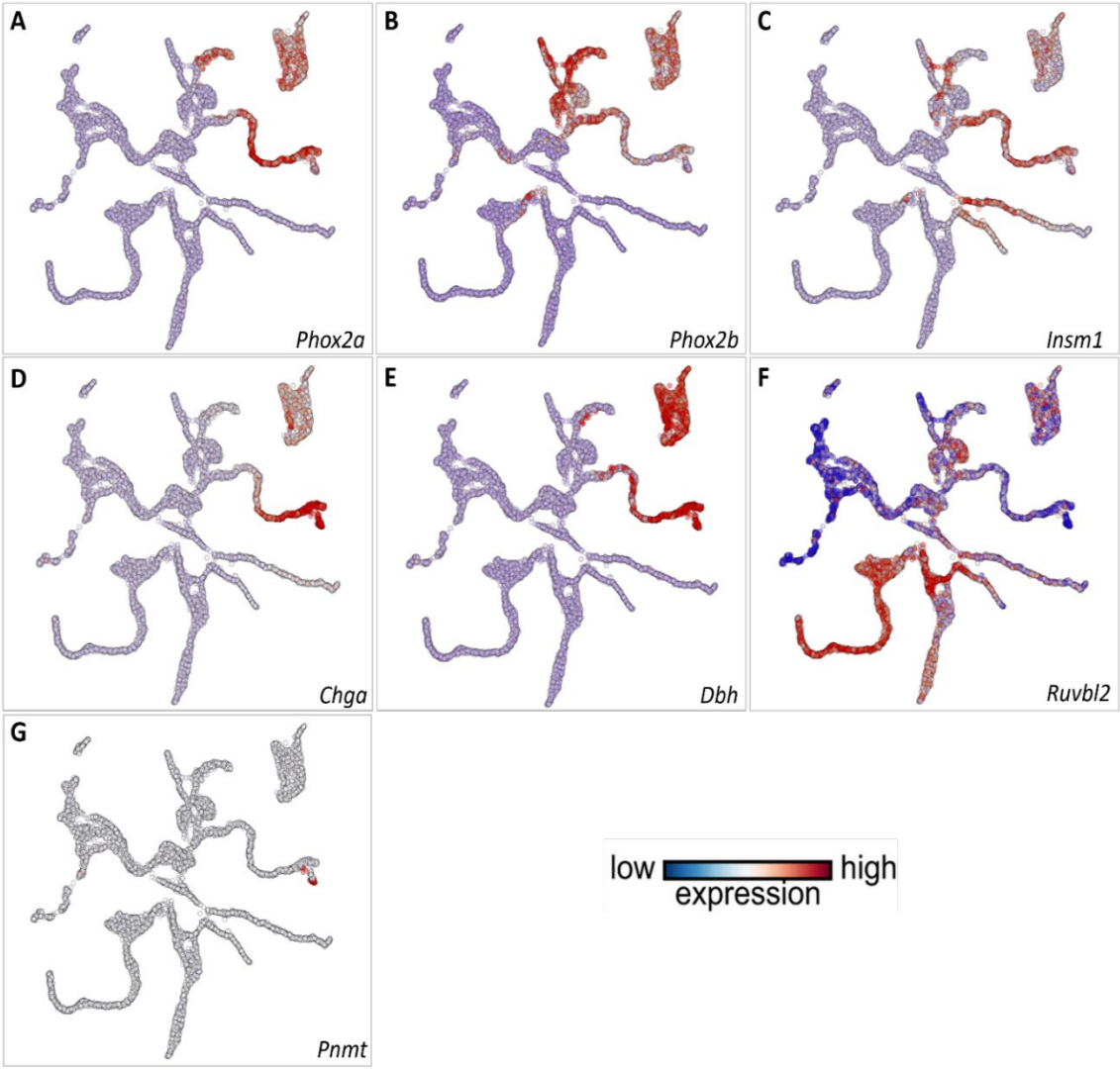

Figure 16:UMAPs (gene-based embedding) showing the expression level of markers of interest within each of the cells of the different anatomical clusters in mouse model. *Obtained with pagoda2 web application created and made available by the Adameyko Lab in 2022. A-C: Expression levels of SA specifier marker genes. Both Phox2a (A) and Insm1 (C) are both well expressed in the CC branch, whereas Phox2b (B) is expressed at early lineage biasing of the CC branch, but not much during further differentiation and developmental time points. All three genes are expressed in varying levels in the enteric neuron and/or glia branch of the enteric nervous system and in the sympathetic neurons cluster. D-G: Expression levels of CC specific markers. Both Chga and Dbh are highly expressed in the CC branch during development and in adult tissue (makes up the overhang on the end of the branch). Dbh in particular, is also highly expressed in the sympathetic neurons (E). Expression of Ruvbl2 is not found in the CC branch but rather in the mesenchyme, and cranial and trunk NC branches (F). Pnmt is exclusively expressed in cells of the CC branch (G).*

3.2 Expression profiles of key marker genes identified for both adrenal medulla and adrenal cortex development

To gain temporal information on genes of interest expression at different developmental time-points of *X. laevis*, expression profiles were established by reverse transcription, RT-PCR (Fig. 17). RNA of embryos (n=10) at key developmental stages was extracted. Developmental time points chosen were unfertilized egg (1-cell), blastula (NF stage 10.5), neurula (NF stage 14), late neurula (NF stage 20), organogenesis at early tailbud (NF stage 24), onset of pronephric kidney development at tailbud (NF stage 27), and organogenesis and late tailbud stages (NF stage 33 and NF 37), as well as organogenesis at tadpole (NF stage 42 and 45). RNA was converted into cDNA and used in RT-PCR to establish expression profiles. New primers were designed to run the PCR on genes of interest were the riboprobe was provided by another lab (*phox2a*, *chga* and *insm1*). For the genes we cloned ourselves, the primers designed for this process were used also for running this PCR. The same number of PCR cycles (37) was used for all genes, but elongation time and annealing temperature were adjusted according to gene insert sizes and primer sequences. A housekeeping gene, *gapdh*, was used as a standard positive control and as a loading control. Water was used as a negative control.

Gapdh was expressed throughout development, expression was very low at NF stage 10.5 and cannot be seen on the figure, due to saturation issues with the other stages, although the band was found to be present when imaging (Fig 17). In contrast to (Session et al., 2016) RNA-sequencing data obtained from Xenbase, most genes of interest are not found to be expressed at NF stage 27. Here, I hypothesis technical issues in cDNA synthesis. Generally, signal intensity was good for most genes. Only *pnmt* showed low signal intensity. *Nr5a1* showed no expression possibly due to contamination of the primers. Expression for each gene of interest is described in their individual sections.

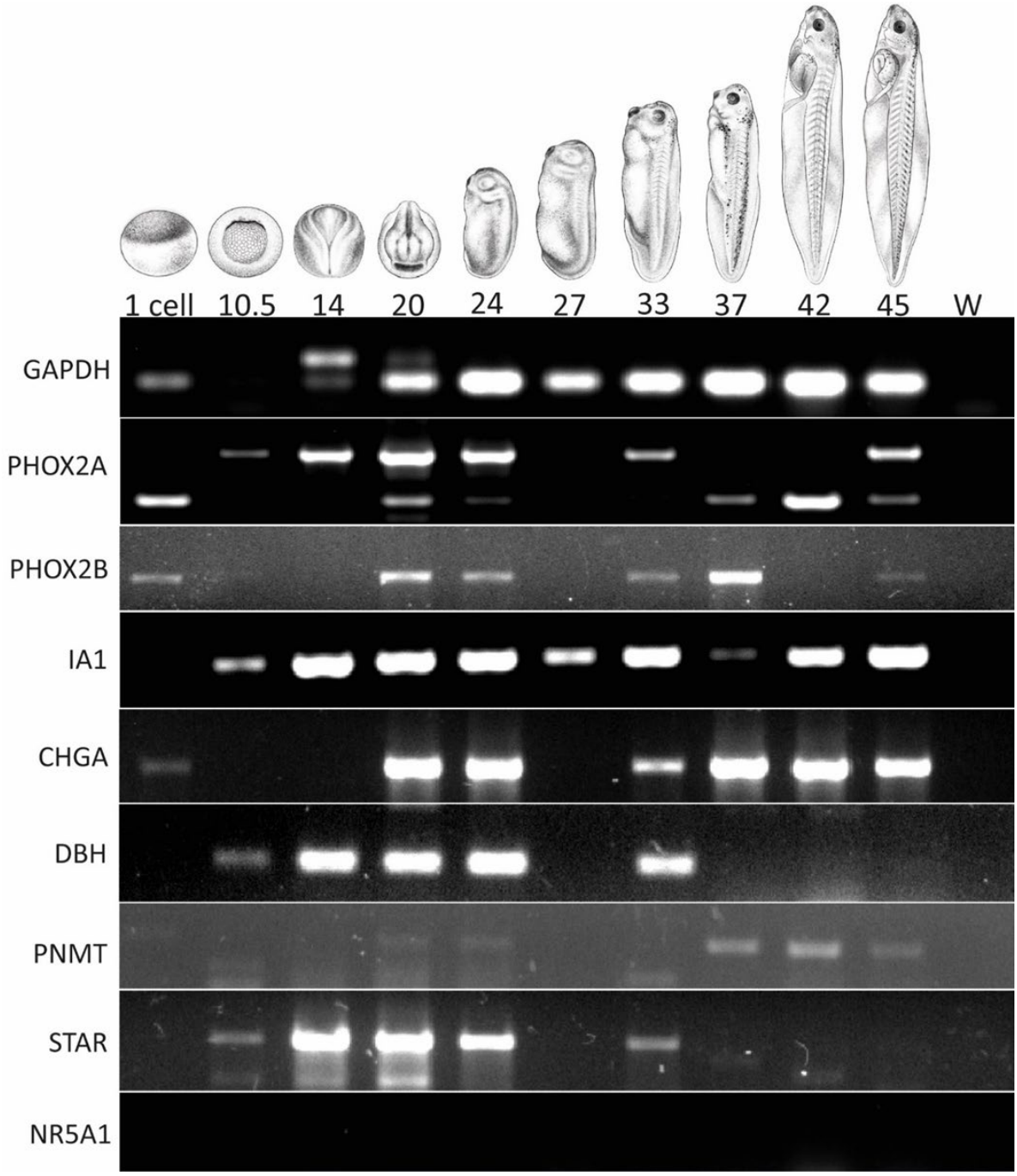

Figure 17: Expression of adrenal gland markers, both for chromaffin and steroidogenic cells, during developmental stages of X. laevis.

Analysis of RT-PCR of mRNA from egg (1 cell stage) to tadpole stage 45. Xenopus developmental stages are shown at the top according to Nieuwkoop and Faber, 1994. Drawings of the developmental stages are taken from Zahn 2022. Name of genes are indicated on the left. RT-PCR was only performed on the final list of key identified markers. Gapdh was used as a positive control and water (W) was used as a negative control.

3.3 Characterisation of AM markers during embryogenesis by Wholemount in *in situ* hybridisation

To visualise the spatial and temporal expression levels of the genes of interest at different stages during *Xenopus* embryogenesis, WISH with digoxigenin (DIG) labelled antisense RNA probes was performed. *Xenopus* embryos are staged according to Nieuwkoop and Faber (Nieuwkoop and Faber, 1994), based on morphological criteria and are therefore annotated with NF. The main stages visualized were late neurula (NF 19/20), early to late tailbud stages (NF 24-40) and tadpole stage NF 45. These stages represent both the onset and duration of pronephric kidney organogenesis, up until fully formed pronephric kidney, prior to undergoing metamorphosis. Pronephric kidney development in *X. laevis* is a well-studied process. The pronephros is an embryonic kidney, essential for survival in larvae of both fish and amphibians (Raciti et al., 2008). In *Xenopus*, pronephros development begins at early neurula (NF stage 12.5), with the specification of mesodermal cells of the intermediate mesoderm (IM) to become renal progenitors, driven by signalling pathways such as BMP and Wnt (Fig.18) (Desgrange and Cereghini, 2015). From NF stage 15, the pronephric anlage is formed, expressing genes such as *lim1* and *pax8 (Chan et al., 2018a; Jones, 2005)*. The structure elongates and by NF stage 24, undergoes an epithelial to mesenchymal transition to form the epithelial pronephric duct, which elongates caudally, eventually opening to the cloaca (Desgrange and Cereghini, 2015; Raciti et al., 2008). In the most proximal region, three ciliated funnels, the nephrostomes, open into the coelom to direct coelomic waste into the proximal tubules (Fig. 18, blue). Glomus morphogenesis begins at NF stages 29–30 with capillaries arising from the dorsal aorta. Blood filtration starts at NF stages 35-36 and, at NF stage 40, the kidney begins excretory functions (Raciti et al., 2008).

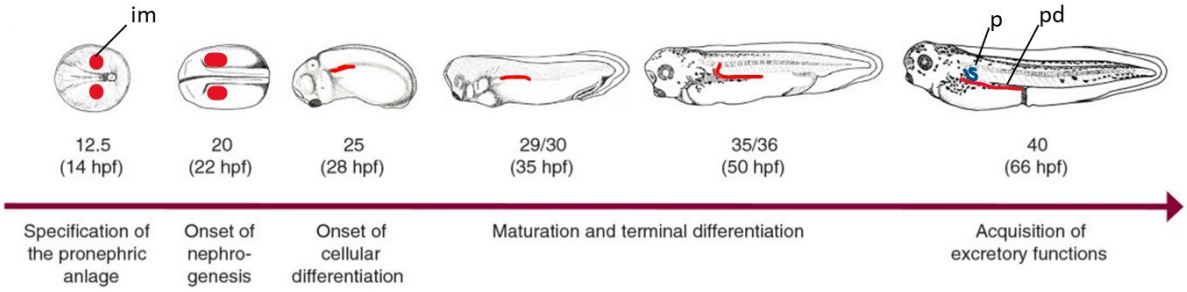

Figure 18: Schematic of pronephric kidney development in Xenopus.
Pronephric kidney development begins around NF stage 12.5, when the pronephric anlagen (red) are induced from the IM by surrounding tissues. NF stage 20 sees the onset of nephrogenesis and by NF stage 25, the epithelial pronephric duct is formed which elongates and matures during late tailbud stages (NF stage 29-36). At NF stage 35-36, the pronephric kidney can filter the blood, and from NF stage 40 is capable of excretion. The figure was created by and taken from (Raciti et al., 2008), with adaptations made according to (Chan et al., 2018a). Hpf, hours post fertilisation; im, intermediate mesoderm; p, pronephros; pd, pronephric duct.

A riboprobe for the pronephric kidney marker *pax8* was made and a spatial and temporal expression map created (Fig. 19). This was used to compare the location and expression of adrenal markers to the pronephric kidney marker *in situ*. Our initial assumption was that the CCs of *Xenopus* embryos would develop within or along the pronephric kidney during embryogenesis.

Gaining insights into the mechanism of how the normal AG develops is vital for research on the pathophysiology of this organ. Some important genes and proteins are introduced, and their expression during development characterized in the following. These could mark important starting points to fate-map AG development in *Xenopus.*

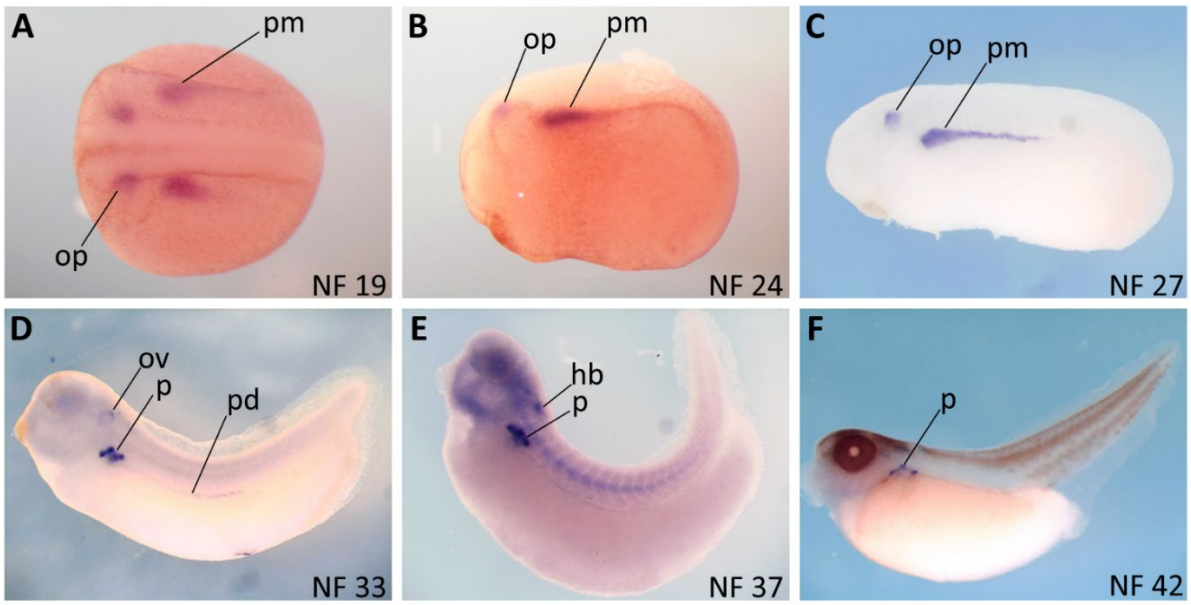

Figure 19: Spatiotemporal expression map of control marker pax8, involved in the development of the pronephric kidney during X. laevis embryogenesis.
Late neurula (A) embryo is imaged dorsally, with the anterior side of the embryo on the left and the posterior on the right. All other embryonic stages are imaged ventrally with the same orientation. Kidney fields form at early neurula stage from the intermediate mesoderm, and the pronephric mesenchyme is seen on each side of the neural tube (A). Pax8 is also expressed in the forming otic vesicle, here the otic placode can be seen anterior to the kidney fields on each side of the neural tube (A). Pronephric anlage undergoes medio-lateral patterning during earl tailbud stages (B,C). From late tailbud (D,E), the pronephric tubule has formed and is apparent. At NF stage 33, the pronephric duct running all along the midline of the embryonic body is clearly visible. Pax8 expression in the otic vesicle is also seen. At tadpole (F), we mainly observe expression of the nephrostomes on the tubules. Pm, pronephric mesenchyme; pd, pronephric duct; p, pronephros; op, otic placode; ov, otic vesicle.

3.3.1 Reptin (*ruvbl2*) marks nephrostomes and not adrenal medulla in *Xenopus*

One of the first markers chosen to characterize the position and development of the AG in *Xenopus* was *ruvbl2*. The highly conserved RUVBL2, or RuvB-like 2, belongs to the AAA+ family of ATPases, and is a crucial player in many cell activities such as DNA replication, repair, and gene regulation (Wang et al., 2022a). Further, RUVBL2 contributes to the maintenance of genomic stability through its role in DNA repair, chromatin remodelling, telomere maintenance, and cell cycle regulation (Wang et al., 2022a).

Ruvbl2 was found to be expressed in *Xenopus*, labelled as *xReptin*, and showed a 94% identity to human/mouse homologs (Etard et al., 2000). In the following, we will refer to this gene simply as *reptin*. *Reptin* has been implicated to play a critical role in embryonic development and gene expression regulation in *Xenopus* (Etard et al., 2005). Expression of *reptin* was described in pre-migratory NC and during later stages of development, *reptin* transcripts were found in the mandibular, hyoid, branchial crest, and in different regions of the brain (Etard et al., 2000). Regional expression of *reptin* in the area of the developing pronephros, labelled as adrenomedullary according to the authors (Fig.20) (Etard et al., 2005) sparked our interest. Here, we characterize the expression of *reptin* in *Xenopus* further.

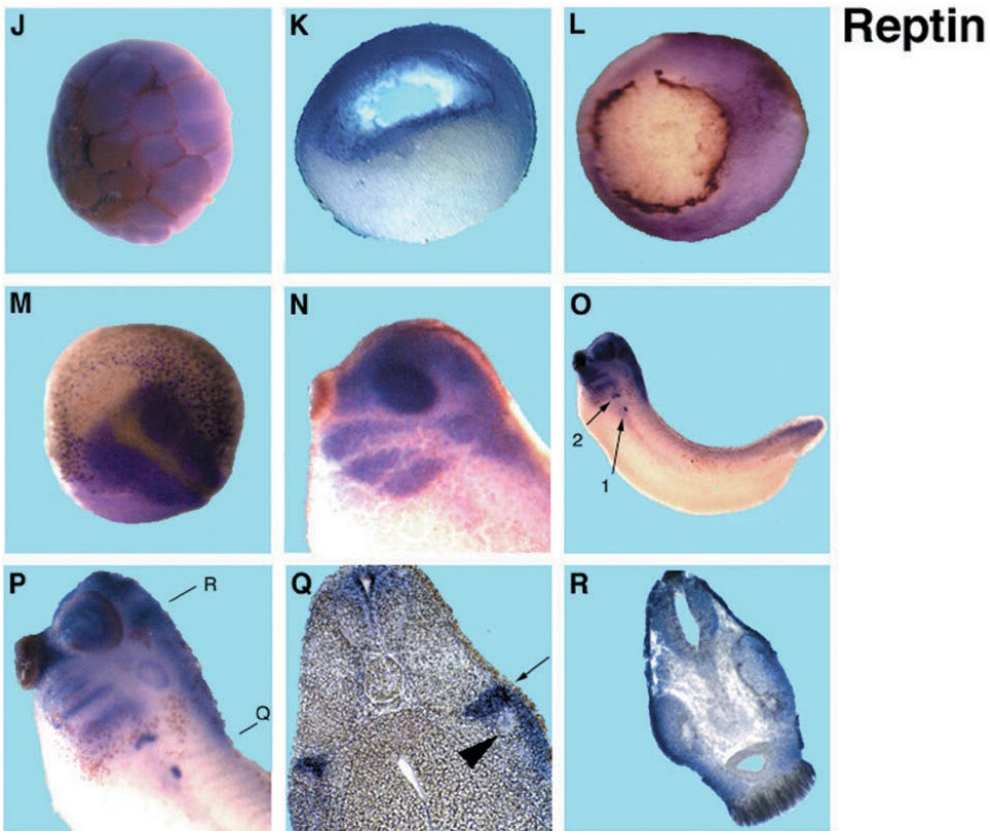

Figure 20: Whole-mount in situ hybridization analysis of Xreptin (J–Q) from Etard et al. (2000).
The authors describe the expression of two separate structures, 1 and 2 (O,P), whereas structure 1 is identified as adrenomedullary cells and structure 2 remains unknown. The black arrow in (Q) indicates the pronephric tubulus which is not stained, and the arrow marks staining in the adrenomedullary cells.

The WISH probe for *ruvbl2* was generated from the plasmid containing *reptin* that was previously first isolated and cloned by the Doris Wiedlich lab (Etard et al., 2005).

As we were particularly interested in the expression discovered during late tailbud development (NF stage 33 and onwards), we mainly performed WISH of *reptin* at tailbud and late tailbud stages. At NF stage 27, when the pronephric tubules of the pronephric kidney forms and expression of pronephric kidney marker *pax8* can be easily detected (Fig. 21), we did not observe any expression of *reptin* in the region of the pronephric kidney (Fig. 21 A). At NF stage 33, we observe expression of *reptin* in three circular looking structures that are located in the area of the pronephric tubule (Fig. 21 B), compared to the two structures that

were previously described by Etard et al. (Fig, 20 O,P,Q). The location of these structures in the area of the pronephric tubule colocalises with the expression of the marker *pax8* (Fig.21). Here, *pax8* marks the localisation of the pronephros and the pronephric duct at this stage of development (Fig. 10E). We further observed expression of *reptin* in the pronephric duct (Fig. 21B). This expression pattern is still observed at NF stage 37, where the circular structures are still strongly expressed, and the pronephric duct expression has further elongated (Fig. 21 C).

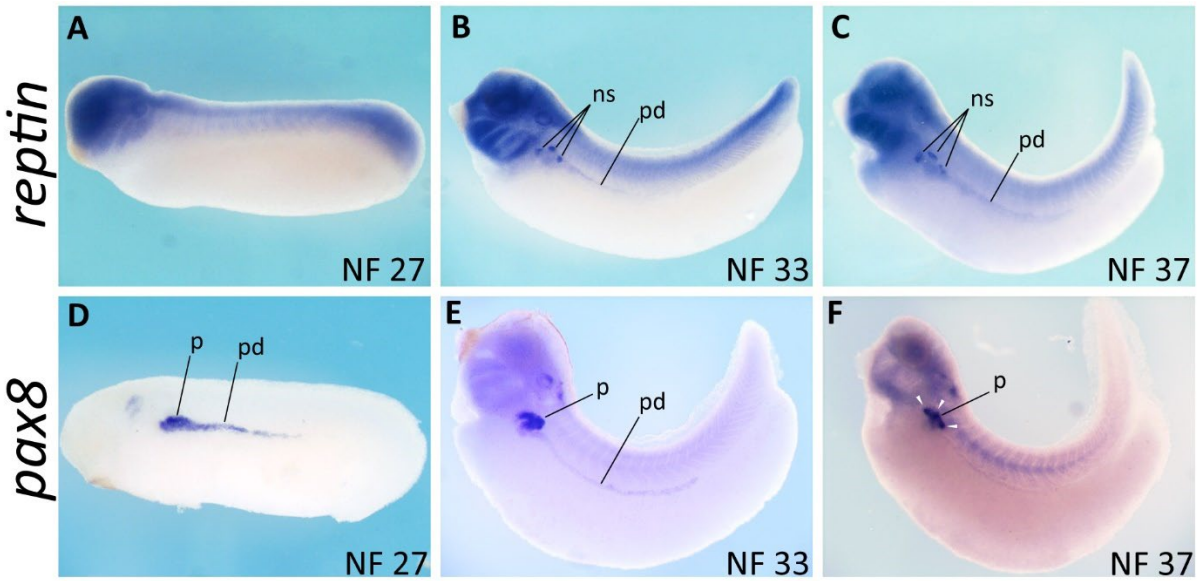

Figure 21: Wholemount in situ hybridisation analysis of reptin and pax8 during late tailbud development in X. laevis.
Embryos are imaged ventrally with the anterior side to the left. Reptin shows no expression in the region of the developing pronephric kidney at NF 27 (A) but is expressed in nephrostomes of the pronephric tubule at NF stage 33 and 37 (B, C). Expression of reptin is also found in the distal tubules of the pronephric kidney at late tailbud (C). Pax8 is continuously expressed in the pronephric tubule and duct from NF stage 27 to NF stage 37 (D-E). White arrowheads indicate area of nephrostomes (ns) in pax8 expression. Ns, nephrostomes; p, pronephros; pd, pronephric duct.

Trying to identify the structures highlighted by *reptin* mRNA expression, we took advantage of the vast work and publications on pronephric kidney development in *Xenopus.* Raciti et al. in 2008 provided a comprehensive analysis of the gene expression patterns in the pronephric kidney of *Xenopus*, elucidating the remarkable similarity between nephron tubule organization in *Xenopus* pronephros and the mammalian metanephros (Raciti et al., 2008).

The authors provide a schematic representation of the *Xenopus* pronephric kidney at NF stage 35/36 (Fig. 22), which is close to the stage where we observe our expression pattern of interest with *reptin.* The scheme describes three structures present at the anterior end of each pronephric tubule, the nephrostomes (NS). Nephrostomes are small openings or funnel-like structures found in the excretory systems of some invertebrates and lower vertebrates, where they serve as the entrance to the tubules, allowing fluid from the body cavity to enter the nephric tubules for filtration (Desgrange and Cereghini, 2015; Raciti et al., 2008). These specialized structures are lined by a group of multi-ciliated cells and play a crucial role in the filtration and elimination of waste materials during kidney development (Desgrange and Cereghini, 2015). They progress over time, contributing to the formation of the mature structure and are implicated in the development of the gonad (Desgrange and Cereghini, 2015). In *Xenopus*, the nephrostomes are marked by the expression of specific marker genes and proteins including *pax2* and *cldn19,* which are known to be associated with pronephric development and function (Raciti et al., 2008). In the paper, the authors have analysed the expression of *cldn19* (Claudin-19) to validate the pronephric segmentation in *Xenopus*. Cldn19 is a member of the claudin family of tight junction proteins, which are crucial for the formation and maintenance of epithelial barriers (Raciti et al., 2008). It has been shown, that *cldn19* is expressed in nephrostomes of *Xenopus* (Fig. 23) *(Raciti et al., 2008)*, where it is involved in the formation and maintenance of the tight junctions of the nephrostomes (Raciti et al., 2008).

Based on the description of the *Xenopus* pronephric kidney schematic by (Raciti et al., 2008) (Fig. 22), and comparing the expression pattern of *cldn19* mRNA WISH to *reptin* mRNA WISH, we hypothesise that the circular expression structures are NS of the pronephric tubules. This hypothesis challenges that *reptin* is involved in the formation of the AM, in *Xenopus*. Therefore, we excluded *reptin* as a marker to characterize the development of the AG in *Xenopus*.

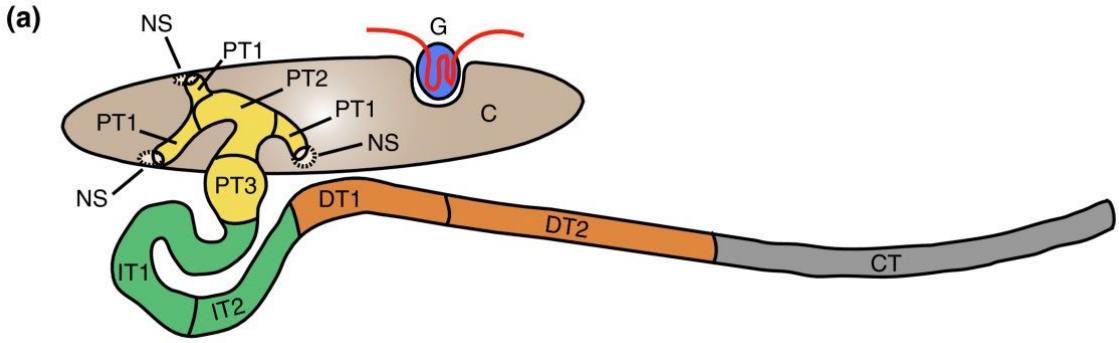

Figure 22: Schematic of Xenopus pronephric kidney at NF stage 35/36
Nephrostomes (NS) can be found at the anterior end of each proximal tubule. Nephrostomes are ciliated funnels that connect the coelomic cavity (C) to the nephron and serve as entrance to the filtration system that is the kidney. The pronephric kidney is distinguished by four tubular compartments, the proximal tubules (PT, yellow; PT1, PT2, and PT3), intermediate tubule (IT, green; IT1 and IT2), distal tubule (DT, orange; DT1 and DT2), and connecting tubule (CT, grey). Figure taken from and created by (Raciti et al., 2008).

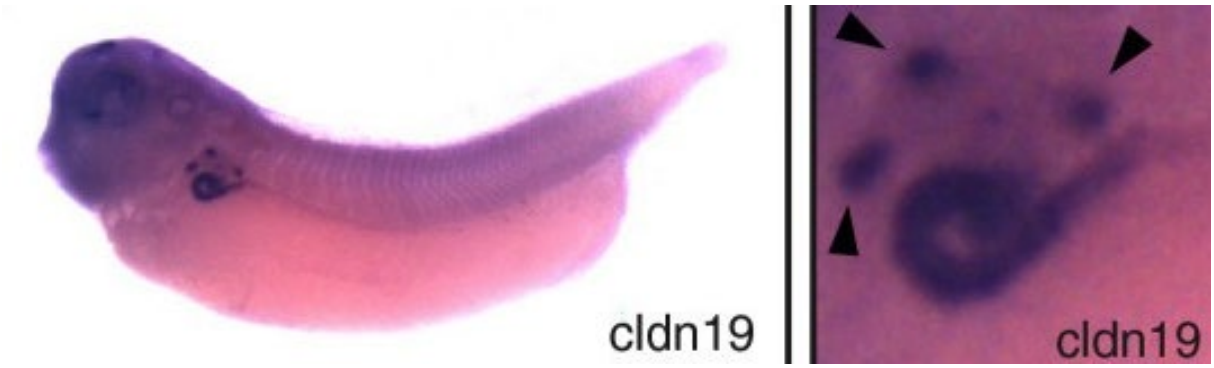

Figure 23: Wholemount In Situ Hybridisation of pronephric tubule marker Cldn19
Cldn19 is expressed in the intermediate tubule and nephrostomes (black arrowheads). Figure taken from and created by (Raciti et al., 2008).

3.3.2 Phox2a

The homeodomain transcription factor *Phox2a* plays a crucial role in the development of the peripheral autonomic nervous system in vertebrates (Flora et al., 2001). It is a key player in the specification of the SA lineage, as part of a complex network of transcription factors (TFs) (Coppola et al., 2005; Huber, 2006). *Phox2a* is part of a paralogous homeobox gene pair together with *Phox2b*, meaning they have similar expression patterns and bind the same target sequences (Coppola et al., 2005). Together, this paralogous pair is involved in the development of the autonomic and sensorimotor neurons in all vertebrates (Coppola et al., 2005). In mice, both *Phox2* genes are expressed in all autonomic ganglia (sympathetic, parasympathetic and enteric) and in the three epibranchial-placode-derived distal ganglia of the cranial nerves as well as in various structures of the central nervous system (CNS) (Coppola et al., 2005). Phox2b is a key player in the development of parasympathetic neurons as well as for the differentiation of medullary respiratory neurons and serotonergic neurons in the hindbrain (Coppola et al., 2005).

Phox2a is found to be primarily expressed in sympathetic neurons and is vital in the expression of noradrenergic features (Hirsch et al., 1998). Importantly, *Phox2a* is a positive regulator of the expression *of Th* and *Dbh*, two catecholaminergic biosynthetic enzymes essential for the production of adrenaline and nor-adrenaline (Hirsch et al., 1998; Huber, 2006). This underscores its significance in the regulation of catecholamine biosynthesis and neuronal differentiation. While the *Phox2* genes have similar functions in some neuronal populations, and are co-expressed in the same lineages, they do so in a distinct temporal order and are not functionally equivalent (Coppola et al., 2005). By conducting reciprocal gene replacement experiments of the *Phox2* genes in mice, it was revealed that *Phox2a*, which is induced by *Phox2b*, is unable to replace *Phox2b* function during development of SA cells (Coppola et al., 2005; Huber, 2006). When *Phox2a* was absent, the development of CCs and sympathetic neurons was not affected, meaning that either *Phox2a* is not vital for the development of these cells, or that its function can be largely compensated by the function of *Phox2b* (Huber, 2006). It could also indicate that *Phox2a* expression is more important for the noradrenergic functionality of these cells through its regulation of the *Dbh* promoter.

However, due to the previous description of *phox2a* as characterising noradrenergic cells in *Xenopus* by Wiley and Colleagues (Wylie et al., 2015), and its important role in the establishment of the SA lineage in mammals, it was chosen as a potential marker gene in this project to trace the development of CCs of the AG in *Xenopus*.

The *phox2a* RNA WISH probe was generated from a plasmid containing X*phox2a.S* (short chromosome variant), that was kindly provided by Dr. Eric Bellefroid. The *Xphox2a.S* gene in *X.laevis* was first isolated and the clone created by the Zimmerman lab (Talikka et al., 2004).

Based on the *X. laevis* RNA-Seq data on Xenbase (Data from Session et al. 2016), *phox2a* expression in transcripts per million (TPM) sharply rises from NF stage 8 and first peaks at NF stage 10 (Fig. 24). Afterwards, expression is dropping to relatively low levels by NF stage 15 throughout 25 and then rising again with another high peak at NF stage 35-36 (Fig. 24).

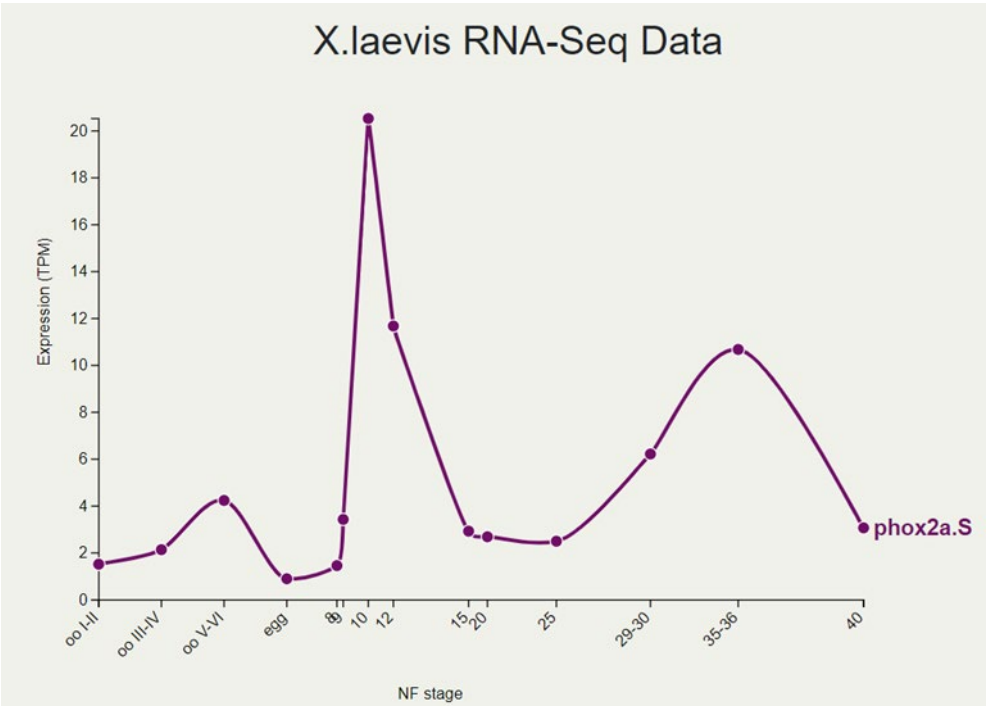

Figure 24: RNA sequencing data of phox2a.S
Graph shows expression in transcripts per million (TPM) on the Y-axis, and the developmental stage of measured expression on the X-axis, taken from Xenbase (Session et al., 2016). Overall expression of phox2a.S is high throughout development, with the x-axis reading between 1

and 20 TPM. Phox2a.L chromosome variant is not correctly annotated and therefore not included.

Phox2a spatial and temporal expression has been previously characterized up to NF stage 35/36 (Talikka et al., 2004). A curious occurrence was observed with the RT-PCR of the *Phox2a.S* primers (Fig. 17), which is the presence of two bands in many developmental stages. Based on BLAST results, we observed that there is no significant similarity with other RNA sequences within *X. laevis* RNA (taxid:8355). Therefore, we cannot determine the nature of the second amplicon band that we observed (Fig. 17). Since *phox2a.L (long chromosome variant)* has not been annotated in *X. laevis*, we suggest that the second amplicon we observed may be the *phox2a.L* variant. However, from these results we cannot say whether the nature of the second band is a degenerated gene, which has become non-coding, or whether it might simply not have been characterized as of now. Looking at the *X. laevis* genome browser, we observed on the *phox2a.S* locus that the gene is annotated on the L Chromosome (Fig. 25). Additionally, on the *X. laevis* genome browser, we were unable to identify *phox2a.L* on chromosome S. Based on synteny results using *inppl1a.L,* we were unable to identify *phox2a.L* on chromosome S. This was due to the large number of uncharacterized genes in that region of the genome. However, when the *phox2a*.S gene was first characterized in *X. laevis*, a splice variant *Xphox2a.2* was characterized. This is identical at the nucleotide sequence level to *phox2a*.S within 5'UTR and N-terminal protein coding sequences, lacking the homeo- and C-terminal protein coding domain (Talikka et al., 2004). No real difference in spatial and temporal expression between the two variants was observed by WISH (Talikka et al., 2004). Therefore, our designed primers may have detected the *xphox2a.2* splice variant in addition to the main transcript.

The predicted size of the amplicon is 560bp, correlating with the observed lower band (Fig. 17). When performing RT-PCR with *phox2a* primers, it was found to be present nearly unanimously throughout embryonic development (Fig. 17). A strong band is observed at 1 cell stage, but not at developmental stage 10.5 or stage 14, which matches the sharp drop of RNA seq. expression of *phox2a.S* on Xenbase (Fig. 17 and Fig. 24). However, we expected to observe a band, basing on the amount of RNA present between NF stage 10.5-12 on the Xenbase dataset. We observe a weak band at NF stage 24 and no band for NF stage 27. This was

expected due to a potential problem with cDNA synthesis of this developmental stage. *phox2a* is present from late tailbud stage NF 37 until tadpole stage (Fig. 17).

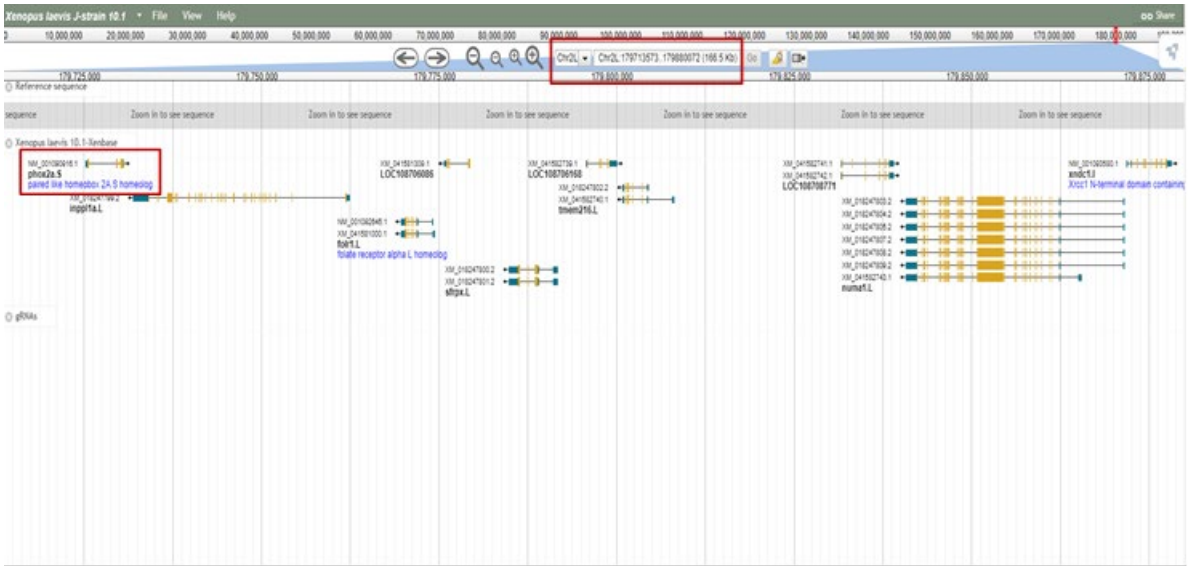

Figure 25: Screenshot of Xenopus laevis Chromosome 2L showing the position of the phox2a.S gene.
From the naming of the gene, we can notice that there was a mis-annotation in the genome browser. We further cannot identify the presence of a phox2a gene on the S chromosome.

Expression mapping of *phox2a* by WISH (Fig. 26) started from late neurula stage (NF stage 19/20) and showed a punctuated pattern of single cells at the anteroventral region of the embryo, underneath the cement gland (Fig. 26 A). Previous studies have shown that this punctuated expression of *phox2a* is first observed during neurula stage (NF stage 14/15) and was labelled as noradrenergic neurons (NA) (Wylie et al. 2015). From this point on, we decided to label these cells as NA cells, to stay in accordance with previous descriptions. These presumable NA-cells expression can be observed throughout early and late tailbud stages (NF stage 22 to NF stage 33), during which these cells seem to either migrate or are pushed by embryonic growth towards the midpoint of the dorsoventral axis of the embryo (NF stage 27 -33) (Fig. 26 A-D). Some of the NA cells can also be seen in the head region of the embryo around the branchial arches, cranial and sympathetic ganglia, which also express *phox2a* from NF stages 27 onwards (Fig. 26 B-E). These structures have previously been identified as cranial ganglia, the facial (VII), glossopharyngeal (IX) and vagus (X) nerves (Coppola et al., 2005;

Talikka et al., 2004). At tailbud NF stage 30, we also see expression in a migrating population of cells that extend from the posterior hindbrain region in a thin line past the somites and neural tube, downwards to the anterior part of the embryos body, where it extends to each side in an oval shape (Fig. 26 C). Based on this expression pattern, we presume this to be vagal NC, which will give rise to enteric neurons and ganglia. This is likely the expression we then observe at tailbud NF stage 40 (Fig. 26 E), where we can see a line of expression following the vagal nerve (vn), which we assume are migrating NCCs. The individual cells that are extending from this linear expression along the vn, likely form enteric neurons. At tadpole stage 45 (Fig. 26 F), we no longer observe expression of our NA cells, migrating NC cells or enteric neurons. However, we still observe expression in the presumed locus coeruleus (LC) and a cranial ganglion. The expression observed from NF stage 40 is discussed in further detail in section 3.6.

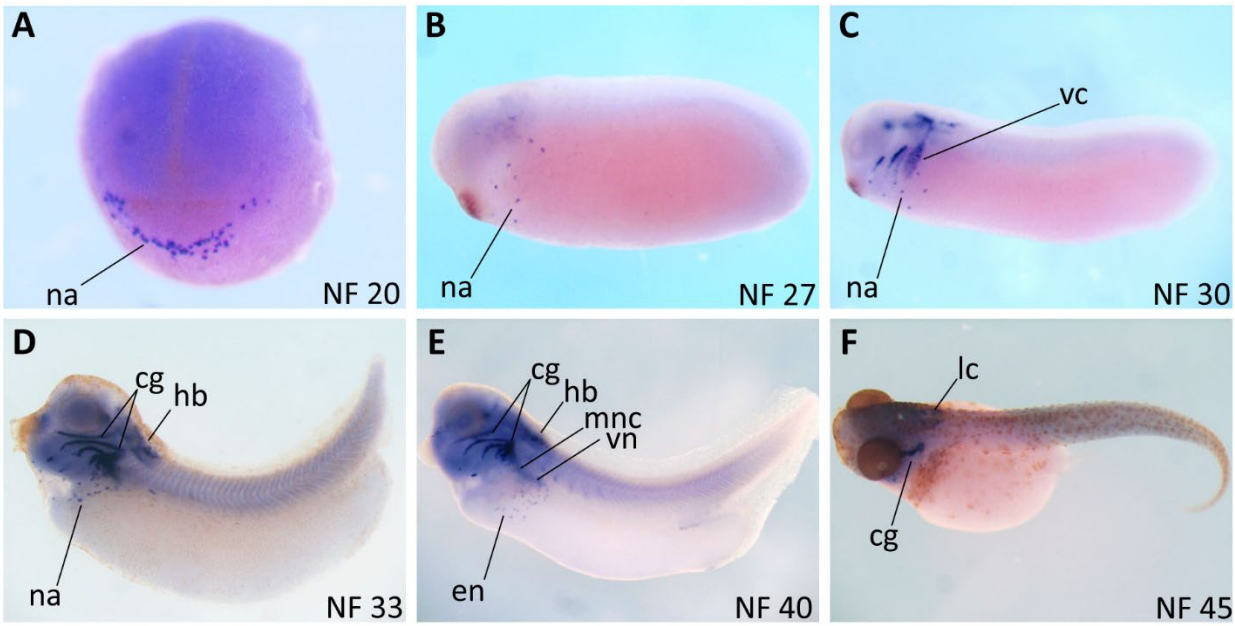

Figure 26: The spatial and temporal expression pattern of phox2a during Xenopus laevis embryogenesis.
Embryos are presented in lateral view with anterior to the left and posterior to the right. Phox2a is expressed in numerous individual cells below the cement gland, labelled as NA cells (A). The NA cells become less numerous and more interspersed (B, C) at tailbud stages and then cluster below the branchial arches at late tailbud stage (D). NA cells are not found after late tailbud NF 33 (E, F). Phox2a is also strongly expressed in migrating vagal neural crest cells (C) and various cranial ganglia (C-F). Expression is also strong in the hindbrain (C-E), and in the locus coeruleus (F). From late tailbud (E), migrating neural crest cells are seen moving along the vagal nerve. From this location, single cells are seen extending out from the expression, likely giving rise to enteric neurons along the GI tract. Cg, cranial ganglia; En, enteric neuron; hb, hindbrain; lc, locus coeruleus; mnc, migrating neural crest; Na, noradrenergic neuron; vc, vagal crest.

3.3.3 Phox2b

The *phox2b* gene is a TF vital for the development of most central and peripheral noradrenergic neuron populations in vertebrates and often described as the master regulator of the SA lineage, specifically of CCs and neurons of the peripheral nervous system (Manethova et al., 2023). Both *phox2* genes are homeodomain TFs, meaning they function as regulators of the expression of various genes involved in development and cell differentiation due to their highly conserved DNA binding homeodomain (Duverger and Morasso, 2008). As mentioned above, both *phox2* genes are expressed in all autonomic ganglia and within the

CNS, they are involved in the development, specification, and migration of neurons of the locus coeruleus, branchial and visceral motor neurons of the brainstem and for oculomotor and trochlear nuclei in the isthmus region (Coppola et al., 2005; Vermeiren et al., 2020).

When *phox2b* is absent, both the development of CCs and sympathetic neurons ceases early on in embryogenesis (Huber, 2015; Pattyn et al., 1999). Furthermore, due to its key involvement of visceromotor neurons located in ganglia of the sympathetic, parasympathetic and ENS, absence of *phox2b* leads to the absence, or drastic reduction, of these NC derived structures as well (Vermeiren et al., 2020).

The *PHOX2B* gene has been identified to play an essential role in the predisposition to the childhood malignancy neuroblastoma (Mosse et al., 2004). *PHOX2B* alterations were found to be a significant factor in the initiation of neuroblastoma tumorigenesis, particularly in patients with NC derived diseases, such as congenital central hypoventilation syndrome (CCHS) and Hirschsprung Disease. These were much more likely to develop this tumour (5-10%) compared to the general population (0.01%) (Barr and Applebaum, 2018; Rohrer et al., 2002). *PHOX2B* mutations are present in 6-10% of familial neuroblastoma cases and occur in about 2% of sporadic cases of neuroblastoma (Barr and Applebaum, 2018).

Although, *phox2b* has been previously characterized in *Xenopus*, mostly in the development of placodal-derived cranial nerves (Talikka et al., 2004), no thorough WISH experiments mapping of *phox2b* expression exists. *Phox2b*, based on its key role in CC development in mammals, was determined as an essential gene to analyse for this project.

The *phox2b* gene was isolated by PCR and primers were designed for the L chromosome variant (800bp) as the TPM expression was slightly higher in the RNA seq. Dataset on Xenbase (Fig. 17) and WISH probe for *phox2b* were generated by PCR as described in the methods chapter.

RNA-seq. expression of *phox2b.L* in *X. laevis* begins and peaks at Blastula (NF stage 9) with 9.37 TPM, after which it falls to its lowest expression level at Neurula (NF stage 15) with 1.68 TPM (Fig. 27). From early tailbud to late tailbud, expression levels have an increasing trend,

the highest here being at 4.12 TPM at late tailbud (NF stage 35/36) after which they begin to drop again (Fig.27).

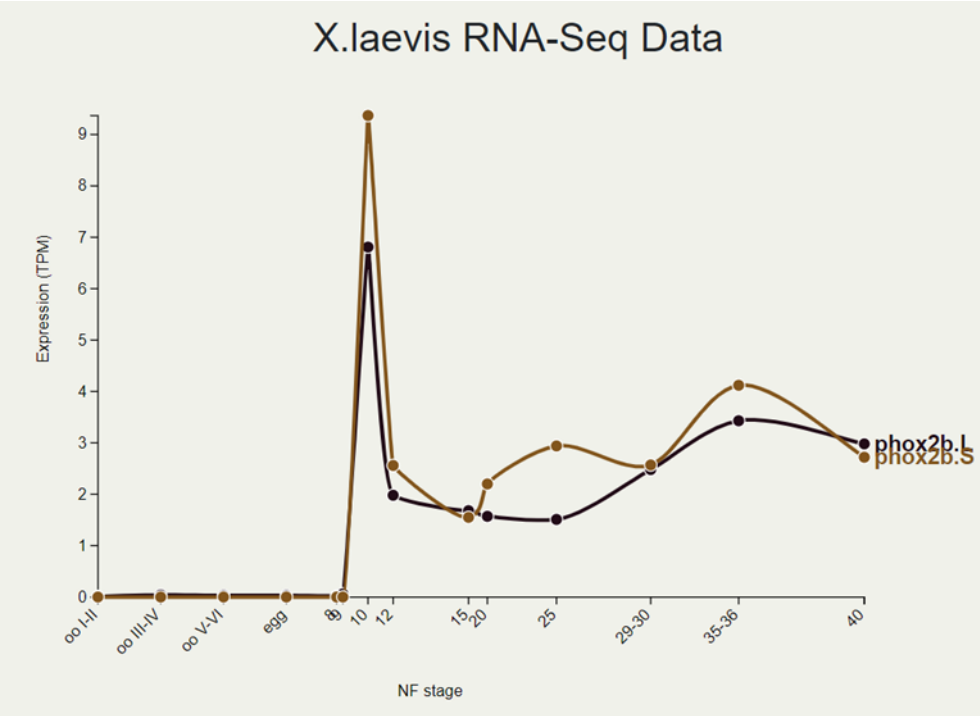

Figure 27: RNA sequencing data of phox2b
Graph is showing expression in transcripts per million (TPM) on the Y-axis and the developmental stage of measured expression on the X-axis taken from Xenbase (Session et al., 2016). Expression ranges from 0.0-10 TPM. Overall, phox2b.L variant seems to be expressed slightly more during developmental time-points and was therefore used for making the WISH probe.

WISH for *phox2b* at Neurula (NF stage 20) shows specific expression at either side of the anterior neural tube (Fig.28 A). This is probably in the region that will give rise to the hindbrain. Excitingly, we also observed the characteristic punctuated single cell expression that was observed previously with *phox2a* (Fig. 26 A and Fig. 28 A). Again, noradrenergic (NA) cells are situated at the anteroventral side of the embryo, just beneath the cement gland and can be seen expanding toward the midline of the ventral embryo at early tailbud (NF stage 20 and NF24) (Fig. 28 A and B). At tailbud (NF stage 30), these cells have again become more interspersed along the anteroventral side of the embryo. There is also strong expression in the

hindbrain, although at this stage, there is much background noise, making it hard to further distinguish structures that may express *phox2b,* at this developmental stage (Fig. 28 C). During late tailbud (NF stage 33), expression of *phox2b* is still strong in the single NA cells, although they have become less frequent, and can also be found in numerous other structures in the head (Fig. 28 D). These include expression in the hindbrain, in the cranial ganglia, including IX and X (glossopharyngeal nerve, vagus nerve) and the anterodorsal ganglia (behind the eye) as described previously (Talikka et al., 2004). During late tailbud growth (NF stage 40), expression is seen along the vagal nerve (Fig. 28 E). Expression in these cells seem to extend outwards of this line, appearing to move downwards along the ventral side of the body. The further the line of *phox2b* expression at the vagal nerve extends towards the ventral midline, the further these elongated single cells spread across the anterior to mid-body within the outer endoderm (Fig. 28 E, MNC). This expression, seen at developmental NF stage 40, is nearly identical to the expression we observed with *phox2a* at the same developmental timepoint (Fig. 26 E and Fig. 28 E). Again, based on the importance of the *phox2* genes in the development of the ENS, the neurons and ganglia, we hypothesise that we see migrating neural crest cells along the vagus nerve, that differentiate and give rise to neurons and ganglia along the gastro-intestinal tract. At this stage of development, *phox2b* expression also becomes visible in the dorsal root ganglion (DRG), while the expression in the hindbrain and cranial ganglia is still strong (Fig. 28 E). However, we can only see expression of very few NA cells just below the branchial arches. At tadpole NF stage 45 (Fig. 28 F), NA cells are no longer visible, but we can see expression of enteric neurons across the GI tract of the tadpole, and we also see expression along the vagus nerve or in proximity to the pronephric duct.

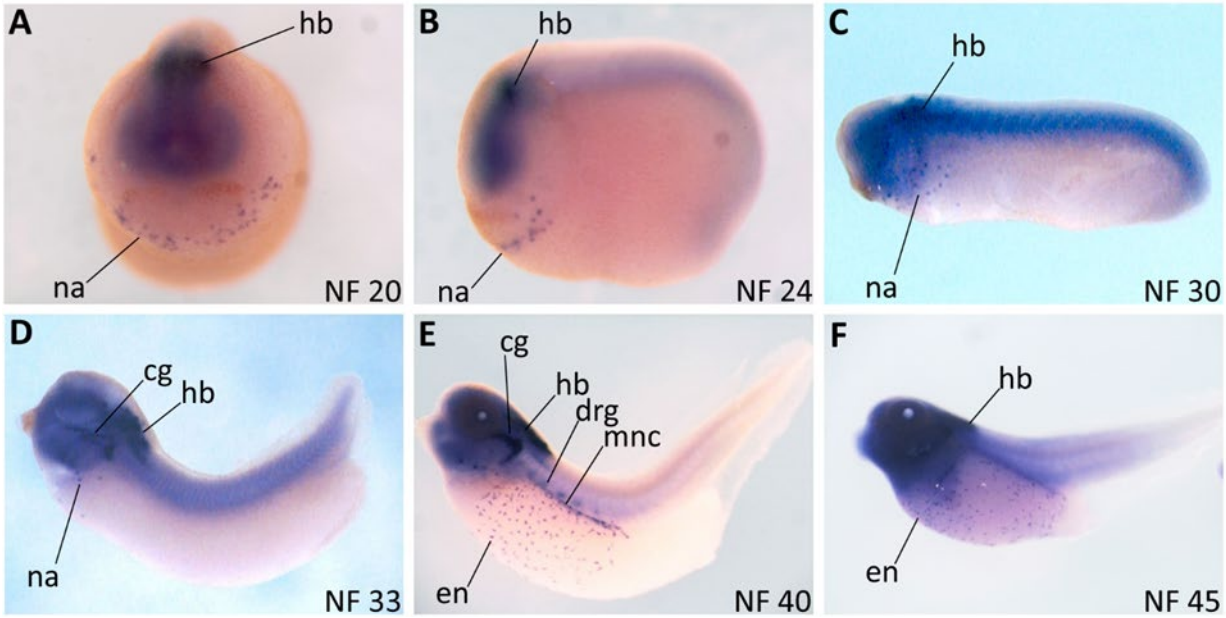

Figure 28: Spatial and temporal expression map of SA marker gene phox2b during X. laevis embryogenesis.
Embryos are positioned in lateral view, with the anterior to the left side and posterior to the right. NA cells are found from late Neurula (A) at the anteroventral side. NA cells then appear on either side of the cement gland at tailbud stage (B) and are found behind the branchial arches, across the anterior body of the embryo (C). NA cell become less interspersed and frequent in number just below the branchial arches (D, E) and are no longer expressed at tadpole stage (F). Expression of phox2b is strong throughout development in the hb (A-F), and in cranial ganglia, cg (D, E). From late tailbud we see expression of migrating neural crest cells (mnc) along the vagal nerve (E, F), giving rise to enteric neurons (en) and ganglia. Cg, cranial ganglia; drg, dorsal root ganglion; en, enteric neuron; hb, hindbrain; mnc, migrating neural crest; na, noradrenergic neuron.

3.3.4 *Insm1*

Insulinoma associated 1 (INSM1) is a zinc-finger TF that functions as a neuroendocrine specific transcriptional regulator, which is highly conserved in various species (Lan and Breslin, 2009). INSM1, is primarily expressed in the developing neuroendocrine tissue and nervous system of mammals, where it plays a crucial role in their differentiation and maturation of embryonic neurogenesis (Mahalakshmi et al., 2020). These neuroendocrine tissues include endocrine cells of the pancreas, pituitary thyroid and parathyroid, pineal gland, the GI-, and respiratory endocrine system as well as of the SA lineage (Lan and Breslin, 2009). INSM1 is essential also for orchestrating various aspects of neuronal differentiation during development, such as the

early differentiation of sympathetic neurons, sensory neurons of the DRG, and olfactory neurons (Chen and Lan, 2022; Wildner et al., 2008). Furthermore, INSM1 is found to be often (over)-expressed in neuroendocrine tumours, and has become a useful marker for neuroendocrine tumour diagnostics as well as being a potential novel biomarker for neuroblastoma (Chen and Lan, 2022; Maleki et al., 2021). Of particular significance for this project is the role of INSM1 in CC development within the AM. *Insm1*-deficient mice show a delay in CC development and proliferation, which later proved lethal in foetal mice (Wildner et al., 2008). In particular, Insm1-deficient mice show a down-regulation of *Pnmt* and *Chga*, two crucial markers for successful CCs development and adrenaline synthesis (Wildner et al., 2008) (See sections 3.4.1 and 3.4.3). During *X. laevis* embryogenesis, *insm1* expression has been shown to be regulated by *phox2* and *hand2* and is likely recruited by Ascl1/Mash-1 to support endocrine differentiation of CCs (Parlier et al., 2008).

In *Xenopus*, *insm1* mRNA expression has previously been shown during embryogenesis from NF stage 13 to NF stage 24 in neural plate primary neurons (Parlier et al., 2008). Additionally, expression is detected in the uncharacterized punctuated cells beneath the cement gland by lab members of Dr. Eric Bellefroid, who also provided this plasmid to us (*insm1.L*) (Parlier et al., 2008). Furthermore, expression has been shown in the retina and brain of tadpoles and in WISH on isolated dorsal and ventral pancreatic buds, where it was found to be essential for specification of GI and pancreas endocrine cells (Horb et al., 2009). However, there is no full spatial and temporal expression map of *insm1* during embryogenesis in X. *laevis*, while its involvement in AM development (assuming chromaffin cells) has been suggested but not proven (Parlier et al., 2008).

Looking at the RNA-seq. data set on *insm1* in *X. laevis*, expression is high throughout development from NF stage 1 until NF stage 40, ranging from 13.2 to 44.6 TPM (Fig. 29). From NF stage 9, expression rises to its peak at NF stage 29/30 after which it settles at 35.38 TPM. When comparing the RNA-seq. expression of *insm1* to our RT-PCR data of *insm1*, *insm1* is again highly present continuously from NF stage 10.5 until tadpole stage NF 45 (Fig. 17). Only at NF stage 37, *insm1* detection was low, which might be explained by the slight dip in RNA-seq. expression of *insm1* at the same developmental stage (Fig. 17 and Fig. 29).

To characterise the expression pattern of *insm1* in *Xenopus* and its possible role in CC development, we mapped the spatial and temporal expression profile from late Neurula (NF stage 19/20) through to tadpole stage (NF stage 45).

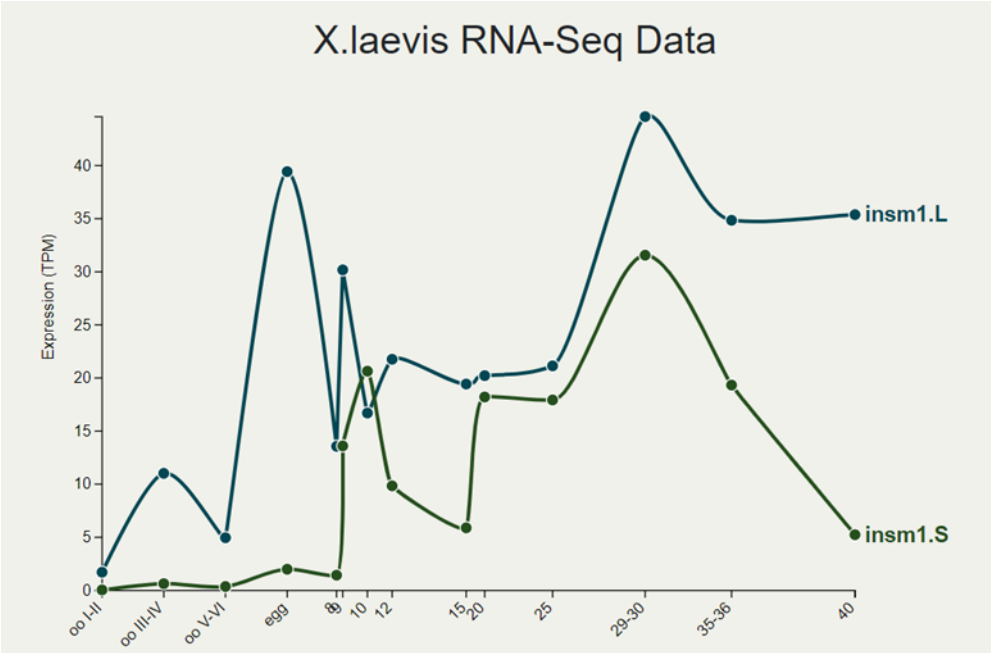

Figure 29: RNA expression analysis of insm1 chromosome variant L and S from to late tailbud NF stage 40 taken from Xenbase (Session et al., 2016).
Insm1 is continuously expressed throughout embryogenesis, with its highest peak at NF stage 29/30. Overall, the insm1.L variant is found to have a higher expression than the S variant. Expression is high throughout development, with expression reading from 0.0 to over 40 TPM.

As previously shown by Parlier and colleagues (Parlier et al., 2008), neurula embryos show punctate cells just below the cement gland, similarly as described in our SA markers at this developmental stage (Fig.26 and Fig. 30 A). Additionally, *insm1* expression at this stage is seen in many structures, such as olfactory and optic placode, in the brain (forebrain/midbrain border), in migrating NCCs, and along the neural tube. At early tailbud (NF stage 24), the NA cells have expanded more dorsally within the embryo above the cement gland (Fig.30 B). Strong expression is also seen in the optic field, olfactory placode, the midbrain, forebrain , in migrating cranial NC as well as in the hindbrain (HB) and along the neural tube. At NF stage 30, the NA cells have become less frequent and are also found interspersed along the midline of the dorsal and ventral side of the embryo (Fig.30 C). No NA cells are found in the head of the embryo. Strong expression is observed in the hindbrain and forebrain, the optic field

(presumptive lens, PL) and in cranial ganglia (likely trigeminal ganglion) (CG). Expression is also observed in the pineal gland (PI) (Fig. 30 C).

From NF stage 33, NA cells have become sparse, located posterior to the branchial arches, between the area of the pronephros and the heart field (Fig. 30 D). At this developmental stage, expression is observed along the pronephric tubule and the head region of the pronephros. Strong expression is seen in the forebrain, midbrain, hindbrain, neural tube, and optic field as well as in cranial nerves (Fig. 30 D). At late tailbud (Fig.30 E) the expression along the pronephric tubule has become shorter and intermitted. Elongated and isolated cells, stained within the outer side of the endoderm have appeared, and seemingly stem from this intermitted line expression along the pronephric tubule of the embryo. These cells are likely migrating NCCs that move along the vagus nerve as described for both *phox2* genes at the same developmental stage (Fig. 26 and 28 E). Finally, at NF stage 45, individual cell expression is seen across the whole gut of the tadpole (Fig. 30 F). As *insm1* has been shown to give rise to endocrine cell of the GI tract (Horb et al., 2009), we assume that this is the expression pattern observed.

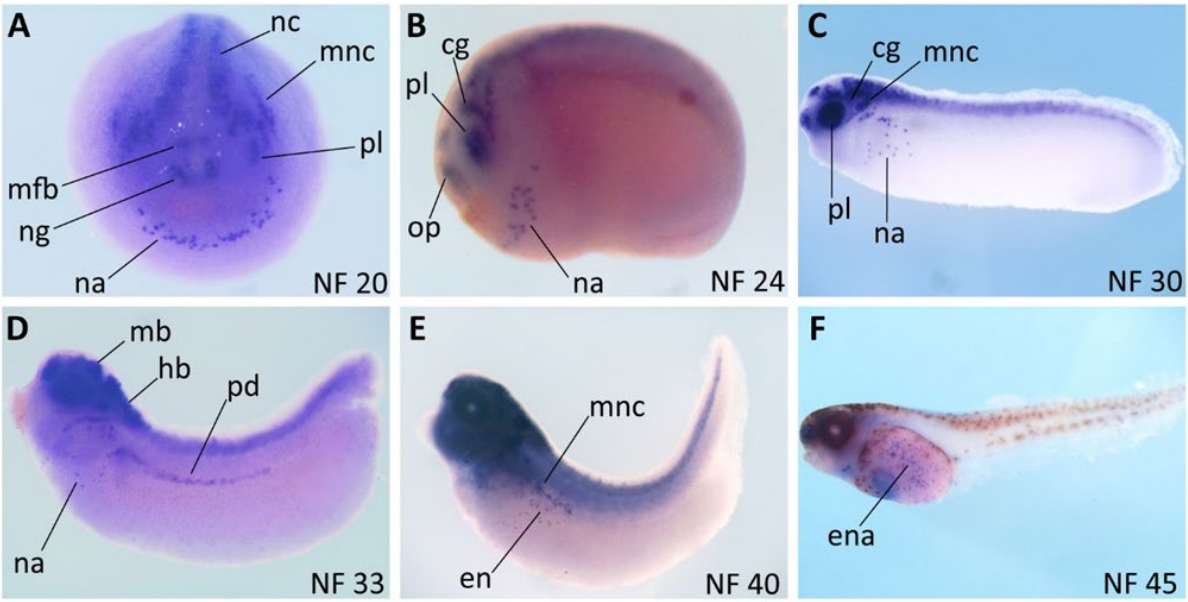

Figure 30: Temporal and Spatial expression analysis of insm1 during X. laevis embryogenesis by WISH.

Embryos are presented in lateral view with anterior to the left and posterior to the right. Insm1 expression is found within a variety of structures within the embryo throughout development. At late Neurula, expression is seen in NC and MNC as well as in the NA cells again located in front of the cement gland and many structures in the head (pl, mfb, ng) (A, B). Noradrenergic cells are found closer to the midline of the embryo at NF stage 24 (B) and are centrally located in the embryo at NF stage 30 (C). After few cells are left anterior to the branchial arches at NF stage 33 (D), no expression of NA cells is observed at NF stage 37 (E). At this stage, migrating NCCs are seen along the vagal nerve, and expression of enteric neurons is found extending from the vn across the midline of the embryo. At NF stage 45 (F), numerous individual cell expression was found across the GI tract of the tadpole, likely expressing in NA cells of the GI tract and pancreas. Cg, cranial ganglia; en, enteric neurons; ena, enteric noradrenergic neuron; hb, hindbrain, midbrain – forebrain; mnc, migrating neural crest; na, noradrenergic neuron; nc, neural crest; ng, neural groove; op, optic placode; pd, pronephric duct; pl, presumptive lens.

3.4 Characterisation of chromaffin cell markers during *Xenopus* development by WISH

3.4.1 Chga

Chromogranin A (CHGA) belongs to the chromogranin/secretogranin family and is located within the secretory granules of CCs. Here, CHGA is co-stored and co-released with

catecholamines adrenaline and noradrenaline (D'amico et al., 2014). Chromogranin expression correlates with the number of secretory vesicles present in neuroendocrine cells (Gut et al., 2016). CCs have gained their name from a particular characteristic to these cells; when staining them with chromium salts (potassium dichromate or chromium trioxide), they exhibit a distinct brown or yellowish coloration due to the presence of catecholamines in the abundant secretory granules found within CCs (Diaz-Flores et al., 2008). Chromogranin A was named for being first discovered within the chromaffin granules of the AM (D'amico et al., 2014). While the presence and function of CHGA in the AM of mammalian species has been known for decades, this is not the case for lower vertebrate species. In zebrafish the presence of the *chga* ortholog was found to be spatially separate from genes expressed in the pronephros, the AC, and the SA neurons/CCs expressing *dbh*, even 7 days post fertilisation (dpf) (Xie et al., 2008). In *X. laevis*, *chga* was shown to be expressed both in GI-, and pancreatic endocrine cells of isolated whole gut and pancreas tissue during late tailbud stage of embryogenesis (Horb and Horb, 2010). However, *chga* has not been previously used in *Xenopus* to characterize CCs of the AM, and no spatial and temporal expression map of *chga* in wholemount of *Xenopus* embryos exists.

Chga was chosen as a potential specific marker for pinpointing the location and development of CCs of the AG in *Xenopus*.

Chga expression in *Xenopus* has not been well characterized and has only been described by WISH in endocrine cells of isolated whole gut tissue of late tailbud stages (Horb et al., 2009). The plasmid containing *chga*, chromosome variant S, was kindly gifted to us by Dr. Marko Horb. There is no existing RNA-seq. data of *chga* on Xenbase for *X. laevis* but is available for *X. tropicalis*. Based on results of the RT-PCR on key stages of *X. laevis* embryonic development, *chga* was found to be present in low levels in 1 cell stage embryos (Fig.17). *Chga* is then highly present from late Neurula NF stage 20 to tadpole stage NF 45. No expression was found at NF stage 27, but this seems to be an error in the obtaining of the cDNA at this stage of development and should be repeated in future experiments (Fig. 17).

Mapping of expression of the *chga* transcripts by WISH began at late Neurula/early tailbud stage (NF stage 19/20), where a strong pattern of numerous punctuated individual cells was

observed just beneath the cement gland (Fig. 31 A). This pattern was remarkably alike to that of previous characterized marker genes *phox2a, phox2b and insm1* (Fig. 26, 28 and 30 A). Additionally, expression was detected along the neural fold in the region of the developing hindbrain (Fig. 31 A). At tailbud NF stage 27, NA cells have become more interspersed and fewer in number. At this stage, expression in the hindbrain, and just behind the eye is detected, though it is unclear if this is otic placode, vesicle or a specific ganglion (Fig. 31 B). We see a similar picture just a few stages later, at NF stage 30 (Fig. 31 C), where we see more NA cells present across the anterior body of the embryo. At late tailbud stage (NF stage 33), expression is strong along the neural tube, the pineal gland and in the NA cells, which are positioned more centralized in the embryo (Fig. 31 D). At NF stage 40, these cells have become fewer in numbers and are clustered together in the region above the heart and beneath the pronephros (Fig. 31 E). Expression is still present in the pineal gland and in the hindbrain. Based on the literature of *chga* expression in zebrafish (Xie et al., 2008), the clustered structure between the head and beginning of the somites is likely to be the superior cervical ganglion (SCG), providing sympathetic innervation to the head. At pre-metamorphic tadpole NF stage 45, NA cells are clustered at a point in the gastrointestinal tract, which also contains endocrine CCs (Fig. 31 F). Expression in the pineal gland and hindbrain is also strong.

This pattern of individual cells like the ones we have reported for *phox2a* and *phox2b* has not been described yet for *chga* neither in *Xenopus* nor in *Dario rerio*.

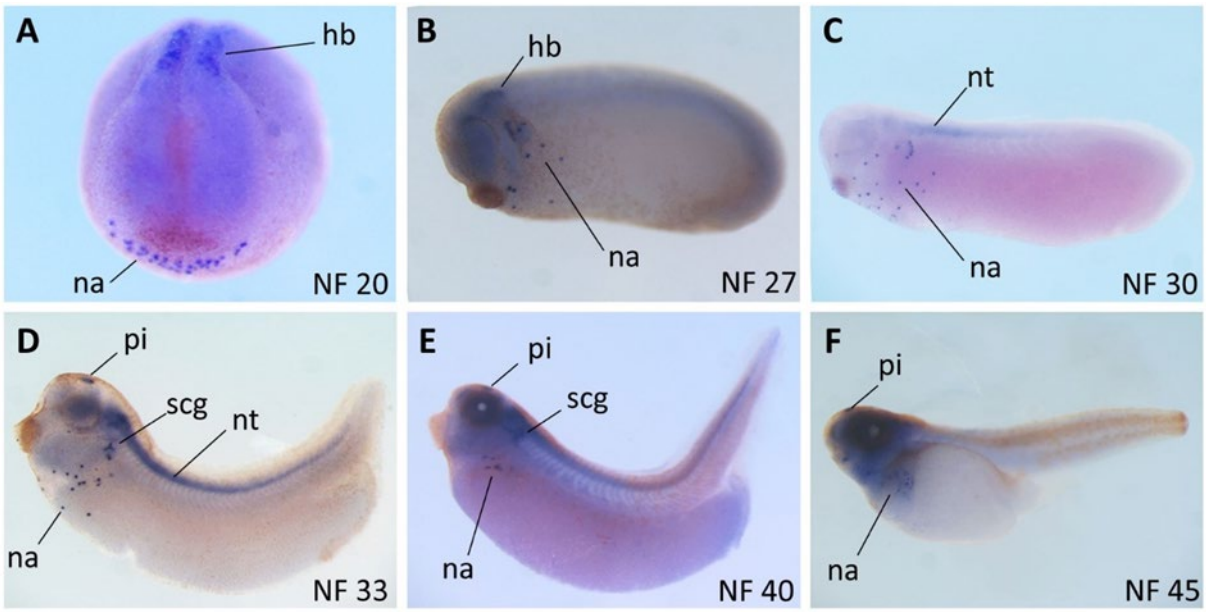

Figure 31: Spatial-temporal expression of chga mRNA by WISH from late Neurula (A) to tadpole (F).
Embryos are shown in the lateral view, with anterior to the left (A-F). At late Neurula, NA cells are expressed at the dorsoventral side (A) and during progressing stages of development move toward the centre of X. laevis embryos in an interspersed fashion (B-D). At late tailbud (E), na cells have clustered closer together beneath the head. At tadpole stage (F), expression of chga is seen in individual cells within the gut but nowhere else. Chga is expressed strongly in the neural tube (C, D) as well as in the pineal gland (D-F) and the hindbrain (A, B, D-F). na, noradrenergic; hb,hindbrain; nt,neural tube; pi,pineal gland; scg, superior cervical ganglion.

3.4.2 Dbh

Dopamine-beta-hydroxylase (DBH) is a vital enzyme in the biosynthesis of catecholamines noradrenaline and adrenaline, catalysing the conversion of dopamine to noradrenaline. Both the expression of *Dbh* and *Th (Tyrosine hydroxylase)* are used as markers in chick, mouse, and zebrafish to characterize the differentiation of the peripheral sympathetic nervous system (PSNS) and CCs of the AM, marking the acquisition of the noradrenergic neurotransmitter phenotype which is characterized by the expression of noradrenaline (Ernsberger et al., 2000; Filippi et al., 2010). Phox2a further acts as a critical positive regulator of *Dbh* expression, as it is required for the expression of both *Th* and *Dbh* (Hirsch et al., 1998; Huber, 2015) In zebrafish, *dbh* expression is initially detected in the superior cervical ganglion at 2 dpf, slightly after the first expression of *th* in the same complex. At 28 dpf, mature CCs express both *th* and *dbh* in

the anterior head of the kidney (An et al., 2002). *Dbh* in the CNS is exclusively expressed in the locus coeruleus and the medulla oblangata in zebrafish larval and juvenile brain (Filippi et al., 2010).

Expression of *dbh* has not been previously characterised by WISH in *Xenopus*. The mRNA WISH probe was generated in the Wheeler lab by cloning. Primers were designed as described in section 2.5.1 for the S chromosome variant. RNA-seq. data on Xenbase (Data from Session et al. 2016) for S chromosome *dbh* shows that *dbh* is present throughout *Xenopus* embryonic development starting from NF stage 10 up until NF stage 40, but expression is low (between 0.2 and 2.0 TPM) compared to the expression of other markers (Fig. 32). After first detection around NF 10, there is a sharp rise from NF stage 15 and reaches the maximum expression of 2.0 TPM at NF stage 24 until NF stage 30, after which expression begins to slowly decrease (Fig. 32).

Our RT-PCR results of *dbh* matches well with the just described RNA-seq expression of *dbh* in X. *laevis*. *Dbh* presence is first detected at NF stage 10.5 and seems to be highly present from NF stage 14 through to NF stage 33, after which, *dbh* is no longer detected (Fig.17). Again, no presence of *dbh* is detected at NF stage 27, which again is likely due to a mistake in cDNA collection of this developmental stage and needs to be repeated in future experiments.

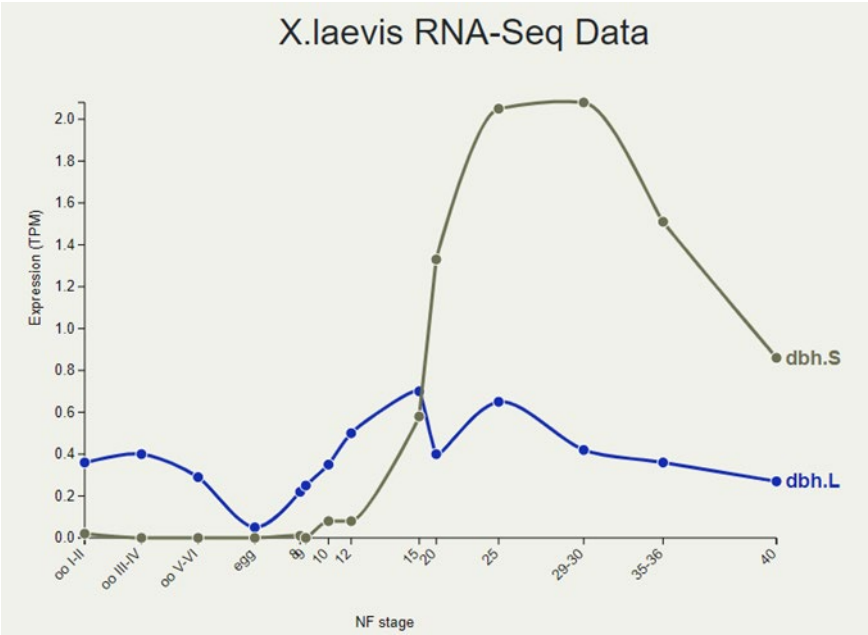

Figure 32: Expression analysis of dbh RNA sequencing data during Xenopus laevis embryogenesis taken from Xenbase (Session et al., 2016).
Dbh chromosome variant S is expressed more and was therefore chosen for making the riboprobe. Dbh RNA expressions starts to rise from NF stage 15 and peaks at NF stage 29-30.

As seen with the other markers, WISH on late neurula embryos (NF stage 20) with *dbh* reveals strong expression of numerous single cells (NA cells) at the anteroventral side of the embryo, again beneath the cement gland (Fig. 33 A). At early tailbud (NF stage 24), the *dbh* expressing cells begin to move/expand away from the anteroventral side and up towards the midline (Fig. 33 B). Numerous NA cells expressing *dbh* are seen across the anterior embryonic body at NF stage 30 (Fig. 33 C). At tailbud stage (NF stage 33), NA cells show strong expression and have again become dispersed and less in numbers (Fig. 33 D). Some cells can be seen in the head of the embryo, beneath the forming eye, while the vast majority are in the anterior part of the embryo's body between the spine and the heart field. At late tailbud (NF stage 40) the NA cells have again clustered together, as seen with *chga* expression (Fig. 33 E), at the anterior body in the region of the embryonic heart and the pronephros. The shape of the NA cells has also changed from well-rounded, frequently occurring individual cells to an elongated shape of individual cells, that are less in number (Fig. 33 E). At this stage of development, further expression is observed in the hindbrain (likely the locus coeruleus), in some cranial ganglia and DRG. A few cells express *dbh* next to the eye at this stage. At pre-metamorphic tadpole

stage NF 45, very few NA cells are still expressed in the anterior body, while expression in the hindbrain is strong and some expression is still observed in the DRG and in the pronephros region (Fig. 33 F).

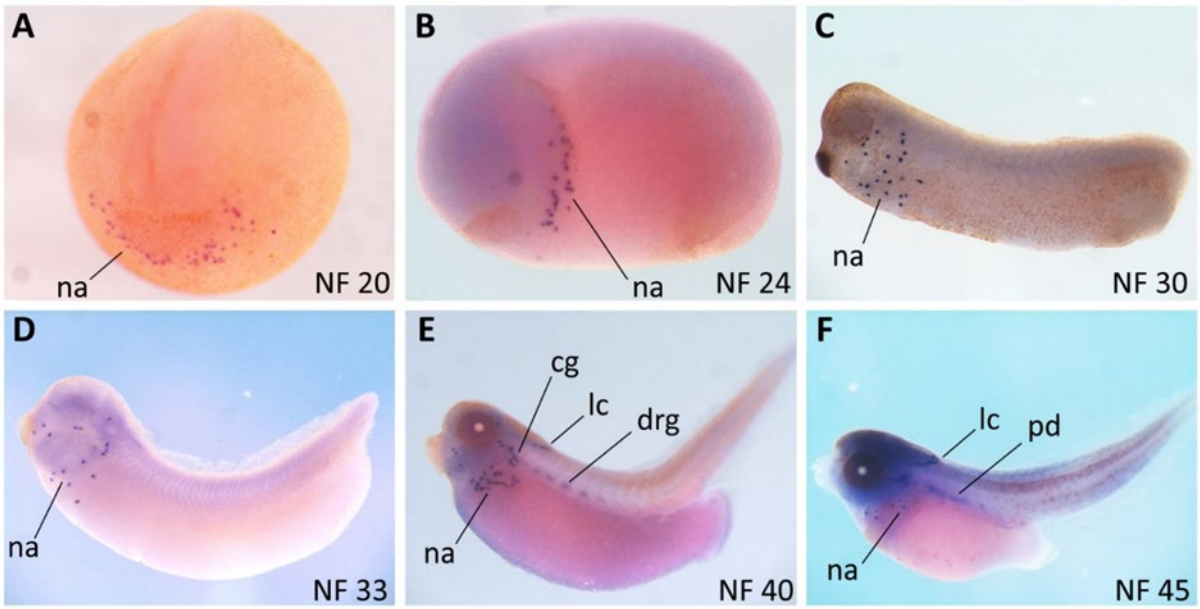

Figure 33: Spatial and temporal expression of dbh mRNA in X. laevis by WISH from late neurula to tadpole.
Anterior view of late Neurula embryo shows expression of numerous individual na cells as described for previous CC markers at the anteroventral side beneath the cement gland (A). Lateral view of early to late tailbud stage embryos show na cells moving toward the centre of the xenopus embryos and become more interspersed (B-E). At NF 33, some individual cells group together (D) just beneath the otic vesicle (ov) and form cranial ganglia (cg) visible at NF 40 (E). At this stage, some na cells are also present in the head. At NF 40, na cells again cluster together beneath the head and above the heart region of the embryo and cells are no longer well rounded but seem to have elongated. At tadpole stage (NF stage 45, F), we observe expression of a few na cells beneath the head and expression along the region of the pronephric kidney. Expression of dbh mRNA is further detected in the hindbrain (hb), likely the locus coeruleus (lc), from late tailbud to tadpole (D-F), and in the drg (E). Cg, cranial ganglia; drg, dorsal root ganglia; lc, locus coeruleus; na, noradrenergic neuron; pd, pronephric duct.

3.4.3 Pnmt

The gene *Phenyl ethanolamine N-methyltransferase* (*PNMT*) serves as a marker for adrenergic function. The enzyme PNMT is responsible for catalysing the conversion of noradrenaline to adrenaline, a key step in the synthesis of the stress hormone adrenaline within CCs of the AM

(Wong, 2003). The synthesis of adrenaline by PNMT is essential for the "fight-or-flight" response, a fundamental physiological reaction to stress (Watts et al., 2021). In humans, adrenomedullary CCs are mainly responsible for the production, storage and release of the hormone (>95%) into the bloodstream (Berends et al., 2019). Expression of *PNMT* outside of the AGs is restricted to a few neurons within the CNS.

Adrenergic cells are easily identified by immunohistochemical staining for PNMT, where they make up roughly 80% of total CCs in rats and mice, and nearly a 100% in humans (Wong, 2003). In zebrafish, *pnmt* expression has been used to label CCs within the interrenal gland. Chromaffin-like cells, which are *th* and *dbh* double positive, are found migrating to the interrenal gland from the SCG at 2 dpf (Morrison et al., 2016). At 3 dpf, *pnmt*/*th* double positive cells were found at the SCG, which suggests that CCs are specified before migration to the kidney (Morrison et al., 2016). Complete maturation of sympathetic ganglia and CCs in zebrafish is reached at 28 dpf (An et al., 2002). Not much detail is provided on how exactly these cells develop and shape between 3 dpf and 28 dpf. However, *pnmt* expression seems to be difficult to locate in zebrafish and has not been well characterized. Also, *pnmt* spatial-temporal gene expression has previously not been characterized in *Xenopus*.

WISH on *pnmt*, was carried out with probes generated by cloning from PCR products as described in section 2.5.1. Primers were designed for the L chromosome variant. The *X. laevis* RNA sequence dataset on Xenbase reveals a general low expression (TPM) of *pnmt* throughout embryonic development. *Pnmt* expression levels first rise steadily from NF stage 1 (where expression starts out at 1.01 TPM) until NF stage 9 where it reaches peak expression of 3.55 TPM (Fig. 34). By NF stage 12 throughout NF stage 15, expression drops to nearly 0. A small rise in expression happens at NF stage 20 to 1.52 TPM and stays at similar expression levels until NF stage 29/30 where it starts to drop off again to 0.42 TPM at NF stage 35/36. At NF stage 40, expression levels are at 0.81 TPM (Fig. 34).

Pnmt was found to be present by RT-PCR in low levels at late neurula and tailbud NF stage 24, absent again in NF stage 27, as well as in NF stage 33, and present throughout late tailbud NF stage 37 to tadpole NF stage 45 (Fig. 17).

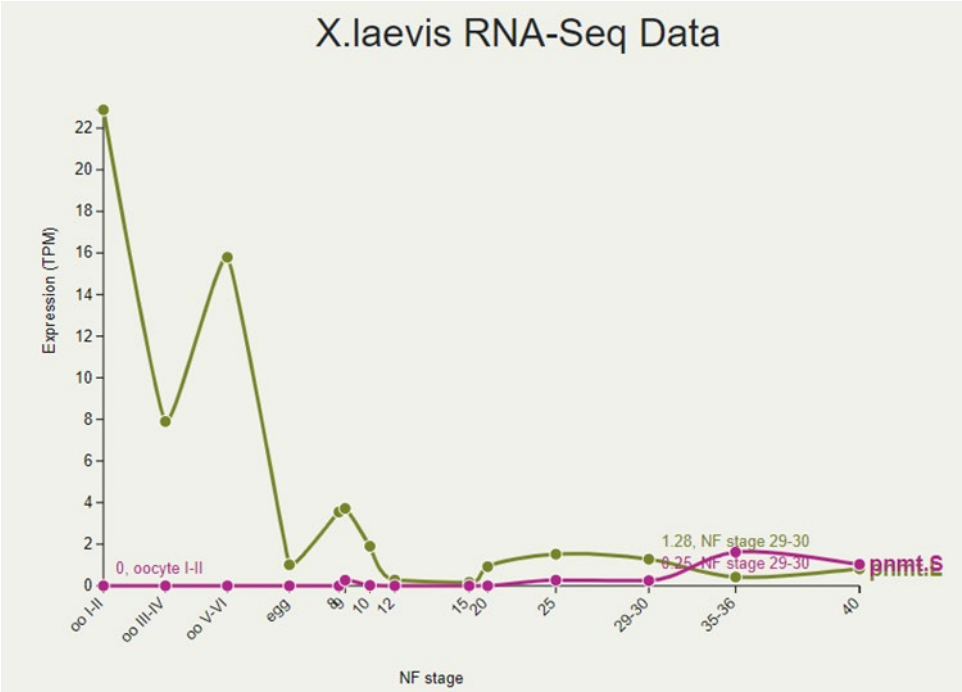

Figure 34: Expression analysis of pnmt RNA in Xenopus laevis during embryogenesis taken from Xenbase (Session et al., 2016).
Expression is measured between 0.0 and 22 TPM. Overall, pnmt levels for both chromosome variants are relatively low throughout development, whereas pnmt.L variant shows a slightly higher expression overall and was therefore chosen for creating a riboprobe.

Mapping of *pnmt* expression took place at late neurula, but no expression was found this early in development (not shown). At tailbud (NF stage 27), *pnmt* expression is observed in the characteristic punctuated single cell expression. These cells are seen at the anteroventral side of the embryo, beneath the cement gland, and along the anterior body of the embryo, around the ventral to dorsal midline (Fig. 35 A-C). Some NA cells are also located in the head, just below the branchial arches, while a few cells are located towards the dorsal side of the embryo, behind the eye field and around the anterior somites. At late tailbud (NF stage 33), expression in NA cells have become sparse and the remaining cells are mainly located in the anterior body endoderm (Fig. 35 C). At this stage, expression of *pnmt* is first observed in a specific structure in the hindbrain regions. After NF stage 33, *pnmt* expression is only observed

in a structure in the hindbrain, which we provisionally suggested to be the locus coeruleus (LC), and nowhere else (Fig. 35 D, E).

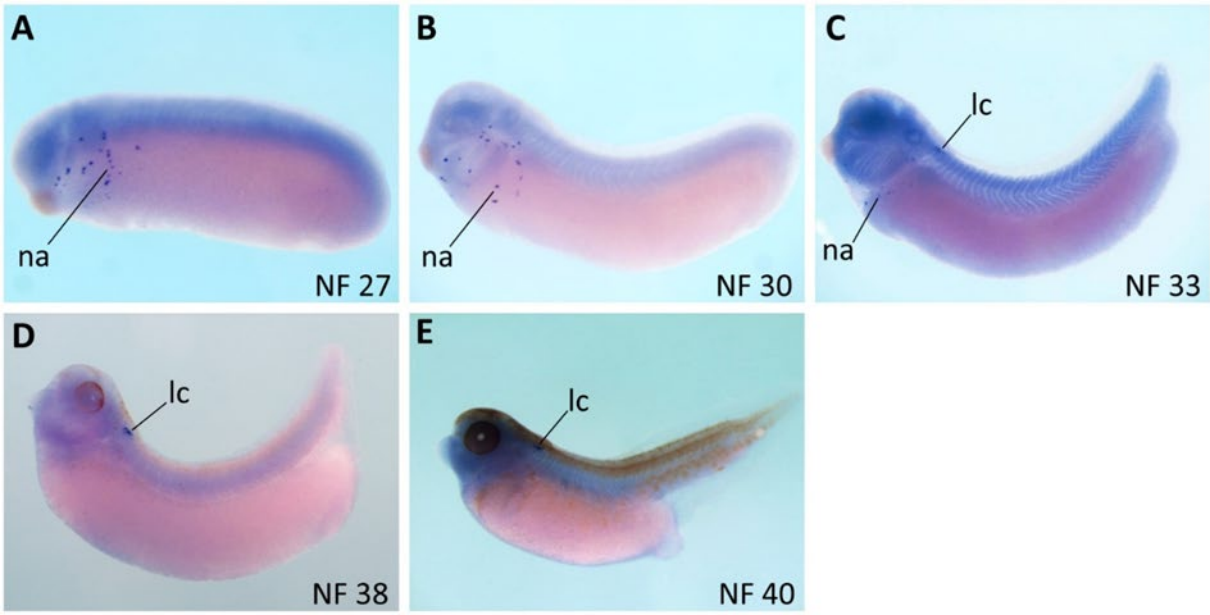

Figure 35: Spatial-temporal expression of pnmt mRNA during X. laevis embryonic development by WISH.
Embryos are arranged with the anterior side to the left and the posterior to the right and all embryos are imaged ventrally. Expression of pnmt is first detected at tailbud (A), again showing individual na cells that are interspersed around the head region and midline of the anterior region of the embryo. NA cells become more interspersed and fewer in number during tailbud development (B, C) and are no longer detected by WISH after NF 33. Expression in a localized hindbrain region, likely the locus coeruleus is detected at late tailbud (C-E). na, noradrenergic; lc, locus coeruleus

3.4.4 Th

Tyrosine hydroxylase (*TH*) gene encodes the protein that catalyses the first, rate-limiting step, in catecholamine synthesis, converting L-tyrosine to L-dihydroxyphenylalanine (L-Dopa). In mouse embryos, all CCs express Th (Kastriti et al., 2020). Th is expressed both in adrenaline and noradrenaline producing CCs in mice (Kastriti et al., 2020) and was therefore chosen as a promising marker gene to locate adrenomedullary CCs in *Xenopus*. Expression of *th* has previously been shown at neurula (NF stage 20) until early tailbud (NF stage 24) (Wylie et al., 2015) and shows the same punctate pattern of cells we have observed with our markers *phox2a*, *phox2b*, *insm1*, *chga,* and *pnmt*.

WISH probes for *th* were generated from PCR products and the gene obtained by cloning as described. Primers for cloning were designed for the L variant. The *X. laevis* RNA-seq. data from Xenbase for *th.L* shows an overall low expression throughout embryonic development (Fig. 36). A first small peak in expression is seen at late neurula (NF stage 20), with a value of 0.45 TPM. Expression then slopes to 0.31 TPM at early tailbud (NF stage 25) and then starts to increase again, with the highest expression at late tailbud (NF stage 35/36) with 1.69 TPM. Expression then drops quickly to 0.7 TPM at NF stage 40.

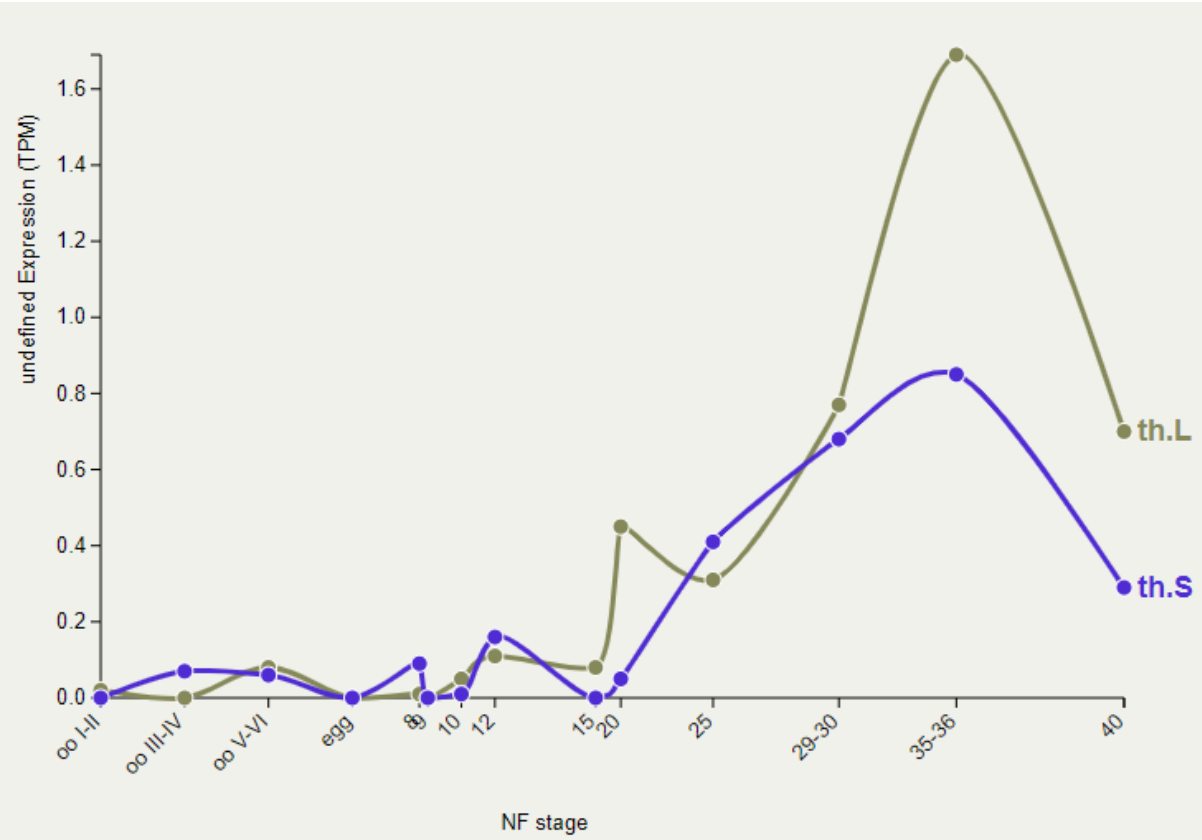

Figure 36: Expression analysis of th RNA in Xenopus laevis during embryogenesis taken from Xenbase (Session et al., 2016).
Expression is measured between 0.0 and 1.6 TPM. Th levels for both chromosome variants are relatively low throughout development, whereas th.L variant shows a slightly higher expression overall and was therefore chosen for creating a riboprobe.

Unfortunately, we experienced issues making a riboprobe with both the existing plasmid containing the *th* insert (L variant, full length) and cloning *th (L variant)* ourselves. Both riboprobes showed high, nonspecific binding, resulting in a strong background, when performing WISH. Therefore, we only got very few images of *th* during *Xenopus* development that, however, confirm the presence of the single punctate cells as previously shown by Wylie and colleagues (Wylie et al., 2015) and potentially like our expression patterns for *dbh* and *chga*.

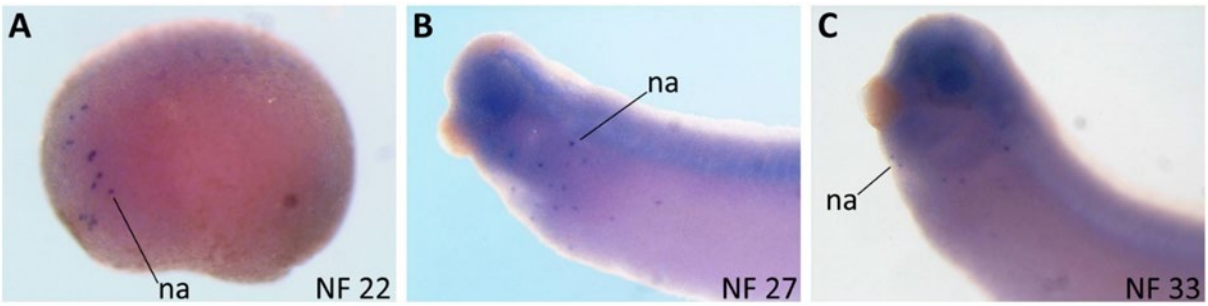

Figure 37: Characterization of th expression during embryogenesis in X. laevis using WISH. *Embryos are presented with the anterior on the left and the posterior to the right. Tailbud embryos are only shown from head to mid-body region to better visualize the NA cells. We clearly observe NA cells expressed on each side of the cement gland at NF stage 22 (A), already interspersed and appearance like previously explored CC markers. During tailbud stage, NA cells are found interspersed across the anterior part of the embryonic body (B), while at late tailbud stage we observe very few NA cells just beneath the branchial arches and a few below the otic vesicle (C). na, noradrenergic*

3.5 Direct staining of catecholamine-producing cells in *Xenopus laevis*

From a histological point of view, there are few methods that are currently used to identify CCs in a sample. These methods have been used by histologists from the mid '50s, and one of these, as mentioned above, gives the name to CCs, which requires the use of potassium dichromate. The limitation of these techniques is that they have to be used on mature CCs (Coupland and Hopwood, 1966; Hopwood, 1969).

In this chapter, we have characterised the expression of multiple candidate marker genes important for CC development and maturation. For most of these genes, we observed a specific, punctuated pattern that have been labelled as NA neurons and that we suggest being putative CCs.

In order to test if the single cells pattern (the noradrenergic neurons) that we observed by WISH using marker genes (such as *chga*, *dbh* and *th*) can be attributed to mature CCs, we decided to use the original potassium dichromate staining on *Xenopus laevis* tailbuds and tadpoles. This staining, which requires the fixation of the tissue with a solution of formaldehyde and potassium dichromate, is supposed to generate a brown precipitate in the cytoplasm of the mature CCs. This variation in colour is due to the oxidation of chromium salts

by the action operated by catecholamines (adrenaline and noradrenaline). In order for this process to occur, it requires the presence of catecholamines and, therefore, mature CCs.

We first performed the potassium dichromate experiment following the original protocol in wholemount embryos. However, we failed in identifying any specific staining. Therefore, we decided to modify the protocol by either pre-treating the embryos with proteinase kinase, or by increasing the colorimetric reaction to one week, in accordance with the canonical WISH protocol, or even doing both. Unfortunately, none of these variations produced conclusive results, on any of the developmental stages that we analysed (NF stage 31 and NF stage 45) (Fig. 38). However, we only performed this staining on wholemount embryos rather than on the kidneys itself. We could have tried to perform either sections of the stained embryos or dissect out kidneys of various developmental stages and perform the protocol, followed by sections. As the kidneys of *Xenopus* are extremely small at the embryonic stages, it would be recommended to first attempt this protocol with froglets (NF stage 59 to 66) and move backwards to earlier stages once a successful staining has been established.

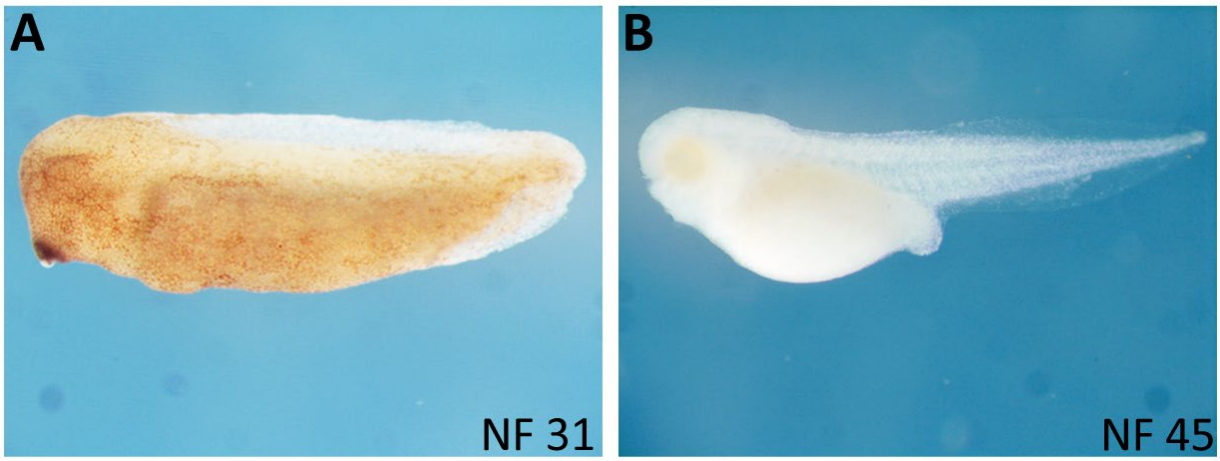

Figure 38: Dichromate staining on wholemount X. laevis embryos to identify mature chromaffin cells.
Dichromate staining was performed as described by (Qiu et al., 2013), with no observed staining in both tailbud NF stage 31 (A) or at tadpole NF stage 45 (B). The only observed effect is a yellowish coloration in the eye field and beneath the somites at NF stage 45.

Being unable to confirm the true nature of the cells that we identified by using the dichromate staining, we decided to use a more direct approach, and to perform immunofluorescence (IF), staining embryos with an anti-adrenaline antibody (LSBio, LS-C295834-100).

Adrenaline and noradrenaline are stored into vesicles of mature CCs, where they can be promptly released into the blood stream. Performing an IF using anti-adrenaline antibody in whole *Xenopus* embryos should provide important information about the location of CCs with these embryos.

An important factor to consider when using antibodies for any kind of assay (Western blot, chromatin immunoprecipitation, co-immunoprecipitation, IF, and others) is the ability of the antibody to react with the antigen in different organisms. We know that the same protein in different animals can have slight variations in the primary, secondary or tertiary structure, or at the level of post-translational modification. These differences can affect the capacity of an antibody to bind that protein across different species. Luckily, we did not have to worry about this technical aspect, during the selection of the primary antibody against adrenaline, since this is a small molecule, and it is the same across all species.

After performing IF on some sections of a NF stage 59 froglet of *Xenopus laevis*, we did not observe any staining, for the samples that we analysed, nor for any of the various antibody concentrations that we tested (data not shown). A difficulty here might have been that we used Alexa Flour 488, which gives a high autofluorescence background signal in *Xenopus*. Most likely though, the protocol used for the IF needed more optimisation as it was not yet established in the Wheeler lab as well as possibly adjusting the fixing time of tissues to be sectioned.

Future experiments, including potassium dichromate and IF using anti-adrenaline, on adult frog tissue are needed to assess the validity of these methods in *Xenopus*, and would provide important information about the maturity of the CCs that we identified by WISH using our specific markers. Also, it would be important to perform these assays at different developmental time points, in order to understand when *Xenopus laevis* embryos start producing catecholamines and where these CCs are located.

3.6 Expression in the developing enteric nervous system?

While characterizing the expression of the putative CCs during *Xenopus* embryogenesis, we noticed another interesting expression pattern at late tailbud development with a few of our chosen marker genes. From late tailbud development NF stage 35/36 to NF stage 40, we see a linear expression pattern initially extending in close proximity of the facial nerves at the midline of the anterior embryo, which is particularly visible with marker *phox2a* (Fig 26).

For both *phox2* genes, we observed two distinct cellular populations originating from the vagal NC. The first population elongating antero-posteriorly, in a segmented pattern, which we suggest being associated with the vagal nerve, as is well-documented in other model organisms. The second population of cells, that appear to be more elongated singular cells, unlike the well-rounded NA neurons, seem to develop in a dorso-ventral pattern, and are likely enteric neurons and/or glia. Interestingly, the appearance of this second population of cells seems to be dependent on the elongation of the vagal nerve. Following elongation of the vagal nerve, more and more enteric neurons seem to appear across the developing GI tract of *Xenopus* embryos, colonising the entirety of the GI system around stage NF 40, once the vagal nerve reaches the cloaca of the embryo (Fig. 39 and Fig. 40).

This expression pattern also seems to be visualized at NF stage 37 (Fig. 30) with *insm1*. At tadpole stage, this expression is still visible for *phox2b* and *insm1*, but no longer visualized with *phox2a*.

After some literature review and discussions, we hypothesised that this expression pattern, marked by the three SA specifier genes, is showing the developing enteric nervous system (ENS) in *X. laevis*. This process has not been visualized or well-studied in *X. laevis*, especially not by using WISH. None of the gene's expression have been characterized this thoroughly before nor has their involvement in ENS development in this animal model been studied. We therefore wanted to characterize this process more, despite it not being part of our main research question of this thesis project.

The ENS of vertebrates is made up of a large network of neurons and glia cells, which make up the intrinsic nervous system of the gut and is essential in the maintenance of normal GI

function, which encompasses motility, blood flow as well as mucosal transport and secretion (Kuil et al., 2021; Nagy and Goldstein, 2017). The majority of the ENS arises from vagal NCCs, which migrate from the hindbrain into and along the entire length of the GI tract, using the fibres of the outgrowing vagus nerve (Kuil et al., 2021). The more posterior lying enteric glia are derived by sacral NCC's in mammals (Kuil et al., 2021). However in zebrafish, no evidence of sacral NC contribution to the ENS has been found (Kuil et al., 2021). Additionally, more recent research has shown that the vagus NC derived enteric neurons are actually derived from a dual population of vagal NC and a population of vagus nerve associated-SCPs, which contribute to neurons of the anterior gut (Espinosa-Medina et al., 2017).

Failures in NC development and migration are known to cause a variety of developmental disorders, the NCPs. A NCP affecting the ENS is Hirschsprung's Disease, which is characterized by a lack of ganglionic cells in the distal portion of the bowel, due to problems in ENS development (Rao and Gershon, 2018).

The TF PHOX2B plays a crucial role in the development of the autonomic NS and therefore also the ENS. It is essential for the formation of all autonomic ganglia, including enteric ganglia, and absence of PHOX2B leads to absence of enteric glia cells in the ENS (Nagy and Goldstein, 2017).

The role of *PHOX2B* in the development of the ENS seems to be highly conserved among vertebrates. The GI system of zebrafish closely resembles that of mammals, and the ENS development is comparable to that of mouse and human, in relation to gene expression and functional studies. This is frequently conducted with *phox2b* transgenic reporter lines such as Tg (−8.3phox2bb:keade)^{em2tg} and Tgbac (phox2bb:eGFP)^{w37tg} to mark migrating enteric NCCs and differentiating neurons (Kuil et al., 2021). *Phox2b* expression was even found in the developing gut of the non-jawed vertebrate sea lamprey (Green et al., 2017). Additionally, it was revealed that the sea lamprey lacks a vagal NC subpopulation, with their ENS developing from late migrating trunk NC-derived SCPs (Green et al., 2017).

While *Xenopus* ENS development has not been well characterized, and not by WISH, the ease of genetic manipulation, quick external development, and closer evolutionary relation to

humans than zebrafish could make it an invaluable additional animal model in the study of ENS development and diseases. During this project, we found the previously described pattern for both *phox2* genes (sections 3.3.2 and 3.3.3), suggesting the visible expression pattern during late tailbud development to be visualizing migrating NCCs along the extending vagus nerve, giving rise to most likely enteric glial populations that can be seen extending from the vagal nerve (Fig. 39, Fig. 40, red arrowhead).

During vagus nerve medio-lateral extension, we observe the enteric neuronal/glial progenitors separate/detach from the vagus nerves current end location, and spread across the whole length of the developing GI tract of *Xenopus* embryos (Fig 39 and Fig 40). While the role of *phox2b* in enteric specification and differentiation of enteric NC is well known and studied, the expression of *phox2a* in enteric neurons is thought to be more restricted to a subset of enteric NCCs (Pattyn et al., 1999) However, its role in the development of this population is much less-well defined.

We have seen a near identical expression for both *phox2* genes during ENS formation in the late tailbud developmental stages. Curiously, we could see two distinctly separate linear expression patterns around the pronephric kidney area for *phox2a* expression. At the start of enteric NCCs migration along the vagus nerve, we see another linear expression pattern (black arrowhead) dorsally to the vagus nerve, just beneath the somites (Fig. 39 B-D). This could potentially show expression of *phox2a* along the/within the pronephric kidney, and would raise more questions about how and when exactly the NA neurons/CCs become associated with the kidney during *Xenopus* embryo development. We see no more evidence of expression in this region after NF stage 38 (Fig. 39) and did not observe the same expression pattern for *phox2b*. However, it could mean that we see expression of *phox2a* in the vNC giving rise to enteric glia, whereas the linear expression pattern above the vagus nerve could be derived from tNC, giving rise to sympathoadrenal progenitors which should be spatially segregated from the vNC.

Finally, while also observing the same expression pattern with *insm1* (Fig. 30 E), we decided to not follow it up more closely. This was due to the *insm1* riboprobe, not being as clean during late-stage development, leading to a high background staining that disturbed clear

visualization. We know *insm1* is crucial for the development of pancreatic and GI endocrine cells, both in mammals and in *Xenopus* (Horb et al., 2009). While *insm1* is vital in neurons and endocrine development of the CNS and peripheral nervous system (PNS) (Jacob et al., 2009; Wildner et al., 2008), no clear implication of its involvement in enteric neuron and glial populations has been indicated. When looking at the UMAP embedding of expression in different anatomical populations in mice, we can see *phox2a* clearly expressed in the enteric neuron lineage, while *phox2b* was expressed both in glia and neurons of the ENS and in the biased 'hub' state SCPs (Fig 16 B). For *insm1,* we saw expression in the bifurcation branches for both enteric neurons and glia cells but not within the differentiated branches. This could mean that *insm1* also plays a role in the differentiation of enteric glia and neurons, or that we have visualized enteroendocrine cell development at this stage of development.

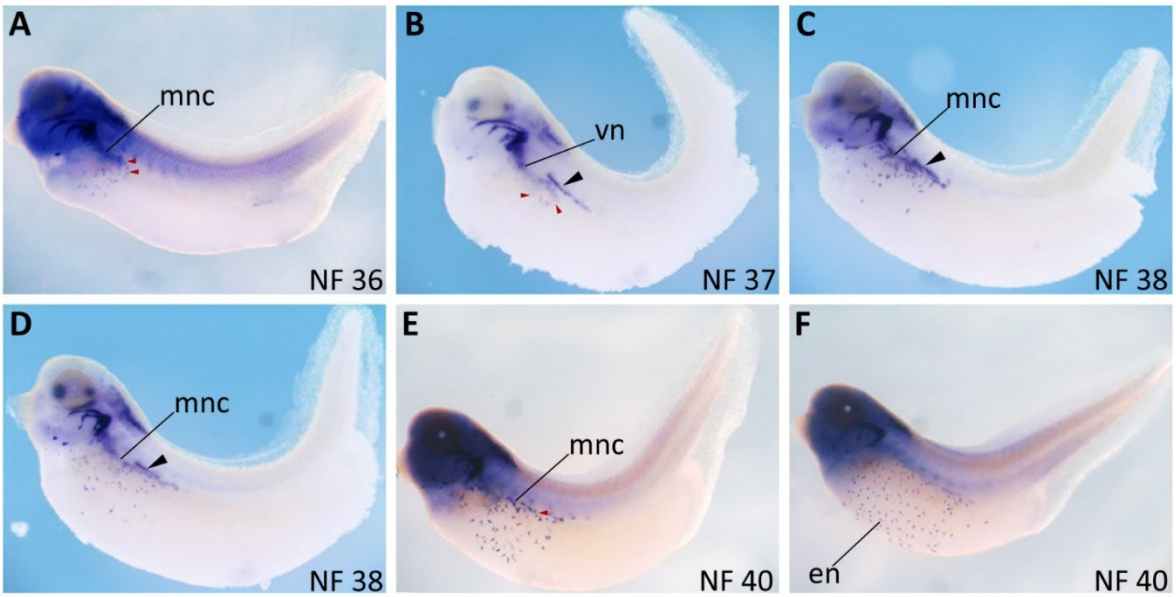

Figure 39: Phox2a ENS development expression analysis during late tailbud NF stages 36 to 40.

Embryos are viewed laterally and are orientated with the head anterior and tail posterior. Expression of vNC migrating along the vagus nerve (vn) is visible around NF stage 36/37 (A). As the VN extends medio-laterally along the embryonic body (B-F) during late tailbud development, we see single cells exiting the VN (red arrowheads) and spread across the developing intestines. The further the VN extends, the further the single cells, likely enteric neurons (EN) and glia, extend across the intestines. After NF stage 40 (F), we no longer see expression of phox2a in the ENS. Additionally, we see a separate linear expression dorsally to the VN at NF stage 37/38 (black arrowhead) that might show expression of phox2a along the pronephric kidney. Vn, vagus nerve, mnc, migrating neural crest.

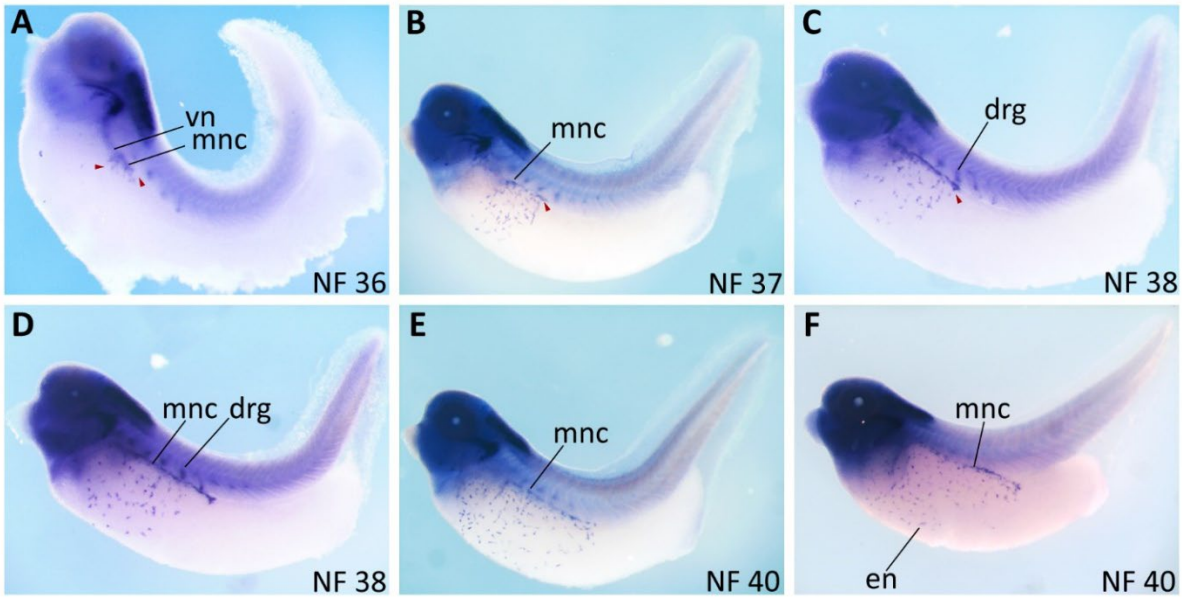

Figure 40: Phox2b ENS development expression analysis during late tailbud NF stages 36 to 40.

Embryos are viewed laterally and are orientated with the head anterior and tail posterior. Expression of vagal NCCs migrating along the vagus nerve (vn) is visible around NF stage 36/37 (A). As the VN extends medio-laterally along the embryonic body (B-F) during late tailbud development, we see single cells exiting the VN (red arrowheads) and spread across the developing intestines. The further the VN extends, the further the single cells, likely enteric glia based on phox2b being known to give rise to this population in mammals, extend across the intestines. We also see the VN in close association with the dorsal root ganglia that express phox2b (A-E). Drg, dorsal root ganglia; mnc, migrating neural crest; vn, vagus nerve.

3.7 Discussion

This chapter aims to identify and characterize the location and development of NC-derived CCs of the AM in *X. laevis* during embryogenesis. Although *X. laevis* has long served as a valuable model organism in the study of developmental biology, not much is known about the structure, location, function, and development of the AG. This is particularly true for the study of CCs within this model. The sparse literature that has been identified in the context of this project has merely hinted at a presence of CCs. No thorough characterisation of this cell type in *Xenopus* has taken place yet. Therefore, this result chapter is the first effort to understand and characterize the development of CCs in this animal model, to develop *Xenopus* as a model organism for normal development of the AM.

3.7.1 Reviewing existing markers

We initially set out to repeat and confirm the two previous gene markers that have been suggested to show expression in the developing AM in *X. laevis* during embryogenesis: *ruvbl2/reptin* and *insm1*.

Reptin was suggested to possibly be the first marker of AM CCs in *X. laevis* based on expression being found in the region of the developing pronephros (Etard et al., 2005). After creating the probe and performing *in situs* on several developmental stages during *X. laevis* embryogenesis, we quickly concluded that *reptin* was not showing expression of adrenomedullary cells. We however saw expression in nephrostomes of the pronephric kidney, which are responsible for waste excretion in the tadpole. We therefore dismissed *reptin* as a potential marker of AM development.

Next, we sought to investigate the expression of *insm1* during *X. laevis* embryogenesis. We hypothesised that it could be a genuine marker of the AM, due to previous work from Parlier and Colleagues. Here, the authors characterized the expression of *insm1* in early development of *X. laevis* embryos, between NF stage 11-27 and found it to be expressed in previously uncharacterized scattered individual cells located at the anteroventral side of early tailbud

embryos (Parlier et al., 2008). These cells were labelled by the authors as being noradrenergic (NA) neurons, based on the same staining being achieved with a riboprobe for *tyrosine hydroxylase* (*th*) (Parlier et al., 2008). Additionally, they discovered the NA neurons express and are regulated by *phox2a* and *hand2* at early tailbud stages, two markers for NC derived progenitors (Parlier et al., 2008). Staining was also observed dorsally to the pronephros, between the tubule and somites, identified by them to possibly be adrenomedullary cells. (Parlier et al., 2008).

Initially, we had great trouble with creating a functional riboprobe for this marker, and had it dismissed for a long time during this PhD project. However, due to the previous characterisation and its clear importance in CCs development and their proper differentiation in mammals, we were adamant on further characterizing the expression of this marker. Therefore, only towards the end of this project, were we able to confirm the previously observed expression by Parlier and Colleagues and add *insm1* to our list of markers that characterize a population of NA neurons in *Xenopus* embryos, which is further discussed in the following paragraphs.

3.7.2 The noradrenergic neurons - Sympathoadrenal lineage specifiers?

In this chapter, we wanted to investigate the location and development of the adrenal CCs in *X. laevis* embryos using carefully pre-selected markers from our initial literature review. Markers were categorized in two groups: SA specifier genes, important for the development of the CCs, composed of *insm1*, *phox2a* and *phox2b*, and marker genes that are presented within CCs and/or perform key roles in the synthesis of adrenaline and noradrenaline which included *chga*, *dbh*, *th*, and *pnmt*. We expected to see expression of these genes in the area of the developing pronephric kidney mainly during early to late tailbud organogenesis. We hereby hypothesised that the CCs would develop from within the developing pronephros, as this is the case in zebrafish, and expression of our selected CC marker genes would likely be mainly located in the head kidney. However, to our great surprise, we observed the dotted individual cell patterns for all our key selected marker genes (a summary of expression for our

key markers is shown in Fig. 42 and Fig. 43). These cells have been previously labelled as being noradrenergic neurons (NA), starting from the initial description by Parlier and Colleagues, with their characterization of *insm1* gene expression in *X. laevis* embryos, and followed by the characterisation of punctate cells at the same anteroventral position in early embryogenesis for *phox2a*, *th* and the heart and neural crest derivatives expressed 2 (*hand2*) by Wylie and Colleagues (Parlier et al., 2008; Wylie et al., 2015). We hereby speculate, that the described noradrenergic neurons are indeed either CCs, CC precursors or chromaffin-like cells that perform the function of CCs prior to metamorphosis in *X. laevis* embryos. With all three of our SA specifier marker genes, we observed expression of a multitude of the punctuated individual cells from our earliest point of developmental stage tracing, the late neurula NF stage 19/20, initially beneath the cement gland at the anteroventral side of the embryo and expressed up until late tailbud stages (summarised in Fig. 42 and Fig. 43). These cells all appear to be lying within the sub-epidermis. Previously, it was also found that NA neurons were expressed by another vital TF for the specification of sympathetic ganglia neurons and neuroendocrine CCs, the NC marker *Hand2.* In mice, *Hand2* was found to be essential in determining the noradrenergic phenotype in the sympathetic nervous system , playing a crucial role in catecholamine biosynthesis, although not required for initial sympathetic neuron formation and differentiation (Morikawa et al., 2007). To confirm this, we performed *in situs* with a *hand2* riboprobe during tailbud development NF stages 27 and 30 and could indeed visualize expression of the NA neurons with this marker gene (Fig. 41).

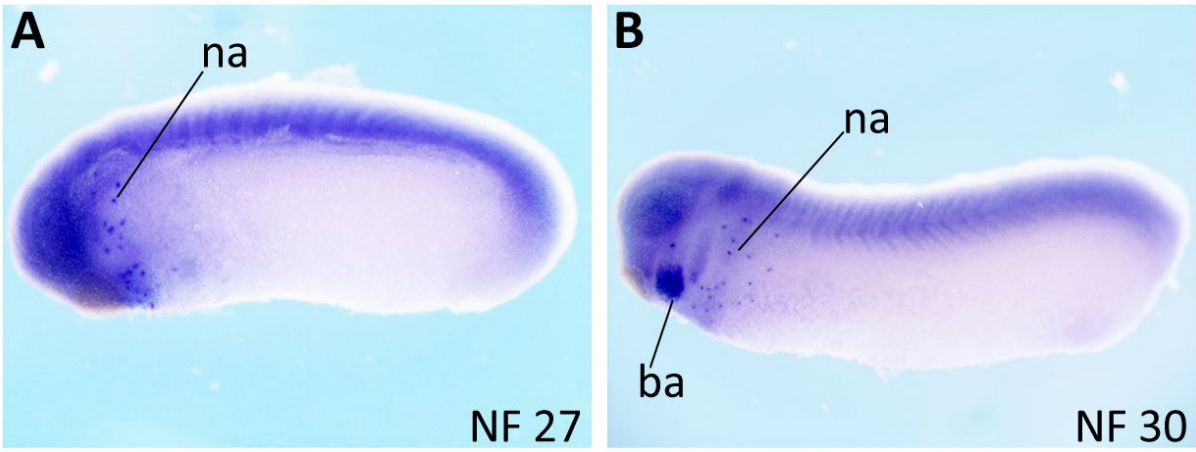

Figure 41: WISH of NC marker gene hand2 showing its expression during X. laevis tailbud development.
The NC marker gene hand2 was implicated by two previous publications to also be expressed in NA neurons , which we can hereby confirm. At early tailbud NF stage 27 (A), we see numerous NA neurons close to the cement gland and in the heart region as well as across the anterior embryonic body. Further along during tailbud stage (B), these cells have become more interspersed across the anterior body, similarly, to previously characterized putative CC marker genes. Additionally, hand2 expression is seen in the lower parts of the branchial arches. Ba, branchial arches; na, noradrenergic neuron.

This finding was supported by a later publication, where the authors characterized a population of anteroventral noradrenergic cells within early *Xenopus* embryogenesis (NF stage 10-22) (Wylie et al., 2015). The authors observed single punctuated cells, which expressed markers characteristic of NA cells in the sympathetic nervous system and neuroblastoma cells. These markers included *hand2*, *phox2a* and *th*, and the expression was consistent with the previously labelled NA neurons from Parlier and Colleagues. *Phox2a* expression in NA cells was seen as early as NF stage 14/15, shortly after appearance of the NC and is seen at the anteroventral side until NF stage 22 (Wylie et al., 2015). Both *hand2* and *th* expression is present after first expression of *phox2a* from NF stage 18/19 in the same location and become more intense from NF stage 20-22. The authors further reported transient expression of *ascl1* from NF stage 14/15 in these cells (Wylie et al., 2015). We observed this as being not clearly evident from the provided images and did not include *ascl1* in our own characterization of the development of CCs, despite its well documented key role in neuronal differentiation in the CNS and PNS (Parkinson et al., 2022). However, *ascl1* expression in NA cells, again sub-

epidermally, has been shown clearly in the anteroventral region of *X. laevis* embryos at late Neurula stages by Talikka and Colleagues (Talikka et al., 2004), when they initially characterized the expression of *phox2a* and *phox2b* in *Xenopus*. The authors implied these cells playing a potential role as heart field progenitors, due to their location of expression being in the developing heart field. While we have not further confirmed the expression of NA cells with *ascl1* ourselves, *ascl1* is known to accompany *phox2a* and *phox2b* expression in the activation of the catecholaminergic differentiation program. This further supports the implication of these cells being potential CC progenitors or performing chromaffin-like roles during embryogenesis prior to metamorphosis. Again, due to our expected expression of marker genes in the developing pronephric region, we did not pick up on this reported expression at the start of this project. Future experiments should include making a riboprobe for *ascl1* to characterize its expression throughout embryonic development, first confirming its expression in the NA neurons between NF stage 14-23 and then assessing if this expression is maintained in these cells at later stages of development. Interestingly, Wylie and Colleagues (Wylie et al., 2015) dismissed the use of gene marker *phox2b*, despite its key role in SNS precursor development and maintenance, due to it not being found to be expressed in the NA cells in its initial characterisation (Talikka et al., 2004). We clearly observed *phox2b* expression in NA cells from late neurula to tailbud stages (Fig.28). We do acknowledge that the *phox2b* riboprobe was not easy to clone in the first place. Overall, the expression took longer to develop, which coincides with a higher background noise making visualization of these NA cells especially hard. This might be the reason that the expression patterns we report in this project, and that will be further discussed, have not been visualized previously. Unfortunately, we did not characterize expression of our marker genes of interest prior to late neurula stages. It would have been interesting to see, if *phox2b* expression would appear slightly before that of *phox2a* and *insm1* expression, as is described in the literature in mouse (Coppola et al., 2005; Huber, 2006), though our RT-PCR results (Fig. 17) suggest otherwise. In mammals, *Phox2b* is expressed early during SNS development whereas *Phox2a* expression emerges slightly afterwards (Coppola et al., 2005). Therefore, we could speculate that *phox2b* expression in the NA cells might coincide with the induction of the NC in *Xenopus* embryos, which begins between NF stage 12.5 and 13.

In summary, we found expression of the NA cells for all three SA specifier markers *phox2a, phox2b* and *insm1* starting from late neurula to late tailbud NF stage 33. After the cells become less frequent and/or do not express these markers in the NA cells at these stages anymore. We do not see appreciable differences in the amount of NA cells or shape of NA cells between the markers between NF stage 19/20 – 24 (Fig. 42). From tailbud stages, NA cells are found across the anterior body of the embryos in a more interspersed manner, but do not seem to be following a certain directionality and are not found in exactly the same places across the three markers. After NF stage 27, NA cells become less frequent for both *phox2* markers, whereas more seem to still be present/still express *insm1*. At NF stage 33, few NA cells seem to converge below the branchial arches for all three markers and cannot be clearly visualized after this developmental time-point.

3.7.3 NA neurons expressing CCs specific markers

Along with our chosen SA specifier marker genes, our key genes of interest to localize CCs in *X. laevis* where genes that are reported to be directly present in CCs like *chga*. Further, we looked at genes that produce enzymes, which play a direct role in adrenaline and nor-adrenaline synthesis and therefore are implied directly to be within CCs. These included marker genes *dbh*, *th* and *pnmt*. Neither *chga*, *dbh* or *pnmt* gene expression had been previously characterized during *Xenopus* embryogenesis. *Th* had been shown to be expressed in the NA cells by Wylie and Colleagues, but we struggled to get clean expression with both the probe made from a plasmid insert already present in the lab or the probe made from designing and cloning ourselves. Despite these difficulties, we could repeat and confirm previous results, showing that we do see NA cells during early tailbud development with *th* expression, even though there was a strong background noise (Fig. 37). *Chga* had previously been shown to be present in endocrine cells of dissected intestines from developmental stage NF 44 (Horb and Horb, 2010), but gene expression during embryogenesis had not been characterized previously. *Chga* was one of the first marker genes we characterized in this project and was our first indication of the punctuated cell pattern we observed later with all our chosen key marker genes (Fig. 31). In humans, DBH and CHGA are both vital for

catecholamine synthesis, storage and release and are co-expressed in CCs of the AM (D'amico et al., 2014; Ernsberger et al., 2000; Wildner et al., 2008). For both marker genes, we saw the single cell expression throughout all stages of our chosen developmental time points (NF stage 19/20- NF stage 45). These two genes were the only markers that still showed expression in the NA neurons at tadpole stages (Fig. 43), as our SA specifier genes did not show expression in the NA neurons after late tailbud stages. Both markers show expression in a multitude of the NA neurons, compared to the SA specifier genes, they seem to be present in more cells (Fig. 42 and Fig. 43). Particularly *dbh* seems to express in a higher number of cells in total (Fig. 33). From NF stage 33, cells become less frequent in number, and we begin to see expression of these cells cluster together below the branchial arches (Fig. 33 D). From NF stage 39-40, *dbh* expressing cells look less rounded and more elongated (Fig. 33 E). This is no longer the case at NF stage 45, where we see a few cells beneath the branchial arches, but also expression along the pronephric kidney, which we don't see with any other marker (Fig. 33 F).

The fact that expression is seen over a longer period of time during development with both *chga* and *dbh* could mean that, at these stages, cells have become fate restricted and have fully differentiated to chromaffin cells/chromaffin-like cells. Further, they might no longer express genes that were required for their initial development and specification such as the *phox2* markers. Both phox2 proteins are known to directly bind to the promotor and regulate the expression of noradrenergic biosynthesis genes *th* and *dbh* and activate the noradrenergic differentiation program (Morikawa et al., 2007). The absence of expression in the NA neurons starting from NF stage 40 (Fig. 43) suggests that the initial phase of noradrenergic specification and differentiation regulated by the *Phox2* genes has been successfully completed. Based on the expression of *dbh* and *th*, we can assume that these CCs are already capable of producing nor-adrenaline from an early developmental time point. Unfortunately, we do not know if *dbh* and *chga* expression comes on earlier than NF stage 19/20 by WISH. Our RT-PCR for dbh shows it faintly being present as early as NF stage 10.5, and we see strong bands from NF stage 14, just after NC formation, up until NF stage 33. Chga was faintly present at NF stage 1 and then again is found to be present strongly from NF stage 20 until NF stage 45. The presence of dbh this early in development, combined with the fact that Wylie and Colleagues found *th* expression in these cells starting from NF stage 18/19, makes us assume

that this is the earliest time-point of catecholamine synthesis. However, we need to keep in mind that *chga* has been shown to be expressed in enteroendocrine and pancreatic endocrine cells in *Xenopus* during embryogenesis (Horb and Horb, 2010). Indeed, expression of this marker at NF stage 45, indicates the location of either pancreatic endocrine cells or of the intestinal endocrine cells. However, although enteroendocrine cells are a type of neuroendocrine cell, they mostly secrete serotonin and other peptides and do not seem to produce or secrete nor-adrenaline (Bellono et al., 2017). These cells are likely just another cell type expressing *chga* as its secretory protein, responsible for release and storage of other hormones. Therefore, expression in these cells does not interfere with the assumption of *chga* and *dbh* showing expression of CCs related to the AM, as we assume that enteroendocrine cells would not show expression of either *th* or *dbh*, necessary for catecholamine biosynthesis and seen to be expressed in the characterized NA cells.

While we saw reliant expression of *chga* and *dbh* throughout development, this was not the case for *pnmt*. *Pnmt* was initially our high-priority marker, as the pnmt enzyme is the rate-limiting step in adrenaline production in CCs (Bechmann et al., 2021; Wong, 2003). We therefore thought it to be the most important one. We did see expression of this gene in the single cells during late tailbud development (NF stage 27-33) (Fig. 35). At later developmental stages, *pnmt* expression was localized to a small structure in the brain and was no longer visible in NA cells (Fig. 35). *Pnmt* expression was indicated to be very low during *X. laevis* embryogenesis based on our RT-PCR results (Fig. 17) and the RNA-sequencing data from Xenbase. Generally, it seems that *pnmt* expression is hard to localise *in vivo* by WISH. In zebrafish, when characterising the expression of *chga* in the interrenal gland, the authors reported being unable to visualize *pnmt* expression (Xie et al., 2008). No further literature could be found characterising the genes expression by WISH in amphibians or teleosts. Finding *pnmt* expression in the NA neurons around tailbud stage suggests that the cells have gained the ability to synthesize adrenaline from tailbud stages. The amount of cells expressing *pnmt* seemed to be less than cells expressing *dbh* and *chga* (Fig. 35 and Fig. 42). This could be based on CCs in mammals being distinguished between adrenaline producing and nor-adrenaline producing. While all CCs are able to produce nor-adrenaline, only a sub-population of CCs express PNMT and are capable of synthesizing adrenaline. In adult frogs (*Rana pipiens*), Pnmt

enzyme tissue distribution and activity were found to be widely present across several organs, whereas in rats, adrenaline synthesis was mostly specific to the AM, due to its activity dependency from adrenal cortex (AC) corticosteroids (Wurtman et al., 1968). It was suggested that, in frog, adrenaline serves as a neurotransmitter, rather than a hormone like it does in mammals, and it is not dependant on inducing signals from the AC (Wurtman et al., 1968). This is likely supported by our findings that the developing AC and CCs are spatially separate throughout embryogenesis.

In summary, the expression in punctate single cells of all of our chosen markers to characterize developing CCs in *X. laevis* was not at all expected. We had anticipated expression of our chosen markers in close relation to the developing pronephric kidney, and at later time-points of development. Therefore, we initially limited the WISH probe characterisation between developmental NF stages 27-45 as this is the time point of pronephric kidney organogenesis. We later went further back in early embryogenesis and found all marker cells to be expressed from NF stage 19/20. Due to previous findings of NA neurons appearing as early as NF stage 13/14, in association with the induction of the NC tissue that gives rise to CCs of the AM, it would have been interesting to characterize our marker gene expression from that early in development. Due to *th* being found to be expressed in these cells from NF stage 18/19, we hypothesise that this is the earliest developmental time-point that the NA neurons are fully functional and can synthesize noradrenaline. We have not found any association of these cells with the pronephric kidney during embryogenesis. This implies that there is no formation of an actual AM organ tissue *per se*, and that NA neurons might become intermingled with the interrenal tissue sometime during pre-, pro-, or after metamorphosis, which would be a frog specific process.

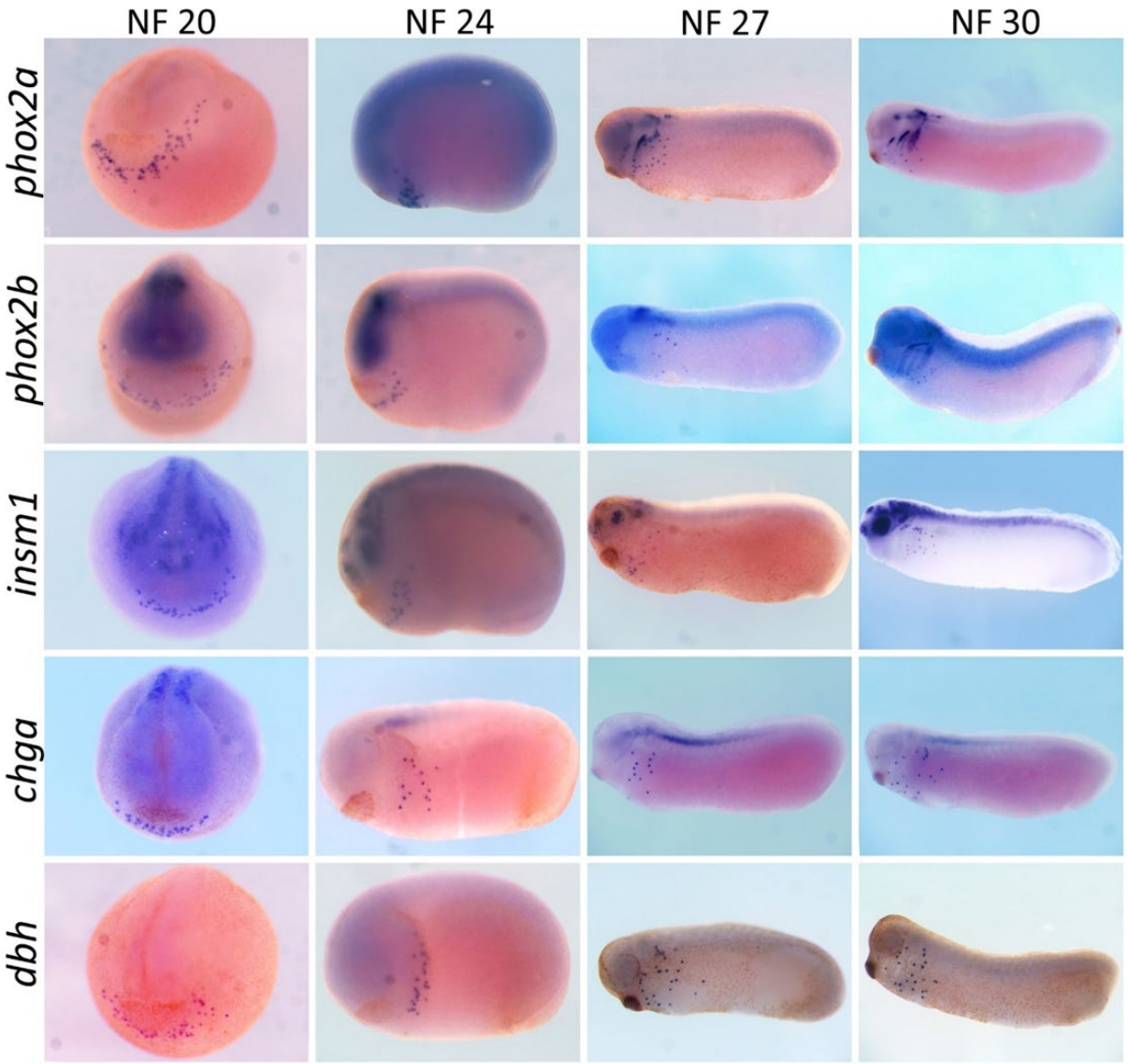

Figure 42: Comparison of spatial-temporal expression of key markers of chromaffin cell development during embryogenesis in X. laevis from developmental stage NF 19/20 – NF 30.

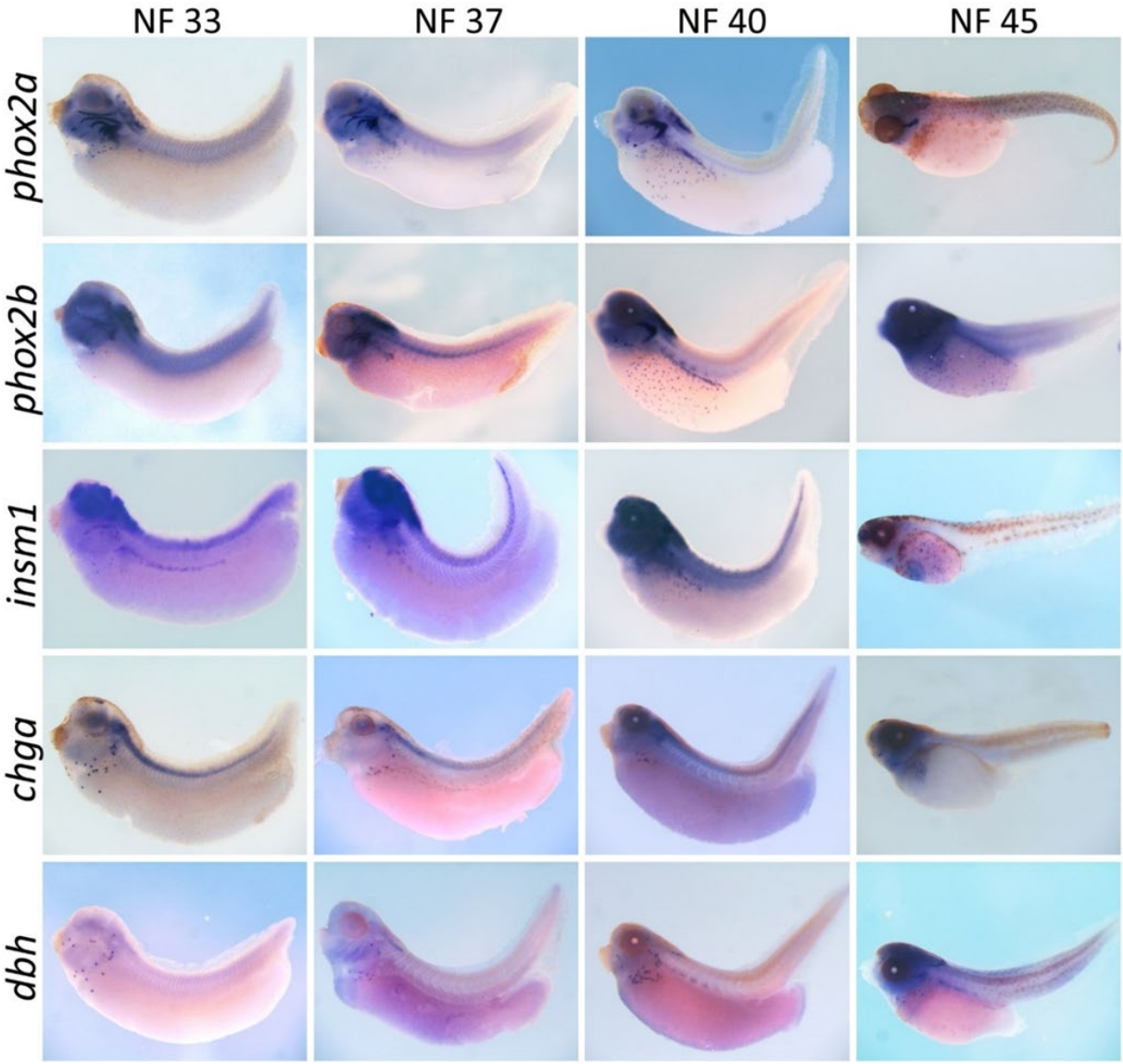

Figure 43: Comparison of spatial-temporal expression of key markers of chromaffin cell development during embryogenesis in X. laevis from developmental stage NF 33 – NF 45.

3.8 Are the characterized noradrenergic neurons neural crest derived?

In mammals, CCs of the AM are known to be derived from trunk NCCs, with the great majority of mammalian CCs being derived from late migrating NCCs that associate with peripheral nerve axons. These NCCs then gain SCP properties, and use the axons to reach the adrenal primordium (Furlan et al., 2017). Here, the cells detach and undergo transcriptional transitory state and differentiate to CCs (Furlan et al., 2017). This process has recently been shown to also be conserved in zebrafish, both for SCP-to neuron and SCP to CC transition (Kamenev et

al., 2021). However, in zebrafish, CCs associate with the interrenal gland, developing within the head kidney while still staying intermingled, and not associating to defined organ structure (Bacila et al., 2021). In the *Xenopus* model system, we did not see an association with the pronephric kidney, at least during embryogenesis. What is further important is that we see expression of NA cells appear soon after initial NC initiation, and we see expression of the NA cells first arise at the anteroventral side of embryos. This would imply that the NC can migrate much further than currently assumed in this model, or that these cells are not derived from the NC.

That these NA neurons are indeed NC-derived was demonstrated by Wylie and Colleagues who, following the discovery of marker genes expressing in the NA neurons, inhibited NC migration by interfering with slug function using a dominant negative slug (dnSlug)(Wylie et al., 2015). This blocking of NCCs migration on one side of the developing *Xenopus* embryos caused a loss of the putative chromaffin like precursors/NA neurons.

This question will be further addressed in chapter 6.

4 Chapter IV: Characterisation of adrenal cortex markers during Xenopus development by WISH

4.1 Introduction

In Chapter 3.1.1 we have summarized what was previously known about the structure of the adrenal gland in *X. laevis*, also in comparison to other amphibian species. We concluded that there is very little known about the general structure of the AG, and we could not find any information on AG development during embryogenesis. In the following, we want to provide more detail on what is known about the structure and function of the adrenal cortex (AC) in this model species.

The development of the AC has been studied during different stages of metamorphosis in *X. laevis* in the 1970s. Steroid synthesis was found to begin during the initial phases of pro-metamorphosis (NF stage 50) and reached their peak activity at the metamorphic climax (Kloas et al., 1997). Measuring whole-body concentration of the adrenal steroids, corticosterone and aldosterone, during *X. laevis* development has revealed stage-dependant changes. No presence of corticosteroids could be detected prior to late tailbud stages and only very small amounts of corticosterone, and even less amount of aldosterone, were found at NF stage 35 (Kloas et al., 1997). Generally, corticosterone levels were found to rise earlier than aldosterone levels (Kloas et al., 1997). At NF stage 40, both steroids were present in detectable amounts (Kloas et al., 1997). At this stage, steroidogenic adrenal cells are morphologically reported in the dorsal nephric region, as well as the presence of steroid dehydrogenase (Hanke, 1978; Kloas et al., 1997; Nieuwkoop and Faber, 1994). Here, the highest levels of corticosteroid levels were measured during pre-and pro-metamorphosis and not during the metamorphic climax reported by a previous study (Kloas et al., 1997).

In teleost's, the development of the steroidogenic cells of the interrenal gland has been well established and, while the interrenal gland is structurally different, it seems to perform the same function as the AG in mammals. Structurally, the interrenal gland in zebrafish consists of dispersed clusters of steroidogenic and CCs embedded at the head kidney, and develops in parallel with the kidneys during embryogenesis (Bacila et al., 2021; Hsu et al., 2003). Primordial interrenal cells, derived from intermediate mesoderm, are initially detected through the expression of *ff1b* (SF-1 ortholog), as bilateral clusters within the pronephric primordium between 22-27 hpf (Bacila et al., 2021; Liu et al., 2003). These cells start to

separate from the pronephric structures, converge to the midline and merge into a single, distinct structure at 30 hpf (Bacila et al., 2021). The organ then acquires steroidogenic identity, marked by the expression of the gene steroidogenic acute regulatory protein (*StAR)*, amongst others (Bacila et al., 2021). CCs progenitors are characterized by the expression of *dbh*, converging bilaterally to the region of steroidogenic cells at 2 dpf, where they overlap (Bacila et al., 2021). At 5-7 dpf, CCs are fully enveloped by the steroidogenic tissue, with no distinct layers between them (Bacila et al., 2021).

Presently, there is no comprehensive study of AG development, or specifically on AC development *in X. laevis* during embryogenesis. Additionally, no spatial and temporal expression map exists of this organ at any stage of development. Although this thesis was initially focussed on studying the development of the NC-derived CCs in *Xenopus* during embryogenesis, the absolute lack of knowledge of the AG, and lack of any specific markers and expression maps led us to extend the research also to characterising the development of the AC. We expected this to help aid in general localisation of the AG in *X. laevis*, as well as generating a more holistic picture of this organ's development and function in this model species. Due to the highly conserved nature of steroidogenic tissue development across mammalian and non-mammalian species (human, mouse, zebrafish, fruit fly) we chose genes *nr5a1* and *star* to trace AC development in this project. *Nr5a1* is as a crucial regulator and transcriptional activator of AC/interrenal gland formation and induces the transcription of *star* (Bacila et al., 2021).

Additionally, we included cytochrome P450 17a1 (*cyp17a1)* as a potential marker gene for active steroidogenesis during development, due to its vital role in interrenal cortisol biosynthesis in humans (Bacila et al., 2021). However, this gene was later dismissed as potential marker due to a lack of specific staining with the synthesised WISH riboprobe. Upon further investigation, we discovered that zebrafish have two *cyp17a1* genes: *cyp17a1* and *cyp17a2*, and only *cyp17a2* was detected in the interrenal gland at 120 hpf, whereas *cyp17a1* showed no significant expression (Weger et al., 2018). Based on our complete lack of *cyp17a1* expression, and the lack of active expression of the cyp17a1 isoform in zebrafish in the interrenal gland, we chose to solely focus on *nr5a1* and *star*.

Therefore, during this chapter I will characterize the expression pattern of the steroidogenic genes *nr5a1* and *star* during *Xenopus laevis* embryogenic development and investigate their role in the development of the AG.

4.2 Nr5a1

The gene *nuclear receptor subfamily 5 group A member 1* (*NR5A1*) encoding for the protein steroidogenic factor 1 (SF-1) plays an essential role in the development and differentiation of steroidogenic tissues including the AC, the gonads and the pituitary gland (Hoivik et al., 2010). *Nr5a1* is highly conserved across species, including vertebrates and invertebrates, with orthologs found in various species belonging to the NR5A subfamily of nuclear receptors. Human and mouse *Nr5a1* gene shares a 95 % homology. When deleting the *Nr5a1* ortholog of *Drosophila melanogaster*, fushi tarazu factor 1 (*FTZ-F1*), the mouse *Nr5a1* can substitute and rescue the deletion *in vivo*. In zebrafish, two co-orthologues of *nr5a1* have been identified, *ff1b* (*nr5a1a*) and *ff1d* (*nr5a1b*) which are required for both interrenal and gonadal tissue development. Also here, *ff1b* was the earliest molecular marker to be detected in the developing interrenal tissue within the pronephric field of zebrafish embryos (Yi-Wen, 2007).

During mouse development, SF-1 is one of the earliest TFs expressed within the AGP forming from the urogenital ridge (E9.0) that will give rise both to the AC and the gonads (Hoivik et al., 2010). Following the separation of the gonadal and adrenal anlagen at E11.5, *SF-1* is consistently expressed throughout gestation within the developing steroidogenic region of the adrenal gland in all three zones (zona glomerulosa, zona fasciculate and zona reticularis) of the adult AC (Hoivik et al., 2010).

SF-1 protein (Nr5a1) targets genes encoding the cytochrome P450 steroid hydroxylase (CYPs) and 3β steroid dehydrogenase (3βHD), stimulating the expression of nearly all factors involved in cholesterol mobilization and steroid hormone biosynthesis (Hoivik et al., 2010). Hereby, it regulates the expression of various enzymes involved in steroidogenesis, the process in which steroid hormones such as cortisol, aldosterone, and androgens are synthesized from cholesterol, thereby also regulating adrenal and gonadal formation, as well as sex

determination and differentiation (Hoivik et al., 2010; Meinsohn et al., 2019). Due to the regulatory function of steroidogenic enzymes, *Nr5a1* expression is found in all steroidogenic tissues in the body as well as being expressed in the non-steroidogenic ventromedial hypothalamic nucleus. This region is associated with energy balance, thermoregulation and sexual behaviour, and pituitary gonadotropes (Hoivik et al., 2010). SF-1 also regulates genes encoding factors involved in cholesterol transport such as *steroidogenic acute regulatory protein* (*StAR*) (Hoivik et al., 2010). SF-1 induces *STAR* expression both through promoter binding but als by acting as an enhancer of the *STAR* transcription start site (Meinsohn et al., 2019).

While the AC and the AM are derived from different tissues and are (in most species) structurally separated, a minimal crosstalk exists between these two tissues through glucocorticoid signalling (Unsicker et al., 2013). The expression of PNMT is dependent on glucocorticoids from the AC which assists in the development of norepinephrine-secreting CCs into epinephrine secreting ones through upregulation of PNMT expression (Unsicker et al., 2013).

Mice lacking *Nr5a1* show a delayed expression of *Pnmt* and a reduced number of developing CCs (Lohr et al., 2006). However, the absence of an AC in *Nr5a1* deficient mice does not seem to have an effect on CCs differentiation (Gut et al., 2005).

Overall SF-1 has emerged as a master regulator of endocrine tissue development involved in reproductive function, stress response and body homeostasis, underscoring a vital role in upkeeping hormonal balance and proper physiological function.

4.2.1 *Nr5a1* RNA sequencing data

Based on its vital function in development, maintenance and steroidogenesis of the AC, *nr5a1* was chosen as the main marker to identify and locate the AC in *Xenopus*. *Nr5a1* has not been previously characterized in *Xenopus*. Primers were designed for the S chromosome variant. Probes were generated by PCR cloning as described in the previous chapter.

RNA seq. data from *X. laevis* on Xenbase shows that *nr5a1* is generally expressed at low levels throughout embryonic development (Fig. 44). The highest peak of *nr5a1* expression is at NF stage 9, with 1.39 transcripts per million (TPM), and drops close to 0 TPM by NF stage 12 and stays low until NF stage 25. The smallest increase in expression happens at NF stage 29/30 to 0.06 TPM and after NF stage 35/36, expression continuously rises to 0.13 TPM at NF stage 40, where the measurements end (Fig. 44). Unfortunately, our RT-PCR did not reveal any specific amplicon of the *nr5a1* during different developmental stages. Generally, expression of *nr5a1* is very low, but it was revealed that the primers originally used for generating the *nr5a1* probe had been contaminated (Fig. 17, Chapter 3). Due to time-constraints, we were unable to repeat this experiment with a new set of the designed primers.

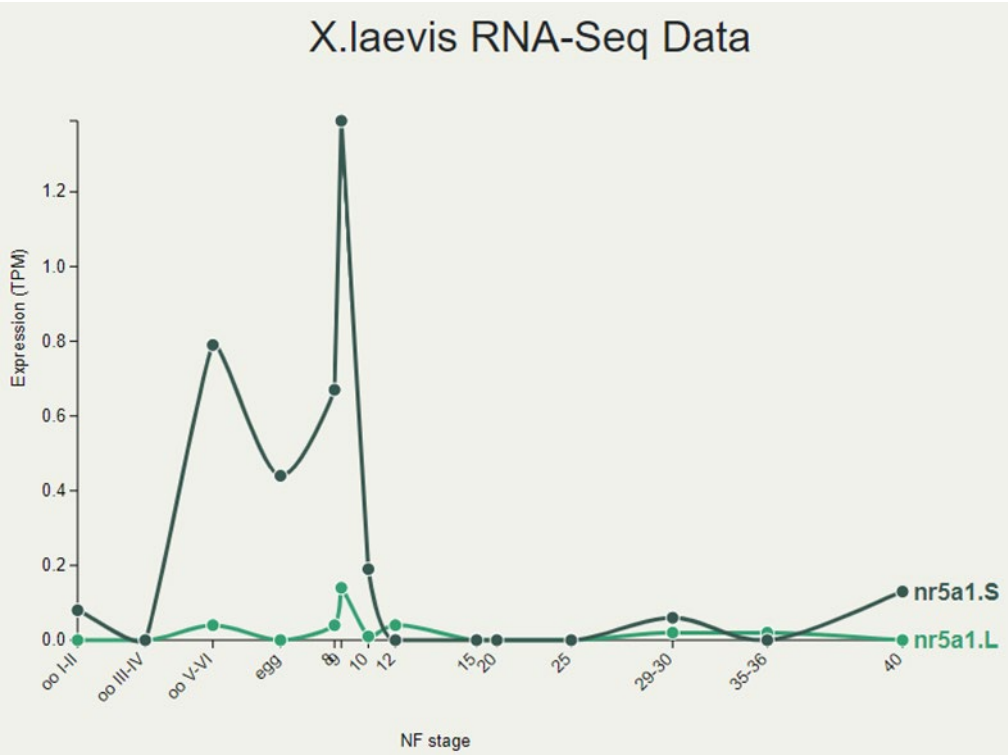

Figure 44: RNA sequencing data of nr5a1 in Xenopus laevis during embryogenesis taken from Xenbase (Session et al., 2016).
Expression of both chromosome variants is relatively low, but the S variant is slightly higher expressed. Generally, the TPM is extremely low, the scale is lowered to 0.0-1.4 TPM compared to most other scales of other gene markers.

4.2.2 *Nr5a1* in WISH

In accordance with the RNA expression just described by PCR, no expression was detected by WISH in neurula (NF stage 19/20) or early tailbud stages (NF stage 22-24) in *X. laevis* embryos. First detection of *nr5a1* expression is seen at tailbud (NF stage 27 and 30) (Fig. 45 A, B), matching the small peak of expression at this stage that is visible in the RNA seq. data set. At this stage, a small, weak line of expression in the area of the pronephros is detected. This expression seemingly elongates throughout further development in the pronephric area and becomes stronger. At late tailbud (NF stage 38), *nr5a1* expression is strong and seems to be expressed somewhere below or near the region of the developing pronephros (comparison of expression patterns see Fig. 50), along parts of the pronephric duct. It is not possible to determine this potential overlap of expression patterns without performing double in situs (DISH) or HCR with both probes. Additionally, at this developmental stage, we can also detect expression just behind the eye field (Fig. 45 C). Based on known expression of *Nr5a1* in mammals (Bashamboo and McElreavey, 2010; Wang et al., 2013), this is likely the hypothalamic nucleus (hypn), or possibly the pituitary gland, but less likely. Unfortunately, this pattern cannot be confirmed simply by comparing the literature and would require further experiments such as performing a double in situ hybridisation (DISH) or HCR with another gene known to be expressed in this anatomical structure and/or performing sectioning and comparing the location of the staining to a sectioned atlas of the brain. Unfortunately, we could not find anatomy labelling of this structure in *Xenopus*, and the main anatomy atlas (Hausen and Riebesell, 1991) ends at NF stage 28, making the determination of anatomical structures and later stages in development difficult.

At NF stage 40 through to pre-metamorphic tadpole (NF stage 45), expression in the previously described region of the pronephric duct is still strong and less interspersed (Fig. 45 D, E).

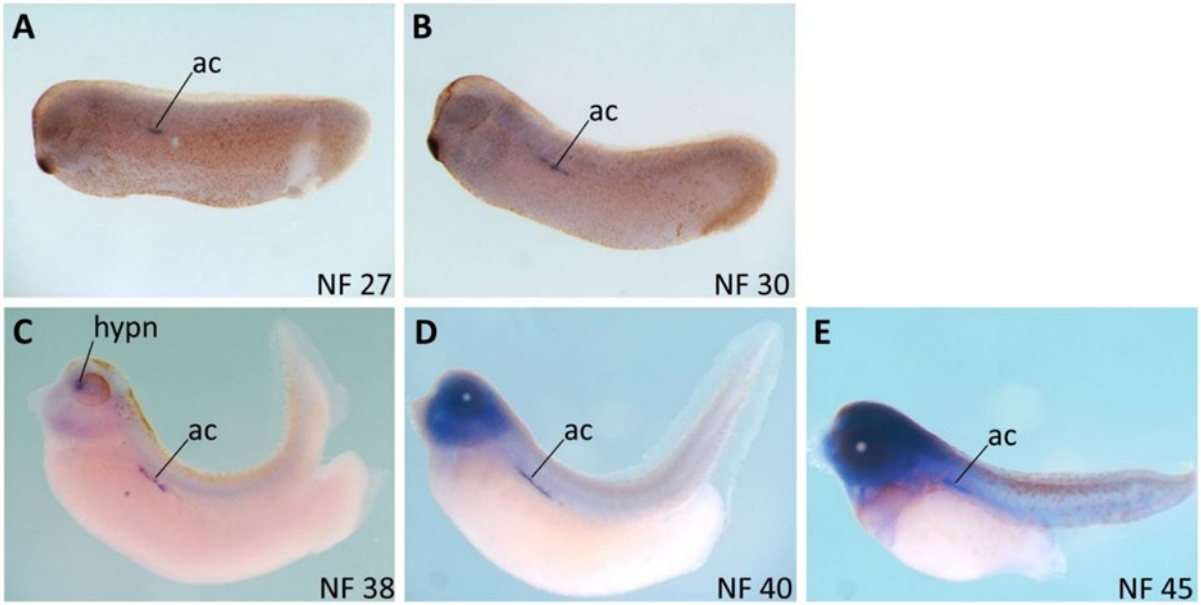

Figure 45: Spatial and temporal expression atlas of nr5a1 during X. laevis embryogenesis by WISH.

Embryos are presented with the anterior to the left and the posterior to the right. Expression of nr5a1 is first seen at NF stage 27, where it appears medio-laterally, just beneath the somites, as a short linear expression (A). Throughout tailbud stages, this nr5a1 expression undergoes medio-lateral patterning and elongates (B-D). At tadpole stage, nr5a1 expression is still visible as a short linear expression medio-laterally (E). Based on the role in adrenal cortex development in other vertebrate species, and the location of the expression in the area of the pronephros, we assume that this indeed is the developing adrenal cortex . Expression of nr5a1 is also clearly visible in a small structure, anterior to the eye but within the brain of X. laevis. Based on literature of expression of this gene, we identify this expression to be in the hypothalamic nucleus (C). ac, adrenal cortex; hypn, hypothalamic nucleus.

4.3 Star

Steroidogenic acute regulatory protein (*STAR*) gene is vital in steroid hormone synthesis and strongly conserved among vertebrate groups (Bacila et al., 2021), but has not been previously characterized in *Xenopus*.

STAR is involved in cholesterol transport and is the key rate-limiting step in the synthesis of steroids (Bauer et al., 2000). STAR facilitates the transporting of cholesterol to the inner mitochondrial membrane, where it is converted into pregnenolone by CYP P450, the precursor of all steroid hormones (Wehrenberg et al., 2001). Mutations in STAR result in congenital lipoid adrenal hyperplasia, as patients carrying this mutation are unable to synthesize sufficient levels of adrenal and gonadal steroids (King et al., 2002). If left untreated, these patients die shortly after birth (King et al., 2002).

STAR homologs have been identified in *Osteichthyes*, avian and amphibian vertebrates. This suggests that function of STAR protein is well conserved among vertebrates as well as the overall process of steroidogenesis and the enzymes involved (Bauer et al., 2000).

In zebrafish, *star* has been used to study organogenesis of the steroidogenic interrenal cells, and was found to be expressed in the forebrain, gonads and the interrenal primordium (To et al., 2007). Generally, *star* is described as a robust marker for the interrenal gland.

4.3.1 *Star* RNA sequencing data

Primers for cloning this gene were designed for the S chromosome variant in *X. laevis* and WISH probes obtained from PCR products. Like *nr5a1*, *star* does not seem to be highly expressed during *Xenopus* development based on the RNA sequencing data set found on Xenbase (Fig. 46). RNA expression of *star* shows two small spikes followed by steep drops at blastula (NF stage 9) with TPM at 0.04 and at Neurula (NF stage 15) with 0.11 TPM. Expression then increases at tailbud (NF stage 25) to 0.19 and rises again from late tailbud (NF stage 35/36) to its peak at 0.26 TPM at tadpole stage (NF stage 40) with an increasing trend (Fig.

46). Our RT-PCR shows *star* being present from NF stage 10.5, with strong presence during NF stages 14-24, again absence in NF stage 27 (as we have seen with many markers likely due to a fault in obtaining cDNA for this stage), and faint expression at NF stage 33 (Fig. 17). After NF stage 33, *star* was not found to be expressed in later tailbud stages, in stark contrast to the RNA-seq. data described.

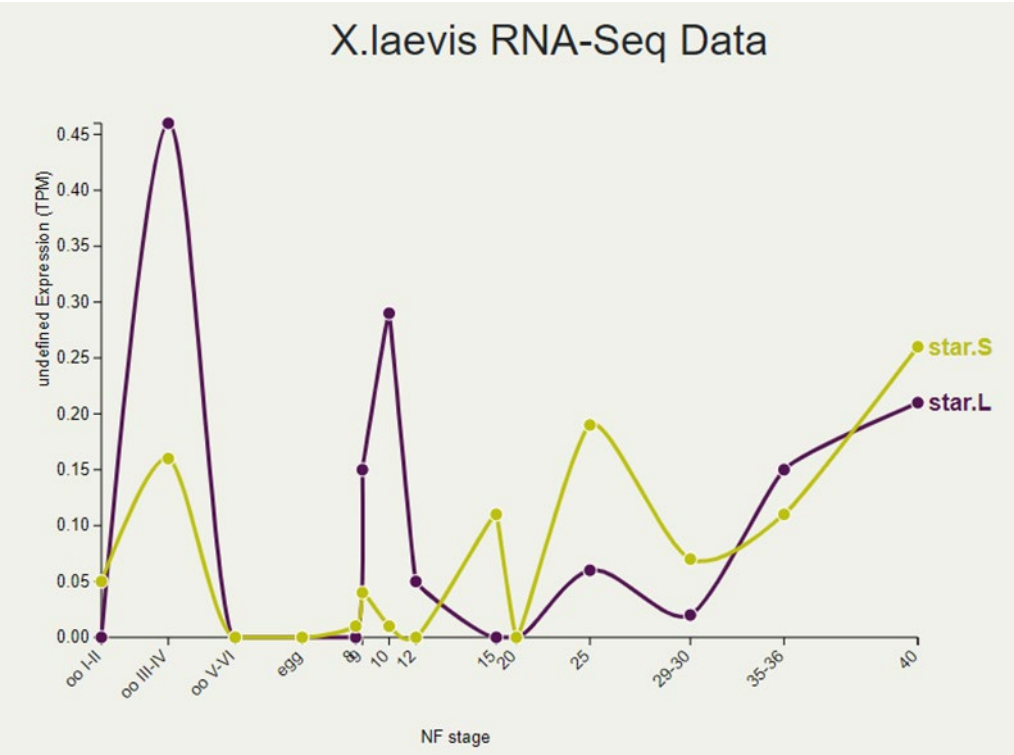

Figure 46: Xenopus laevis RNA-sequencing data for Star taken from Xenbase (Session et al., 2016).
Like with nr5a1, expression of both chromosome variants is very low, and the axis has been adjusted to be able to show the curve from 0.0 to 0.45 TPM.

4.3.2 *Star* in WISH

No expression signal was detected by WISH prior to late tailbud (Fig 47 A, B) NF stage 33. Like the expression seen with *nr5a1* WISH probes, expression of *star* mRNA appears as a thin line in the region of the pronephric duct, which extends medio-laterally during late tailbud (NF stage 33 to 40) and at tadpole stage (NF stage 40-42) of development (Fig. 47 B-D). Additionally, expression is visible in the hindbrain region of the embryo from late tailbud (NF

stage 33) and stays consistent throughout further development (NF stage 37/38 to NF stage 42). This expression in the hindbrain matches expression of several other markers used throughout this project, including *chga*, *dbh* and *pnmt* and likely also the hindbrain expression seen with *phox2a* and *phox2b*. This expression is specific to a local structure in the hindbrain and is likely the locus coeruleus, based on information on the function of this structure and the specific genes it seems to have expressed (see section 4.5.3).

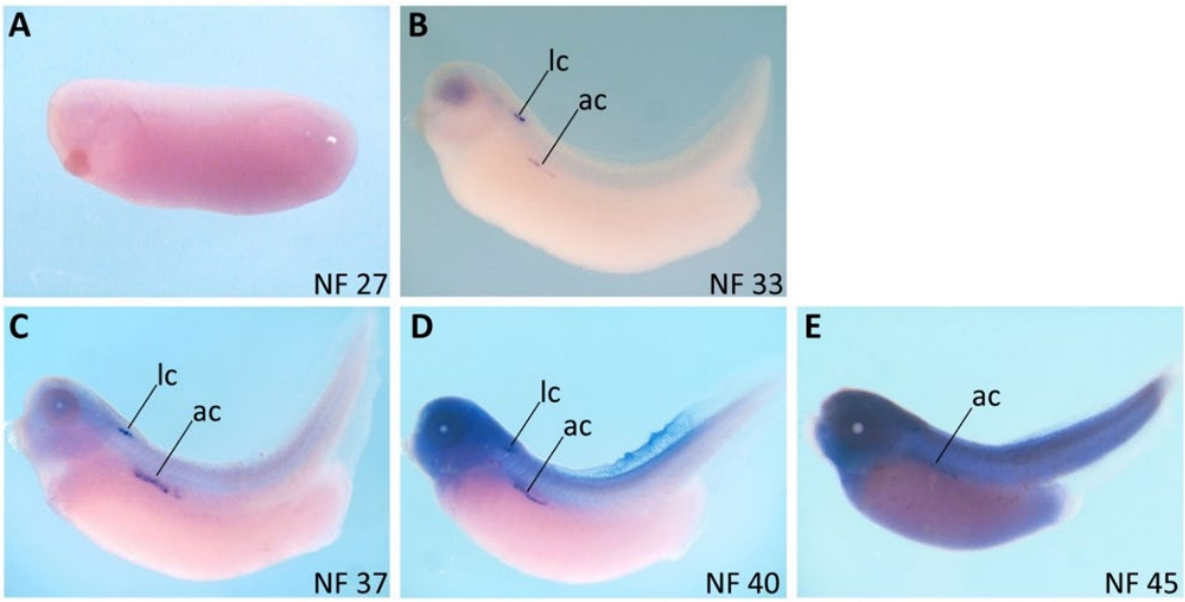

Figure 47: Spatial and temporal expression map of steroidogenic marker star during X. laevis embryogenesis.
Embryos are presented with the anterior on the left and the posterior to the right, embryonic stages are imaged ventrally. Star was not found to be expressed prior to late tailbud NF stage 33 (B). Here, expression is located beneath the somites and seems to extend ventrally beneath the somites during tailbud development (B-E). This expression pattern is assigned to be expression of the adrenal cortex, based on knowledge of this gene's expression location in other species. Additionally, we see expression in a hindbrain structure, also from late tailbud, that is likely the locus coeruleus. ac, adrenal cortex; lc, locus coeruleus

4.4 Pgat

When discussing the WISH results obtained by *nr5a1* and *star* to mark the AC, we came along one major issue of this project: As previously described, the AC arises from the AGP which, as the name suggests, gives rise to both the steroidogenic AC, but also the gonads. The gonads make gametes and are comprised of the ovaries in females and testes in males. These reproductive organs in vertebrates perform both gametogenesis (the production of functional

gametes for fertilization) and hormone production (gonadal steroids regulating physiological functions such as reproduction, maintenance of secondary sexual characteristics and various metabolic processes (Dreher, 2015).

These two steroidogenic tissues develop along the kidney. When looking at the structure and location of the presumptive gonads in *X. laevis*, the gonads appear on the ventral side of the developing kidney(Fig. 48), just as is presumed with the developing AG (Fig. 14,Chapter 3.1).

In *Xenopus*, the gonads develop along nearly the entire length of the mesonephros (Piprek et al., 2014). The genital ridges arise as parallel folds along the ventral surface of mesonephroi on both sides of the dorsal mesentery around NF stage 45 (Piprek et al., 2014; Wylie and Heasman, 1976). Gonadal formation is initialized when primordial germ cells (PGCs) migrate from the gut through the dorsal mesentery to the ventral surface of the vena cava, which is located between both mesonephroi (Piprek et al., 2017). PGCs are precursor cells, which are found in the germ line of most animals, giving rise to gametes (Machado et al., 2005). This migration to the presumptive gonadal ridge takes place between NF stages 44-49 (Wylie and Heasman, 1976). At NF stage 50, gonads are still sexually undifferentiated and contain few germ cells (Wylie and Heasman, 1976).

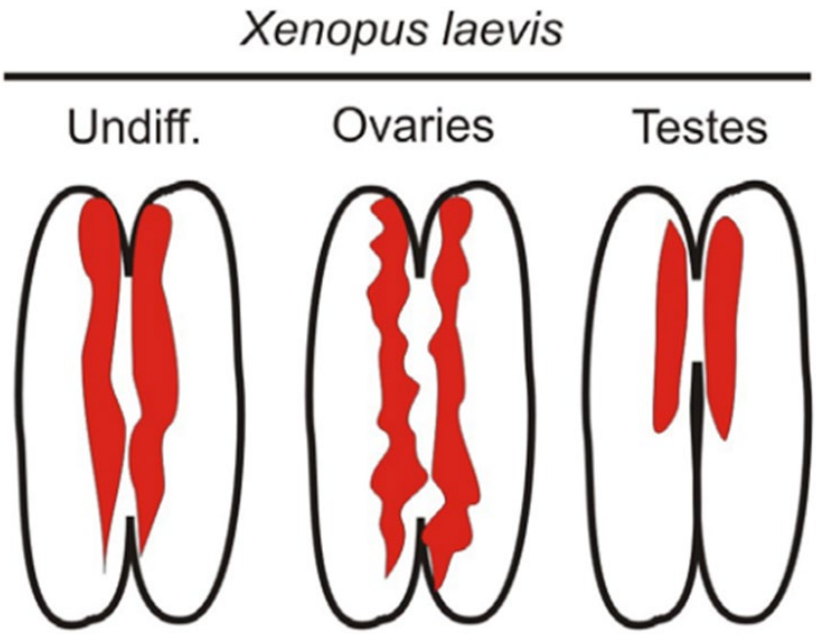

Figure 48: Schematic of gonadal structure and morphology in X. laevis.
Gonadal structure and morphology in X. laevis prior to differentiation (left) and after undergoing sexual differentiation to either ovaries or testes which are structurally different. Undifferentiated gonads are defined between NF stage 49-53 and ovarian development occurs after NF stage 53. From NF stage 55, visible differences in length are seen between long ovaries and short testes. The image was taken directly from (Piprek et al., 2014).

4.4.1 *Pgat* in WISH

Despite the difficulty in distinguishing gonads and the AC by expression pattern alone, we decided to look at the expression of the PGCs in *Xenopus* to determine their spatial-temporal separation from our presumed developing AC. Therefore, we created a riboprobe for the well-established PGC marker *pgat* (primordial germ cell-associated transcript protein) by cloning. The probe was designed for chromosome variant L. Pgat is an integral part of the germ plasm, and an excellent marker of migrating PGCs in *X. laevis* (Machado et al., 2005). We only looked at PGCs expression from tailbud stages, to compare them to AC markers.

We observed *pgat* expression starting at NF stage 30, where multiple PGCs were visualized in the posterior midline of the embryo, clustered together (Fig. 49 A). At NF stage 33, PGCs

appear in the dorsal posterior region of the endoderm, underneath the somites. While the expression seemed to be mainly in close proximity of the epidermis, some PGC cells have begun to migrate laterally and are more viscerally in the embryo. Later, during tailbud development, from NF stage 37, more cells have migrated towards the mediolateral region of the embryo (Fig. 49 C). At NF stage 40, all PGCs can be seen just beneath the somites, in the medio-lateral body axis, and they are again clustered together (Fig.49 D).

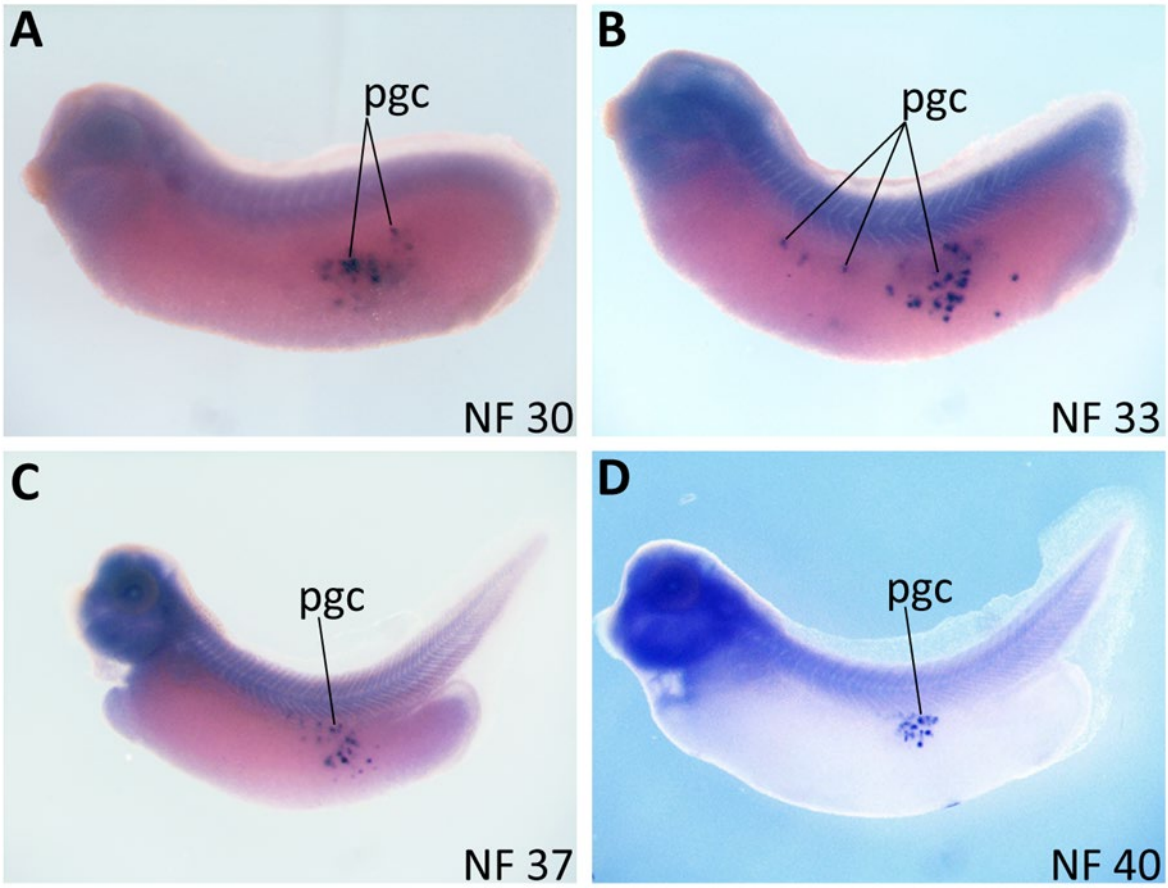

Figure 49: Spatiotemporal expression of primordial germ cell marker pgat during tailbud development of X. laevis.
PGCs are initially located as a cluster of well-rounded cells at the posterior medio-lateral side of the embryo (A). Cells become more interspersed and begin migrating towards the area of the presumed formation of the genital ridges from NF stage 45. Cells migrate anterior and medio-laterally, and appear more visceral (B-C). At NF stage 40, all PGCs have migrated just beneath the somites (D). pgc, primordial germ cells

4.5 Discussion

4.5.1 Expression of AC markers during *X. laevis* development is in the anticipated area of the embryonic kidney

In this chapter, we explored the expression of three genes of interest to mark the development of the adrenal cortex in *X. laevis,* during embryonic development. Using WISH with these marker genes, we wanted to pinpoint the location of the AC formation during embryonic development. Further we wanted to explore whether AG development in *Xenopus* is similar to mammals and other vertebrae species, even if it is not an entirely conserved process. *Xenopus* pronephric kidney development has been thoroughly studied, and *Xenopus* has been proven to be useful in studying human diseases affecting this organ, offering a simplified model to the more complex mammalian kidney (Nenni et al., 2019). If we can model AG development in this organism, this could enable *Xenopus* to emerge as another vital research model in the study of adrenal physiology and disease. Presently, there is no information on how this organ develops in *Xenopus* and if it holds a similar function and importance.

Both chosen AC markers *nr5a1* and *star* are well known marker genes involved in the development of the adrenal gland and onset of steroidogenesis across vertebrate species. *Cyp17a1* was additionally chosen for its role in cortisol biosynthesis and its part in androgen production. With these three marker genes, we hoped to cover all aspects of steroidogenic tissue formation, early steroidogenesis, and the active steroidogenic tissue. None of these three genes have previously been characterized in *Xenopus*.

All three genes showed a good percentage identity (protein-protein) to *Homo sapiens, Mus musculus* and *Danio rerio*, although the percentage identiy of *cyp17a1* in both *Homo sapiens* and *Mus musculus* was lower (50.31% and 47.93% respectively) than in *Danio rerio* (94%). Clones of these genes were obtained by cloning as described in section 2.5.

We performed spatial-temporal expression analysis of our genes of interest using WISH during embryonic development to investigate AC development. None of the three genes showed expression prior to tailbud stages. The earliest gene expression to be detected was *nr5a1*, which was expressed initially as a short line, just below the somites, medio-laterally at

embryonic NF stage 27 (Fig 45). From NF stage 33, expression in the same region was detected for both *star* and *nr5a1* (Fig.50). The linear expression pattern extends medio-lateral for both genes during tailbud stages and was still visible at tadpole stage (Fig. 50). The expression for both these markers was in the expected region, near the developing pronephric kidney. When comparing the expression of *nr5a1* and *star* to the expression pattern of the pronephric kidney marker *pax8* (Fig. 50), we can see that expression of these genes might overlap with the ones of the pronephric duct. No expression is seen in the region of the pronephric tubules.

No expression in the region of the pronephric kidney was detected for marker gene *cyp17a1* and is therefore likely not expressed in the developing AC in *Xenopus* (see Fig. 52 F). In fact, we can exclude the possibility of technical errors during the WISH, since we observed a staining in the hindbrain, that we hypothesize to be the LC (see section 4.5.3, Fig. 52) Therefore, it was dismissed as a marker for the AC in *Xenopus*.

When we compare the expression of our steroidogenic markers to our CC markers (Chapter 3), we can clearly see that their expression patterns do not overlap. This is not surprising, in some ways, as these organs develop from separate tissues. CCs are NC derived and, in mammals, innervate the adrenal primordium at a later time point of development. The steroidogenic AC develops from the intermediate mesoderm, and gives rise to the adrenal primordium (Pihlajoki et al., 2015). However, this result clearly shows that the NA cells that we think might give rise to CCs in *Xenopus,* or perform CCs function prior to metamorphosis, develop at different developmental time-points, and do not seem to associate with the AC markers. Still surprising is the fact that NA cells were already expressed at late neurula stage (Fig. 42). Some previous work has even shown that the expression of *phox2a*, *insm1* and *th* in NA cells starts as early as NF stage 15/16 (Wylie et al., 2015). In stark contrast to this, our AC markers were not expressed prior to tailbud organogenesis, with *nr5a1* being first visualized at NF stage 27, whereas *star* was not seen to be expressed prior to NF stage 33 (Fig. 47). In other animal species, steroidogenic tissue develops first, giving rise to the adrenal primordium in close vicinity to the embryonic kidney, which is later innervated and colonised by catecholaminergic CCs (Ehrhart-Bornstein and Bornstein, 2008).

The presence of the NA cells long before the apparent initial formation of steroidogenic tissue, as observed with our WISH, indicates that these cells might develop earlier, in *Xenopus,* than expected. Further, our data show no direct indication of being in close association with steroidogenic tissue. This is unusual, as there seems to be evidence for crosstalk between steroidogenic cells and CCs, as is the case in mammalian species (Bechmann et al., 2021; Ehrhart-Bornstein and Bornstein, 2008).

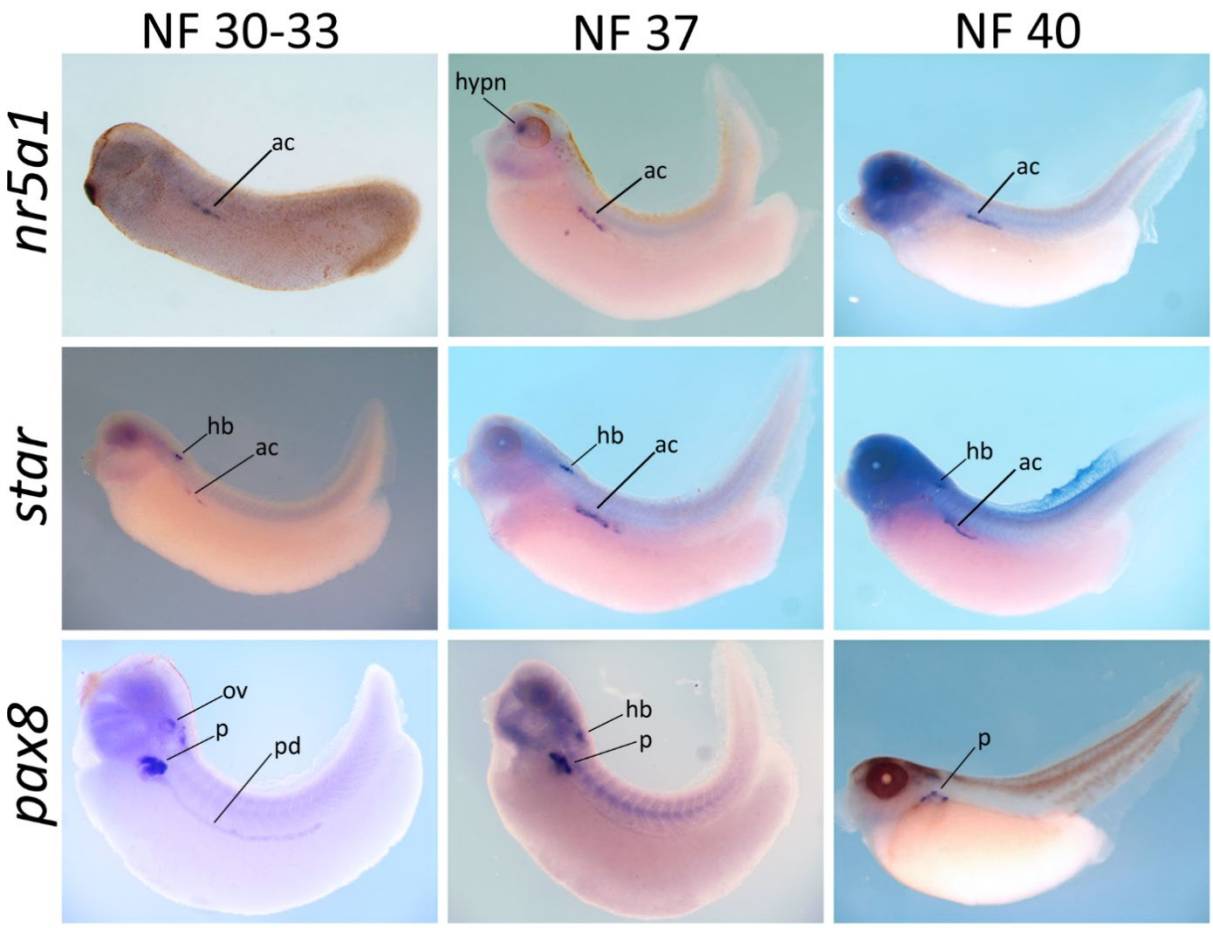

Figure 50: Expression comparison of markers for the AC to the expression of pronephric kidney marker pax8.

Pax8 was used as control during late tailbud development stages in X. laevis. Embryos are imaged laterally are orientated with the anterior to the left and posterior on the right. Both chosen AC markers nr5a1 and star are expressed in the anticipated area that seems to be close to the developing pronephric duct. Expression of AC markers extend medio-laterally during late tailbud development, whereas pax8 expression begins to be localized in the pronephric tubules at later stages. Both star and pax8 are expressed in the hindbrain. ac, adrenal cortex; hypn, hypothalamic nucleus; hb, hindbrain; ov, otic vesicle; pt, pronephric tubule; pd, pronephric duct.

4.5.2 Distinguishing the adrenal cortex from the developing gonads

Despite our initial excitement and conclusion to having located the AC during *X. laevis* embryogenesis, by using evolutionary strongly conserved marker genes, there is one issue that we must consider carefully before defining this expression. The AC of human and rodents originates from the AGP, a common progenitor for both the AC and the gonads (Cheng et al., 2022). Gonads are the reproductive organs giving rise to testes and ovaries and produce the gametes and hormones essential for reproduction. Although the AC is the major source of steroid hormones in vertebrate bodies, gonads also produce steroid hormones, which are required for reproduction (Cheng et al., 2022).

Both tissues have an initial and maintained expression of *nr5a1 (Rotgers et al., 2021)*. Additionally, *de novo* synthesis of all steroid hormones, in all steroidogenic tissues including the interrenal gland, gonads and brain, begins with the transport of cholesterol into the mitochondria, performed by our marker gene *star (Tokarz et al., 2013)*. Therefore, both of our highly specific, and highly conserved maker genes are also found to be expressed in the developing gonads.

Initially, in vertebrates, the gonads form as sexually bipotent structures known as genital ridges, through the transformation of coelomic epithelium into a cluster of somatic cells (Piprek et al., 2016). The early genital ridges are a group of somatic SF1-positive cells, called gonadal precursor cells, derived from proliferating coelomic epithelium (Piprek et al., 2016).

When we compare the expression of PGC marker *pgat* to that of *star* and *nr5a1* we can clearly see that, at NF stage 30, both are expressed spatially separated (Fig. 51). From NF stage 33, we can see that some PGCs have migrated more medio-laterally and could be well in the area of *nr5a1* and *star* expression (Fig.51). At NF stage 37, we observed most PGCs migrating towards the posterior end of where we visualized *nr5a1* and *star* expression (Fig. 51). We observed the same kind of expression also at NF stage 40.

As the genital ridge does not form prior to NF stage 45, according to the limited existing literature (Piprek et al., 2017; Wylie and Heasman, 1976), we could presume that the observed expression of *nr5a1* and *star*, which was observed between NF stages 27 to 45, is to be

attributed to the developing AC. This would only be based on the developmental time point of our observed expression pattern. Unfortunately, available literature is based on cell morphology and structure, rather than gene expression (Hanke, 1978; Kloas et al., 1997). Therefore, we cannot exclude the possibility that the structure observed by WISH using *nr5a1* and *star* probes could also show the formation of precursors of the genital ridge, and not the AC. As described earlier, the genital ridges highly express SF-1 throughout vertebrate species, and while there is no literature proving this case in *Xenopus*, we can likely presume that, due to the highly conserved developmental processes of these organs among vertebrates, this would be the case.

To further investigate the relation between the AC and the PGCs, a DISH or Hybridisation Chain Reaction (HCR) should be used, to allow for visualization of possible co-expression/co-localisation of different genes within the same embryo. Furthermore, there seems be no thorough investigation of how the gonads develop in *Xenopus* prior to sexual differentiation. Additionally, there is no literature found on gene expression during early gonadal development. This strongly encourages the opportunity to study the developmental process of the gonads in *Xenopus* and to elucidate if these processes are evolutionary as well conserved as they appear to be across different model species.

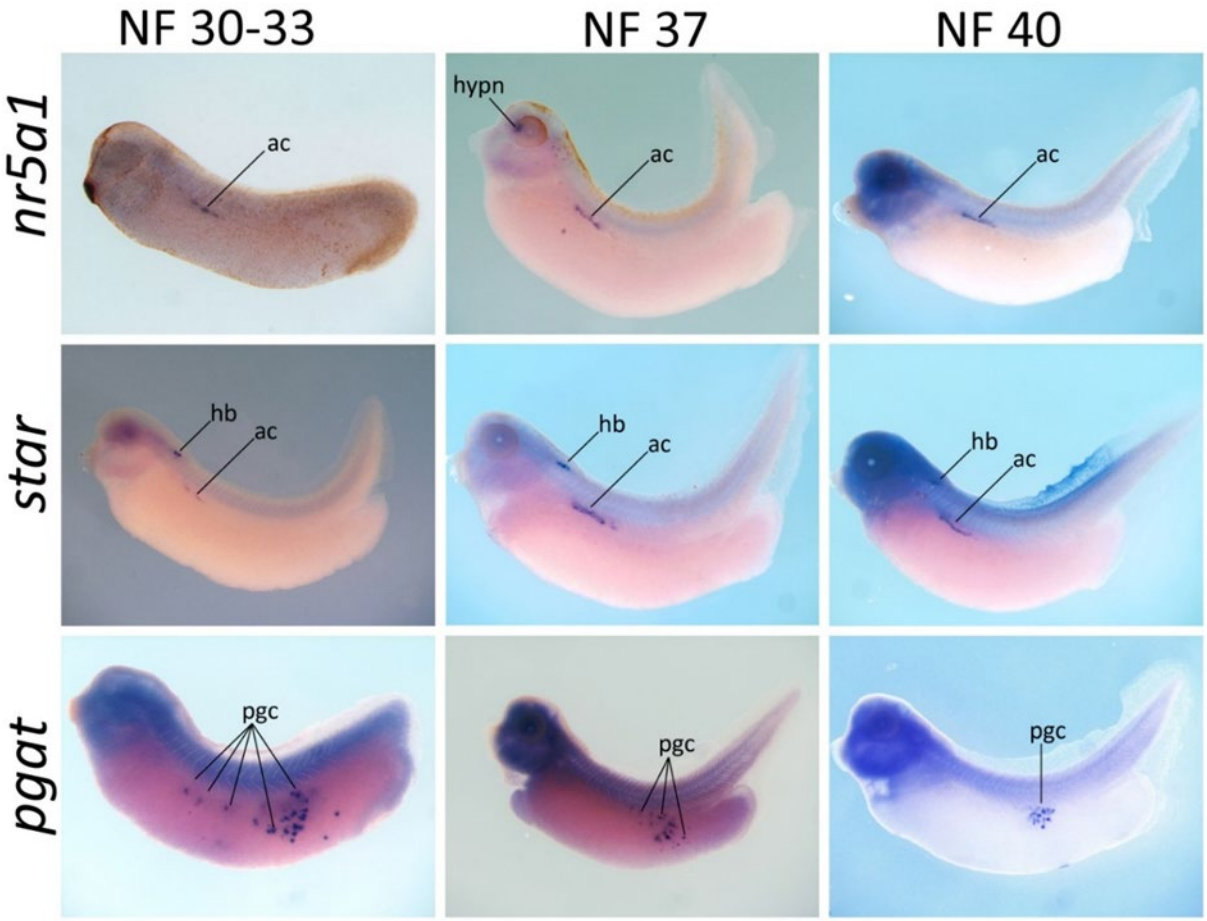

Figure 51: Comparison of expression of adrenal cortex markers star and nr5a1 to gonadal primordial germ cell marker pgat during tailbud developmental stages in X. laevis. *Embryos are imaged laterally and arranged with the anterior to the left and posterior to the right. Gene names are indicated on the left and staging is found at the top. Expression of cortex markers nr5a1 and star both starts in the anterior side of the embryo, just beneath the somites, and follows medio-lateral extension throughout development. PGCs are found more to the posterior side of the embryo, at the midline, and cells migrate dorsally and anterior throughout tailbud stages, and eventually cluster just beneath the mid-posterior somites, at NF stage 40. Expression of cortex markers to PGCs markers is spatially distant throughout, only at NF stage 40 do PGCs look to be in close proximity to the posterior end of cortex expression. It does not look like the expression would co-localize. ac, adrenal cortex; hypn, hypothalamic nucleus; hb, hindbrain; pgc, primordial germ cell*

4.5.3 Identifying the hindbrain expression pattern – locus coeruleus?

One other expression pattern we consistently visualized with multiple marker genes during this project, and that we wanted to discuss is the hindbrain expression pattern we saw with marker genes *phox2a* and *phox2b*, *dbh*, *pnmt*, *star* and *cyp17a1*, that we hypothesise to be the locus coeruleus (LC). (Fig. 52)

The LC is a vertebrate specific, small group of NA cells situated within the brainstem, with extensive axons projecting throughout the brain, providing noradrenaline (Wang et al., 2022b). The LC regulates many fundamental brain functions, including the "fight-or-flight" stress response, and sleep and wake cycles (McKinney et al., 2023). Among non-mammalian vertebrates, such as birds, reptiles, amphibians, and fish, structures analogous to the LC have been identified as well as a correlation between the number of LC neurons and the complexity of the species' nervous system (Wang et al., 2022b). Zebrafish only possess between 10-20 LC neurons, whereas humans have up to 50.000 cells withing this structure (Wang et al., 2022b). The LC, while strongly evolutionary conserved, has not been extensively studied among non-mammalian species.

Neurons of the LC are identified by their immunoreactivity for enzymes critical in NA biosynthesis, specifically *th* and *dbh* (Benarroch, 2018). In *Xenopus*, noradrenaline as well as *dbh* and *th* were found to be present in the LC homolog by immunohistochemistry (González and Smeets, 1993). We clearly see expression of *dbh* in a specific HB region (Fig.52) that is indicated by literature to be the LC (McKinney et al., 2023; Yokogawa et al., 2007; Zhang et al., 2011). However, we did not study the expression of *th* thoroughly enough to visualize expression in that region. *Phox2a* and *Phox2b* are both required for the generation of neurons of the LC and it's regulation of the noradrenergic phenotype (Vermeiren et al., 2020). Mice with a null mutation in the *Phox2a* gene completely lack a LC (Morin et al., 1997). While expression in this structure with these two markers is not clearly distinguishable from the overall expression in the HB, the well-defined role in the development and expression of the LC in the literature, indicates that the expression we see in the HB with these two markers is indeed the LC (Fig. 52, indicated by black arrowheads)(Pattyn et al., 2000; Vermeiren et al., 2020). *Pnmt* is known to be present in specific neurons in the brain stem of mammals, but not directly in the LC. However, adrenergic fibres immunoreactive to PNMT have been traced into the LC in the human and rat brain (Kitahama et al., 1985). However, the direct function of this interaction is not known yet.

Based on the location and similarity of expression pattern to that of *dbh*, we hypothesise that *pnmt* may be expressed in the LC of *Xenopus* embryos, or in a structure closely associated to

the LC, which likely interacts with the LC to regulate the stress response in the brain. However, *pnmt* expression has not been characterized in *Danio rerio* nor *Xenopus laevis*.

In the mouse brain, both Star and Cyp17a1 were found to be immunoreactive in the LC nuclei, implicated to play a role in the regulation of stress and hormone secretion in the brain (Chen et al., 2022). We found that both of these genes were expressed in a specific HB region in the brain of *Xenopus* embryos, that positionally matches the expression of *dbh* in the LC (Fig. 52).

While the observed expression pattern in the HB of the above presented markers is seemingly highly specific to the function and location of the LC, our observations are purely speculative, on the basis of pre-existing literature and structural morphology of *Xenopus* embryos. To further confirm this hypothesis, we would need to perform functional assays, and analysis of protein expression by immunohistochemistry and look at other markers?

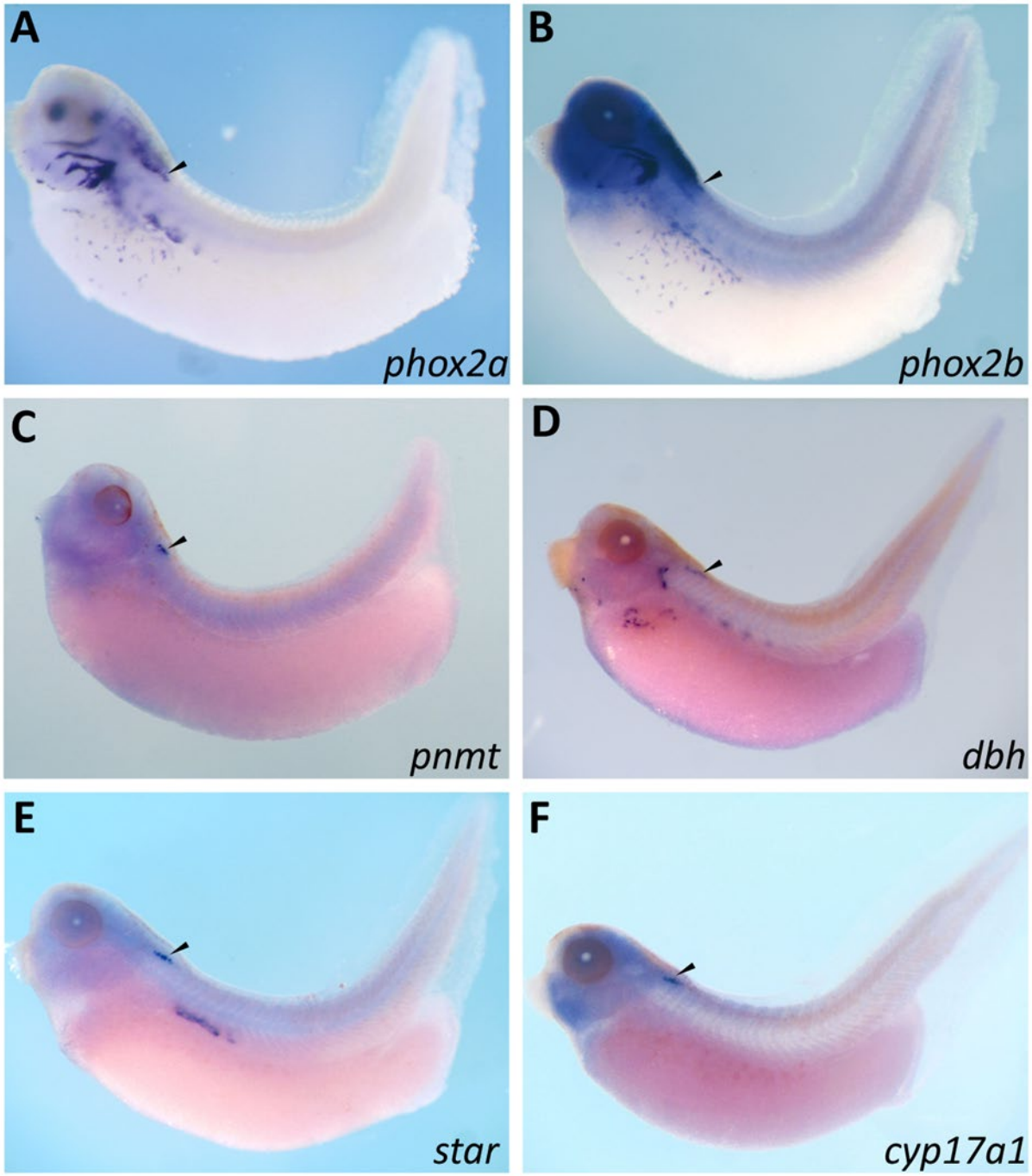

Figure 52: Summary of marker genes that show expression in a hindbrain structure, likely the locus coeruleus (lc) in X. laevis at NF stage 40.

All embryos are viewed laterally and orientated with the anterior side to the left and posterior to the right. Embryos show the most expression in this structure between NF stage 37-40 and all embryos are shown at these stages. Both the location of the expression, as well as the marker genes expressing this pattern, indicates the structure being the LC (homologue) in Xenopus laevis embryos, which is responsible for noradrenaline production and distribution in the brain. The LC is strongly conserved evolutionary among vertebrates and is located in the brain stem, specifically deep within the pons, indicated with black arrowheads.

4.6 Summary of Chapter III and IV

In these two chapters, we investigated the development of the AG in *Xenopus laevis* during embryogenesis by performing WISH, using selected marker genes on key developmental time-points of organogenesis. While anticipating expression along the pronephric duct of the developing pronephric kidney, we came across a rather curious expression pattern of numerous singular and well-rounded cells appearing at the anteroventral side of the embryo at NF stage 19/20. These cells then seem to move/expand towards the anterior midline of the embryo, where they cluster together around NF stage 40, posterior to the branchial arches and beneath the region of the anterior pronephros (Fig.53, purple dots). This was the case for nearly all chosen CCs markers. Upon further investigation we learnt that this population of cells had been previously identified as noradrenergic neurons (NA neurons), using some of our chosen marker genes including *phox2a* and *th*. Based on previous publications and our thorough characterization of these NA neurons, using multiple marker genes identified as being directly expressed in CCs or involved in NC specification and differentiation to the SA lineage, we postulate that these cells are indeed early CCs markers of *X. laevis* during embryogenesis. Furthermore, previous research by Wylie and Colleagues has indicated that these cells are derived from the NC, and expression in the cells for some of the markers begins as early as NF stage 14 (neurula). This aspect of this cell population will be further addressed in Chapter 6.

This revealed two things: First, these NA neurons/CCs do not associate with the pronephric kidney or the AC prior to metamorphosis and, second, the regionality and time-point of expression of NA marker genes indicates that the NC may migrate much further in the embryo than currently assumed during *Xenopus* embryogenesis.

We further investigated AG development during embryogenesis by characterizing the spatio-temporal expression of marker genes involved in AC development. We used markers *nr5a1* and *star*, which are both involved in steroidogenic tissue formation and steroidogenesis and have not yet been characterized in *Xenopus*. Both markers were expressed in the area of the developing pronephric kidney (Fig. 53, blue line) and are therefore likely showing development of the AC in close association with the pronephric kidney.

For a comparison of gene expression patterns between Xenopus laevis and Xenopus tropicalis see Appendix chapter 9.1.

Additionally, we looked at the spatio-temporal migration of PGCs in relation to the formation of the supposed AC (Fig. 53, pink). We did not see PGCs expressed in close association to our AC expression during embryogenesis, and therefore assume that the gonadal tissue has not fully formed during this developmental time point, and that we did identify the AC with these markers.

Lastly, we characterized another key NC-derived developmental process: the development of the ENS in *Xenopus laevis* with two of our CC development marker genes: *phox2a* and *phox2b*. At late tailbud, we see expression of both markers in developing vagal NCCs moving along the vagus nerve, giving rise to ENS and enteric glia along the developing intestine (Fig. 53, dark blue neurons). This has not been characterized before and is not well-studied in this animal model.

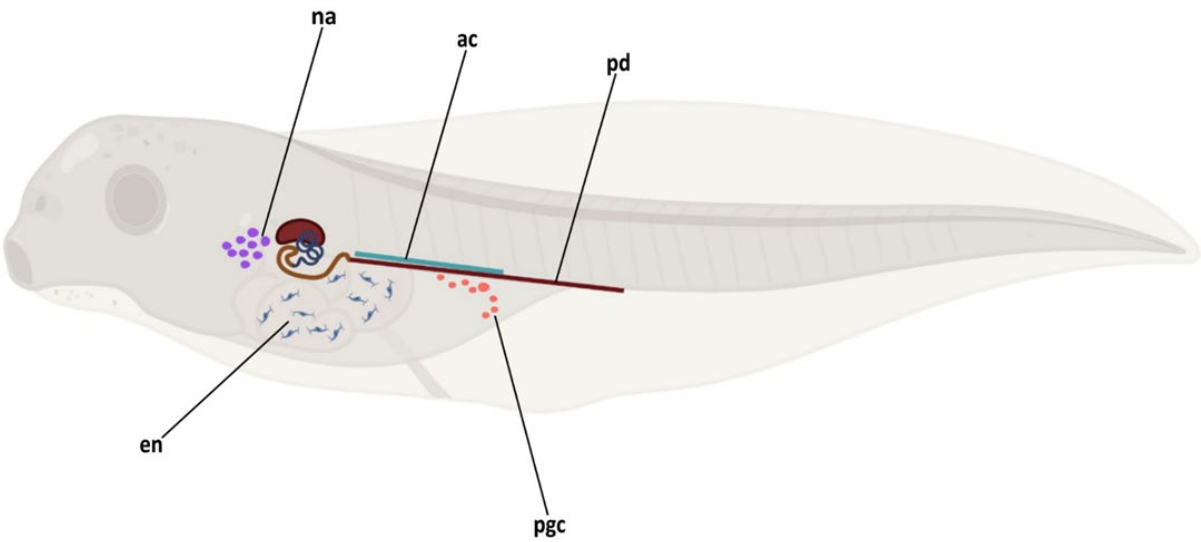

Figure 53: Summary of expression patterns identified and described throughout the process of characterizing the developing adrenal gland in Xenopus laevis.
We first identified well rounded, single cells, that have been labelled as being noradrenergic and suggest them as chromaffin cells of the developing X. laevis embryos (na, purple). Next, we characterized the development of the adrenal cortex (ac, blue). This develops in close association with the pronephric duct (pd, brown) of the developing kidneys, as previously anticipated. To exclude the possibility of the expression labelled as AC potentially showing the developing gonads, we characterized the spatio-temporal expression of primordial germ cells (pgcs, pink), which migrate through the embryo into the developing gonadal tissue, where they differentiate to either ovaries or testes. We did not see the PGCs in close association with the AC during embryogenesis, assuming the gonadal tissue has not been fully formed yet, and therefore conclude to have correctly identified the developing AC with our chosen marker genes nr5a1 and star. Finally, some of our chosen marker genes for CCs development and differentiation are also involved in the development of enteric neurons (en, dark blue) and glia formation of the ENS. We visualized expression of migrating NCCs along the vagus nerve, giving rise to EN and glia along the developing GI tract of X. laevis embryos. This developmental process has never been characterized in this animal model before, and neither has the expression of the genes involved in the process (phox2a/b) and therefore presents another novel gene expression profile.

5 Chapter V: Performing Hybridisation Chain Reaction to multiplex genes showing presumptive CCs and the AC

5.1 Introduction

In the previous chapters we have identified several markers of interest to characterise the development of CCs and the AC during *Xenopus* development. To our surprise, our chosen marker genes, including genes important for the initial development and differentiation of both sympathetic neurons and CCs (*phox2a/b* and *insm1*), neuroendocrine secretory protein (*chga*), and catecholamine biosynthesis enzyme (*dbh*), all showed expression in numerous punctated single cells in the anteroventral region of *Xenopus laevis* embryos. We have also seen expression of these single cells with genes encoding for catecholamine biosynthesis enzymes *th* and *pnmt*, as well as with another SA differentiation marker, *hand2*. We have characterised the expression of these cells from late neurula stages until tadpole. Additionally, previous research by Parlier and colleagues found this exact expression pattern of individual cells beginning at the anteroventral side of *Xenopus* embryos as early as neurula NF stage 14/15 with marker genes *ascl1*, *phox2a*, *hand2* and *th*. Based on the expression of these specific marker genes, that are all involved in sympathetic neuron development, Parlier and Colleagues labelled these cells as being NA neurons (Parlier et al., 2008).

While it is likely that these cells, marked by genes crucial for the development of the SA lineage and catecholamine phenotype, are indeed expressing the same markers, this has not been definitively shown.

To confirm that the individual punctate cells pattern we characterised and labelled as being NA neurons share a similar expression profile, we performed in situ hybridization chain reaction (HCR) using our key markers of interest. HCR allows us to hybridise multiple different RNA probes and tag them with distinct fluorophores within the same embryo. This enables us to study co-expression patterns of key genes from our previous chapters involved in SA development. Simultaneous detection of different mRNA species could help us identify which genes are active together within the same cell. This will take us a step further in confirming these cells as either embryonic CCs, or precursors of such cells. The HCR method has the advantages of having high sensitivity and effective background suppression. Using the HCR RNA-FISH protocol and probes designed by Molecular Instruments (MI) further provides us with a reliable method to verify the expression patterns we have characterised with our WISH

probes. This double-check approach also ensures the accuracy and consistency of our findings, strengthening the validity of our observed gene expression patterns.

5.1.1 Hybridisation Chain Reaction – HCR™ RNA-FISH

Hybridization Chain Reaction (HCR) is an enzyme-free, fluorescent in situ hybridization technique that allows for the spatial visualization of gene expression, offering insights into various developmental stages and the precise localization of genes of interest. HCR facilitates the visualization, evaluation, and analysis of gene expression at both tissue and subcellular levels (Kufukihara et al., 2022). This technique is notably more sensitive than traditional WISH, enabling the simultaneous detection of multiple RNA targets within the same embryo, enabling the analysis of gene expression patterns of different genes (Choi et al., 2018). This is not easily accomplished by WISH, and requires making additional probes that have to be labelled with FITC, or by performing immunohistochemistry. Both options are time-intensive and have some additional disadvantages: Fast-red staining is not as visible as WISH. IHC in *Xenopus* is severely limited by the amount of antigens that are made for this model species, and the lack of antigen-targets tested for most.

The HCR process involves using DNA hairpins, which are short DNA oligonucleotides that form a hairpin loop structure. In HCR, two types of DNA hairpins are used: initiator hairpins and monomer hairpins. Initiator hairpins have a single-stranded region complementary to a specific target nucleic acid sequence. Upon binding to their target sequence, the initiator hairpins undergo a conformational change that exposes a new single-stranded region (Tsuneoka and Funato, 2020). Monomer hairpins have two single-stranded regions, one of which binds to the exposed region of the initiator hairpin, leading to a conformational change and further exposure of new single-stranded regions. This creates a chain reaction where additional monomer hairpins bind, resulting in signal amplification. As the split-initiator probes (P1 and P2) each carry half of the initiator sequence, no signal amplification can take place if probes bind non-specifically. To date, there is no established HCR-FISH protocol for use on *Xenopus laevis* by MI and few publications have used this technique in this model

species. An additional goal of this work was, therefore, to introduce and establish HCR RNA-FISH protocol in the Wheeler laboratory. We used the HCR RNA-FISH protocol designed for whole-mount zebrafish embryos and larvae with a few adaptions, mainly on length and concentration of proteinase K (PK) treatment, and adding an additional bleaching step prior to the start of the protocol (see section 2.8)

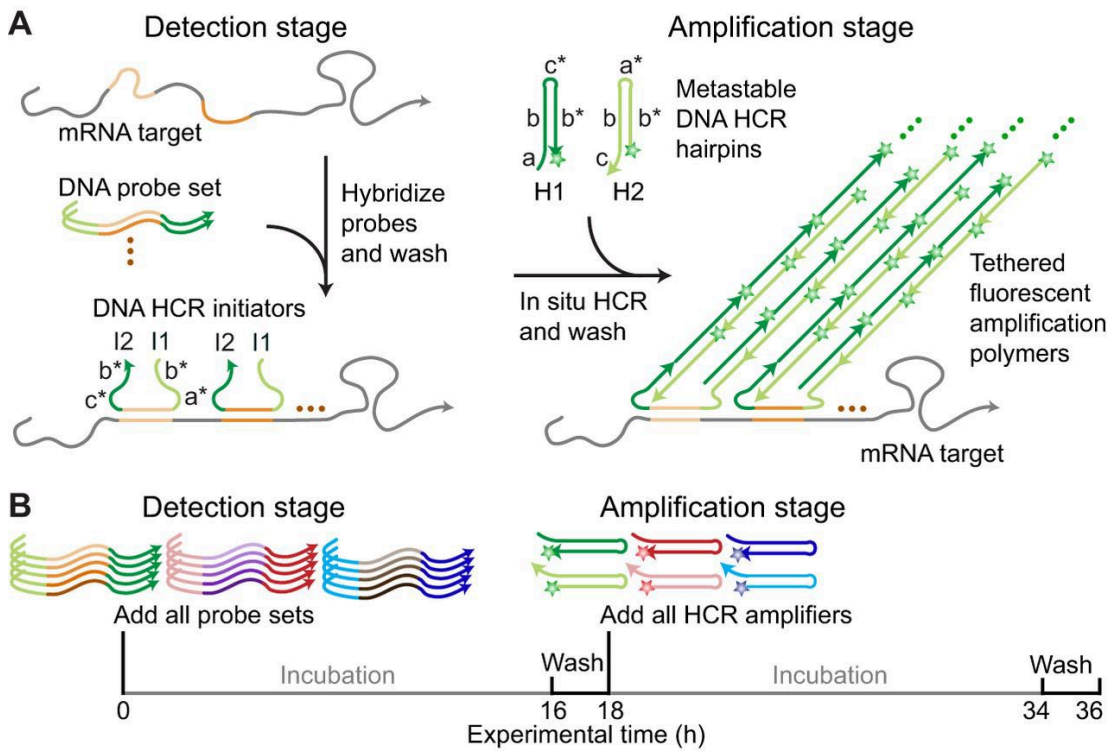

Figure 54: Schematic of a two stage, multiplexed in situ hybridisation chain reaction (HCR). *A: In the detection stage, DNA probes equipped with DNA HCR initiators (I1 and I2) bind to their respective mRNA targets by hybridization. Unbound probe is subsequently washed away. During the amplification stage, DNA HCR hairpins (H1 and H2) penetrate the sample. The initiator then triggers chain reactions as fluorophore-labelled H1 and H2 hairpins sequentially open and assemble into fluorescent amplification polymers which remain tethered to the target site. Unused hairpins are again washed away and samples can be imaged using a two-photon- or confocal microscope. B: Experimental timeline of HCR protocol remains consistent no matter the number of targets, and takes around two days to complete. Image created by and taken from (Choi et al., 2016).*

5.2 HCR RNA-FISH testing, targeting *phox2b* and *pax8*

To assess the functionality of the HCR RNA-FISH protocol in *Xenopus laevis* with our target probes, we initially performed HCR using only a single probe. We decided to test our kidney marker pax8 at tailbud NF stage 37 (Appendix Figure 1). The protocol is performed using in situ hybridization kits from MI, and was performed initially in accordance with their official whole mount zebrafish protocol. To obtain the probes, including the one used to identify *pax8* expression, mRNA sequences for our genes of interest were sent to MI company, who provides a kit with the in-situ probes, and the required buffers and amplifiers. Probes were designed using accession numbers from the Ensembl gene browser. Probe sequences designed by MI are not provided by the company.

The pronephric kidney marker *pax8* probe was designed to be used with amplifier B4 + Alexa Flour 647. The SA master regulator *phox2b* was designed to be used with amplifier B1+ Alexa Fluor 546 or Alexa Fluor 594. Optimisation of the control marker gene pax8 at tailbud stages was the starting point for adapting the HCR protocol for use in Xenopus laevis. After adapting the incubation time and concentration of PK to the parameters we used for our WISH protocols (See section 2.7), we obtained a good signal of pax8 in far red (Alexa Fluor 647). However, using Alexa Fluor 546 (orange) with our probes designed with amplifier B1, generally resulted in weak signal, compared to background fluorescence, and this fluorophore was therefore dismissed from further usage (Appendix Figure 2). Using Alexa Fluorophore 594 with our *phox2b* probe generally provided a stronger signal, especially in the cranial ganglia (Fig. 55 A).However, we were unable to visualize the NA neurons at NF stages 30-37 with the provided probe. While troubleshooting this, we realised that we provided MI with the mRNA sequence for the L chromosome variant, rather than the S chromosome variant we used to design our WISH probe for *phox2b*. This could mean that the *phox2b.L* variant is only expressed in the cranial nerves while the *phox2b. S* variant is expressed in both cranial nerves and the NA cell. If this is the reason why we were unable to visualize the NA neurons with the probe or if this was due to other challenging factors we encountered, such as strong auto fluorescent background or the intense expression signals in the facial ganglia and hindbrain that may have overshadowed weaker signals in the smaller single cells we were hoping to target, we are not sure.

Despite these issues, we obtained robust fluorescent signals for both *pax8* and *phox2b* and performed HCR with both probes in the same embryo at NF stage 37, to assess if we are able to still obtain good signal when using two probes within the same embryo, and to see if there is co-expression of *pax8* and *phox2b* along the pronephric kidney (Fig. 55).

Pax8 expression is observed in the pronephric tubule and weak expression along the pronephric duct (Fig. 55 B). Weaker expression of *pax8* at late tailbud stage is consistent with *pax8* WISH probe expression and correlates with decreasing overall *pax8* mRNA presence at later stages, as shown by RNA seq. data (Session et al., 2016). Expression of *phox2b* was less intense when compared to the signal obtained when performing *phox2b* HCR alone, and only visible in the facial ganglia. No coexpression was observed between *pax8* and *phox2b*. *Phox2b* was excluded from further HCR co-expression experiments based on the above mentioned technical difficulties.

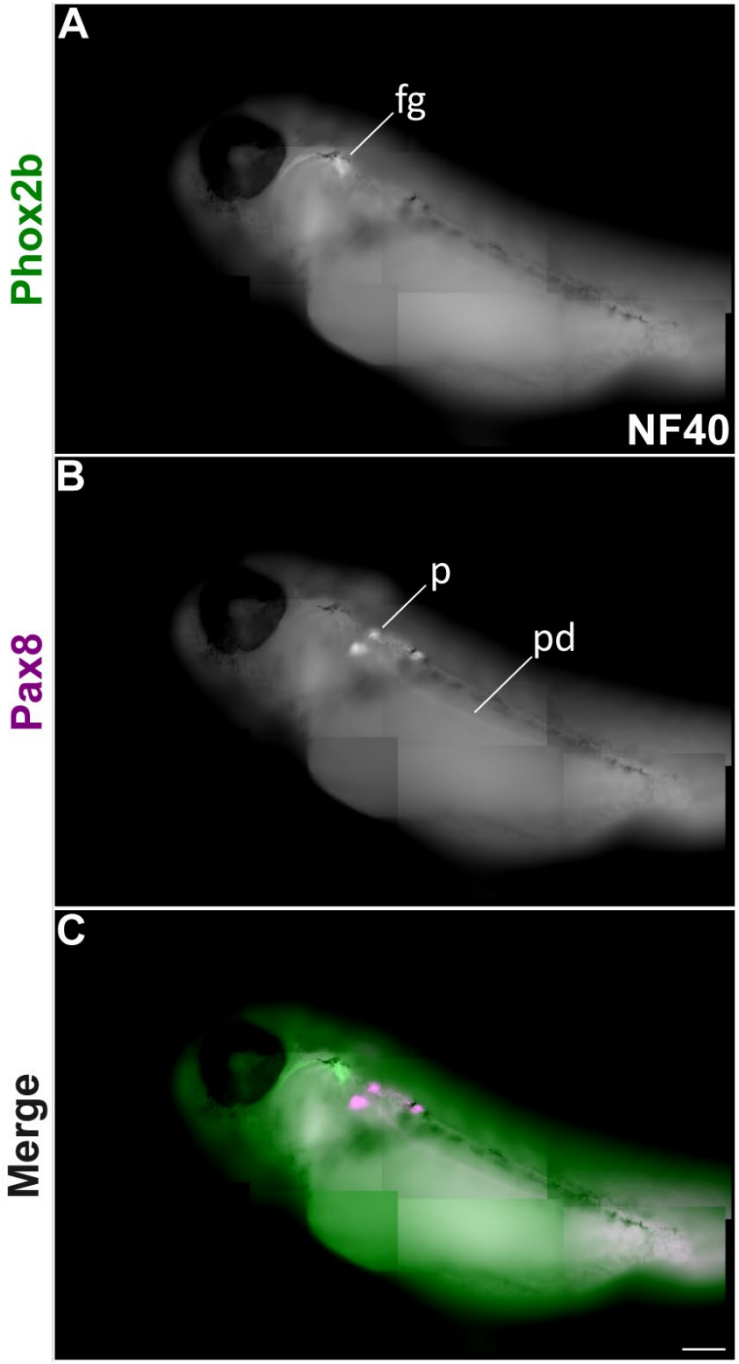

Figure 55: HCR expression of SA specifier marker phox2b and control gene pax8 in Xenopus laevis embryo NF stage 40.

Embryo is a lateral view with anterior to the left. To first test HCR detection of markers in Xenopus laevis with a slightly revised protocol, we performed HCR in NF stage 40 embryos with phox2b (A, green) and pax8 (B, magenta). Phox2b was labelled with 594 (red) and pax8 with 647 (Far-red) as these wave lengths gave the strongest signal with the least amount of background. Phox2b is expressed in facial ganglia, while pax8 is expressed in the pronephric tubules and weakly along the pronephric duct. Markers show no co-localization. Scalebar, 200 µm. Fg,facial ganglia; P, pronephros; Pd, pronephric duct;

5.3 HCR co-expression analysis targeting *phox2a* and *dbh*

To see if SA TF marker gene *phox2a* and catecholamine biosynthesizing enzyme gene *dbh* are co-expressed in the same NA cells, we performed our adapted HCR protocol with both these markers at early tailbud NF stage 30. This stage was selected as this was the time point where the punctuated single cells were clearly visible with both WISH probes at this developmental stage.

The *phox2a* HCR probe was designed to be used with amplifier B1 + Alexa Flour 647 or Alexa Fluor 546. The *dbh* HCR probe was designed to be used with amplifier B2+ Alexa Fluor 594.*Phox2a* expression was detected in the facial ganglia and in some single NA cells across the anterior body of the embryo (Fig. 56 A). *Dbh* was solely expressed in the NA cells across the anterior body, as was the case with the WISH probe for *dbh* (Fig. 56 B). When merging both imaging channels, we observed co-expression of the *phox2a* and *dbh* gene in the NA cells (Fig. 56 C). To further assess co-expression in these cells, we decided to measure the signal intensity of the two genes using ImageJ and then Excel to visualize the resulting graph (Fig. 57). On the x-axis, we have the distance measured in micrometres (µm), representing the spatial location along a line drawn through two selected cells (indicated by white arrow heads, Fig. 56 C'). The y-axis shows the signal intensity in arbitrary units (AU) for both genes, indicating the levels of gene expression. In the graph, we observed distinct spikes in signal intensity at specific points along the x-axis. Each spike represents the location where the signal for each gene is the highest. The superimposed spikes for the two genes suggest that the genes are expressed in the same cells.

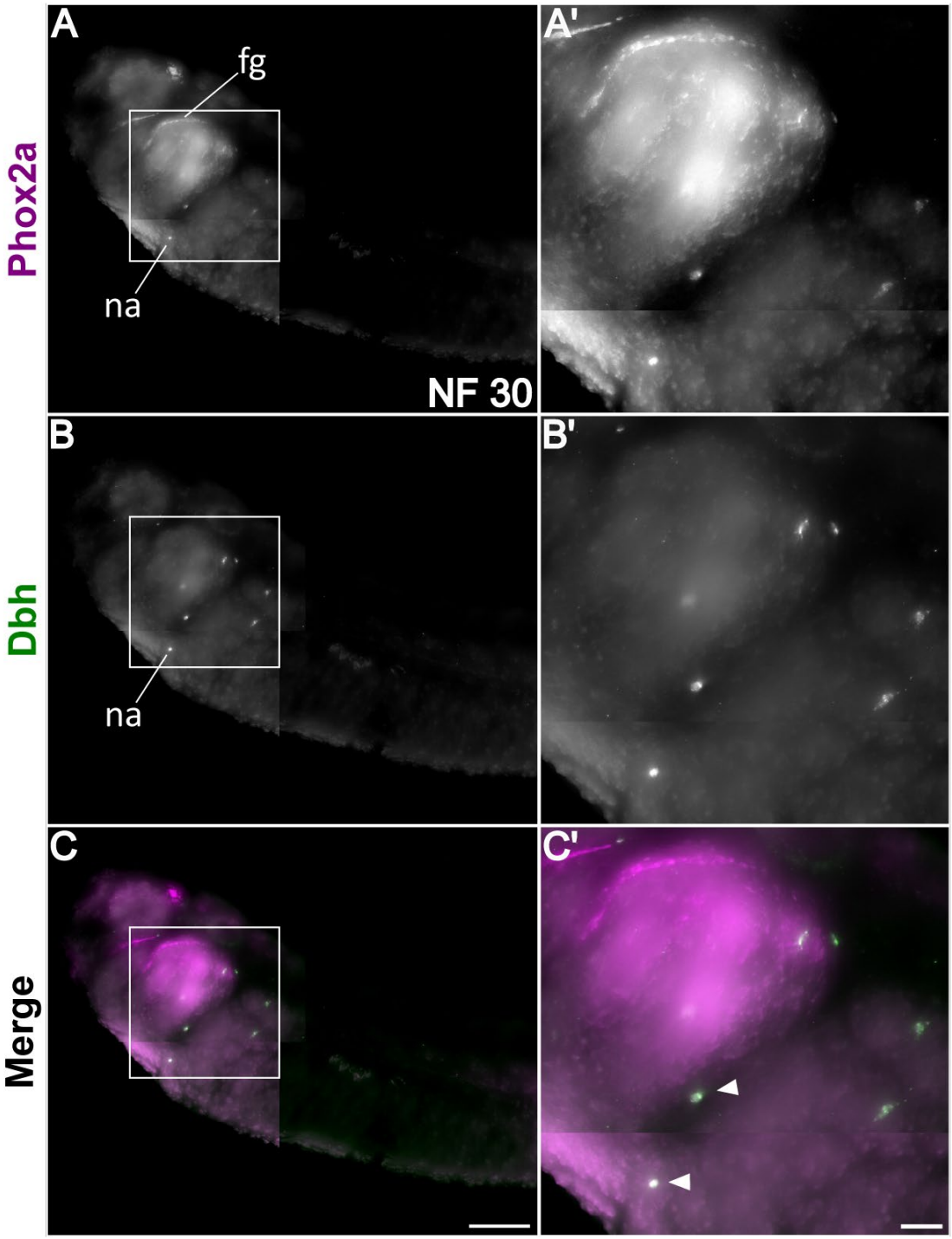

Figure 56: Co-expression of SA fate specifier gene phox2a with catecholamine biosynthetic enzymes dbh in Xenopus laevis.

HCR detection of phox2a (A, A', magenta) and dbh (B, B', green) at NF stage 30. Phox2a is expressed in facial ganglia and NA cells (A, A'), whereas dbh expression is visualised solely in NA cells. Co-localisation is seen in cells in the anterior body of the embryo (C,C', white). Co-expression is highlighted in zoomed inset (C'), and area of zoom in is indicated by the white squares. Cells used for co-expression analysis (Fig.4) are indicated by white arrows. Scale bars 200 µm (C), 50 µm (C'). Fg, facial ganglia; na, noradrenergic neuron;

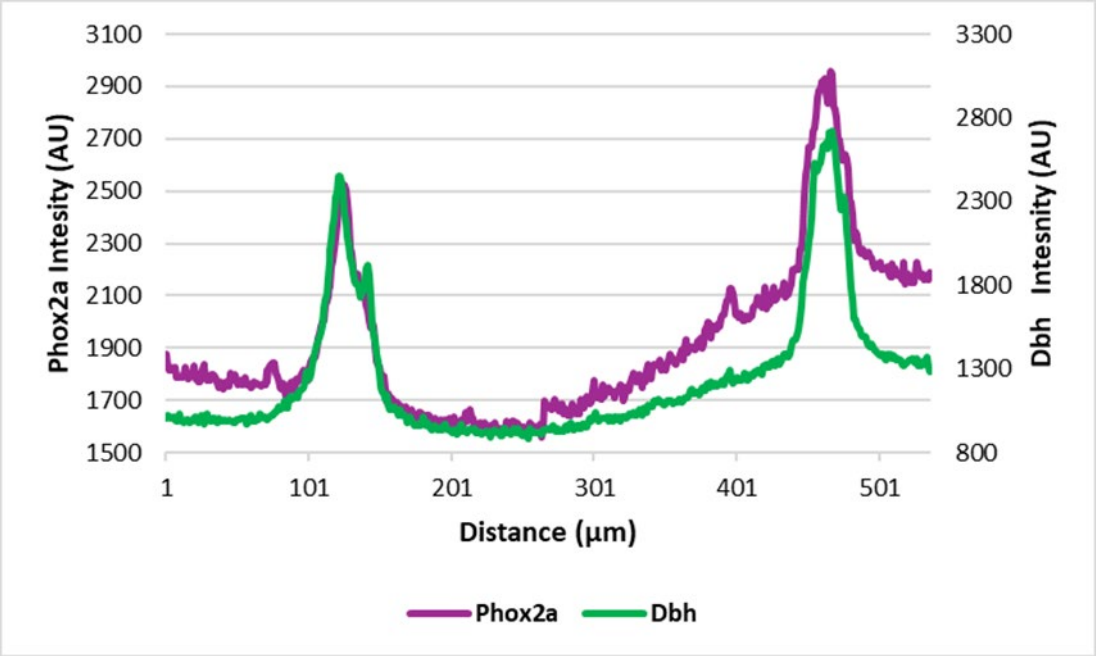

Figure 57: Co-expression analysis of phox2a and dbh at NF stage 30.
The graph shows the signal intensities of genes phox2a (magenta) and dbh (green), measured from the HCR expression obtained in X. laevis embryos. By drawing a line through two selected cells, we used ImageJ to measure the signal intensities along this line The x-axis represents the distance in micrometres, and the y-axis shows the signal intensity in arbitrary units (AU) for both genes. The spikes in the graph indicate the highest expression levels. The overlapping peaks demonstrate that both genes are co-expressed in the same cells.

5.4 HCR co-expression analysis of *phox2a* and *chga*

After confirming co-expression of *phox2a* and *dbh* in putative CCs, we wanted to repeat the same experiment with markers *phox2a* and *chga*, which encodes for one of the neuroendocrine secretory proteins present in secretory vesicles of CCs.

The *chga* HCR probe was designed to be used with amplifier B3+ Alexa Fluor 488.

When using Alex Fluor 488 we experienced excessive autofluorescence and were unable to see any specific signals within the embryo, particularly individual cells. We therefore decided against further use of this fluorophore and instead used Alexa fluor 647 to combine with B3 amplifiers. With Alexa Fluor 647 we got evident staining results of multiple individual NA cells along the anterior embryonic body (Appendix Figure 3). This result matches the expression pattern characterised with the *chga* WISH probe. For the colocalisation experiment, we

performed HCR with *phox2a* in combination with Alexa Fluor 594. When carrying out HCR for both *phox2a* and *chga* within the same embryos at early tailbud NF stage 30, we again observed co-expression within the NA cells (Fig. 58). We performed signal intensity analysis as described above to further assess coexpression in these cells. The resulting graph showed spikes of higher signal intensity at our measured cell points along the x-axis for both genes, suggesting that these genes are co-expressed in the same cells (Fig. 59).

However, we noticed a clear reduction in signal intensity of *phox2a* in this experiment compared to the expression signal we get when performing HCR with the *phox2a* probe on its own and in the experiment together with *dbh*. Specifically, we did not observe expression of *phox2a* in the facial ganglia or in the hindbrain. We therefore need to be cautious when assuming the expression of *phox2a* and *chga* within the same NA cells. It could be, that there is a chance there is some bleed-over signal from the red (594) and far red (647), that may have been measured as signal in the wrong channel. However, considering that the stainings produced in this experiment by the two probes do not completely overlap (as visible with the brain staining for *chga*), a bleed-over effect is not necessarily the case and there could have been a technical issue that we can not exclude. Based on previous HCR experiments with the *chga* probe on its own, we are definite of *chga* expression in the NA cells (Appendix Figure 3). We would have liked to repeat this experiment to get more clear signals from both markers in the same embryo and would suggest this as a future experiment.

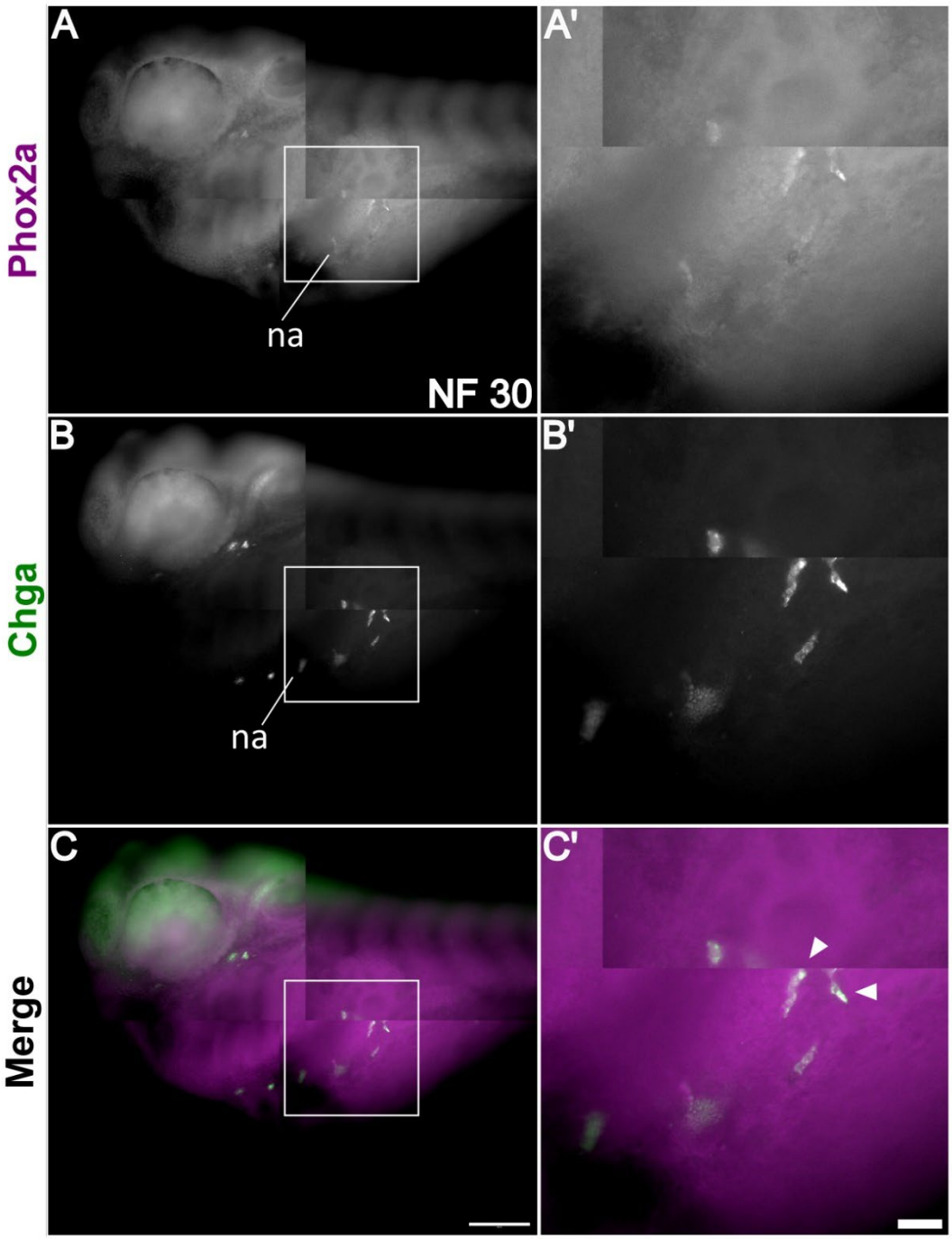

Figure 58: Co-expression of SA specifier gene phox2a and neuroendocrine secretory protein chga in Xenopus laevis embryo.

HCR detection of phox2a (A, A', magenta) and chga (B, B', green) at NF stage 30. Phox2a is expressed in facial ganglia (not seen) and NA cells, whereas chga expression is visible in both NA cells and in the CNS. Co-localisation is seen in cells in the anterior body of the embryo (C,C', white). Co-expression is highlighted in zoomed inset (C'), and area of zoom in is indicated by white box. Cells used for co-expression analysis are indicated by white arrow heads. Scale bars 200 µm (C), 50 µm (C').

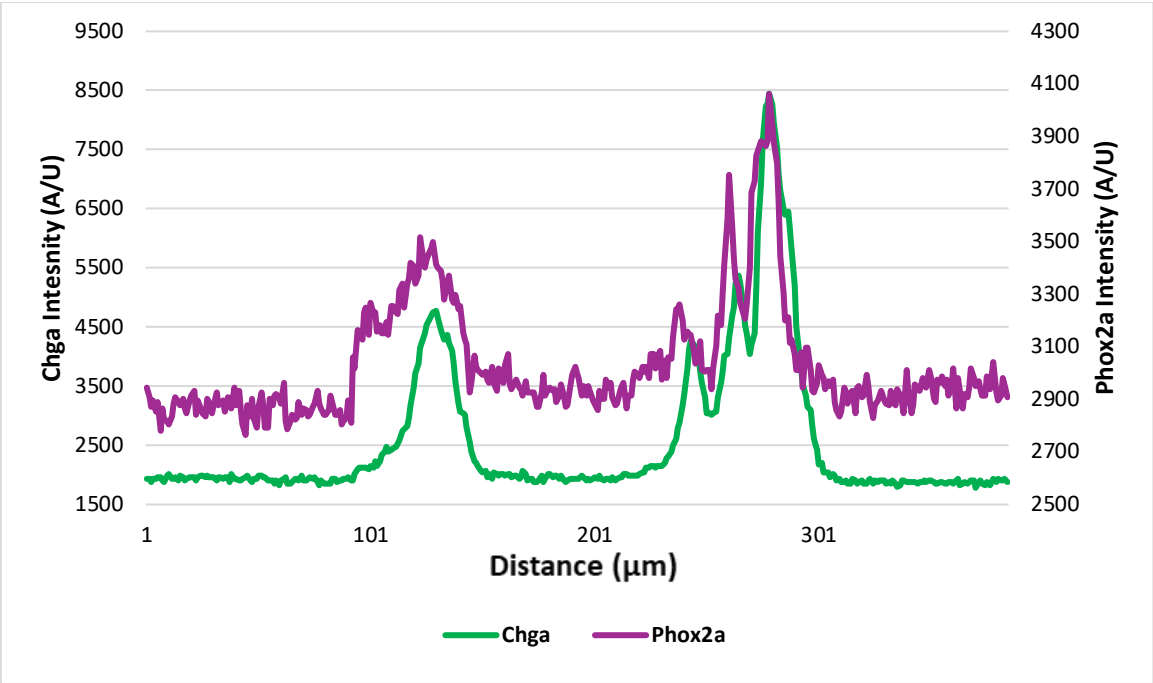

Figure 59: Coexpression analysis of phox2a and chga in indicated cells at NF stage 30. *The graph shows the signal intensities of genes phox2a (magenta) and chga (green), measured from the HCR expression obtained in Xenopus laevis embryos. The x-axis represents the distance in micrometres, and the y-axis shows the signal intensity in arbitrary units (AU) for both genes. By drawing a line through two selected cells (white arrow heads, Fig. 5), we used ImageJ to measure the signal intensities along this line. The spikes in the graph indicate the highest expression levels. The overlapping peaks demonstrate that both genes are expressed in the same cells.*

5.5 HCR co-expression analysis targeting *chga* and *dbh*

Now that we have detected co-expression with SA specifier TF gene *phox2a* with both *chga* and *dbh*, we also wanted to see if the neurosecretory protein gene *chga* and the catecholamine biosynthesis enzyme gene *dbh* would also be co-expressed in the presumptive NA neuron/CCs. We performed our HCR protocol with both these markers at early tailbud NF stage 30.

The *dbh* HCR was again combined with Alexa Fluor 594 and the *chga* HCR probe with Alexa Fluor 647. Both probes were clearly expressed in single NA cells across the anterior body of the embryo (Fig. 60). We also observed *chga* expression in the CNS, albeit a weak signal. *Chga* signal was stronger than the expression of *dbh*. This seems to be due to a higher auto

fluorescent background signal in Alexa Fluor 594. However, a possible explanation might also be due to higher levels of *dbh* mRNA levels in these cells or, another possibility, is that *dbh* probe designed by MI has a better affinity for its own target that the probe designed against *chga* mRNA. However, this can not be determined by HCR as the method is not quantitative.

Again, when merging both imaging channels, we observed co-expression of the *chga* and *dbh* genes in the NA cells (Fig. 60 C). White arrowheads mark the two NA cells used for co-expression intensity analysis. We again performed signal intensity analysis as described above, in order to further assess co-expression in these cells. The resulting graph showed overlapping spikes of higher signal intensity at our measured cell points, along the x-axis for both genes, suggesting that the genes are expressed in the same cells (Fig. 61).

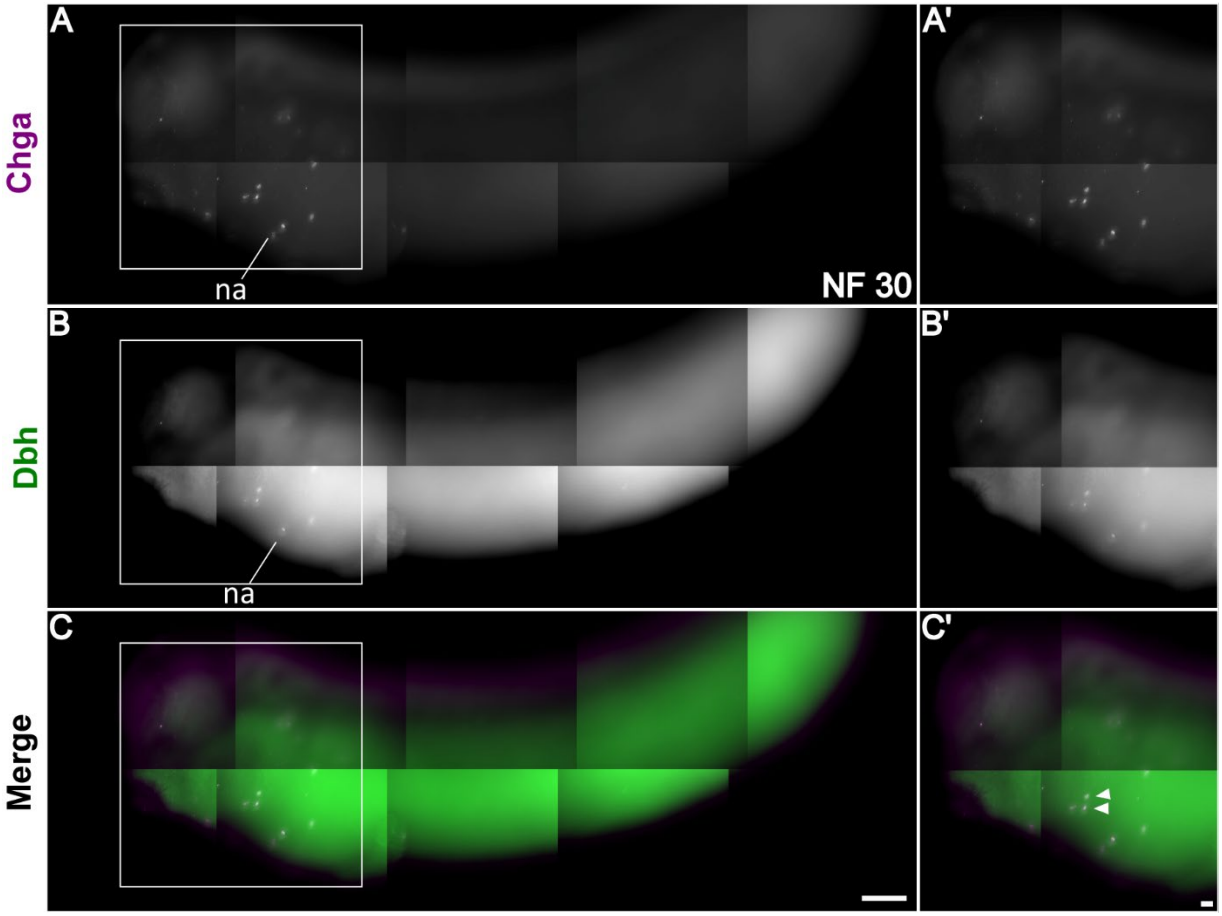

Figure 60: Co-expression of neuroendocrine secretory protein chga and catecholamine biosynthesis enzyme dbh at NF stage 30.

HCR detection of chga (A, A', magenta) and dbh (B, B', green) at NF stage 30. Chga expression is visible in both NA cells and in the CNS, whereas dbh is solely visible in NA cells. Co-localisation is seen in cells in the anterior body of the embryo (C,C', white). Co-expression is highlighted in zoomed inset (C'), and area of zoom in is indicated by the white box. Cells used for co-expression analysis are indicated by white arrows. Scale bars 200 µm, 50 µm.

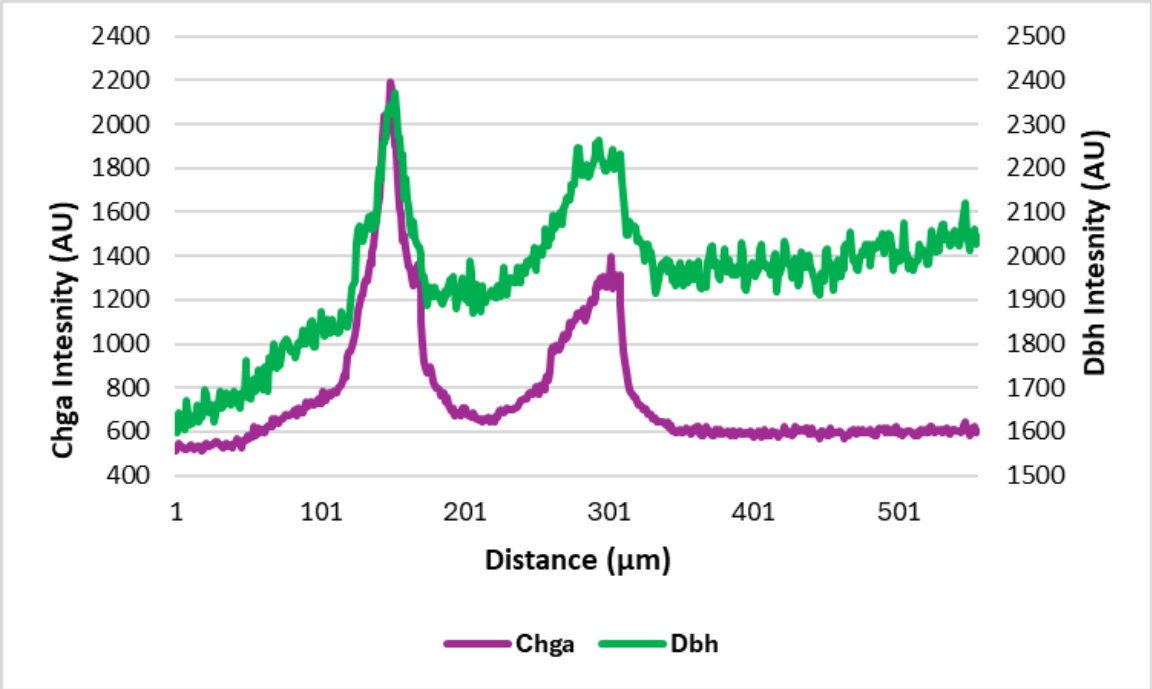

Figure 61: Co-expression analysis of chga and dbh in indicated cells at NF stage 30.
The graph shows the signal intensities of genes chga (magenta) and dbh (green), measured from the HCR expression obtained in Xenopus laevis embryos. The x-axis represents the distance in micrometres, and the y-axis shows the signal intensity in arbitrary units (AU) for both genes. By drawing a line through two selected cells (white arrow heads, Fig. 6), we used ImageJ to measure the signal intensities along this line. The spikes in the graph indicate the highest expression levels. The overlapping peaks demonstrate that both genes are expressed in the same cells.

5.6 Discussion of CC marker genes co-expression analysis by HCR RNA-FISH

CC development is governed by a complex transcription network involving key TFs such as Phox2a/b, Ascl1, Insm1 and others, which regulate the expression of genes necessary for the differentiation and function of these cells (Huber et al., 2002)

In addition to catecholamines, CC granules contain various proteins essential for catecholamine production and secretion, including chromogranins A and B, enkephalins, calcium ions, and the enzymes Dbh and Th (Kataoka et al., 1985; Winkler and Fischer-Colbrie, 1992). To further confirm that the multiple individual cells that we have characterized in Chapter 3 with several marker genes, and labelled as being NA neurons, are indeed expressed

in the same cell, we performed HCR, using two marker genes at a time within the same embryo. We have successfully observed co-expression of *phox2a* and *dbh* at developmental NF stage 30. As a reminder, Phox2a is a vital TF in the network of SA lineage specification and is found to be expressed in sympathetic neurons while Dbh is an enzyme vital in the catecholamine biosynthesis. Furthermore, Phox2a is vital in the expression of noradrenergic features, being a positive regulator of *th* and *dbh* expression (Hirsch et al., 1998; Huber, 2006). We also observed coexpression of *phox2a* with *chga* in the same NA cells we previously characterized by WISH. However, we have experienced issues in this experiment with the expression of *phox2a*. In this experiment, *phox2a* expression could not be observed in the facial ganglia or in the hindbrain structures, where it is usually strongly expressed during this stage of development. We did observe strong expression of *chga* in the NA cells. To exclude the chance, that the expression of *phox2a* and *chga* observed within the same NA cells was simply down to some bleed-over signal of the two red channels (red/594 and far red/647), this experiment needs to be confirmed. We postulate that the presence of two separate peaks does indicate two different probes, while bleed-over signal likely would look similar but at a much lower signal intensity.

Finally, we observed co-expression of catecholamine biosynthesis enzyme dbh, and chga, which is typically present in secretory vesicles of neuroendocrine cells. These results support the characterization of these three selected marker genes that we have identified to play an important role in NA neuron development in *Xenopus laevis*. Co-expression of these cells gives us a promising indication that the previously characterized cells may be putative CCs, although they do not seem to align in a specified structure (which would act as an embryonic adrenal gland, in *Xenopus*) in the developing embryo, at least prior to tadpole stage. Our findings from this chapter on co-expression, and our previous chapter 3, characterizing marker genes for putative CCs development, seem to align with results from a very recently published research article that reports on finding trunk sympathetic neurons in the sea lamprey (Petromyzon marinus) (Edens et al., 2024). Previously, it was thought that jawless vertebrates, like the sea lamprey, lack peripheral sympathetic ganglia and these types of neurons are a novelty to jawed vertebrates (Edens et al., 2024; Ernsberger and Rohrer, 2024). Here, the authors, by performing multiplex HCR, showed that each core SA TF gene *Ascl1*, *Phox2*, and *Hand2* were

co-expressed with *Th* and *Dbh* in these putative neurons. The co-expressing cells were found in small clusters along the trunk region in a bilateral pattern at late embryonic stages (Fig. 62), therefore differing in location from our identified NA cells that are mostly at the anterior region of *Xenopus laevis* embryos.

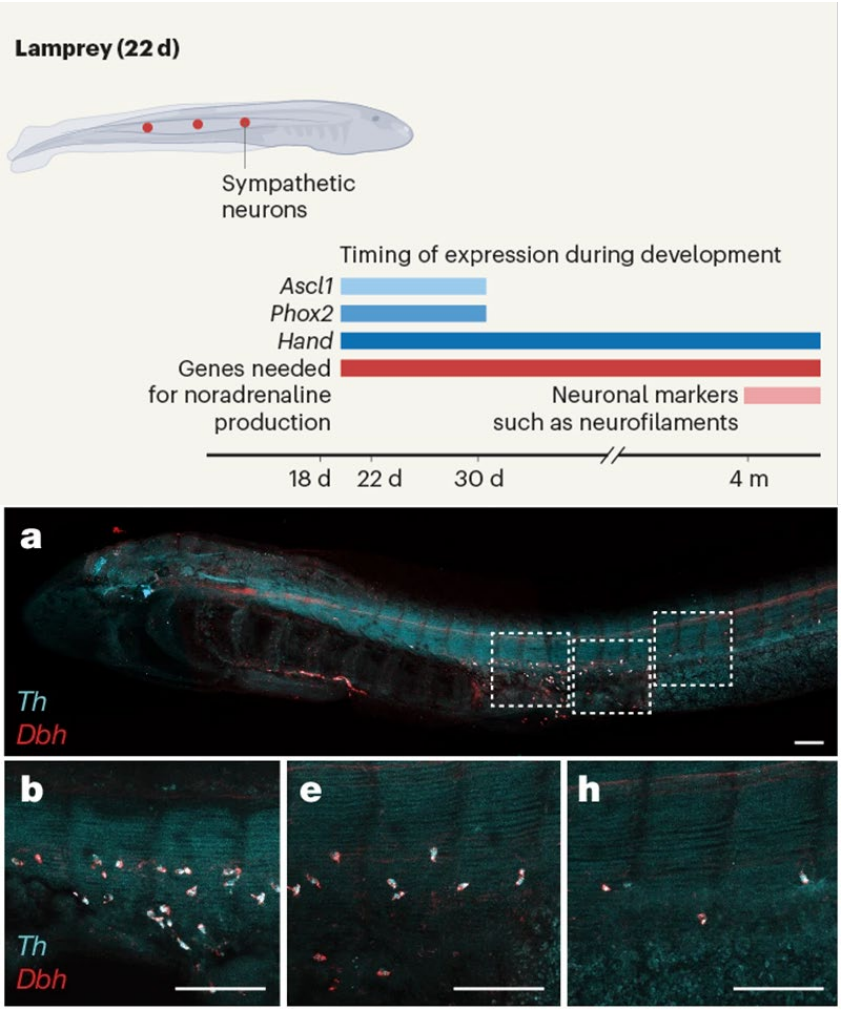

Figure 62: New discovery demonstrates the presence of sympathetic neurons in lamprey that co-express catecholamie biosynthesis enzymes th and dbh.
A very recent study conducted by the Bronner laboratory has shown that sympathetic neurons are present in jawless vertebrates the sea lamprey. These neurons develop bilaterally in the trunk region (indicated by red colouring in top schematic). Compared to other species, the time course of sympathetic neuronal differentiation is slow, with catecholamine enzyme expression first being detected at T28 (tailbud larvae). However, embryonic development and hatching in sea lamprey is much slower compared to zebrafish or frogs. Coexpression of catecholamine biosynthesis enzymes was shown by HCR, presented in the lower figure at T28. Top schematic was created by and taken from (Ernsberger and Rohrer, 2024). The figure was made in response to findings presented by (Edens et al., 2024), and the lower figure was taken from this publication.

Furthermore, as these cells have now been described by several different studies as NA sympathetic neurons, we have no way yet of distinguishing these cells as putative CCs, based on the markers these cells express. Unfortunately for us, sympathetic neurons and CCs share a complex gene network that governs their development and differentiation from NC progenitors. Based on their ability to both synthesize noradrenaline, these two cell types also share the expression of *th* and *dbh*. To truly distinguish the identified NA cells as putative CCs, we would have to show the coexpression of *pnmt* in some of these cells. We did observe *pnmt* expression in some of these cells in chapter 3, but struggled to get definite expression at later stages of development. Obtaining reliable expression with WISH for *pnmt* seems to be a struggle also in the zebrafish model. When characterizing *chga* expression in zebrafish (Xie et al., 2008), the authors reported they were unable to detect *pnmt* expressing cells by WISH, despite RT-PCR data detecting *pnmt* transcript at 7dpf, at juvenile stage. The authors noted that transcript expression was relatively low in comparison to *dbh* and *th* and concluded that the difficulties in *pnmt* visualization by WISH is likely due to low levels of *pnmt* transcripts and/or a scarcity of CCs expressing *pnmt* during early embryogenesis. Future experiments in *Xenopsu laevis* should address this and co-expression analysis of *pnmt* with some of the markers we have shown in this work needs to be done.

Despite promising results of our co-expression experiments, there are several challenges we faced with this technique that we would like to address here, and should be solved for future successful experiments.

While HCR RNA-FISH provides us with an easy approach to multiplex different mRNA targets within the same embryo, we experienced high autofluorescence background signal with most markers. Autofluorescence was especially high with Alex Fluor 488 and 546 and had to be excluded from further use. This limited our multiplexing capabilities and use of fluorescent markers to just two: Alexa Fluor 647, which showed the least amount of background noise and most clear expression signals, and Alexa Fluor 594 which still showed autofluorescence, but strong expression of marker probes. High amount of autofluorescence background signal in *Xenopus* is likely due to the high amount of lipids present – due to yolk being in all cells of the embryos unlike in zebrafish where the yolk is separate from the embryo- particularly around the area of interest to us for visualizing the single cells at the anterior end of the

embryo. To navigate this issue, we should set up confocal microscopy with a spectral detector and adjusting parameters, such as exposure time and gain to improve the visualization of weaker signals from autofluorescent background. We could additionally try using Alexa Fluor 405 (blue) and sample the autofluorescence by performing detection and amplification controls. Generally, we need to define better background suppression with the HCR protocol by further optimising the number of washes, buffers used and possibly finding a way of deyolking the embryos. Furthermore, we need to investigate why we observed irregularities in signal presence and intensity when multiplexing. We sometimes struggled with absent or weak signals of one marker when multiplexing two probes at the same time, despite them both working fine when individually tested, as seen in the case of our co-expression experiment with *phox2a* and *chga*. We are unsure about how and why this irregularity of signal detection occurs. Not knowing the sequence for each of the probe poses some questions. One possibility might be that the probes for the different genes might have some complementarity, which can result in cross-reaction between them, leading to lack or absent signal, though this is unlikely. However, further optimisation of the protocol needs to be done for it to provide consistent results. In future experiments, we would have liked to perform multiplexing of the above performed experiments also at multiple stages of development and, if possible, multiplexing up to three probes. This would have been useful in order to identify if NA cells express all three marker genes *chga*, *dbh* and *phox2a* at the same developmental time points and in the same area. We also would have liked to order a *pnmt* HCR probe and perform multiplexing with marker genes *chga*, *dbh* and *phox2a*. Additionally, we would have liked to multiplex *phox2a/b* with our kidney marker *pax8* to see if their expression overlaps at later stages of development (NF stage 37-40). Finally, using HCR to perform spatio-temporal expression analysis at tadpole stage would have been interesting in order to see if we can still detect NA cells at these stages. We struggled performing WISH at this late stage as probes require a long time at this stage to develop colouring, leading to high background noise.

In conclusion, the work of this chapter was a first trial for using HCR RNA FISH in *Xenopus laevis,* and establishing the method in the Wheeler laboratory. Despite some technical difficulties and issues with strong autofluorescence, we have firstly confirmed that some of the markers we have established as putative CCs markers show the same expression pattern

in the NA cells. Most importantly, several of these markers (*dbh* and *chga*, *phox2a* and *dbh*) are co-expressed within the NA cells. This is true for key SA TF gene *phox2a* with catecholamine biosynthesis gene *dbh*, as well as *dbh* with neuroendocrine secretory protein coding gene *chga*. This, for one, confirms that these markers indeed have characterised the same cell type and, potentially, we would see co-expression for our other markers in the NA neurons. Secondly, the co-expression of these markers confirms these cells as being sympathetic neurons. If future experiments could show co-expression of these marker genes with *pnmt* within the same cell, this would finally confirm these cells as embryonic CCs. Future experiments should also show co-expression with other SA specifier markers, such as *ascl1,* or CCs differentiation marker *insm1*, and show co-expression across different embryonic developmental stages.

5.7 Performing Hybridisation Chain Reaction to multiplex genes to separate presumptive adrenal cortex and primordial germ cells

In our previous chapter, we investigated the spatio-temporal expression of the genes *star* and *nr5a1* in developing *Xenopus laevis* embryos, in order to determine the development and location of the putative AC. Both *star* and *nr5a1*, known for their roles in steroidogenic tissue formation and steroidogenesis, were expressed in the same region of the developing pronephric kidney, suggesting their involvement in AC development. However, it is known in the literature that these genes are also expressed in gonadal tissue, which is anatomically adjacent to the kidney and thus the presumptive AC (Pignatti and Flück, 2021; Piprek et al., 2017). To differentiate between AC and gonadal tissues, we performed in WISH using the marker gene *pgat* to track the migration of PGCs and their relation to the AC.

Building on this work, we aimed to perform HCR RNA-FISH using either *star* or *nr5a1*, with *pgat* to simultaneously visualize their expression within the same embryo. This experiment helped us to further distinguish the presumptive AC from the developing gonads, and the relation between the migrating PGCs in the embryonic body to the location of our cortex marker at the stages tested.

We chose developmental NF stage 40 (late tailbud) for this experiment, as at this stage, with normal WISH, we struggle with pigmentation and high background signals. Additionally, at this stage, PGCs should have migrated further towards the genital ridges to innervate the gonadal tissue, and therefore be closer to our presumptive AC marker expression.

5.7.1 HCR RNA-FISH targeting *pax8* and *pgat*

First, we wanted to see the relationship between the pronephric kidney to the developing gonads, using PGCs marker *pgat* to see how close PGCs are to the developing kidneys.

The *pax8* HCR probe was designed to be used with amplifier B4 + Alexa Flour 647. The *pgat* HCR probe was designed to be used with amplifier B2+ Alexa Fluor 594.

We obtained strong signals for both probes. *Pax8* was detected in the hindbrain and in the pronephric tubules, as expected. Expression could also be seen faintly in the pronephric duct at NF stage 40. *Pax8* expression during this stage of development seems to generally decrease, based on RNA sequencing data of *pax8* from Xenbase (Session et al., 2016), and expression in the hindbrain and pronephric tubules was dominant, making visualization in the area of the pronephric duct harder. PGCs detection was also strong using Alexa Fluor 594, with multiple PGCs being visible towards the posterior side of the embryo. When merging the two channels, we could see that the PGCs were in close association with the posterior end of the pronephric duct (Fig. 63).

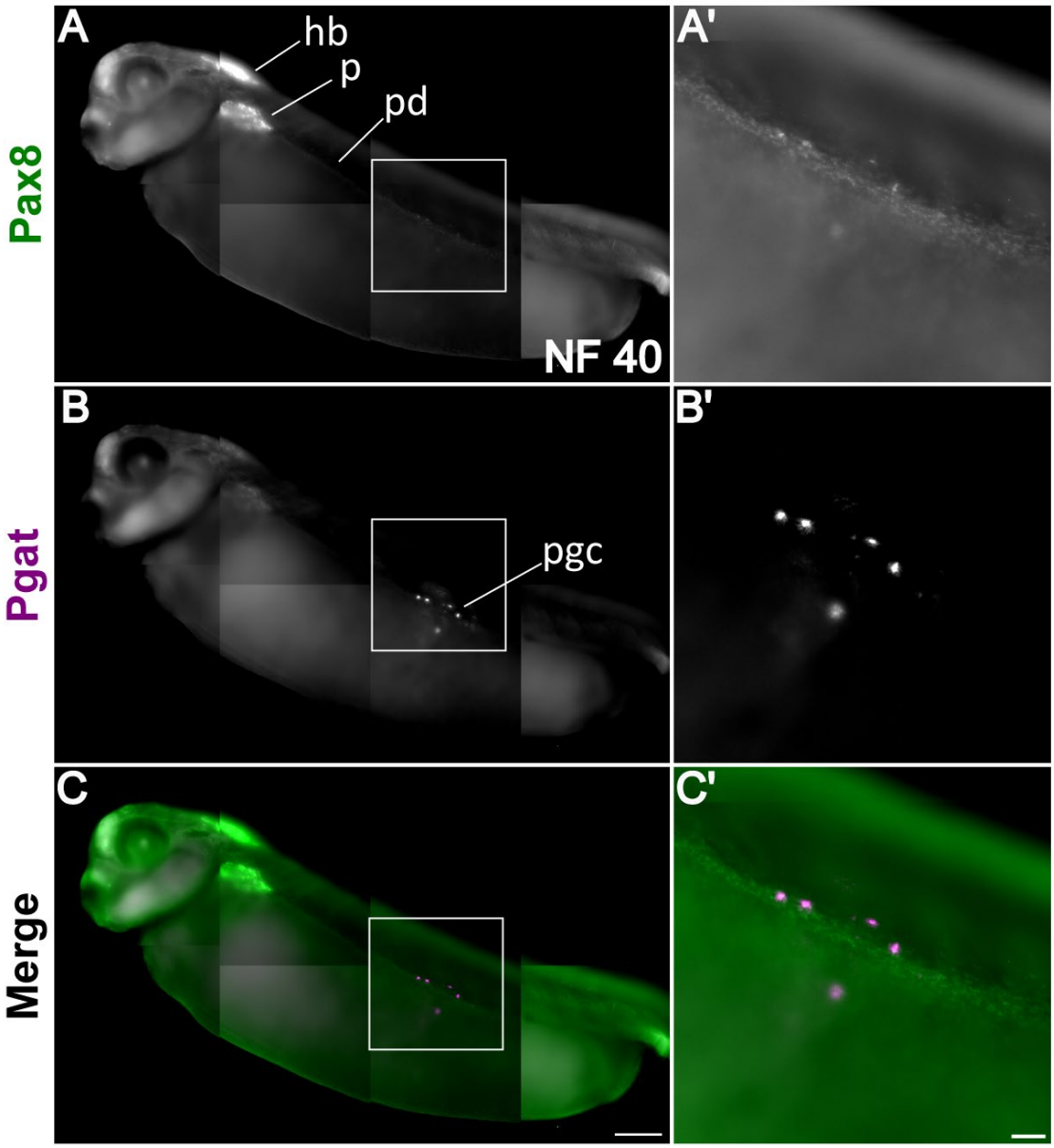

Figure 63: HCR detection of pronephric kidney marker pax8 and PGCs marker pgat at NF stage 40.

HCR detection of pax8 (A, A',) and pgat (B, B',) in Xenopus laevis embryo. Pax8 is expressed in the pronephric kidney (tubules and duct) and in the hindbrain (A, A'). Expression in the pronephric duct is weak at late developmental stages and possibly less prominent due to strong expression in the tubules and hindbrain. Pgat expression is solely found in PGCs that will invade the gonads and give rise to ovaries or testes (B, B'). At late tailbud stage, PGCs (magenta) are found in close association with the posterior pronephric duct (green) (C,C',), highlighted in zoomed inset (white box). Scale bars 200 µm (C), 50 µm (C'); hb, hindbrain; p, pronephric tubule; pd, pronephric duct; pgc, Primordial germ cells.

5.7.2 HCR RNA-FISH targeting *nr5a1* and *pgat*

Next, we performed HCR RNA-FISH targeting both *nr5a1* and *pgat* mRNAs.

The *nr5a1* HCR probe was designed to be used with amplifier B4 + Alexa Flour 647 and strong detection in the anticipated regions was visible both in the hypothalamic nucleus (HYPN) and the presumptive AC, just below the somites (Fig. 64). The expression was consistent with the regions of *nr5a1* expression, characterized with the *nr5a1* WISH probe (Fig. 45, section 4.2.2). PGCs were again detected using the *pgat* HCR probe with Alexa Fluor 594. We observed expression in multiple PGCs, mostly at the posterior end of the embryonic body. Here, we could observe the presence of some PGCs further along the region of the pronephric kidney, migrating more towards the mid-line of the embryo. We did not observe co-expression of *nr5a1* and *pgat* at this stage of development, when merging both channels.

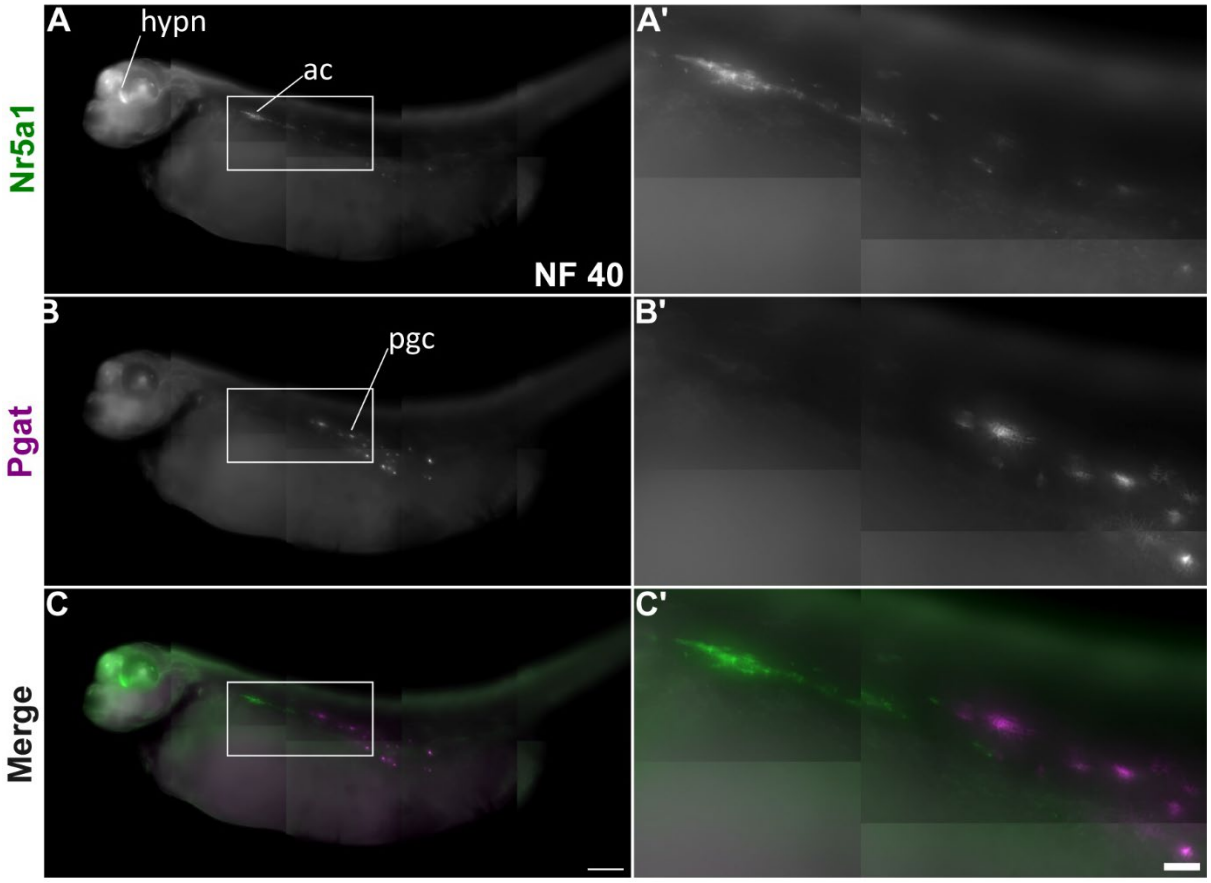

Figure 64: Expression of steroidogenic marker nr5a1 and PGCs marker pgat at NF stage 40. *HCR detection of nr5a1 (A, A', green) and pgat (B, B', magenta) in Xenopus laevis embryo. Nr5a1 is expressed in steroidogenic tissue along the developing kidney (putative AC) and in the HYPN, behind the eye field (A, A'). Pgat expression is solely found in PGCs (B, B'). At late tailbud stage, PGCs are found in close association with nr5a1 expression, highlighted in zoomed inset (white box), but no overlap was seen at this stage of development (C, C', white). Scale bars 200 µm (C), 50 µm (C'); ac, Adrenal cortex, pgc, Primordial germ cells; hypn, hypothalamic nucleus.*

5.7.3 HCR RNA-FISH targeting *star* and *pgat*

Finally, we performed HCR RNA-FISH targeting both *star* and *pgat*. The *star* HCR probe was designed to be used with amplifier B4 + Alexa Flour 647, and strong detection in the anticipated regions was observed both in the presumptive AC, just below the somites (Fig. 65). The expression was consistent with *star* expression characterized by WISH. PGCs were detected using the *pgat* HCR probe with Alexa Fluor 594. Also here, we observed expression in multiple PGCs, mostly at the posterior end of the embryonic body. Consistent with previous observations, we could detect expression of some PGCs further along the region of the

pronephric kidney, seeming to have migrated further towards the mid-line of the embryo. We did not observe co-expression of *star* and *pgat* at this stage of development, when merging both channels.

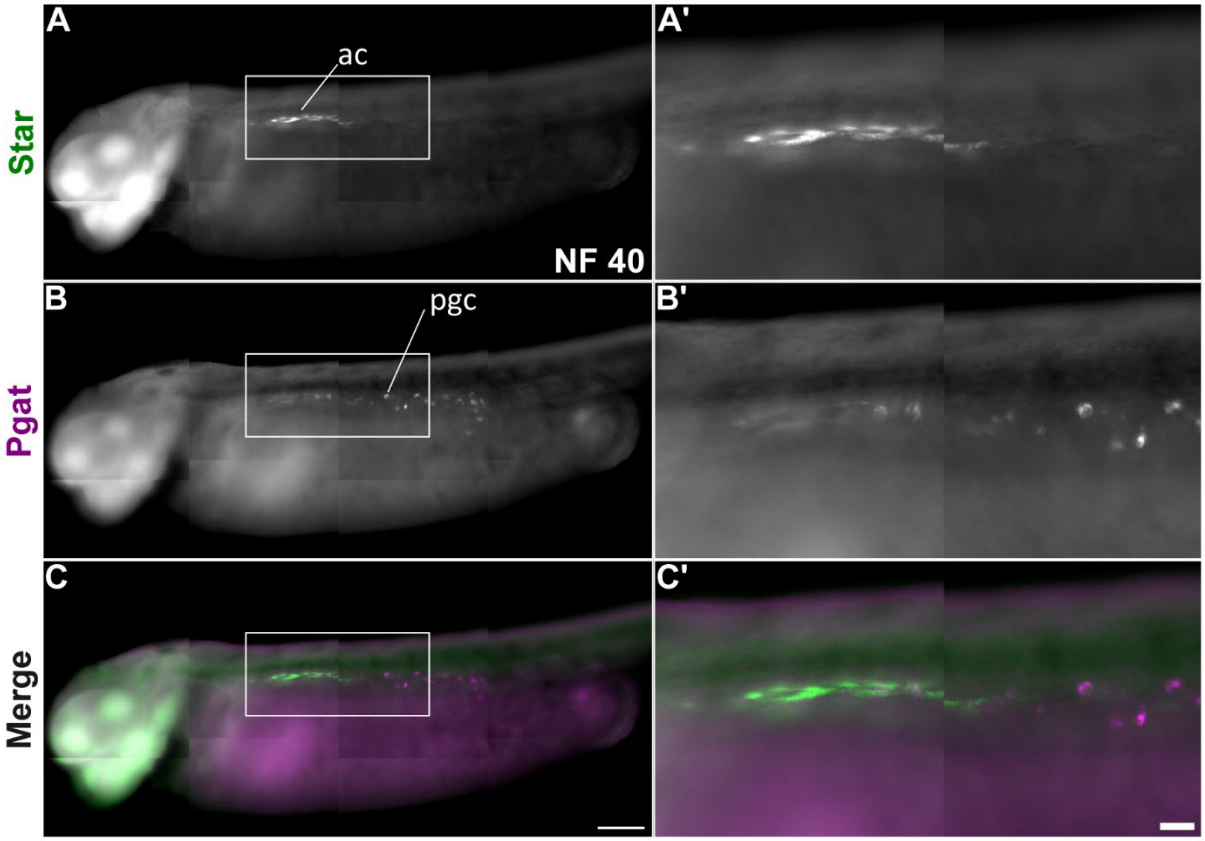

Figure 65: Expression of steroidogenic marker star and PGCs marker pgat at NF stage 40. *HCR detection of star (A, A', green) and pgat (B, B', magenta) in Xenopus laevis embryo. Star is expressed in steroidogenic tissue along the kidney (suggested as the AC) (A, A'). Pgat expression is solely found in PGCs (B, B'). At late tailbud stage, PGCs are found in close association with star expression, highlighted in zoomed inset (white box), but no overlap was seen at this stage of development (C,C',). Scale bars 200 µm (C), 50 µm (C'); ac, Adrenal cortex; pgc, Primordial germ cells.*

5.8 Discussion

The aim of these experiments was to separate gonadal tissue from our putative AC expression signal. We, therefore, chose to continue marking the expression of PGCs using *pgat* and performing multiplex HCR RNA-FISH experiments in order to exclude the possibility of PGCs showing co-expression with AC marker genes *nr5a1* and *star*. We therefore chose late stages

of embryonic development (NF 40). When multiplexing *pgat* with either *nr5a1* or *star*, we could see that the migratory trajectory of the PGCs is close to where we see expression of our presumptive AC markers. While we could find many publications on determining sexual differentiation of the gonads in the developing frog, we could not find information of gonadal tissue formation, genes expressed in this tissue, and differentiation processes prior to pre-metamorphic stages. The general model of gonad development seems to be accepted as being universal for all vertebrates.

In amphibians, the presumptive gonads develop from two longitudinal thickenings of the coelomic epithelium, located on the ventral part of the mesonephros, along both sides of the gut mesentery (Roco et al., 2021). This process is similar to that in other vertebrates, where PGCs of extragonadal origin migrate to the gonadal anlagen. Once they arrive, they form undifferentiated gonads composed of both germ and somatic cells. In some amphibian species, as seems to be the case for *Xenopus laevis*, the genital ridges only become evident upon the arrival of the PGCs at the presumptive gonad. This developmental process ensures that the germ cells are integrated into the developing gonadal structure, which is crucial for the formation of functional reproductive organs (Roco et al., 2021). The migration of PGCs from the median genital ridge to the coelomic walls is completed by NF stage 46 in *Xenopus laevis*. By NF stage 48, the paired genital ridges form folds that protrude into the coelomic cavity (Wylie and Heasman, 1976). At NF stage 49, somatic cells from the mesonephric region enter the genital ridges, forming the medullary tissue of the future gonad (Houston and King, 2000).

Each gonadal anlage typically contains between 25 to 30 PGCs, which remain inactive, and the gonads are sexually undifferentiated up until NF stage 52. At this stage, PGCs can differentiate into female or male gametes, depending on the sexual identity of the surrounding somatic tissue (Kloc et al., 2001).

To properly distinguish *nr5a1* and *star* expression in either the gonads, the AC or in both, we would need to carry out HCR RNA-FISH again with our chosen markers at post-embryonic stages (NF stage 48-52) and perform sectioning. Sectioning the embryo at these stages will allow us to distinguish the different tissue types and expression within with greater precision.

Another possibility to distinguish these two tissues during embryogenesis, is to characterize the expression of other markers of gonad development such as *wt1* and *gata4 (Pihlajoki et al., 2015)*. These two genes are upregulated in gonadal specification from the AGP. However, the difficulty with these two genes is that *wt1* is also expressed in the kidney, and can therefore also not be used to clearly distinguish between the two tissues. In *Xenopus*, *gata4* is important in endoderm and cardiac development, as well as in gonadal differentiation. When looking at the community platform Xenbase, WISH images of *gata4* submitted to the page, do not show specific expression in the kidney region. Not much literature on initial gonadal tissue development during embryogenesis in this model species could be found and this process has not been mapped by spatio-temporal gene expression. This could be a future research project and needs to be further understood to examine the developmental relation between the gonads and the AC.

In conclusion, I have now shown the presence of *nr5a1* and *star* expression along or within the pronephric kidney, both by WISH and by HCR RNA-FISH. Based on their known function and importance in AC development, and their role in steroidogenesis of the AC in other vertebrate species, I have labelled these genes as being putative markers also for the AC development in *Xenopus laevis*. While I have seen no evidence of co-expression of our putative AC marker genes with PGCs marker gene *pgat* during embryogenesis, I still suggest the above mentioned future experiments to exclusively define the structures as the AC and to separate it fully from the developing gonads.

6 Chapter VI: Morpholino knockdown of the NC

6.1 Introduction

In Chapter 3, we identified a population of single, well-rounded cells arising within the anteroventral region of *Xenopus* embryos, that were previously suggested to be NA neurons. This was based on a series of markers that were shown to be expressed in this cell population which included *ascl1*, *phox2a*, *hand2* and *th*. We have further shown the expression of additional NA markers in these cells, including *phox2b*, *chga*, *dbh* and the adrenergic marker *pnmt*. We have additionally shown that these cells do not stay at the anteroventral side of the embryo but begin to be more interspersed across the anterior body of *Xenopus* embryos up until NF stage 40. After this stage, we are no longer able to visualize these cells by WISH. We further postulate the NA neurons to be indeed early CCs during embryogenesis based on the markers we found to be expressed and co-expressed. Both sympathetic chain ganglia and CCs of the AM are derived from a series of SA progenitors which express *Ascl1/Xasha1*, *Phox2a/b*, *Hand2* and *Insm1* (Huber, 2006; Shtukmaster et al., 2013). These proteins are vital to acquire a NA fate and in turn initiate the transcription of catecholamine synthesizing enzymes *Th* and *Dbh*.

As we assume that these cells are CCs, they should therefore be NC-derived. However, the appearance of this cell population as early as NF stage 13/14, as described for markers *ascl1* and *phox2a* by previous studies, poses a few questions. Firstly, the described cells arise at the anteroventral region of the developing *Xenopus* embryos, which is not the expected location for developing and migrating SA progenitors. In fact, this cell population should arise from trunk NCCs that, in other vertebrate species, emerge from the dorsal neural tube and migrate ventrally, towards the dorsal aorta. Additionally, the majority of CCs in both mouse and zebrafish vertebrate models, are derived from peripheral nerve-associated SCPs, which are themselves derived from late migrating NCCs. Secondly, enhancing the issue with the location of the CCs population in *Xenopus,* is the timing of their first appearance at the anteroventral region. The NC in *Xenopus* is not known to have migrated or emerged at the anteroventral side of embryos this early during development. Cephalic NC migration in *Xenopus* begins around NF stage 19-20, coinciding with the nearing completion of the neural folds closure to form the neural tube (Theveneau and Mayor, 2012) (Fig. 66 and 67). However, little is known about TNCCs migration, or the cues that guide *Xenopus* TNCC to the ventromedial pathway

taken by TNCC of other vertebrate models to form the trunk PNS (Mayor and Theveneau, 2013; Vega-Lopez et al., 2017). No thorough lineage tracing of trunk NCC in *Xenopus* has been performed, and no research has been done yet to assess the involvement of SCPs in NC lineage derivatives.

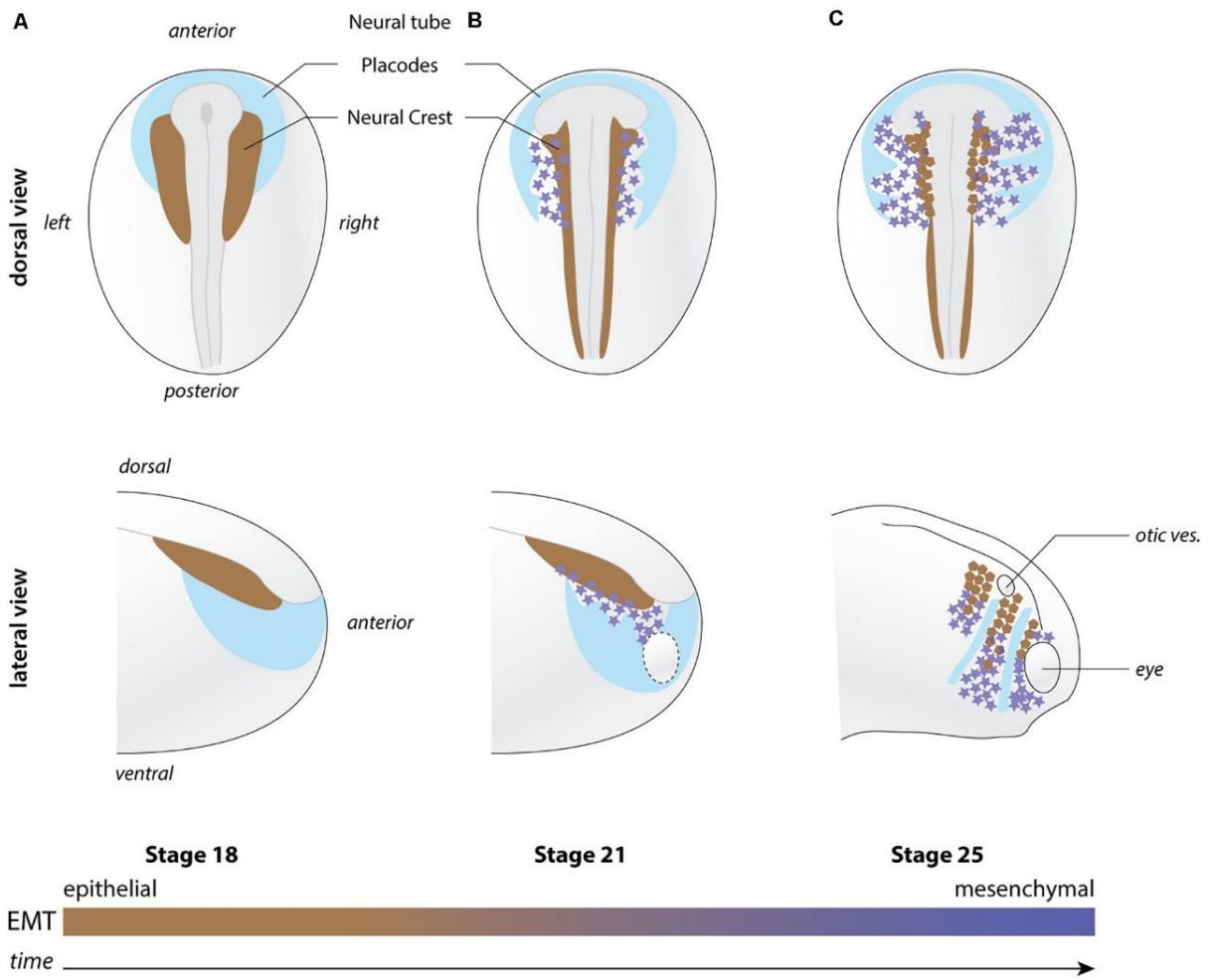

Figure 66: Overview of neural crest migration in Xenopus embryos from late Neurula to early tailbud development.

The diagram shows the position of NC cells (brown and magenta) at pre-migration (NF stage 18) to early migration (NF stage 21) and late migration (NF stage 25) in relation to the placodal region (light blue). This figure illustrates the current knowledge of NC migration in Xenopus embryos, which shows that NC migration only begins at NF stage 18 in a dorso-ventral fashion whereas, in this study, we see expression of likely NC-derived cells at the anteroventral stage, reported as early as NF stage 14 for phox2a. Generally, expression of NC cells is seen at the anteroventral side from NF stage 19/20, shortly after NC migration begins. The figure was created by and taken from (Barriga and Theveneau, 2020). EMT, epithelial-to-mesenchymal transition; otic ves., otic vesicle

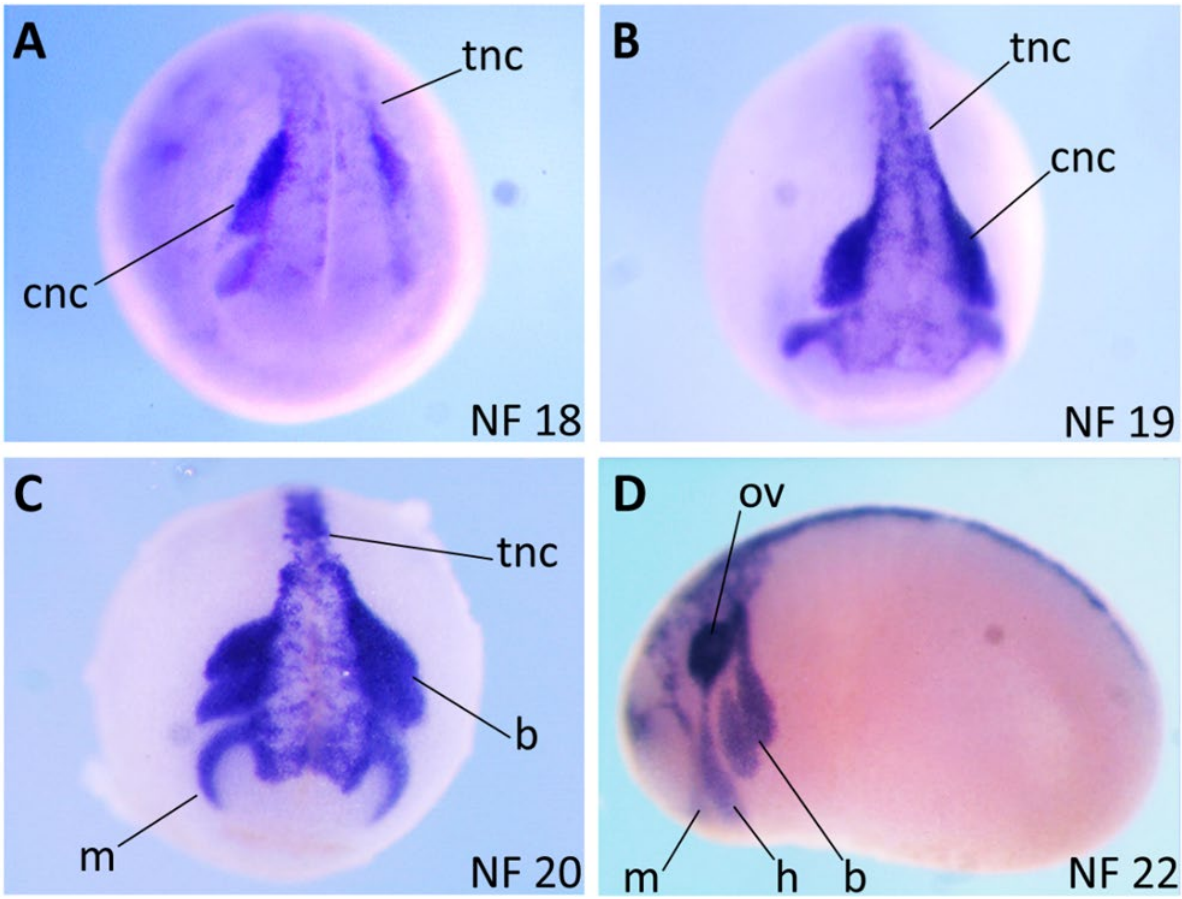

Figure 67: Expression profile of NC marker Sox10 during early Xenopus embryogenesis by WISH.

Embryos are viewed from the anterior side (A-C), or orientated lateral with anterior side to the left and posterior on the right. Expression of sox10 first emerges in the prospective NC around NF stage 12.5, in Xenopus embryos (not visualized). At Neurula (A, B), sox10 is expressed both in cephalic NC (cNC) and trunk NC (tNC). At late Neurula stage (C, D), sox10 positive cells have begun to migrate laterally and ventrally, and expression can be observed in the mandibular, hyoid and branchial arches as streams of NC of the migrating cNC subpopulation, as well as in the otic vesicle (ov). The tNC is clearly visible along the entire anterior-posterior axis. However, we see no sox10 expression at the anteroventral side of the embryo at these stages of developmental, nor do we see tNC migrating this far anterior to the location of the NA neurons. cnc, cephalic neural crest; tnc, trunk neural crest; b, branchial; h, hyoid; m, mandibular; ov, otic vesicle

To study if the described cell population is indeed derived from the NC, we decided to make use of a morpholino (MO) knockdown (KD) strategy, a commonly used technique which allows for loss-of-function studies in *Xenopus*.

The use of antisense MO oligonucleotides has been an essential tool in developmental biology to study the molecular function of genes in embryonic development. Hereby, synthetic MOs are designed to inhibit gene expression by blocking mRNA translation. They do so by either binding to the translational start site (ATG-MOs) of the targeted mRNA molecule, or blocking the splicing of mRNA, therefore producing a non-functional protein. This selective KD of specific target genes is particularly useful to study gene function in the frog model *Xenopus*, but it has also been used in chicken *(Gallus gallus*), sea urchins (*Nematostella*) and zebrafish *(Danio rerio*) model organisms which allowed enormous advances in the understanding of developmental mechanisms (Blum et al., 2015).

To confirm the NC origin of this cell population, we decided to knock down two vital NC genes: *foxd3* and *sox10* in independent experiments. Both genes are essential in different aspects of NC development, ranging from induction to late migration. We opted for two genes, rather than performing the experiment with only one, because we wanted to make sure that the observed phenotypes (if any) would have been associated with defects of NC development, and not to some possible off-target effect due to an imperfect MO.

6.2 Foxd3 MO KD effect on NA neurons/putative Chromaffin cells

Forkhead Box D3 (Foxd3) is an embryonic TF essential for NC development. In *Xenopus*, both *foxd3* and *snail2* are known bona fide markers for the presumptive NC and play essential roles in the specification and migration of the NC (Sato et al., 2005). Both *snai2* and *foxd3* are activated from NF12-12.5, and *foxd3* plays a vital role in controlling the NC stem cell state and promoting EMT. KD of *foxd3* in *Xenopus* causes a reduction in the expression of NC regulatory factors including *snail2*, *sox10*, *twist* and *ets-1*, as well as causing defects in NC migration (Sasai et al., 2001; York and LaBonne, 2022).

The foxd3 MO and the foxd3 control MO were designed and validated in *Xenopus* embryos previously by Sato and colleagues (Sato et al., 2005). Embryos were injected on one side of a two-cell stage embryo (Fig. 68) and left to develop initially to NF stage 13, which shows first induction of the NC, and then further to our key developmental NF stage 19/20 to assess the effect of *foxd3* KD on the NA neuron population. A dose response for *foxd3* MO was set at 20 ng, 40 ng and 60 ng to determine a concentration at which we observe a consistent NC reduction phenotype, determined by WISH with NC marker *sox10* at NF stage 13 and 20.

We observed a mild reduction of NC marker *sox10* expression and possibly an inhibition of migration using 20 ng of MO, but the reduction was not strong (Fig. 69). At 40 ng, embryos were beginning to die after NF stage 14 and showed clear signs of toxicity. At 60 ng all the injected embryos died during neurulation (data not shown). We therefore decided to inject 30 ng of *foxd3* MO, which allowed the embryos to survive up to NF stage 20 (Fig. 69). Our control MO injection showed no phenotype, nor an increased mortality, when compared to the wild type (WT) embryos.

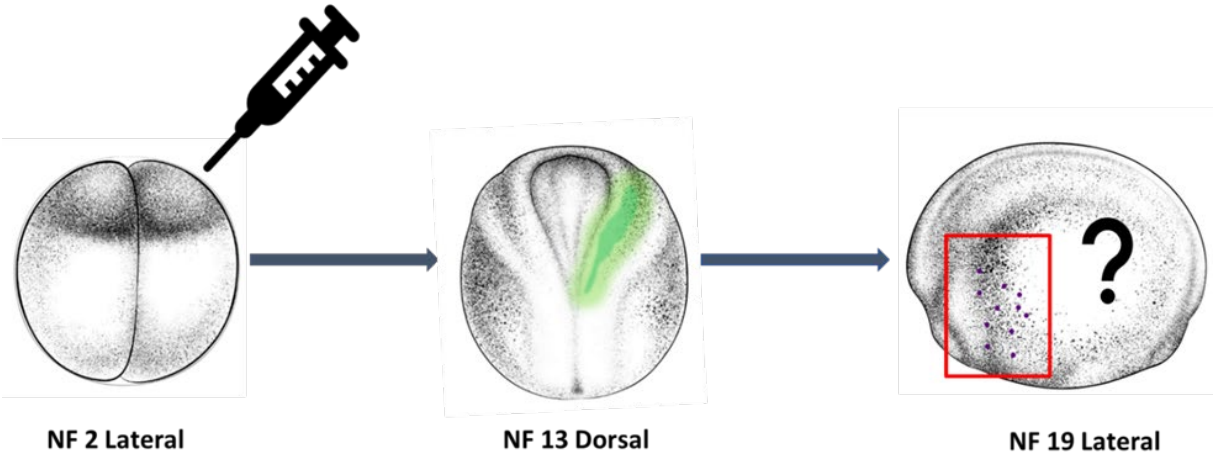

Figure 68: Schematic showing the process of the Morpholino Knockdown experiments to inhibit NC development.
Embryos were injected with either foxd3 MO (30ng) or sox10 MO (16ng), together with GFP mRNA (25ng) into one blastomere of a two-cell stage embryo. Embryos were left to develop first until early Neurula (NF stage 13), which is when the NC is first induced and visible by WISH. We were able to distinguish the injected side from the uninjected side by using GFP, which was also used to control that embryos were correctly injected (green). Embryos were then allowed to further develop until late Neurula (NF stage 19/20) and in situ hybridization was performed with CCs markers to see if there was a reduction or complete lack of NA neurons/CCs, purple dots) on the MO injected side of the embryo, compared to the uninjected side. Figure was created with Xenopus illustrations from Natalya Zahn (2022).

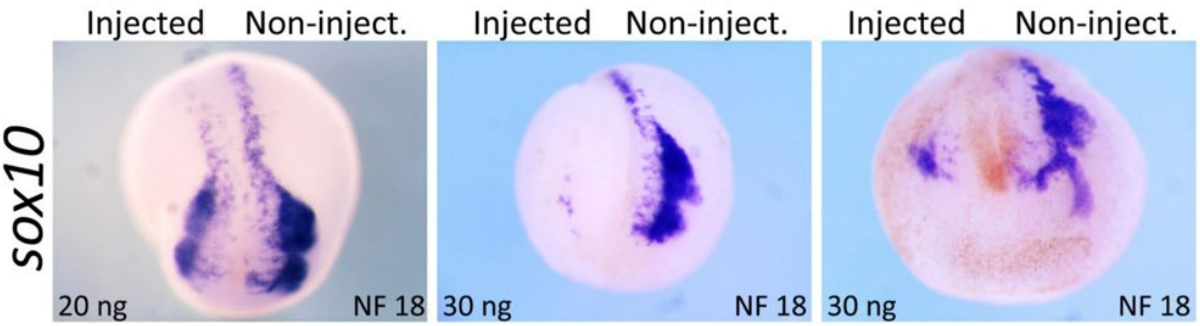

Figure 69: Dose response experiment of foxd3 Morpholino injected on one side (left) of a two-cell stage X. laevis embryo.

Embryos are viewed dorsally (A, B) or from the anterior side (C). After injection, embryos are left to develop until late Neurula (NF stage 18) and WISH was performed with NC marker sox10 to assess the degree of NC hindrance by the KD. Dose response revealed that 20 ng foxd3 MO was not enough to significantly reduce NC development on the injected side, whereas 40 ng and 60 ng Foxd3 MO injection led to toxicity phenotype, leading us to settle on 30ng injections, that show a clear reduction in the NCCs population, both for cephalic and trunk crest. ng, nanograms; non-inject., non-injected.

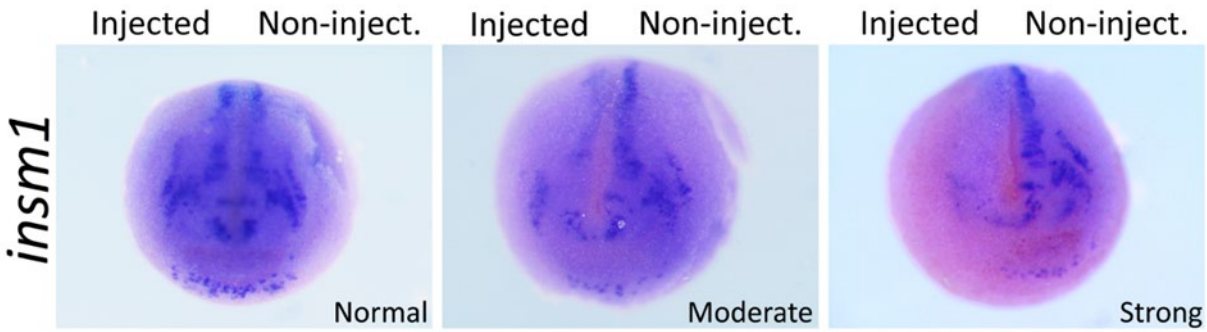

Figure 70: Example of phenotype categorization/scoring following foxd3 KD on one side of a two-cell stage embryo with insm1 mRNA expression.

Following KD, embryos were left to develop until NF stage 19/20, fixed and WISH was performed on insm1. Observed phenotypes were categorized as no effect on NA neuron number (normal), reduction in NA neuron number (moderate) and complete lack of NA neurons (strong). Insm1 is widely expressed in the developing nervous system and is vital in neuroendocrine development and differentiation in vertebrates. Insm1 showed a strong reduction in NA neurons as well as in overall expression on the injected side, lacking migrating NC, midbrain and NA neuron expression. non-inject., non-injected;

To investigate the effect of NC KD on our NA neuron population, we performed WISH on NF stage 19/20 in *X. laevis* embryos using marker genes *phox2a*, *insm*, *chga* and *dbh*. The KD phenotype achieved with the foxd3 MO was categorized into normal (no observed effect on NA neurons), moderate (clear reduction in number of NA neurons) and strong (complete lack of NA neuron staining) as demonstrated with gene expression of *isnm1 (Fig. 70).*

Results of knockdown phenotype for all tested marker genes are shown in Fig. 71 .

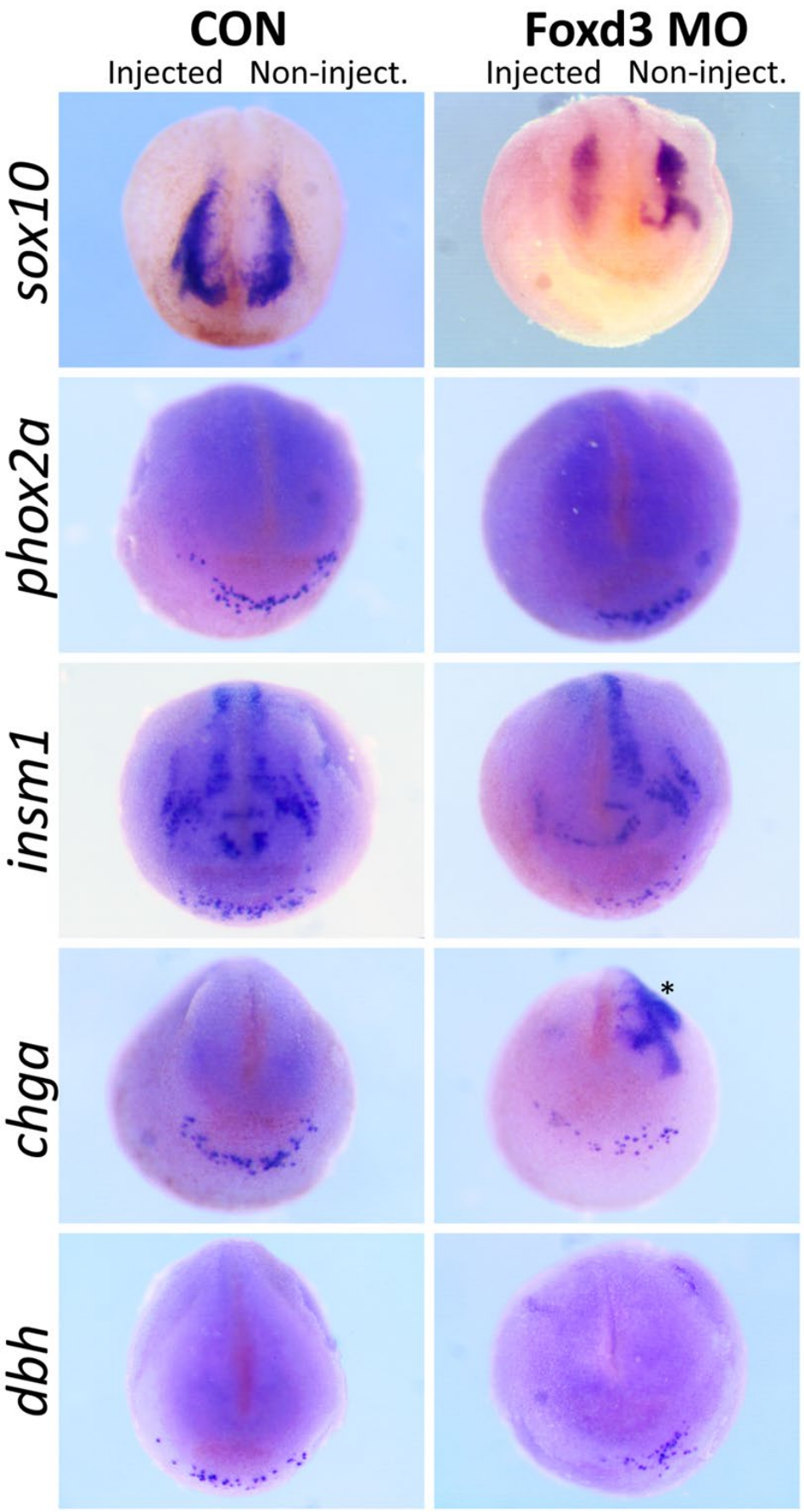
CON
Injected
Non-inject.
Foxd3 MO
Injected
Non-inject.
sox10
phox2a
insm1
chga
*
dbh

Figure 71: The effect of NC inhibition by foxd3 MO knockdown in X. laevis.
Embryos were fixed at NF stage 19/20, when the NA neuron population is clearly visualized at the anteroventral side of the embryos, beneath the cement gland. Embryos are viewed anteriorly. Embryos were injected on one side of a two-cell stage embryo (injected side always on the left, uninjected control side on the right of the embryo) with 30ng of either control MO or foxd3 MO, plus 25 ng GFP to trace the side of injection. The left column (control MO) are representative embryos injected with the control MO, which shows that there is no obvious phenotypic effect on the NC, and no difference between injected and non-injected side in the amount of NA cells and their distribution. The right column (foxd3 MO) shows a clear difference between the foxd3 MO injected side (left) and the uninjected side (right) for all our CCs marker genes. We see a reduction in our NC control marker gene sox10, with clear reduction in overall NCCs expression and reduced migration of cNC. Both phox2a and insm1 show a complete absence of NA neurons staining on the injected side, compared to the uninjected side. For marker insm1, we additionally see a strong reduction in migrating NC and NA expression. For chga, we see a clear reduction in the number of NA neurons, but no complete reduction in the cells. Asterisks mark NC expression that was visualized by sox10 probe, which was mixed in with the chga probe but is not expressed by chga itself. We can clearly see that the NC has been nearly completely blocked on the injected side. Dbh shows a clear absence of NA neurons on the injected side while the control side shows a high amount of dbh expressing cells. The control injection shows no reduction in cell number. CON, control morpholino; MO, Morpholino oligonucleotide; non-inject., non-injected.

KD of NC marker foxd3 using 30 ng of MO was performed in two biological replicates as well as the control injections. Embryos injected with our control MO showed no phenotype for the NC marker *sox10* (100% normal), and less than 10% of moderate phenotype for our four NA neuron markers (Fig. 72). All controls are shown on the left side of the graph (Fig. 72). Loss of function of *foxd3* at NF stage 19/20 showed a strong reduction in NC expression and migration in our NC control marker *sox10* (n=39). In total, 24 embryos showed a strong phenotype (61.5 %), or a moderate phenotype (n=10; 25,6%) and only 5 embryos showed no effect after KD (12,8%). SA lineage marker *phox2a*, had a complete absence of NA neurons in 31.4 % of embryos (n=22 of n=70 total injected), while 40% (n=28) showed a moderate phenotype, with a clear reduction of the amount of NA neurons on the injected side, when compared to the non-injected side. Also, our neuroendocrine differentiation marker *insm1* was clearly affected when the NC was knocked down. In total we had 47 embryos injected with the *foxd3* MO and 51.1% (n=47) of injected embryos showed a complete lack of NA neurons on the injected side compared to the non-injected side. 36.2 % of embryos had a clear reduction in number of NA neurons on the injected side. *Insm1* showed a clear reduction in expression also in other tissues such as in the migrating NC, and the CNS expression. As *Insm1* is a key factor in the

neuroendocrine differentiation pathway of the NC into CCs in other mammals, this is a good indicator for us that the NA neuron population seems to be indeed NC derived, and therefore likely to give rise to putative CCs acting as the equivalent of the frog AG. Finally, the genes directly involved in noradrenaline production, storage and release, *chga* and *dbh,* were clearly affected by NC loss-of-function. In absence/reduction of *foxd3*, well over 50% of embryos showed a complete lack of NA neurons on the injected side. In total, we injected 57 embryos of which 39 were lacking the NA population (68,4%) after *chga* staining. Another 21.1% of embryos showed a reduction in NA neuron number. *Dbh* was also affected by NC KD, with 26,7% (n=30) of embryos lacking NA neurons on the injected side and a further 33.3% showed a reduction in NA neuron numbers.

Overall, we observed a clear reduction and loss of expression of our NA neuron/CCs markers on the injected side of embryos following KD of the NC marker *foxd3*. This suggest that the NA neurons/CCs seem to indeed be derived from the NC as is known for CCs of the AM.

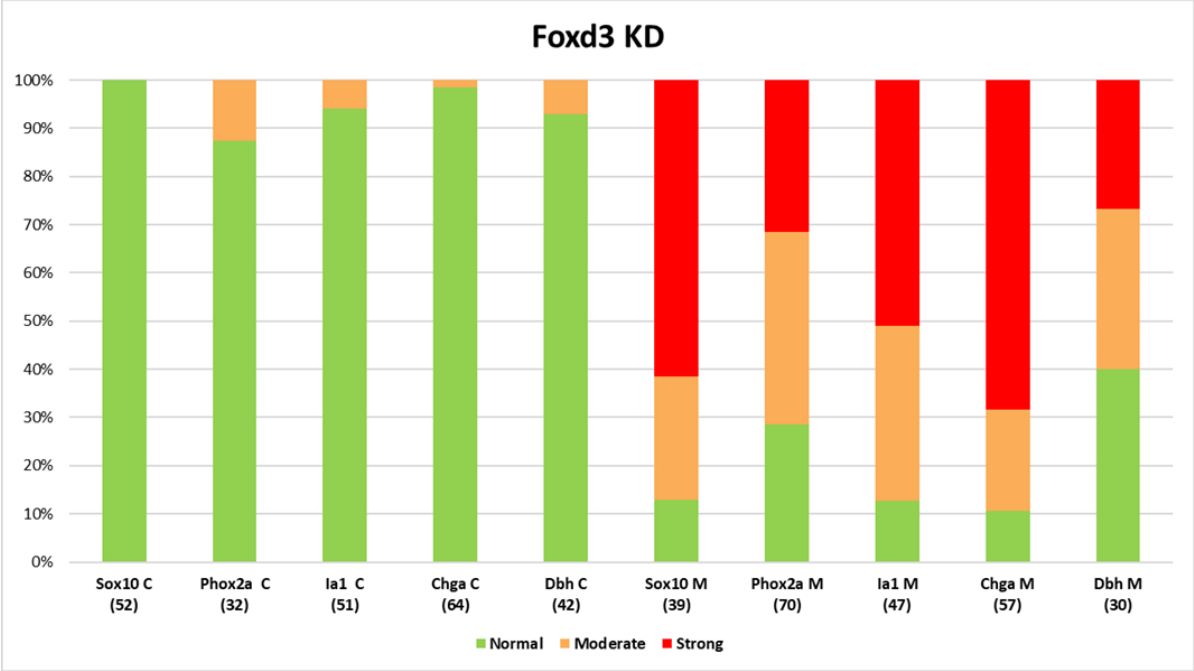

Figure 72: KD of NC marker foxd3 inhibits the expression of CCs/NA neuron markers in the anteroventral region of X. laevis embryos.

Xenopus embryos were injected with foxd3 MO on one side of a two-cell stage embryo to inhibit the NC, together with GFP mRNA as a control tracer. Additionally, a group of X. laevis embryos were injected with a control foxd3 MO to assess injection toxicity and embryonic death. Embryos were allowed to develop until NF stage 19/20 when NA neurons are well visualized with chosen markers at the anteroventral side. Embryos were fixed and WISH performed with CCs marker genes phox2a, insm1, dbh and chga to assess the effect of NC KD on the NA cell population. Additionally, WISH was performed on KD embryos with NC marker sox10 to assess efficiency of NC inhibition. Embryos were scored based on severity of effect on NA neuron/CCs marker genes expression on the injected side, compared to the uninjected side. Normal means no difference was observed on the amount of NA neurons/CCs on the injected side compared to the uninjected. Moderate effect meant a reduction in amount of NA neurons was visualized by WISH on the injected side, and strong indicates there was a complete lack of NA neurons on the injected side. The left side of the graph shows the foxd3 control injected embryos which showed no significant disruption of the NC after injection. The right side shows the foxd3 MO injected embryos, with a clear reduction in NA neuron number for all four CCs marker gens (orange) or complete lack of expression of CC markers (red). Overall, NC inhibition showed a clear reduction in CCs marker gene expression, and the minority of injected embryos showed no effect (green).

6.3 *Sox10* MO KD effect on NA neurons/Chromaffin cells

Sox10 is a transcription factor expressed in pre-migratory and migratory NCCs, and functions in the multipotentiality of these cells *in vitro* and *in vivo*. Sox10 is involved in the differentiation of NCCs into neurons, glia and melanocytes. Initially, Sox10 expression is high in all NC progenitors but, during development, expression is downregulated in the cranial region, while it stays high in trunk NC. Mis-expression of Sox10 during NC development in human causes Waardenburg or Hirschsprung disease (Vega-Lopez et al., 2017). In *Xenopus* embryos, *sox10* is involved in lineage decision making of the NC, rather than the migration of this cell population. To further confirm the results of NA neurons/CCs reduction following inhibition of the NC by KD of *foxd3*, we decided to also perform KD on NC marker *sox10*.

The *sox10* MO used in this experiment was previously designed against the ATG region of *Xenopus sox10 mRNA*, to prevent the initiation of translation, by Honoré and colleagues (Honoré et al., 2003). Previous publications injected between 1 ng and 15 ng of sox10 MO into one cell of a two-cell, four-cell or eight-cell stage embryo. Good results to inhibit *sox10* expression in *Xenopus* embryos at two-cell stage have been achieved using a dose of 10 ng, and letting embryos develop to blastula stage by (Buitrago-Delgado et al., 2018). 10 ng was therefore used as initial dose concentration for creating a dose-response experiment for the sox10 MO. To determine a concentration which would give a consistent phenotype, we injected varying concentrations starting from 10 ng, 12 ng and 20 ng of the sox10 MO into one cell of a two-cell stage embryo, together with 25 ng of *GFP* mRNA. We initially observed good results with 12 ng of sox10 MO, when performing WISH with NC marker *snai2,* to test the efficiency of the injected doses just after NC induction around NF stage 13/14. However, at late Neurula stages NF 19/20, which are our developmental time points of interest, we observed the reduction of the NC on the injected side to not be efficient. As 20 ng of sox10 MO showed signs of toxicity, we therefore repeated our initial *sox10* KD experiment with a dose of 16 ng of sox10 MO (Fig. 73). To assess levels of mortality of WT embryos compared to MO injected embryos, we again used our control MO, and could confirm no excess of mortality, nor obvious developmental defects of the embryos.

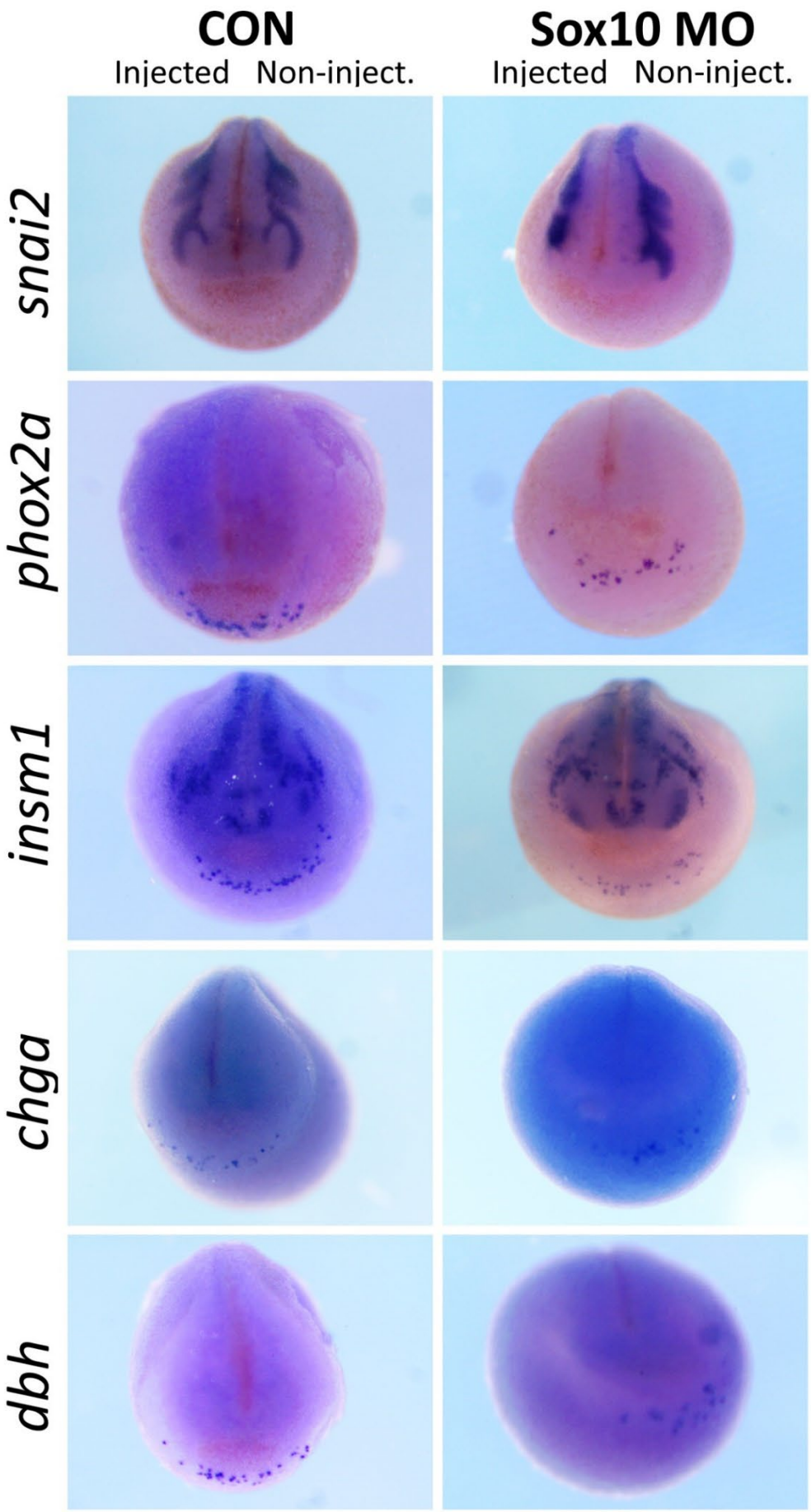
CON
Injected
Non-inject.
Sox10 MO
Injected
Non-inject.
snai2
phox2a
insm1
chga
dbh

Figure 73: The effect of NC inhibition by sox10 MO KD in X. laevis.
Embryos were fixed at NF stage 19/20, when the NA neuron population is clearly visualized at the anteroventral side of the embryos, beneath the cement gland. Embryos are viewed anteriorly. Embryos were injected on one side of a two-cell stage embryo (injected side always on the left, uninjected control side on the right of the embryo) with 16 ng of either control morpholino or 16 ng sox10 morpholino, plus 25ng GFP to trace the side of injection. The left column again shows control (CON) MO injected embryos injected, showing there is no obvious phenotypic effect on the NC, and no difference between injected and non-injected side in the amount of NA cells and their distribution. The right column (sox10 MO) shows a difference between the sox10 MO injected side (left) and the uninjected side (right) for all our CCs marker genes. We see a reduction in our NC control marker gene snai2, with a reduced migration of cNC. The effect of NC KD is lower than in our previous experiment with foxd3 MO. Both phox2a and insm1 show a reduction of NA neurons staining on the injected side, compared to the uninjected side. Insm1, is less affected in overall expression than in our previous KD experiment with foxd3. For chga, we see a clear reduction in the number of NA neurons, as is the case for dbh. Dbh shows a clear absence of NA neurons on the injected side while the control side shows a high amount of dbh expressing cells. The control injection shows no reduction in NA/CCs number. C, control; MO, Morpholino oligonucleotide; non-inject., non-injected.

Due to time constraints towards the end of this projects, sox10 MO KD using 16 ng, was only performed once, but with a large number of embryos injected (Fig. 74). Our NC control marker *snai2* showed a moderate inhibition of the NC at 59.4 % (n=38). Only 3.1% of embryos showed a complete inhibition of the NC (n=2). No effect after MO injection was observed in 37.5% (n=24) embryos. *Phox2a* was less affected by sox10 MO KD compared to previous results with 30 ng of *foxd3* MO KD. Nevertheless, 33.3% of embryos (n=33) showed a reduction in number of NA neurons/CCs expressing our marker genes on the injected side, when compared to the uninjected side. Also, 6.1% (n=6) of the embryos showed a complete absence of NA neurons. *Insm1* expression again, showed the strongest response to NC KD, a total of 52.7% (n=49) embryos show a moderate effect, with a reduction in total NA neurons expressing *insm1* marker on the injected side. 7.5% (n=7) embryos totally lacked *insm1* expression in NA neurons on the injected side. *Chga* had 35.3% (n=24) of the embryos displaying a moderate effect on the injected side, and 8.8% (n=6) of the embryos with a strong score. Finally, *dbh* had a lower score for moderate effect of injections, specifically 23.5% (n=20), but a slightly higher score for strong effect at 14.1% (n=12).

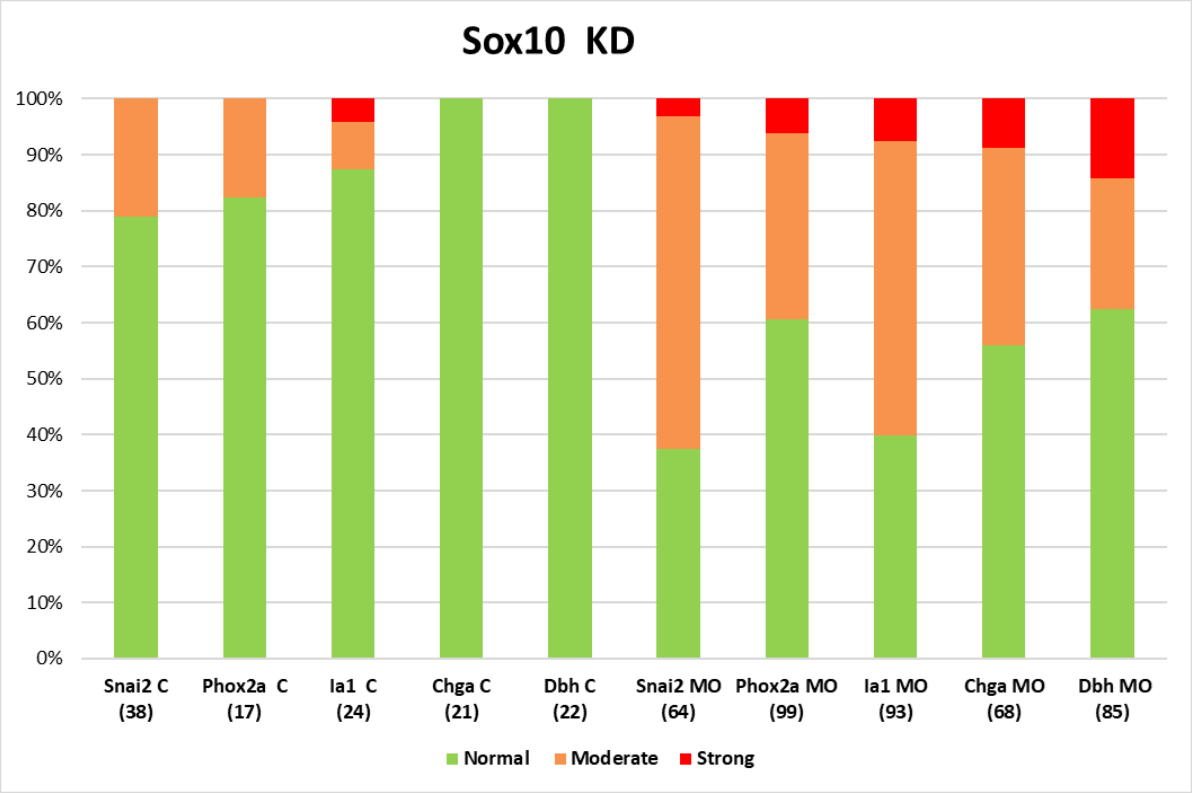

Figure 74: Inhibition of NC development by sox10 KD reduces the number of cells expressing CCs markers on the injected side compared to the uninjected side in X. laevis embryos. *Embryos were injected on one side of a two-cell stage embryo with 16 ng of sox10 MO and 25 ng of GFP mRNA as a tracer control. Injected embryos were left to develop until NF stage 19/20, when the NA neurons/CCs are visualized with selected markers at the anteroventral side of developing X. laevis embryos, and then fixed. WISH was performed with marker genes phox2a, insm, chga and dbh to assess the effect on the NA neuron population following sox10 KD. Embryos were scored compared to the uninjected side based on reduced expression of NA neuron/CC markers and inhibition of NC, assessed by performing WISH with NC marker snai2. Additionally, to assess the success of the injections and toxicity effect, our positive control foxd3 MO was again injected on a group of embryos and WISH performed on the same markers. The control groups showed no reduction in NA neurons expressing markers chga or dbh. Very few embryos showed a reduction in NA neuron numbers following control injection for markers insm1 and phox2a and the NC was found to be moderately inhibited in 20% of injected embryos. Overall, NC inhibition by sox10 KD mostly caused moderate effect on the cell population expressing NA neuron/CC markers, mostly leading to a reduction in expression rather than complete absence of NA neurons. The strongest effect of sox10 KD was again seen with markers insm1. Generally, the KD of sox10 using 16 ng may not have been high enough at these stages of development to fully inhibit sox10 expression, although we saw toxicity effects using 20 ng of sox10 MO.*

6.4 Discussion and Conclusion

In this chapter, we have demonstrated that there is a correlation between the KD of the NC by MOs and the amount of NA neurons arising at the anteroventral side of *X. laevis* embryos at late Neurula stages. We observed a clear reduction in the amount of NA neurons present on the injected side, when compared to the uninjected side of embryos or embryos injected with a control MO. A significant percentage of embryos demonstrated a complete absence of the cell population on the injected side following NC inhibition with the *foxd3* MO and we are therefore suggesting the NA neuron population is indeed derived of the NC. Previous experiments by Wylie and Colleagues also demonstrated this by using a dominant-negative form of slug (dnSlug) to inhibit NC migration (Wylie et al., 2015). When NC migration was blocked, no expression of NA neuron markers *phox2a*, *hand2* and *ascl1* was observed at the anteroventral region of the embryos. We additionally performed MO KD of sox10, another critical TF involved in the early specification and migration of NCCs and in the promotion of NCCs differentiation into neurons and glia of the peripheral nervous system. We observed a moderate effect on the NA neuron population following *sox10* KD, with an overall reduced number of cells expressing CCs marker genes on the injected side compared to the uninjected side. However, less embryos demonstrated a complete lack of NA neurons following NC KD of *sox10* compared to that seen with *foxd3* NC KD though the results of this experiment are still statistically significant. In both experiments, neuroendocrine differentiation marker *insm1* seems to be the most affected by NC knockdown.

There are several possible reasons why we observed a reduced effect of sox10 MO, when compared to the foxD3 MO experiment. The first reason might be due to a higher concentration of *sox10* mRNA, in comparison to *foxD3* mRNA in the developing embryo. This might mean that effective KD may require a higher concentration of sox10 MO, in order to obtain the same knock-down effect on the NC development. Another possible explanation might be in a different silencing effect due to the different bases in the two morpholinos. In fact, as the two morpholino sequences are different, it is possible that they bind to their targets with different affinity. In this scenario, it is possible that foxD3 MO binds with more affinity to its target compared to the sox10 MO. Another reason for the different effects on gene expression using different morpholinos might be due to the biology of the investigated

genes itself. Specifically, it is possible that foxD3 is more important than sox10 to initiate the transcriptional pathway that will lead to phox2a, ia1, chga and dbh synthesis, as it slightly precedes expression of sox10. However, it is not excluded that the real explanation is a combination of all of these reasons, or some other that were not elaborated here.

Finally, while we saw an indication that inhibition of the NC negatively affects the formation of the NA neurons at the anteroventral side of the embryo at late neurula stages, we do not know what the effect may be at later developmental time points. It would have been interesting to trace the development of NA neurons following NC KD further throughout developmental stages to see if they are also inhibited in moving closer to the pronephric tubule, or if signal would be delayed.

It has also become increasingly clear that most research on Xenopus' NC development and expression of NC markers is not studied well after Neurula stages, and there is a significant lack of spatial-temporal mapping of NC markers further in development (Tailbud stages) and would be useful to be addressed in future studies.

7 Chapter VII: General Discussion

7.1 Summary

The data presented throughout this thesis provides a first framework towards the characterization of the development of the AG in the model species *Xenopus laevis*. *Xenopus* is a useful model organism to study and model human diseases, contributing to elucidate NC biology and NCPs (Medina-Cuadra and Monsoro-Burq, 2021). Our lab has successfully used *Xenopus* as a model for compound screenings (Wheeler and Brändli, 2009) that can be useful in testing and identifying novel drug candidates and easily assess how such a drug compound affects an organ's development. In this context, it would be of interest to study how certain drug compounds could affect the AG or AG-associated tumours.

Recently, *Xenopus* has been used as a model organism to study the childhood tumour Neuroblastoma (Corallo et al., 2020; Moreno et al., 2021), which originates from transformed sympathoadrenal (SA) cell precursors derived from TNCCs, and can occur anywhere along the SA nervous system (Barr and Applebaum, 2018; Corallo et al., 2020). Almost half of these tumours are found in the AM (Vo et al., 2014).

However, no research has been done in *Xenopus* to trace the development of the SA lineage, as well as the development of the AG, particularly the NC-derived AM. This lack of fundamental knowledge on the AGs development, comparability and compatibility with the human system provides great challenges in performing research on the SA lineage and SA precursor derived NCPs using *Xenopus*. Even in other vertebrate species, key details of AG development, as well as the origin of tumours associated with the SA lineage and the AG directly, are not well understood (Kameneva et al., 2022). My main goal, therefore, was to establish a spatial and temporal characterisation of the organ's development, in order to be able to use *Xenopus* in the future to further understand the NC-derived CCs and SA tumour development and progression.

Initially, I determined a list of candidate marker genes from the literature in other vertebrate species, such as humans, mice and zebrafish, of AG development, with a focus on CCs development. In Chapter 3, after determining our candidate marker genes, I created riboprobes to perform WISH on such genes, and visualized their expression at different stages

of *Xenopus laevis* embryonic development (starting from NF stage 19/20 up to NF stage 45) to map the location and development of CCs of the AM. I identified a particular expression pattern of punctate cells. The expression is found initially at the anteroventral side of the embryo, and the cells are later visible across the anterior embryonic body. The markers showing this expression pattern included SA specifier genes *phox2a* and *phox2b*, neuroendocrine differentiation marker *insm1*, the neuroendocrine secretory gene *chga*, and genes coding for enzymes vital in the synthesis of catecholamines *dbh*, *th* and *pnmt*. This expression pattern was labelled as showing NA neurons, based on previous publications showing this expression pattern at earlier stages of development (NF stage 14-22) for candidate marker genes *phox2a, insm1* and *th*, as well as for *ascl1*, which is vital in the generation of autonomic neurons and the regulation of neuroendocrine cell development (Parlier et al., 2008; Talikka et al., 2004; Wylie et al., 2015).

These results lead me to hypothesize that these broadly labelled NA neurons are, in fact, putative CCs. As the expression of these cells was not observed in close association to the developing kidney, nor did the cells seem to form a defined structure, I further hypothesized that *Xenopus* do not form an AM structure *per se*, during embryogenesis, and that CCs likely remain individual and loosely intermingled among the developing AC along the ventral side of the adult kidney. This hypothesis reinforces previous observations that this is the structure of the adult *Xenopus* AG (Milano and Accordi, 1983; Perry and Capaldo, 2011).

In Chapter 4, I continued to characterize the embryonic development of the AG in *X. laevis*, this time focussing on the characterization of the mesoderm derived AC. Again, we created a spatio-temporal map by WISH for candidate marker genes *nr5a1* and *star,* which are both involved in steroidogenic tissue formation and steroidogenesis. Both genes were expressed in the region of the developing pronephric kidney, starting from NF stage 30-33 up to NF stage 45, therefore most likely showing the developing AC. While both markers were expressed in the expected region of the embryo, there was one further issue that had to be addressed. As discussed previously, the AC is derived from the AGPs that also gives rise to the reproductive organs, the gonads, which share a similar set of genes involved in their development and functionality, including *nr5a1* and *star*. To distinguish between these two tissues, I also characterized the expression of PGCs marker *pgat*, and concluded that the PGCs are in no

close proximity with the expression characterized for steroidogenic marker genes *nr5a1* and *star*, during embryonic development of *Xenopus*. I therefore concluded that the gonads are not fully formed during embryogenesis, and that I had identified the location and development of the AC.

Both these chapters present, for the first time, the characterisation of expression of multiple genes in *Xenopus laevis* associated with AG development, including *nr5a1*, *star*, *pnmt*, and *dbh*. This is also the first time *chga* has been fully characterized by WISH, while I have also added extensively to the full characterization of *phox2a*, *phox2b* and *insm1,* describing novel expression patterns that have not been previously shown for all three.

Chapter 5 was aimed at establishing a protocol for HCR usage in *Xenopus laevis*, and attempted to confirm that our candidate CCs marker genes are co-expressed within the same putative NA cells, as presumed by previous observations. By performing HCR with two marker genes at a time, I could confirm the co-expression of *phox2a* and *dbh* within the same NA cell, as well as *phox2a* with *chga,* both at NF stage 30. Finally, I observed co-expression of *chga* and *dbh* within the same NA cells again at NF stage 30.

Additionally, I performed HCR with our candidate AC markers together with our PGCs marker *pgat* to confirm, within the same embryo, that there is no overlap between the PGCs and the presumptive AC during embryogenesis, as assumed based on my WISH results in Chapter 4. We did not observe overlap of the PGCs with the presumptive AC at late tailbud stage NF stage 40, further solidifying my assumption that we have indeed characterized the location of the developing AC taking advantage of the markers *nr5a1* and *star* during embryogenesis of *X. laevis*.

In my final result Chapter 6, I wanted to assess if the putative CCs identified in Chapter 3 are NC-derived, further supporting the validity of these cells being CCs. To do so, MO KD of NC genes *foxd3* and *sox10* was performed on one side of a two-cell stage embryo, followed by WISH of our candidate CCs markers. *FoxD3* and *Sox10* are required for NC development and their KD leads to a loss of NC and NC derived tissues. *Foxd3* KD correlated with a reduction in NA neurons on the injected side of the embryo for all marker genes tested *(phox2a, insm1,*

chga and dbh). The same effect was observed with *sox10* KD, although, in this case, the impact on the expression of our marker genes was less severe. This demonstrates a clear relation between the NC and the putative CCs.

This work presents a first effort to characterize the development of the AG during *X. laevis* embryogenesis, yielding unexpected and surprising results, particularly in the characterization of the CCs. Initially, we anticipated that the characterization of CCs development would be a swift and preliminary phase. However, these findings have opened numerous intriguing questions that I would like to address.

7.2 Terminology and cell definition - Sympathetic neuron, noradrenergic neuron or chromaffin cell?

The first task is to define the terminology used to describe the characterized punctate cells with our candidate CCs marker genes throughout this thesis. The terminology found in different aspects of this research has jumped between sympathetic neurons, noradrenergic neurons and CCs. Although all three cell types/definitions share commonalities, such as sharing noradrenaline as their main signalling neurotransmitter, there are some differences to distinguish them. As summarized in Chapter 3, this punctate single cell pattern we have seen was previously discovered in *X. laevis* embryos at the anteroventral side of early tailbud stages for a set of marker genes labelled as noradrenergic (NA) precursor cells, including *phox2a*, *hand2*, *insm1* and *th* (Parlier et al., 2008). These cells expressed markers similar to the developing mammalian sympathetic nervous system (SNS) and were shown to be dependent on BMP signalling, like the developing SNS in mammals. A further research group found the same expression pattern in *X.laevis* embryos during neurogenesis with marker *ascl1,* which is essential for noradrenergic sympathetic ganglion neuron development, and labelled the cells as noradrenergic neurons(Parlier et al., 2008; Wylie et al., 2015). Finding a definition for the term noradrenergic neuron has been difficult, but the following is to the best of my understanding. A noradrenergic neuron is a type of neuron that primarily releases noradrenaline as their neurotransmitter, and can be found both in the CNS, mainly in the locus

coeruleus (LC), and in the PNS (Hirsch et al., 1998; Szabadi, 2013). These neurons are involved in functions like attention, stress response and mood regulation in the CNS, and modulating heart rate, blood pressure and blood flow in the PNS. As NA neurons are described as having a typical neuronal structure with a cell body, axon, dendrites, and synaptic terminals (Kandel et al., 2000; Szabadi, 2013), this cannot be taken as a definition for a putative CCs, as I suggest the cells I identified in this work to be. Although we have continuously labelled these cells as NA neuron, this would be no longer accurate if we can finalize their definition as CCs or chromaffin-like cells, as these cells are able to synthesize and store adrenaline. More work needs doing to make this label a definite, which will be discussed in the following paragraphs.

Another definition and label of a similar cell expression pattern that I came across is sympathetic neuron. Sympathetic neurons are part of the autonomic nervous system, specifically the sympathetic division, as implied by their name and are involved in 'fight-or-flight' (Murtazina and Adameyko, 2023). Compared to NA neurons, these cells are defined by their specific role in the SNS, and can use noradrenaline or acetylcholine as neurotransmitters, whereas NA neurons are a broader category, defined simply by the neurotransmitters they respond to. Thereby, a sympathetic neuron and a noradrenergic neuron could describe one and the same cell type, meaning they use noradrenaline as their neurotransmitter and both are part of the SNS.

However, the sympathetic branch of the autonomic nervous system includes both sympathetic neurons with associated glial cells, as well as neuroendocrine CCs (Murtazina and Adameyko, 2023). Both CCs and sympathetic neurons share multiple characteristics, such as their origin (if distantly) from the NC, the ability to synthesize, store and release catecholamines, along with the expression of catecholaminergic marker enzymes TH and DBH (Shtukmaster and Huber, 2023). However, only CCs can synthesise adrenaline, through the activity of PNMT. Both *PNMT* and *CHGA* are considered CC specific markers, that can help us distinguish between sympathetic neurons and CCs (Shtukmaster and Huber, 2023). As mentioned before, another key difference is the presence of neurites from sympathetic neurons, which are used to communicate and regulate organs, which CCs do not possess nor require, to secrete catecholamines (Shtukmaster and Huber, 2023).

The research article presented by Edens and Colleagues show, for the first time, sympathetic neurons spanning the length of the lamprey trunk, aligned in a sparse, chain-like manner, and expressing genes essential for SA fate development (Edens et al., 2024). Interestingly, these cells were found as single cells and not assembled as ganglia, much like the cells I have characterized in this work. The authors further confirmed that these cells are of trunk NC origin. Curiously, the sympathetic neurons were shown to arise at much later developmental stages than in humans, mouse or zebrafish. The cells were shown (by HCR) to co-express TF genes essential for the SA fate (*Ascl1*, *Phox2 -Phox2b* in jawed vertebrates-, and *Hand2*), as well as enzymes Th and Dbh (Edens et al., 2024). The cells identified in lamprey look remarkably like the cells we have characterized throughout this project in *X. laevis* embryos and are expressing some of the same markers that we have presented and analysed in this project.

An issue I therefore faced, while characterizing the cell expression further, is the fact that CCs and sympathetic neurons share a similar network of TFs regulating their development, including *Ascl1*, *Phox2a*,*Phox2b,Hand2* and others (Chan et al., 2018a; Furlan et al., 2017).

I have shown the expression in the previously labelled NA cells of TFs *insm1*, *phox2a* and *phox2b,* as well as *hand2*. Compared to Edens and Colleagues, I did not show co-expression of these factors in the same cells, although this is a strong presumption, based on the similar pattern of expression and the data presented in lamprey. Additionally, the expression of marker *ascl1* was shown to be present at early tailbud development in *Xenopus* in a similar fashion (Parlier et al., 2008; Wylie et al., 2015). I have also shown the expression of the catecholamine synthetic enzymes, th and dbh. While I have characterized expression of *th* only briefly due to technical difficulties, and have not yet performed co-expression with other candidate markers, previous data shows the expression of *th* in the NA cells as early as NF stage 19/20 (Wylie et al., 2015), in a similar fashion as the other candidate genes. However, the presence of these two enzymes in the labelled NA cells is not enough to distinguish between a sympathetic neuron and a differentiated CC.

Promisingly, the presence of *chga*, which is mostly specific to adrenal CCs (Shtukmaster and Huber, 2023), as well as the co-expression of *chga,* with both *dbh* and *phox2a* within the

labelled NA cells is a strong first indication of these cells being CCs (see chapter 3, section.3.4.1 and chapter 5, section 5.4 and 5.5). *Chga* is vital in chromaffin vesicle formation and binds catecholamines, and is also thought to protect catecholamines against enzymatic degradation until they are secreted (Berends et al., 2019).

The differentiation from SCPs to CCs by RNA-seq analysis by Furlan and Colleagues (Furlan et al., 2017), was shown by the expression of *Chga* and *Th* amongst others in mice (Chan et al., 2018b; Furlan et al., 2017). While some presence of *Chga* has been indicated in the sympathetic neurons of rat superior cervical ganglion, DRG and in enteric neurons (Schäfer et al., 1994), this marker is still considered specific to AM CCs to distinguish them from the sympathetic neurons (Shtukmaster and Huber, 2023).

Another specific marker of AM CCs, specifically adrenergic CCs, is *pnmt*. I have shown that *pnmt* is present and expressed in *X. laevis* embryos at early tailbud, in cells that look like the previous described cell type and are in a similar location (chapter 3, section 3.4.3). I did not observe *pnmt* expression prior to tailbud NF stage 27, or after NF stage 33 (in punctate cells). This lack of *pnmt* prior to early tailbud and in later tailbud could be due to two possible reasons; either these CCs are not fully differentiated and able to produce adrenaline prior to NF stage 27,or the lack of expression in these cells during later tailbud stages could also be due to low levels of transcripts present at these stages (chapter 3, Fig.35). The earliest presence of detected adrenaline in the blood of *X. laevis* has been shown starting from NF stage 40 (Kloas et al., 1997). This is in contrast to our results showing *pnmt* expression between NF stage 27-33, and highlights the need of a more detailed characterization of AG development and the role of adrenaline during embryogenesis. However, the presence of the main enzyme for adrenaline synthesis makes a strong case for CCs being present and differentiated during embryogenesis although not in the area that we anticipated. Furthermore, it is of interest to determine if the expression of *pnmt* at NF stage 27-33 might be correlated to a physiological process developing at these stages that might require adrenaline.

Another interesting morphological observation is the fact that the cells we have characterized are well rounded and show no evidence of the presence of axons and dendrites, based on

WISH and HCR staining. Their structure can especially be highlighted against the elongated enteric neurons we think to have identified by the expression of *phox2a* and *phox2b* as well as with *insm1* during late tailbud development. These cells are structurally more elongated and look neuronal (chapter 3, Fig. 43).

To make a definite case for the characterized NA cells being truly CCs, co-expression of the marker *pnmt* with one or more of the other investigated markers, such as *dbh* and *phox2a,* by HCR at the previous shown stages of development would be required to further prove these cells as being putative CCs or chromaffin-like cells. Another experiment to optimise would be IHC with anti-adrenaline during *Xenopus* embryogenesis. It could be useful to hereby section *Xenopus* embryos and perform the anti-adrenaline IF on those sections, when possible, with a red or far-red fluorophore, in order to minimize autofluorescence. This could show us where adrenaline is synthetised during embryogenesis in the *X. laevis* body, as well as putting the expression into relation with the characterized putative CCs. The presence or absence of adrenaline during *X. laevis* embryogenesis might elucidate if, before metamorphosis, *Xenopus* tadpoles are capable of producing this molecule, giving us an indication about the nature of the putative CCs that we characterised during the course of this project.

Another way to attempt to distinguish these cells as being either sympathetic or CCs could be to examine expression of markers that are specific to sympathoblast, the precursor of sympathetic neurons, and differentiated sympathetic neurons. A good marker gene to test could be cocaine- and amphetamine-regulated transcript (CART) peptide. Sympathetic neuroblast in mice express *Cart*, whereas CCs do not (Chan et al., 2018a). *Cart* could therefore serve as a useful marker to discriminate between the two related but distinct cell lineages.

7.3 Do chromaffin cells in *X. laevis* develop after embryogenesis?

One of the biggest surprises during this project was, firstly, the expression pattern of the punctate cells that I observed with most candidate CC marker genes and, second, them being expressed early in development, and nowhere near the pronephric kidney. The initial hypothesis was that the AG in *Xenopus* will likely develop similarly to the interrenal gland in

zebrafish although, morphologically, the developed AG structure has been described as being more closely related to that of *Urodeles* and particularly Salamandriae (Capaldo, 2023; Milano and Accordi, 1983).

In zebrafish, CCs are visualized as several dispersed clusters in the interrenal region at 2 dpf, by the expression of *dbh*. This would be around NF stage 40-45 in *Xenopus*. From 3 dpf, the cells converge to the midline of the interrenal gland and are in close contact with the steroidogenic cells, shown by the presence of $pnmt^+/th^+$ cells (Morrison et al., 2016; Yi-Wen, 2007). The mechanism of CCs integration within the interrenal gland was unclear until recently. As is the case in mouse, a majority of CCs have shown to be derived from SCPs also in Zebrafish larvae (Kamenev et al., 2021).

At this time point, and with the currently collected data, I am unable to confirm if the development of the AG in *Xenopus* is similar or not to the developing interrenal gland in Zebrafish. I have shown the presence of candidate CCs markers *dbh*, *th* and *pnmt* in the labelled NA cells. However, I have not found a research paper showing a similar expression pattern of numerous single cells in the anterior part of the zebrafish embryos by WISH, as I have characterized in *X. laevis*. It seems, that CC association and innervation of the interrenal gland may occur just after embryogenesis, which would indicate a similar time-point and association of CCs with the AC as described for zebrafish.

WISH expression mapping revealed an early expression of these cells, unexpectedly, at the anteroventral side of the embryo already expressing *dbh*, vital for noradrenaline synthesis. During early to late tailbud development, these cells appear across the anterior embryonic body in an interspersed fashion, without a clear pattern. The latest expression of these cells I was able to visualize by WISH, was at NF stage 40, when the putative CCs are less interspersed and seem to cluster together posterior to the head, between the heart field and the developing pronephros, as seen with markers *chga* and *dbh* (see summary Figure 43, chapter 3). After NF stage 40, I was unable to visualise these putative CCs anymore. This could be either due to limitations of the WISH protocol itself or due to our candidate markers no longer being expressed at later stages of development, which is likely the case for SA development and differentiation markers *phox2a*, *phox2b* and *insm1.* However, that would be surprising for

markers directly involved in catecholamine storage or synthesis like *chga*, *dbh*, *th* or *pnmt*. At later stages of embryonic development (NF stage ~45), I experienced issues with high background staining when performing WISH, likely due to non-specific colour development due to high endogenous alkaline phosphatases activity. Additionally, as embryos develop into tadpoles, the tissue becomes thicker and more complex, which could cause probes and antibodies to become trapped non-specifically or are unable to penetrate deeper tissues. Therefore, I cannot confirm the fate of the putative CCs after NF stage 40, and I do not know if these cells will associate with the kidney, and if so, at which developmental time point.

A study performing single-cell RNA sequencing on 300 pronephric kidneys of WT *X. laevis* embryos at NF stage 40 to characterize the cellular diversity of the *Xenopus* kidney development, also used *dbh* and *pnmt* to distinguish the AM from the pronephric kidney tissue (Corkins et al., 2023). They did find both genes to be expressed in the pronephric kidney at NF stage 40, and identified the AM to be part of the NC cell type (Corkins et al., 2023). They also identified the AC to be present in the pronephric kidney using markers *star* and *cyp11a1* (Corkins et al., 2023).

This raises a few questions on why I didn't observe *dbh* and *pnmt* expression associated with the kidney by WISH, at this stage of development, although still observing the NA cells at this stage.

Future experiments should include performing WISH on embryos between NF stage 40-45 with those two markers, along with marker *chga*. Hereby, I would suggest letting the probes develop for a longer period of time, despite high background staining, and then perform sectioning to determine the precise location of expression. The same experiment should also take place at later stages of development, like premetamorphic stages NF 48 to 54, hereby using sections rather than Wholemount staining, as the tissue is too thick at this point of development.

7.4 Lineage tracing could aid in identifying time points of CCs development and association with the kidney

An experiment that I attempted during this project to identify what happens to the putative CCs after NF stage 40, was the generation of a reporter plasmid, able to detect cells expressing our CCs markers *in vivo*. The general idea was to use a plasmid that contains a directional cloning site, just upstream of either *GFP* (green fluorescent protein) or *RFP* (red fluorescent protein) gene, and to subclone the promoter region of our genes of interest into this plasmid. To pursue this project, I wanted to amplify the ~3000bp upstream of our marker genes, such as *phox2a* or *phox2b*, *insm1*, *dbh* and *pnmt*, and to clone them into this reporter plasmid. Then, following injection of this plasmid at a 1-cell stage embryo, I would have tracked the expression of the GFP during different stages of development, up to NF stage 45. The rationale of this experiment is that the promoters of our maker genes will be active in cells that express such genes. With these promoters being active, it would be possible to observe the expression of the GFP or RFP in such cells. However, in this case, the effect would be a mosaic in which some cells will take up the plasmid and some others would not. Unfortunately, due to time constraints during this project, I was unable to clone and validate such a reporter plasmid.

To avoid the mosaicism problem, a possibility could be to integrate the plasmids inside the genome of the embryos using transgenic technology and looking at F0s and/or growing stable lines. This would not only allow us to overcome the problem of the mosaicism, since all cells of the next generations of embryos would have the plasmid integrated in their genome but would also help us defining the AM later in development, and even in adult frogs.

The question of whether the AG in *Xenopus* develops after embryogenesis was a major issue that I wanted to address in this project, but was pressed on time to do so. Early attempts to perform IF on dissected kidneys of pre-and pro-metamorphic *Xenopus* larvae were either not succesful or inconclusive, therefore, we did not continue this line of experiments. During a secondment period in the laboratory of Prof. Igor Adameyko, a partner of the NEUcrest consortium, an idea was to analyze this question using bioinformatics. Lab members of the Adameyko laboratoy, Dr. Maria-Eleni Kastriti and fellow Ph.D student of the NEUcrest consortium, Irina Poverennaya, helped in searching and identifying a recently published

single-cell atlas on *Xenopus* larvae, comprising four *Xenopus laevis* stages from larvae to juevenile (NF stage 48, 54, 59 and 66) as well as 17 adult tissues (Liao et al., 2022). The goal was to search for potential SA cells in this single cell atlas. The entire analysis was kindly performed by Irina Poverennaya. To identify the clusters of interest that contain SA cells from the dataset only containing the larval stages (Fig. 75 A), we gave a SA signature containing genes listed in Fig. 75 B and calculated the signature expression. The resulting clusters of interest (Fig. 75 C) where the SA signature was expressed the most was further used to identify and distinguish between chromaffin-like cells (Fig. 75 D) and sympathoblast-like cells (Fig. 75 E), based on the average expression of either chromaffin or sympathoblast gene signature. In total, 73 chromaffin-like cells and 298 sympathoblast cells were identified, presented in proportion to the corresponding stages (Fig. 75 F). Individual gene expression from the SA signature can be found in the appendix (Appendix Figure 4). Most chromaffin-like cells were identified at NF stage 48 (n=41), with fewer chromaffin-like cells present at later stages of development (NF 54, n=21; NF 66, n=11). Interestingly, no chromaffin-like cells were present at the metamorphic climax NF stage 59. Sympathoblast-like cells were also most frequent at NF stage 48 (n=161) and at NF stge 54 (n=89), and less frequent during and after metamorphosis (NF 59, n=8; NF 66, n=40). Based on these results, we can see that most chromaffin-like cells are present just after embryogenesis and decrease in frequency during the transition from tadpole and froglet to adult frog, giving us an indication on the developmental time-points that are key to CC development. However, some things need to be taken into account before concluding that most chromaffin-like cells are present at NF stage 48. Firstly, it is possible that not all cells from the larvae have been sequenced. Additionally, cells at adult NF stage 66 are larger in size than they are at NF stage 48 tadpoles, which could result in fewer cell types being sequenced for the adult frog. Unfortunately, the cell atlas did not include embryonic stages that we could use to compare the amount of chromaffin-like cells present at embryogenesis to those at later stages.

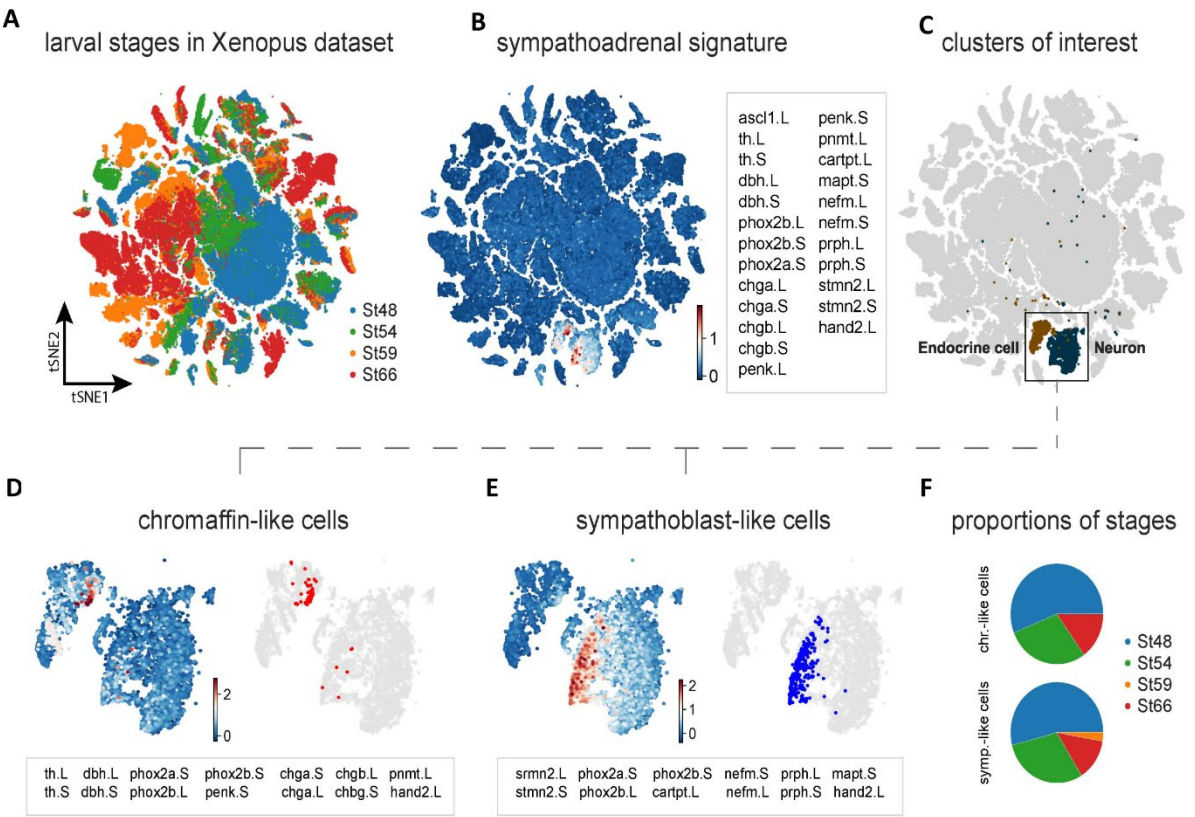

Figure 75: Search for potential SA cells in the single cell atlas of larval Xenopus created by (Liao et al., 2022).
A-C: t-SNE embedding of larval Xenopus single-cell dataset, n = 188020 (taken from [https://doi.org/10.1038/s41467-022-31949-2]). A: Stage distribution. B: Average expression and composition of SA signature. C: Highlighted clusters of interest where the SA signature was expressed the most. The cluster annotation is inherited from the original source ([https://doi.org/10.1038/s41467-022-31949-2]). D: Identification of chromaffin-like cells based on the average expression of chromaffin gene signature. E: Identification of sympathoblast-like cells based on the average expression of sympathoblast gene signature. F: Stage proportion in chromaffin- and sympathoblast-like cells.

7.5 *Xenopus* AG structure may be more closely related to the Sea lamprey

CCs of modern vertebrates are predominantly located near steroidogenic cells, forming the AG. However, evolutionary history suggests a more complex origin, with CCs and steroidogenic cells initially evolving separately, and later coalescing into a composite gland (Kastriti et al., 2020). Apart from their role in the 'fight-or-flight' response, an evolutionary conserved mechanism that responds to environmental and predatory threats, CCs also play a role in

oxygen-sensing , sharing a common evolutionary origin with other oxygen sensing cells (Edens et al., 2024; Kastriti et al., 2020). Oxygen-sensing cells include the glomus cells of the carotid body (small glands on either side of the neck), which are NC-derived, and pulmonary neuroendocrine cells of lung airway epithelia (Hockman et al., 2017). In fish and amphibians, these cells are found in close association with blood vessels. During hypoxia, these serotonergic cells trigger reflexes like hyperventilation, through the release of neurotransmitters (Hockman et al., 2017). For aquatic species, hypoxia-sensing is essential for monitoring oxygen levels in the water (Hockman et al., 2017; Kastriti et al., 2020). Sea lampreys have both cardiac CCs and extracardiac CCs, which are proposed to be the evolutionary precursors of the AM, as they are of NC origin and their main function is considered to be oxygen-sensing (Kastriti et al., 2020; Paiement and McMillan, 1975). Apart from their apparent restriction to the heart, lamprey CCs seem to be incapable of adrenaline biosynthesis, probably due to the absence of a *pnmt* orthologue (Edens et al., 2024). Based on the here characterized cells, that were sometimes present in the head structure of tailbud embryos (see Figure 43, Chapter 3), in close association with the branchial arches, it could be suggested that these cells perform an oxygen-sensing role during embryogenesis. It has been observed that CCs of the AM are oxygen-sensing during perinatal stages of rats and humans (Kastriti et al., 2020). Previously, scattered serotonergic cells have been identified in the internal gills of *Xenopus* tadpoles between NF stage 41and 43, that have been proposed to be homologs of teleost gill hypoxia-sensing neuroepithelial cells (NECs) (Hockman et al., 2017). However, it has been shown that in zebrafish, X*enopus* and lamprey, the NC does not contribute to gill NECs, and these cells are endoderm-derived (Hockman et al., 2017; Kastriti et al., 2020). Therefore, it has been proposed that carotid body glomus cells evolved from the aggregation of NC-derived catecholaminergic CCs, associated with blood vessels in the anamniote pharyngal arches. This data has been supported by the presence of catecholaminergic oxygen-sensing cells identified in close association with blood vessels in the cardiac region and gills of bony fish, that are NC-derived (Hockman et al., 2017; Kastriti et al., 2020). As I saw a relation between NC KD and the amount of cells present in the embryo, it makes it likely these cells are NC-derived. This would speak against the presented theory of these cells being hypoxia sensing NECs, as these were shown to not be NC-derived.

Still, to study if our characterized cells could be oxygen-sensing cells, that are more like glomus cells of the carotid body, WISH with marker genes like *cox4i2*, *gnas* and *rgs4* could be performed, or a co-expression experiment with oxygen-sensing cell specific marker genes and *pnmt* by HCR. However, their similarities on both origin and function could make a proper distinction complicated. It may also be that these putative CCs may perform mainly oxygen-sensing functions prior to metamorphosis and associate with the steroidogenic tissue at later stages of development, as seen with the interrenal gland in teleosts.

It could be plausible that the here identified cells are more similar to the recently identified trunk sympathetic neurons in the sea lamprey. This is based on the shared expression of TFs necessary for sympathetic neuron development and their morphological similarity. This means, *Xenopus* may have a more primitive form of CCs or chromaffin-like cells that are in closer relation to the agnathan than they are to the AG of gnathostomes. Although the presence of the enzyme *pnmt* indicates that these cells have transitioned towards adrenaline producing CCs that we see in gnathostomes. These cells may associate with the kidney just after late embryogenesis.

7.6 Chromaffin-like cells are NC derived

In my final result chapter (Chapter 6), I explored the relationship between the NC and the chromaffin-like cells that I have identified. As CCs of the AM are NC-derived (or more specifically, having a majority arise out of NC-derived SCPs), I wanted to test this relationship and see if inhibiting the formation of the NC affects the development of the chromaffin-like cells. To test this, I performed morpholino KD of either NC genes *foxd3* or *sox10* in one cell of a two-cell stage embryo and performed WISH with candidate CC markers *phox2a*, *insm1*, *chga* and *dbh*. I clearly saw a reduction, up to complete absence, of putative CCs following *foxd3* KD on the injected side, compared to the uninjected side. I also observed a reduction in the number of putative CCs following *sox10* KD on the injected side compared to the uninjected side, although the results were not as strong. Therefore, the data indicates that the putative CCs are derived from the NC.

My data further supports a previous study that showed this relationship between the migrating NC and the expression of NA markers *phox2a* and *hand2*. When Wylie and colleagues inhibited NC migration by dnSlug injections on one side of a two-cells stage embryo, it resulted in the absence of the NA neurons on the injected side (Wylie et al., 2015)

The absence and/or reduction of putative CCs after NC KD further supports my hypothesis that these cells are indeed CCs, but also raises an important question on how far the NC can migrate so early development of the *Xenopus* embryo. The stages of our first reported expression of the putative CCs, NF stage 19/20, is when the cephalic NC is first reported to begin migration from their location adjacent of the lateral ectoderm, on either side of the neural plate. Here, the NC is still mostly epithelial (Theveneau and Mayor, 2012). Once early migration of NC takes place, from NF stage 21, when NC undergoes EMT and becomes more mesenchymal, leading to a shift from medial to lateral migration as was well illustrated and described by Thevenau and Mayor (See Figure 66). Unfortunately, not much information is available on TNCC migration in *Xenopus*. No expression of established NC markers has previously been reported at the anteroventral side of the embryo this early in their development. Furthermore, the presence of these putative CCs arising at the anteroventral side of *Xenopus* embryos has been shown as early as NF stage 14 with markers *phox2a* and *ascl1* (Wylie et al., 2015*)*. This would indicate that the NC and its derivatives may have a further migratory reach then presently known and opens an intriguing aspect of NC research that should be addressed by future research.

To confirm that these cells are NC-derived, a NC ablation experiment could be performed. Hereby the blastomeres that will give rise to the NC would be removed using either a fine-tipped needle or glass pipette. This method could also be performed using a precise laser to ablate the NC without affecting the surrounding tissue. Embryos would then again be allowed to develop until NF stage 19/20 and WISH with our candidate CCs markers be performed to assess if the cells are still present, in absence of a NC population. Fate maps on *Xenbase* indicate the blastomeres with major contributions to the NC (Fig. 76).

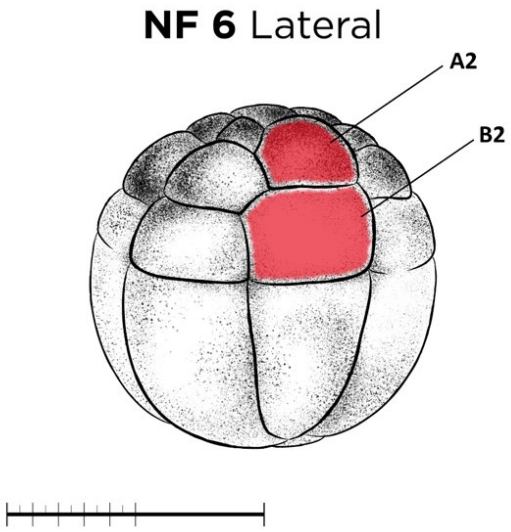

Figure 76: Blastomeres with major contribution to the NC (red).
Blastomeres A2 and B2 give rise to the neural crest and many other anatomical structures. Blastomere A2 gives major contributions to the reinta, spinal chrord, dorsal brain, cranial ganglia, the cement gland, olfactory placode, lens and the head epidermis. Blastomere B2 also contributes to the dorsal brain, spinal chord and central somites. Figure made in accordance to information on Xenbase and image adapted from (Zahn et al., 2022).

Another interesting question to assess in the future would be if the majority of CCs in *Xenopus* also originate from SCPs. This process was recently shown to be evolutionary conserved also in zebrafish (Kamenev et al., 2021), and could possibly explain how the putative CCs are moving within the embryo. Parlier and colleagues have shown previously that HNK-1 immunostaining also labelled the NA anteroventral cells at NF stage 27 (Parlier et al., 2008). Performing double-staining with candidate CCs markers, followed by HNK-1 immunostaining, would be informative to identify if these cells are associated with nerve axons. It would be further intriguing to identify if these cells would associate with peripheral nerve axon and use them as guidance to innervate the forming AC at a later developmental time-point, as SCPs do. An identified marker of SCPs is the proteolipid protein (*Plp*), a major myelin protein (Chan et al., 2018b). In the study of Furlan and Colleagues (Furlan et al., 2017), lineage tracing in mouse was performed using yellow fluorescent protein (YFP) as a reporter from the *Plp1* promoter at E 11.5 (Chan et al., 2018b). YFP activation showed YFP-positive CCs at E 17.5 (Chan et al., 2018b; Furlan et al., 2017). So far, the presence and role of SCPs in *Xenopus*

development has not yet been characterized. A possible starting point could be to characterize the expression pattern of SCPs marker gene *plp1* either by WISH or HCR. RNA-seq data on Xenbase shows a high TPM of *plp1* between NF stage 10-15, and again from NF stage 25 through to NF stage 40 (Session et al., 2016).

7.7 AC vs gonads

While the main focus of this project was to characterize CCs of the AM in *Xenopus*, I also identified key markers of AC development, in order to conduct a holistic characterization of AG development in this model organism. The putative AC genes were found to be expressed in close proximity to the developing kidney during embryogenesis. To finalise this project, and to distinguish if the AC develops separate or within the developing kidney, co-expression of kidney marker *pax8*, along with markers *nr5a1* and *star*, should be performed to see if their expression overlaps. Furthermore, sectioning of these embryos should finalise the location of the structure in relation to the pronephric kidney, as well as being able to tell if the expression is found in the AC, the gonads, or even in both structures that are so close in anatomical position that a separation would only be clear by sectioning of co-expression experiments and different embryonic developmental time-points.

7.8 Concluding Remark

The data presented and discussed in this thesis has been a first attempt at characterizing the development of the AG in *Xenopus* during embryogenesis. While being unable to show an AM-like structure in association with the pronephric kidney at this developmental time point, I have characterized the expression of multiple markers involved in CC development and differentiation, that likely show putative CCs during embryogenesis, as single cells, across the anterior body of the embryo. I have further shown that these cells are likely NC-derived. Additionally, I have identified expression of AC markers genes within the proximity of the developing pronephric kidney, likely showing the developmental time point and genes involved in AC formation. I therefore have identified that the AC and the AM develop separately during embryogenesis and marker genes for the AC and the AM do not overlap. This further indicates that the AG is not fully formed at embryogenesis and may not be fully formed prior to metamorphosis. Finally, I have demonstrated that these chromaffin-like cells are indeed derived from the NC, suggesting an exciting and previously undescribed capacity of the TNCCs to migrate earlier than previously described in the literature. This research contributes to the basic understanding of *Xenopus* organogenesis and furthers the evolutionary characterization of the development of NC-derived CCs.

8 References

Accordi, F., 1991. The chromaffin cells of urodele amphibians. Journal of anatomy 179, 1.

Akkuratova, N., Faure, L., Kameneva, P., Kastriti, M.E., Adameyko, I., 2022. Developmental heterogeneity of embryonic neuroendocrine chromaffin cells and their maturation dynamics. Frontiers in Endocrinology 13, 1020000.

An, M., Luo, R., Henion, P.D., 2002. Differentiation and maturation of zebrafish dorsal root and sympathetic ganglion neurons. Journal of Comparative Neurology 446, 267-275.

Bacila, I., Cunliffe, V.T., Krone, N.P., 2021. Interrenal development and function in zebrafish. Molecular and Cellular Endocrinology 535, 111372.

Barr, E.K., Applebaum, M.A., 2018. Genetic predisposition to neuroblastoma. Children 5, 119.

Barriga, E.H., Theveneau, E., 2020. In vivo neural crest cell migration is controlled by “mixotaxis”. Frontiers in Physiology 11, 586432.

Bashamboo, A., McElreavey, K., 2010. NR5A1/SF-1 and development and function of the ovary, Annales d'endocrinologie. Elsevier, pp. 177-182.

Bauer, M., Bridgham, J., Langenau, D., Johnson, A., Goetz, F., 2000. Conservation of steroidogenic acute regulatory (StAR) protein structure and expression in vertebrates. Molecular and cellular endocrinology 168, 119-125.

Bechmann, N., Berger, I., Bornstein, S.R., Steenblock, C., 2021. Adrenal medulla development and medullary-cortical interactions. Molecular and Cellular Endocrinology 528, 111258.

Bellono, N.W., Bayrer, J.R., Leitch, D.B., Castro, J., Zhang, C., O’Donnell, T.A., Brierley, S.M., Ingraham, H.A., Julius, D., 2017. Enterochromaffin cells are gut chemosensors that couple to sensory neural pathways. Cell 170, 185-198. e116.

Benarroch, E.E., 2018. Locus coeruleus. Cell and tissue research 373, 221-232.

Berends, A.M., Eisenhofer, G., Fishbein, L., van der Horst-Schrivers, A.N., Kema, I.P., Links, T.P., Lenders, J.W., Kerstens, M.N., 2019. Intricacies of the molecular machinery of catecholamine biosynthesis and secretion by chromaffin cells of the normal adrenal medulla and in pheochromocytoma and paraganglioma. Cancers 11, 1121.

Berger, I., Werdermann, M., Bornstein, S.R., Steenblock, C., 2019. The adrenal gland in stress–adaptation on a cellular level. The journal of steroid biochemistry and molecular biology 190, 198-206.

Blum, M., De Robertis, E.M., Wallingford, J.B., Niehrs, C., 2015. Morpholinos: antisense and sensibility. Developmental cell 35, 145-149.

Blum, M., Ott, T., 2019. Xenopus: an undervalued model organism to study and model human genetic disease. Cells Tissues Organs 205, 303-313.

Bolande, R.P., 1974. Neurocristopathies - Unifying Concept of Disease Arising in Neural Crest Maldevelopment. Human Pathology 5, 409-429.

Bronner, M.E., Simões-Costa, M., 2016. The neural crest migrating into the twenty-first century. Current topics in developmental biology 116, 115-134.

Buchholz, D.R., 2017. Xenopus metamorphosis as a model to study thyroid hormone receptor function during vertebrate developmental transitions. Molecular and Cellular Endocrinology 459, 64-70.

Buitrago-Delgado, E., Schock, E.N., Nordin, K., LaBonne, C., 2018. A transition from SoxB1 to SoxE transcription factors is essential for progression from pluripotent blastula cells to neural crest cells. Developmental biology 444, 50-61.

Burns, A., Champeval, D., Le Douarin, N., 2000. Sacral neural crest cells colonise aganglionic hindgut in vivo but fail to compensate for lack of enteric ganglia. Developmental biology 219, 30-43.

Capaldo, A., 2023. The Adrenal Gland of Squamata (Reptilia): A Comparative Overview. Animals 13, 2686.

Chan, W., Anderson, C., Gonsalvez, D.G., 2018a. From proliferation to target innervation: signaling molecules that direct sympathetic nervous system development. Cell and tissue research 372, 171-193.

Chan, W.H., Anderson, C.R., Gonsalvez, D.G., 2018b. From proliferation to target innervation: signaling molecules that direct sympathetic nervous system development. Cell and Tissue Research 372, 171-193.

Chen, C., Lan, M.S., 2022. Interplay: The Essential Role between INSM1 and N-Myc in Aggressive Neuroblastoma. Biology 11, 1376.

Chen, Y., Li, Q., Li, X., Liu, H., Li, P., Hai, R., Guo, Y., Wang, S., Wang, K., Du, C., 2022. Amylin regulates testosterone levels via steroidogenesis-related enzymes in the central nervous system of male mice. Neuropeptides 96, 102288.

Cheng, K., Seita, Y., Moriwaki, T., Noshiro, K., Sakata, Y., Hwang, Y.S., Torigoe, T., Saitou, M., Tsuchiya, H., Iwatani, C., 2022. The developmental origin and the specification of the adrenal cortex in humans and cynomolgus monkeys. Science Advances 8, eabn8485.

Choi, H.M., Calvert, C.R., Husain, N., Huss, D., Barsi, J.C., Deverman, B.E., Hunter, R.C., Kato, M., Lee, S.M., Abelin, A.C., 2016. Mapping a multiplexed zoo of mRNA expression. Development 143, 3632-3637.

Choi, H.M., Schwarzkopf, M., Fornace, M.E., Acharya, A., Artavanis, G., Stegmaier, J., Cunha, A., Pierce, N.A., 2018. Third-generation in situ hybridization chain reaction: multiplexed, quantitative, sensitive, versatile, robust. Development 145, dev165753.

Coppola, E., Pattyn, A., Guthrie, S.C., Goridis, C., Studer, M., 2005. Reciprocal gene replacements reveal unique functions for Phox2 genes during neural differentiation. The EMBO journal 24, 4392-4403.

Corallo, D., Donadon, M., Pantile, M., Sidarovich, V., Cocchi, S., Ori, M., De Sarlo, M., Candiani, S., Frasson, C., Distel, M., Quattrone, A., Zanon, C., Basso, G., Tonini, G.P., Aveic, S., 2020. LIN28B increases neural crest cell migration and leads to transformation of trunk sympathoadrenal precursors. Cell Death Differ 27, 1225-1242.

Corkins, M.E., Achieng, M., DeLay, B.D., Krneta-Stankic, V., Cain, M.P., Walker, B.L., Chen, J., Lindström, N.O., Miller, R.K., 2023. A comparative study of cellular diversity between the Xenopus pronephric and mouse metanephric nephron. Kidney international 103, 77-86.

Coupland, R., Hopwood, D., 1966. The mechanism of the differential staining reaction for adrenaline-and noreadrenaline-storing granules in tissues fixed in glutaraldehyde. Journal of Anatomy 100, 227.

Cryer, P.E., Polonsky, K., 2008. Glucose homeostasis and hypoglycemia. Williams textbook of endocrinology 88, 1589-1590.

D'amico, M.A., Ghinassi, B., Izzicupo, P., Manzoli, L., Di Baldassarre, A., 2014. Biological function and clinical relevance of chromogranin A and derived peptides. Endocrine connections 3, R45-R54.

Därr, R., Kater, J., Sekula, P., Bausch, B., Krauss, T., Bode, C., Walz, G., Neumann, H.P., Zschiedrich, S., 2020. Clinical decision making in small non-functioning VHL-related incidentalomas. Endocrine Connections 9, 834-844.

Denver, R.J., 2013. Neuroendocrinology of amphibian metamorphosis. Current topics in developmental biology 103, 195-227.

Desanlis, I., Felstead, H.L., Edwards, D.R., Wheeler, G.N., 2018. ADAMTS9, a member of the ADAMTS family, in Xenopus development. Gene Expression Patterns 29, 72-81.

Desgrange, A., Cereghini, S., 2015. Nephron Patterning: Lessons from Xenopus, Zebrafish, and Mouse Studies. Cells 4, 483-499.

Di Lorenzo, M., Barra, T., Rosati, L., Valiante, S., Capaldo, A., De Falco, M., Laforgia, V., 2020. Adrenal gland response to endocrine disrupting chemicals in fishes, amphibians and reptiles: A comparative overview. General and comparative endocrinology 297, 113550.

Diaz-Flores, L., Gutiérrez, R., Varela, H., Valladares, F., Alvarez-Argüelles, H., Borges, R., 2008. Histogenesis and morphofunctional characteristics of chromaffin cells. Acta physiologica 192, 145-163.

Dixon, J., Trainor, P., Dixon, M.J., 2007. Treacher Collins syndrome. Orthod Craniofac Res 10, 88-95.

Dongre, A., Weinberg, R.A., 2019. New insights into the mechanisms of epithelial–mesenchymal transition and implications for cancer. Nature reviews Molecular cell biology 20, 69-84.

Dreher, J.-C., 2015. Neuroimaging evidences of gonadal steroid hormone influences on reward processing and social decision-making in humans.

Duverger, O., Morasso, M.I., 2008. Role of homeobox genes in the patterning, specification, and differentiation of ectodermal appendages in mammals. Journal of cellular physiology 216, 337-346.

Edens, B.M., Stundl, J., Urrutia, H.A., Bronner, M.E., 2024. Neural crest origin of sympathetic neurons at the dawn of vertebrates. Nature 629, 121-126.

Ehrhart-Bornstein, M., Bornstein, S.R., 2008. Cross-talk between adrenal medulla and adrenal cortex in stress. Annals of the New York Academy of Sciences 1148, 112-117.

El Faitwri, T., Huber, K., 2018. Expression pattern of delta-like 1 homolog in developing sympathetic neurons and chromaffin cells. Gene expression patterns 30, 49-54.

Ernsberger, U., Reissmann, E., Mason, I., Rohrer, H., 2000. The expression of dopamine β-hydroxylase, tyrosine hydroxylase, and Phox2 transcription factors in sympathetic neurons: evidence for common regulation during noradrenergic induction and diverging regulation later in development. Mechanisms of development 92, 169-177.

Ernsberger, U., Rohrer, H., 2024. The sympathetic nervous system arose in the earliest vertebrates. Nature Publishing Group UK London.

Espinosa-Medina, I., Jevans, B., Boismoreau, F., Chettouh, Z., Enomoto, H., Müller, T., Birchmeier, C., Burns, A.J., Brunet, J.-F., 2017. Dual origin of enteric neurons in vagal Schwann cell precursors and the sympathetic neural crest. Proceedings of the National Academy of Sciences 114, 11980-11985.

Etard, C., Gradl, D., Kunz, M., Eilers, M., Wedlich, D., 2005. Pontin and Reptin regulate cell proliferation in early Xenopus embryos in collaboration with c-Myc and Miz-1. Mechanisms of development 122, 545-556.

Etard, C., Wedlich, D., Bauer, A., Huber, O., Kühl, M., 2000. Expression of Xenopus homologs of the β-catenin binding protein pontin52. Mechanisms of development 94, 219-222.

Filippi, A., Mahler, J., Schweitzer, J., Driever, W., 2010. Expression of the paralogous tyrosine hydroxylase encoding genes th1 and th2 reveals the full complement of dopaminergic and noradrenergic neurons in zebrafish larval and juvenile brain. Journal of Comparative Neurology 518, 423-438.

Flora, A., Lucchetti, H., Benfante, R., Goridis, C., Clementi, F., Fornasari, D., 2001. SP Proteins and PHOX2B Regulate the Expression of the HumanPHOX2a Gene. Journal of Neuroscience 21, 7037-7045.

Furlan, A., Adameyko, I., 2018. Schwann cell precursor: a neural crest cell in disguise? Developmental biology 444, S25-S35.

Furlan, A., Dyachuk, V., Kastriti, M.E., Calvo-Enrique, L., Abdo, H., Hadjab, S., Chontorotzea, T., Akkuratova, N., Usoskin, D., Kamenev, D., 2017. Multipotent peripheral glial cells generate neuroendocrine cells of the adrenal medulla. Science 357, eaal3753.

González, A., Smeets, W.J., 1993. Noradrenaline in the brain of the south african clawed frog Xenopus laevis: A study with antibodies against noradrenaline and dopamine-β-hydroxylase. Journal of Comparative Neurology 331, 363-374.

Green, S.A., Uy, B.R., Bronner, M.E., 2017. Ancient evolutionary origin of vertebrate enteric neurons from trunk-derived neural crest. Nature 544, 88-91.

Griffin, J.N., Liu, K.J., Sempou, E., 2020. Xenopus models of organogenesis and disease. Frontiers in Physiology 11, 542655.

Gut, P., Czarnywojtek, A., Fischbach, J., Bączyk, M., Ziemnicka, K., Wrotkowska, E., Gryczyńska, M., Ruchała, M., 2016. Chromogranin A–unspecific neuroendocrine marker. Clinical utility and potential diagnostic pitfalls. Archives of Medical Science 12, 1-9.

Gut, P., Huber, K., Lohr, J., Brühl, B., Oberle, S., Treier, M., Ernsberger, U., Kalcheim, C., Unsicker, K., 2005. Lack of an adrenal cortex in Sf1 mutant mice is compatible with the generation and differentiation of chromaffin cells.

Guttman, D.E., 1966. Analysis of steroids in mixtures using the kinetics of blue tetrazolium reduction. Journal of Pharmaceutical Sciences 55, 919-922.

Hale, C.L., Niederriter, A.N., Green, G.E., Martin, D.M., 2016. Atypical phenotypes associated with pathogenic CHD7 variants and a proposal for broadening CHARGE syndrome clinical diagnostic criteria. Am J Med Genet A 170a, 344-354.

Hall, B.K., 2000. The neural crest as a fourth germ layer and vertebrates as quadroblastic not triploblastic. Evolution and Development 2, 3-5.

Hanke, W., 1978. The adrenal cortex of Amphibia, General, comparative and clinical endocrinology of the adrenal cortex. Elsevier, pp. 419-495.

Hausen, P., Riebesell, M., 1991. The early development of Xenopus laevis: an atlas of the histology. (No Title).

Heanue, T.A., Pachnis, V., 2007. Enteric nervous system development and Hirschsprung's disease: advances in genetic and stem cell studies. Nature Reviews Neuroscience 8, 466-479.

Hirsch, M.-R., Tiveron, M.-C., Guillemot, F., Brunet, J.-F., Goridis, C., 1998. Control of noradrenergic differentiation and Phox2a expression by MASH1 in the central and peripheral nervous system. Development 125, 599-608.

His, W., 1868. Untersuchungen über die erste Anlage des Wirbelthierleibes: die erste Entwickelung des Hühnchens im Ei. FCW Vogel.

Hockman, D., Adameyko, I., Kaucka, M., Barraud, P., Otani, T., Hunt, A., Hartwig, A.C., Sock, E., Waithe, D., Franck, M.C., 2018. Striking parallels between carotid body glomus cell and adrenal chromaffin cell development. Developmental biology 444, S308-S324.

Hockman, D., Burns, A.J., Schlosser, G., Gates, K.P., Jevans, B., Mongera, A., Fisher, S., Unlu, G., Knapik, E.W., Kaufman, C.K., Mosimann, C., Zon, L.I., Lancman, J.J., Dong, P.D.S., Lickert, H., Tucker, A.S., Baker, C.V.H., 2017. Evolution of the hypoxia-sensitive cells involved in amniote respiratory reflexes. eLife 6, e21231.

Hoek, K.S., Schlegel, N.C., Brafford, P., Sucker, A., Ugurel, S., Kumar, R., Weber, B.L., Nathanson, K.L., Phillips, D.J., Herlyn, M., Schadendorf, D., Dummer, R., 2006. Metastatic potential of melanomas defined by specific gene expression profiles with no BRAF signature. Pigment Cell Res 19, 290-302.

Hoivik, E.A., Lewis, A.E., Aumo, L., Bakke, M., 2010. Molecular aspects of steroidogenic factor 1 (SF-1). Molecular and cellular endocrinology 315, 27-39.

Honoré, S.M., Aybar, M.J., Mayor, R., 2003. Sox10 is required for the early development of the prospective neural crest in Xenopus embryos. Developmental biology 260, 79-96.

Hoppler, S., Wheeler, G.N., 2015. It's about time for neural crest. Science 348, 1316-1317.

Hopwood, D., 1969. Amino acids of the adrenal medulla and the effect of potassium dichromate oxidation on them. Journal of Anatomy 104, 71.

Horb, L.D., Horb, M.E., 2010. BrunoL1 regulates endoderm proliferation through translational enhancement of cyclin A2 mRNA. Developmental biology 345, 156-169.

Horb, L.D., Jarkji, Z.H., Horb, M.E., 2009. Xenopus Insm1 is essential for gastrointestinal and pancreatic endocrine cell development. Developmental dynamics: an official publication of the American Association of Anatomists 238, 2505-2510.

Houston, D.W., King, M.L., 2000. A critical role for Xdazl, a germ plasm-localized RNA, in the differentiation of primordial germ cells in Xenopus. Development 127, 447-456.

Hsu, H.-J., Lin, G., Chung, B.-c., 2003. Parallel early development of zebrafish interrenal glands and pronephros: differential control by wt1 and ff1b.

Huber, K., 2006. The sympathoadrenal cell lineage: specification, diversification, and new perspectives. Developmental biology 298, 335-343.

Huber, K., 2015. Segregation of neuronal and neuroendocrine differentiation in the sympathoadrenal lineage. Cell and tissue research 359, 333-341.

Huber, K., Brühl, B., Guillemot, F., Olson, E.N., Ernsberger, U., Unsicker, K., 2002. Development of chromaffin cells depends on MASH1 function.

Huber, K., Janoueix-Lerosey, I., Kummer, W., Rohrer, H., Tischler, A.S., 2018. The sympathetic nervous system: malignancy, disease, and novel functions. Springer, pp. 163-170.

Huber, K., Kalcheim, C., Unsicker, K., 2009. The development of the chromaffin cell lineage from the neural crest. Autonomic Neuroscience 151, 10-16.

Huber, K., Karch, N., Ernsberger, U., Goridis, C., Unsicker, K., 2005. The role of Phox2B in chromaffin cell development. Developmental biology 279, 501-508.

Jacob, J., Storm, R., Castro, D.S., Milton, C., Pla, P., Guillemot, F., Birchmeier, C., Briscoe, J., 2009. Insm1 (IA-1) is an essential component of the regulatory network that specifies monoaminergic neuronal phenotypes in the vertebrate hindbrain. Development 136, 2477-2485.

Jones, E.A., 2005. Xenopus: a prince among models for pronephric kidney development. J Am Soc Nephrol 16, 313-321.

Kamenev, D., Sunadome, K., Shirokov, M., Chagin, A.S., Singh, A., Irion, U., Adameyko, I., Fried, K., Dyachuk, V., 2021. Schwann cell precursors generate sympathoadrenal system during zebrafish development. Journal of Neuroscience Research 99, 2540-2557.

Kameneva, P., Melnikova, V.I., Kastriti, M.E., Kurtova, A., Kryukov, E., Murtazina, A., Faure, L., Poverennaya, I., Artemov, A.V., Kalinina, T.S., 2022. Serotonin limits generation of chromaffin cells during adrenal organ development. Nature communications 13, 1-21.

Kandel, E.R., Schwartz, J.H., Jessell, T.M., Siegelbaum, S., Hudspeth, A.J., Mack, S., 2000. Principles of neural science. McGraw-hill New York.

Kastriti, M.E., Adameyko, I., 2017. Specification, plasticity and evolutionary origin of peripheral glial cells. Current opinion in neurobiology 47, 196-202.

Kastriti, M.E., Faure, L., Von Ahsen, D., Bouderlique, T.G., Boström, J., Solovieva, T., Jackson, C., Bronner, M., Meijer, D., Hadjab, S., 2022. Schwann cell precursors represent a neural crest-like state with biased multipotency. The EMBO journal 41, e108780.

Kastriti, M.E., Kameneva, P., Adameyko, I., 2020. Stem cells, evolutionary aspects and pathology of the adrenal medulla: A new developmental paradigm. Molecular and Cellular Endocrinology 518, 110998.

Kastriti, M.E., Kameneva, P., Kamenev, D., Dyachuk, V., Furlan, A., Hampl, M., Memic, F., Marklund, U., Lallemend, F., Hadjab, S., 2019. Schwann cell precursors generate the majority

of chromaffin cells in Zuckerkandl organ and some sympathetic neurons in paraganglia. Frontiers in Molecular Neuroscience 12, 6.

Kataoka, Y., Majane, E., Yang, H., 1985. Release of NPY-like immunoreactive material from primary cultures of chromaffin cells prepared from bovine adrenal medulla. Neuropharmacology 24, 693-695.

Kempná, P., Flück, C.E., 2008. Adrenal gland development and defects. Best practice & research Clinical endocrinology & metabolism 22, 77-93.

King, S.R., Manna, P.R., Ishii, T., Syapin, P.J., Ginsberg, S.D., Wilson, K., Walsh, L.P., Parker, K.L., Stocco, D.M., Smith, R.G., 2002. An essential component in steroid synthesis, the steroidogenic acute regulatory protein, is expressed in discrete regions of the brain. Journal of Neuroscience 22, 10613-10620.

Kitahama, K., Pearson, J., Denoroy, L., Kopp, N., Ulrich, J., Maeda, T., Jouvet, M., 1985. Adrenergic neurons in human brain demonstrated by immunohistochemistry with antibodies to phenylethanolamine-N-methyltransferase (PNMT): discovery of a new group in the nucleus tractus solitarius. Neuroscience letters 53, 303-308.

Kloas, W., Reinecke, M., Hanke, W., 1997. Stage-Dependent Changes in Adrenal Steroids and Catecholamines during Development inXenopus laevis. General and comparative endocrinology 108, 416-426.

Kloc, M., Bilinski, S., Chan, A.P., Allen, L.H., Zearfoss, N.R., Etkin, L.D., 2001. RNA localization and germ cell determination in Xenopus. Int Rev Cytol 203, 63-91.

Kuil, L.E., Chauhan, R.K., Cheng, W.W., Hofstra, R.M., Alves, M.M., 2021. Zebrafish: a model organism for studying enteric nervous system development and disease. Frontiers in cell and developmental biology 8, 629073.

Lalli, E., Figueiredo, B.C., 2015. Pediatric adrenocortical tumors: what they can tell us on adrenal development and comparison with adult adrenal tumors. Frontiers in Endocrinology 6, 23.

Lamouille, S., Xu, J., Derynck, R., 2014. Molecular mechanisms of epithelial–mesenchymal transition. Nature reviews Molecular cell biology 15, 178-196.

Lan, M.S., Breslin, M.B., 2009. Structure, expression, and biological function of INSM1 transcription factor in neuroendocrine differentiation. The FASEB Journal 23, 2024.

Le Dourarin, N.M., Smith, J., Teillet, M.-A., Le Lievre, C.S., Ziller, C., 1980. The neural crest and its developmental analysis in avian embryo chimaerast. Trends in Neurosciences 3, 39-42.

Leathers, T.A., Rogers, C.D., 2022. Time to go: neural crest cell epithelial-to-mesenchymal transition. Development 149, dev200712.

Leist, K.-H., Bergerhoff, K., Pehlemann, F.-W., Hanke, W., 1968. Histophysiological investigations of the development of the interrenal organ in the clawed toad (Xenopus laevis Daudin). Zeitschrift für Zellforschung und Mikroskopische Anatomie 93, 105-125.

Liao, Y., Ma, L., Guo, Q., E, W., Fang, X., Yang, L., Ruan, F., Wang, J., Zhang, P., Sun, Z., 2022. Cell landscape of larval and adult Xenopus laevis at single-cell resolution. nature communications 13, 4306.

Litwack, G., 2024. Adrenal Gland. Elsevier.

Liu, Y.-W., Gao, W., Teh, H.-L., Tan, J.-H., Chan, W.-K., 2003. Prox1 is a novel coregulator of Ff1b and is involved in the embryonic development of the zebra fish interrenal primordium. Molecular and Cellular Biology 23, 7243-7255.

Lockett, J., Inder, W.J., Clifton, V.L., 2024. The Glucocorticoid Receptor: Isoforms, Functions, and Contribution to Glucocorticoid Sensitivity. Endocrine Reviews.

Lohr, J., Gut, P., Karch, N., Unsicker, K., Huber, K., 2006. Development of adrenal chromaffin cells in Sf1 heterozygous mice. Cell and tissue research 325, 437-444.

Lumb, R., Tata, M., Xu, X., Joyce, A., Marchant, C., Harvey, N., Ruhrberg, C., Schwarz, Q., 2018. Neuropilins guide preganglionic sympathetic axons and chromaffin cell precursors to establish the adrenal medulla. Development 145, dev162552.

Machado, R.J., Moore, W., Hames, R., Houliston, E., Chang, P., King, M.L., Woodland, H.R., 2005. Xenopus Xpat protein is a major component of germ plasm and may function in its organisation and positioning. Developmental Biology 287, 289-300.

Maguire, L.H., Thomas, A.R., Goldstein, A.M., 2015. Tumors of the neural crest: Common themes in development and cancer. Developmental Dynamics 244, 311-322.

Mahalakshmi, B., Baskaran, R., Shanmugavadivu, M., Nguyen, N.T., Velmurugan, B.K., 2020. Insulinoma-associated protein 1 (INSM1): a potential biomarker and therapeutic target for neuroendocrine tumors. Cellular Oncology 43, 367-376.

Maleki, Z., Nadella, A., Nadella, M., Patel, G., Patel, S., Kholová, I., 2021. INSM1, a novel biomarker for detection of neuroendocrine neoplasms: cytopathologists' view. Diagnostics 11, 2172.

Manethova, M., Gerykova, L., Faistova, H., Drugda, J., Hacova, M., Hornychova, H., Ryska, A., Gabalec, F., Soukup, J., 2023. Phox2B is a sensitive and reliable marker of paraganglioma—Phox2B immunohistochemistry in diagnosis of neuroendocrine neoplasms. Virchows Archiv 482, 679-686.

Martik, M.L., Bronner, M.E., 2017. Regulatory Logic Underlying Diversification of the Neural Crest. Trends Genet 33, 715-727.

Martik, M.L., Bronner, M.E., 2021. Riding the crest to get a head: neural crest evolution in vertebrates. Nature Reviews Neuroscience 22, 616-626.

Mayor, R., Theveneau, E., 2013. The neural crest. Development 140, 2247-2251.

McKinney, A., Hu, M., Hoskins, A., Mohammadyar, A., Naeem, N., Jing, J., Patel, S.S., Sheth, B.R., Jiang, X., 2023. Cellular composition and circuit organization of the locus coeruleus of adult mice. Elife 12, e80100.

Medina-Cuadra, L., Monsoro-Burq, A.H., 2021. Xenopus, an emerging model for studying pathologies of the neural crest. Current Topics in Developmental Biology 145, 313-348.

Meinsohn, M.-C., Smith, O.E., Bertolin, K., Murphy, B.D., 2019. The orphan nuclear receptors steroidogenic factor-1 and liver receptor homolog-1: structure, regulation, and essential roles in mammalian reproduction. Physiological reviews 99, 1249-1279.

Milano, E.G., Accordi, F., 1983. Comparative morphology of the adrenal gland of anuran Amphibia. Journal of Anatomy 136, 165.

Miller, W.L., Auchus, R.J., 2011. The molecular biology, biochemistry, and physiology of human steroidogenesis and its disorders. Endocrine reviews 32, 81-151.

Monsoro-Burq, A.H., 2007. A rapid protocol for whole-mount in situ hybridization on Xenopus embryos. Cold Spring Harbor Protocols 2007, pdb. prot4809.

Moreno, M.M., Barrell, W.B., Godwin, A., Guille, M., Liu, K.J., 2021. Anaplastic lymphoma kinase (alk), a neuroblastoma associated gene, is expressed in neural crest domains during embryonic development of Xenopus. Gene Expr Patterns 40, 119183.

Morikawa, Y., D'Autréaux, F., Gershon, M.D., Cserjesi, P., 2007. Hand2 determines the noradrenergic phenotype in the mouse sympathetic nervous system. Developmental biology 307, 114-126.

Morin, X., Cremer, H., Hirsch, M.-R., Kapur, R.P., Goridis, C., Brunet, J.-F., 1997. Defects in sensory and autonomic ganglia and absence of locus coeruleus in mice deficient for the homeobox gene Phox2a. Neuron 18, 411-423.

Morrison, M., Zimmerman, M., Look, A., Stewart, R., 2016. Studying the peripheral sympathetic nervous system and neuroblastoma in zebrafish, Methods in cell biology. Elsevier, pp. 97-138.

Mosse, Y.P., Laudenslager, M., Khazi, D., Carlisle, A.J., Winter, C.L., Rappaport, E., Maris, J.M., 2004. Germline PHOX2B mutation in hereditary neuroblastoma. The American Journal of Human Genetics 75, 727-730.

Müller, J., Krijgsman, O., Tsoi, J., Robert, L., Hugo, W., Song, C., Kong, X., Possik, P.A., Cornelissen-Steijger, P.D., Geukes Foppen, M.H., Kemper, K., Goding, C.R., McDermott, U.,

Blank, C., Haanen, J., Graeber, T.G., Ribas, A., Lo, R.S., Peeper, D.S., 2014. Low MITF/AXL ratio predicts early resistance to multiple targeted drugs in melanoma. Nat Commun 5, 5712.

Murtazina, A., Adameyko, I., 2023. The peripheral nervous system. Development 150.

Nagy, N., Goldstein, A.M., 2017. Enteric nervous system development: A crest cell's journey from neural tube to colon, Seminars in cell & developmental biology. Elsevier, pp. 94-106.

Nenni, M.J., Fisher, M.E., James-Zorn, C., Pells, T.J., Ponferrada, V., Chu, S., Fortriede, J.D., Burns, K.A., Wang, Y., Lotay, V.S., 2019. Xenbase: facilitating the use of Xenopus to model human disease. Frontiers in physiology 10, 154.

Nieto, M.A., Huang, R.Y., Jackson, R.A., Thiery, J.P., 2016. EMT: 2016. Cell 166, 21-45.

Nieuwkoop, P.D., Faber, J., 1994. Normal table of Xenopus laevis (Daudin): a systematical and chronological survey of the development from the fertilized egg till the end of metamorphosis.

Paiement, J.M., McMillan, D.B., 1975. The extracardiac chromaffin cells of larval lampreys. General and Comparative Endocrinology 27, 495-508.

Pakhomova, N.Y., Strokova, E.L., Korytkin, A.A., Kozhevnikov, V.V., Gusev, A.F., Zaidman, A.M., 2023. The History of the Study of the Neural Crest (Overview). Cell and Tissue Biology 17, 477-491.

Parkinson, L.M., Gillen, S.L., Woods, L.M., Chaytor, L., Marcos, D., Ali, F.R., Carroll, J.S., Philpott, A., 2022. The proneural transcription factor ASCL1 regulates cell proliferation and primes for differentiation in neuroblastoma. Frontiers in Cell and Developmental Biology 10, 942579.

Parlier, D., Ariza, A., Christulia, F., Genco, F., Vanhomwegen, J., Kricha, S., Souopgui, J., Bellefroid, E.J., 2008. Xenopus zinc finger transcription factor IA1 (Insm1) expression marks anteroventral noradrenergic neuron progenitors in Xenopus embryos. Dev Dyn 237, 2147-2157.

Patel, S., Rauf, A., Khan, H., Abu-Izneid, T., 2017. Renin-angiotensin-aldosterone (RAAS): The ubiquitous system for homeostasis and pathologies. Biomedicine & Pharmacotherapy 94, 317-325.

Pattyn, A., Goridis, C., Brunet, J.-F., 2000. Specification of the central noradrenergic phenotype by the homeobox gene Phox2b. Molecular and Cellular Neuroscience 15, 235-243.

Pattyn, A., Morin, X., Cremer, H., Goridis, C., Brunet, J.-F., 1999. The homeobox gene Phox2b is essential for the development of autonomic neural crest derivatives. Nature 399, 366-370.

Perry, S.F., Capaldo, A., 2011. The autonomic nervous system and chromaffin tissue: neuroendocrine regulation of catecholamine secretion in non-mammalian vertebrates. Autonomic neuroscience 165, 54-66.

Pignatti, E., Flück, C.E., 2021. Adrenal cortex development and related disorders leading to adrenal insufficiency. Molecular and cellular endocrinology 527, 111206.

Pihlajoki, M., Dörner, J., Cochran, R.S., Heikinheimo, M., Wilson, D.B., 2015. Adrenocortical zonation, renewal, and remodeling. Frontiers in endocrinology 6, 27.

Pingault, V., Ente, D., Dastot-Le Moal, F., Goossens, M., Marlin, S., Bondurand, N., 2010. Review and update of mutations causing Waardenburg syndrome. Hum Mutat 31, 391-406.

Piprek, R.P., Kloc, M., Kubiak, J.Z., 2016. Early development of the gonads: origin and differentiation of the somatic cells of the genital ridges. Molecular mechanisms of cell differentiation in gonad development, 1-22.

Piprek, R.P., Kloc, M., Tassan, J.-P., Kubiak, J.Z., 2017. Development of Xenopus laevis bipotential gonads into testis or ovary is driven by sex-specific cell-cell interactions, proliferation rate, cell migration and deposition of extracellular matrix. Developmental biology 432, 298-310.

Piprek, R.P., Pecio, A., Kloc, M., Kubiak, J.Z., Szymura, J.M., 2014. Evolutionary trend for metamery reduction and gonad shortening in Anurans revealed by comparison of gonad development. Int J Dev Biol 58, 929-934.

Purves, D., 2019. Brains as engines of association: an operating principle for nervous systems. Oxford University Press.

Qiu, S., Du, Y., Wang, L., Hu, C., 2013. Chromaffin cells of the adrenal gland in the beagle dog. Anat Histol Embryol 42, 144-150.

Raciti, D., Reggiani, L., Geffers, L., Jiang, Q., Bacchion, F., Subrizi, A.E., Clements, D., Tindal, C., Davidson, D.R., Kaissling, B., 2008. Organization of the pronephric kidney revealed by large-scale gene expression mapping. Genome biology 9, 1-21.

Rao, M., Gershon, M.D., 2018. Enteric nervous system development: what could possibly go wrong? Nature Reviews Neuroscience 19, 552-565.

Rocha, M., Singh, N., Ahsan, K., Beiriger, A., Prince, V.E., 2020. Neural crest development: insights from the zebrafish. Dev Dyn 249, 88-111.

Roco, Á.S., Ruiz-García, A., Bullejos, M., 2021. Testis development and differentiation in amphibians. Genes 12, 578.

Rohrer, T., Trachsel, D., Engelcke, G., Hammer, J., 2002. Congenital central hypoventilation syndrome associated with Hirschsprung's disease and neuroblastoma: case of multiple neurocristopathies. Pediatric pulmonology 33, 71-76.

Rotgers, E., Nicol, B., Rodriguez, K., Rattan, S., Flaws, J.A., Yao, H.H., 2021. Constitutive expression of Steroidogenic factor-1 (NR5A1) disrupts ovarian functions, fertility, and metabolic homeostasis in female mice. Faseb j 35, e21770.

Rothstein, M., Bhattacharya, D., Simoes-Costa, M., 2018. The molecular basis of neural crest axial identity. Developmental biology 444, S170-S180.

Saito, D., Takase, Y., Murai, H., Takahashi, Y., 2012. The dorsal aorta initiates a molecular cascade that instructs sympatho-adrenal specification. Science 336, 1578-1581.

Sasai, N., Mizuseki, K., Sasai, Y., 2001. Requirement of FoxD3-class signaling for neural crest determination in Xenopus.

Sato, T., Sasai, N., Sasai, Y., 2005. Neural crest determination by co-activation of Pax3 and Zic1 genes in Xenopus ectoderm.

Sato, T.S., Handa, A., Priya, S., Watal, P., Becker, R.M., Sato, Y., 2019. Neurocristopathies: Enigmatic Appearances of Neural Crest Cell-derived Abnormalities. Radiographics 39, 2085-2102.

Sauka-Spengler, T., Bronner-Fraser, M., 2008. A gene regulatory network orchestrates neural crest formation. Nature Reviews Molecular Cell Biology 9, 557-568.

Schäfer, M.K.-H., Nohr, D., Romeo, H., Eiden, L.E., Weihe, E., 1994. Pan-neuronal expression of chromogranin A in rat nervous system. Peptides 15, 263-279.

Schmitt, S.M., Gull, M., Brändli, A.W., 2014. Engineering Xenopus embryos for phenotypic drug discovery screening. Advanced drug delivery reviews 69, 225-246.

Session, A.M., Uno, Y., Kwon, T., Chapman, J.A., Toyoda, A., Takahashi, S., Fukui, A., Hikosaka, A., Suzuki, A., Kondo, M., 2016. Genome evolution in the allotetraploid frog Xenopus laevis. Nature 538, 336-343.

Shtukmaster, S., Huber, K., 2023. The role of the Notch signalling pathway in regulating the balance between neuronal and nonneuronal cells in sympathetic ganglia and the adrenal gland. PloS one 18, e0281486.

Shtukmaster, S., Schier, M.C., Huber, K., Krispin, S., Kalcheim, C., Unsicker, K., 2013. Sympathetic neurons and chromaffin cells share a common progenitor in the neural crest in vivo. Neural Development 8, 12.

Simoes-Costa, M., Bronner, M.E., 2015. Establishing neural crest identity: a gene regulatory recipe. Development 142, 242-257.

Szabadi, E., 2013. Functional neuroanatomy of the central noradrenergic system. Journal of psychopharmacology (Oxford, England) 27.

Szabó, A., Mayor, R., 2018. Mechanisms of neural crest migration. Annual Review of Genetics 52, 43-63.

Talikka, M., Stefani, G., Brivanlou, A.H., Zimmerman, K., 2004. Characterization of Xenopus Phox2a and Phox2b defines expression domains within the embryonic nervous system and early heart field. Gene expression patterns 4, 601-607.

Tandon, P., Conlon, F., Furlow, J.D., Horb, M.E., 2017. Expanding the genetic toolkit in Xenopus: Approaches and opportunities for human disease modeling. Developmental biology 426, 325-335.

Theveneau, E., Mayor, R., 2012. Neural crest delamination and migration: from epithelium-to-mesenchyme transition to collective cell migration. Dev Biol 366, 34-54.

To, T.T., Hahner, S., Nica, G., Rohr, K.B., Hammerschmidt, M., Winkler, C., Allolio, B., 2007. Pituitary-interrenal interaction in zebrafish interrenal organ development. Molecular endocrinology 21, 472-485.

Tokarz, J., Möller, G., de Angelis, M.H., Adamski, J., 2013. Zebrafish and steroids: what do we know and what do we need to know? The Journal of steroid biochemistry and molecular biology 137, 165-173.

Trochet, D., Bourdeaut, F., Janoueix-Lerosey, I., Deville, A., De Pontual, L., Schleiermacher, G., Coze, C., Philip, N., Frébourg, T., Munnich, A., 2004. Germline mutations of the paired–like homeobox 2B (PHOX2B) gene in neuroblastoma. The American Journal of Human Genetics 74, 761-764.

Tsubota, S., Kadomatsu, K., 2017. Origin and mechanism of neuroblastoma. Oncoscience 4, 70.

Tsubota, S., Kadomatsu, K., 2018. Origin and initiation mechanisms of neuroblastoma. Cell and tissue research 372, 211-221.

Tsuneoka, Y., Funato, H., 2020. Modified in situ hybridization chain reaction using short hairpin DNAs. Frontiers in Molecular Neuroscience 13, 75.

Turchini, J., Cheung, V.K., Tischler, A.S., De Krijger, R.R., Gill, A.J., 2018. Pathology and genetics of phaeochromocytoma and paraganglioma. Histopathology 72, 97-105.

Twigg, S.R., Wilkie, A.O., 2015. A Genetic-Pathophysiological Framework for Craniosynostosis. Am J Hum Genet 97, 359-377.

Unsicker, K., Huber, K., Schober, A., Kalcheim, C., 2013. Resolved and open issues in chromaffin cell development. Mechanisms of development 130, 324-329.

Vega-Lopez, G.A., Cerrizuela, S., Aybar, M.J., 2017. Trunk neural crest cells: formation, migration and beyond. Int J Dev Biol 61, 5-15.

Vega-Lopez, G.A., Cerrizuela, S., Tribulo, C., Aybar, M.J., 2018. Neurocristopathies: New insights 150 years after the neural crest discovery. Dev Biol 444 Suppl 1, S110-S143.

Verhofstad, A.A., Coupland, R.E., Parker, T.R., Goldstein, M., 1985. Immunohistochemical and biochemical study on the development of the noradrenaline- and adrenaline-storing cells of the adrenal medulla of the rat. Cell Tissue Res 242, 233-243.

Vermeiren, S., Bellefroid, E.J., Desiderio, S., 2020. Vertebrate sensory ganglia: common and divergent features of the transcriptional programs generating their functional specialization. Frontiers in Cell and Developmental Biology 8, 587699.

Veschi, V., Verona, F., Thiele, C.J., 2019. Cancer stem cells and neuroblastoma: characteristics and therapeutic targeting options. Frontiers in endocrinology 10, 489775.

Vo, K.T., Matthay, K.K., Neuhaus, J., London, W.B., Hero, B., Ambros, P.F., Nakagawara, A., Miniati, D., Wheeler, K., Pearson, A.D., Cohn, S.L., DuBois, S.G., 2014. Clinical, biologic, and prognostic differences on the basis of primary tumor site in neuroblastoma: a report from the international neuroblastoma risk group project. J Clin Oncol 32, 3169-3176.

Wang, C.-Y., Chen, W.-Y., Lai, P.-Y., Chung, B.-c., 2013. Distinct functions of steroidogenic factor-1 (NR5A1) in the nucleus and the centrosome. Molecular and cellular endocrinology 371, 148-153.

Wang, H., Li, B., Zuo, L., Wang, B., Yan, Y., Tian, K., Zhou, R., Wang, C., Chen, X., Jiang, Y., 2022a. The transcriptional coactivator RUVBL2 regulates Pol II clustering with diverse transcription factors. Nature communications 13, 5703.

Wang, S., Wang, Z., Mu, Y., 2022b. Locus coeruleus in non-mammalian vertebrates. Brain Sciences 12, 134.

Watts, D., Bechmann, N., Meneses, A., Poutakidou, I.K., Kaden, D., Conrad, C., Krüger, A., Stein, J., El-Armouche, A., Chavakis, T., 2021. HIF2α regulates the synthesis and release of epinephrine in the adrenal medulla. Journal of Molecular Medicine 99, 1655-1666.

Weger, M., Diotel, N., Weger, B.D., Beil, T., Zaucker, A., Eachus, H.L., Oakes, J.A., do Rego, J.L., Storbeck, K.H., Gut, P., 2018. Expression and activity profiling of the steroidogenic enzymes of glucocorticoid biosynthesis and the fdx1 co-factors in zebrafish. Journal of Neuroendocrinology 30, e12586.

Wehrenberg, U., Prange-Kiel, J., Rune, G., 2001. Steroidogenic factor-1 expression in marmoset and rat hippocampus: co-localization with StAR and aromatase. Journal of neurochemistry 76, 1879-1886.

Wheeler, G.N., Brändli, A.W., 2009. Simple vertebrate models for chemical genetics and drug discovery screens: lessons from zebrafish and Xenopus. Developmental Dynamics 238, 1287-1308.

Whirledge, S., Cidlowski, J.A., 2010. Glucocorticoids, stress, and fertility. Minerva Endocrinol 35, 109-125.

White, R.M., Cech, J., Ratanasirintrawoot, S., Lin, C.Y., Rahl, P.B., Burke, C.J., Langdon, E., Tomlinson, M.L., Mosher, J., Kaufman, C., 2011. DHODH modulates transcriptional elongation in the neural crest and melanoma. Nature 471, 518-522.

Wildner, H., Gierl, M.S., Strehle, M., Pla, P., Birchmeier, C., 2008. Insm1 (IA-1) is a crucial component of the transcriptional network that controls differentiation of the sympatho-adrenal lineage.

Wilkie, A.O., Johnson, D., Wall, S.A., 2017. Clinical genetics of craniosynostosis. Current opinion in pediatrics 29, 622-628.

William Tank, A., Lee Wong, D., 2011. Peripheral and central effects of circulating catecholamines. Comprehensive Physiology 5, 1-15.

Winkler, H., Fischer-Colbrie, R., 1992. The chromogranins A and B: the first 25 years and future perspectives. Neuroscience 49, 497-528.

Wong, D.L., 2003. Why is the adrenal adrenergic? Endocrine pathology 14, 25-36.

Wulf, A.M., Moreno, M.M., Paka, C., Rampasekova, A., Liu, K.J., 2021. Defining pathological activities of ALK in neuroblastoma, a neural crest-derived cancer. International Journal of Molecular Sciences 22, 11718.

Wurtman, R.J., Axelrod, J., Vesell, E.S., Ross, G.T., 1968. Species differences in inducibility of phenylethanolamine-N-methyl transferase. Endocrinology 82, 584-590.

Wylie, C., Heasman, J., 1976. The formation of the gonadal ridge in Xenopus laevis: I. A light and transmission electron microscope study. Development 35, 125-138.

Wylie, L.A., Hardwick, L.J., Papkovskaia, T.D., Thiele, C.J., Philpott, A., 2015. Ascl1 phospho-status regulates neuronal differentiation in a Xenopus developmental model of neuroblastoma. Disease models & mechanisms 8, 429-441.

Xie, J., Wang, W.-Q., Liu, T.-X., Deng, M., Ning, G., 2008. Spatio-temporal expression of chromogranin A during zebrafish embryogenesis. Journal of endocrinology 198, 451-458.

Xing, Y., Lerario, A.M., Rainey, W., Hammer, G.D., 2015. Development of adrenal cortex zonation. Endocrinology and Metabolism Clinics 44, 243-274.

Yates, R., Katugampola, H., Cavlan, D., Cogger, K., Meimaridou, E., Hughes, C., Metherell, L., Guasti, L., King, P., 2013. Adrenocortical development, maintenance, and disease. Current topics in developmental biology 106, 239-312.

Yi-Wen, L., 2007. Interrenal organogenesis in the zebrafish model. Organogenesis 3, 44-48.

Yokogawa, T., Marin, W., Faraco, J., Pézeron, G., Appelbaum, L., Zhang, J., Rosa, F., Mourrain, P., Mignot, E., 2007. Characterization of sleep in zebrafish and insomnia in hypocretin receptor mutants. PLoS biology 5, e277.

York, J.R., LaBonne, C., 2022. The Development and Evolution of the Vertebrate Neural Crest: Insights from Xenopus. Xenopus, 125-141.

Youson, J.H., 2007. Peripheral endocrine glands. II. The adrenal glands and the corpuscles of stannius. Fish Physiology 26, 457-513.

Zahn, N., James-Zorn, C., Ponferrada, V.G., Adams, D.S., Grzymkowski, J., Buchholz, D.R., Nascone-Yoder, N.M., Horb, M., Moody, S.A., Vize, P.D., 2022. Normal Table of Xenopus development: a new graphical resource. Development 149, dev200356.

Zeineldin, M., Patel, A.G., Dyer, M.A., 2022. Neuroblastoma: When differentiation goes awry. Neuron 110, 2916-2928.

Zhang, J., Darling, R.D., Paul, I.A., Simpson, K.L., Chen, K., Shih, J.C., Lin, R.C., 2011. Altered expression of tyrosine hydroxylase in the locus coeruleus noradrenergic system in citalopram neonatally exposed rats and monoamine oxidase a knock out mice. Anat Rec (Hoboken) 294, 1685-1697.

9 Appendix

9.1 Validating candidate gene markers of chromaffin cell development in *Xenopus laevis* in *Xenopus tropicalis*

The main animal model used for the entirety of this project was *Xenopus laevis*. The advantages of using *X.laevis* over *X.tropicalis* during this project were practical. *X.laevis'* produce larger sized embryos, which are more robust and have a better fertilisation rate. Additionally, *X.laevis* adults are easier in handling, due to their larger overall size and tolerance for a broader temperature range, which corresponds to most room temperatures and does not require heating equipment (Schmitt et al., 2014). These factors, make *X.laevis* exceptionally convenient for laboratory handling.

However, as briefly mentioned in chapter 1.1, there are downsides to *X.laevis* as a model species that can be overcome with the use of X.*tropicalis*. *X.tropicalis* generation time is about 50% shorter than for *X.laevis*, with embryos developing faster and undergoing metamorphosis earlier. Their smaller embryo size also makes them more suitable for use in chemical compound screening, which can be assayed in 96-well plates (Wheeler and Brändli, 2009).

Compared to the tetraploid X.*laevis*, X.t*ropicalis* is diploid, like humans, meaning that its genome is more similar to the human genome in terms of organisation and complexity, facilitating the identification of human orthologs of the genes of interest (Schmitt et al., 2014; Wheeler and Brändli, 2009). The X.t*ropicalis* genome contains orthologs of approximately 80% of known human disease genes (Schmitt et al., 2014). Identifying and validating genes essential for AC and CC development in *X. tropicalis* could strengthen their potential as drug targets or biomarkers for human diseases, such as neuroendocrine tumours, which involve disruptions in chromaffin cell development. Since *X. tropicalis* is highly suitable for genetic manipulation (e.g., CRISPR), it could also be used to perform functional knockouts or overexpression studies to model disease phenotypes and test drugs that may influence gene function.

Generally, validating our findings of chapter 3 and chapter 4 in *X.tropicalis* could add more scientific rigor to our previous findings and help determine whether the gene regulation and

expression patterns observed in *X.laevis* are consistent across both species. Differences in gene expression could highlight evolutionary divergence or functional redundancy, offering further insights into the evolution of chromaffin cells development as well as AC development.

A few of the WISH probes for genes that were found to be vital in CC development and AC development were evaluated at NF stage 32/33 in *X.tropicalis* to confirm consistent gene expression patterns across both *Xenopus* species.

Due to their central role in the development of noradrenergic neuron populations across vertebrate species, WISH with the *phox2* TFs were expected to match the previously characterized expression patterns in *Xenopus laevis*. Unfortunately, *phox2b* was not found to be expressed in X.*tropicalis* embryos using the WISH probe made for *X.laevis* (Fig 1 A). As a reminder, *phox2b* in *X.laevis* at this developmental stage was found to be highly expressed in the NA cells (identified as early CCs or CC precursors), cranial ganglia and the hindbrain. In the tropicalis embryos high background staining is observed in the head and somites, due to a long incubation period of the colour solution. As the primers designed for the phox2b.L variant in *X.laevis* match the coding sequence of *phox2b* in *X.tropicalis* and both *Xenopus* coding sequences align with a percentage identity of 93, the absence of a specific expression pattern is most likely due to a technical error. Therefore, the phox2b WISH probe needs further testing and potential probe optimisation before drawing any final conclusions.

Phox2a was found to be expressed in the NA cells, cranial ganglia and a brain structure just behind the lens field that is consistent with the expression pattern observed in *X.laevis* (Fig 1 B). Interestingly, the expression pattern of the NA cells in *X.tropicalis* seems to show a directionality of these cells moving towards the area of the developing pronephric kidney that we could not clearly distinguish in *X.laevis*, where the NA cells were found closer to the branchial arches. The same observation was made when performing WISH with *dbh* (vital in catecholamine synthesis) and *chga* (neuroendocrine secretory gene) in *X. tropicalis* (Fig 1 C and D). Both these markers showed expression of multiple NA cells across the anterior body of the

embryos, consistent with the expression pattern we characterized in *X.laevis*.

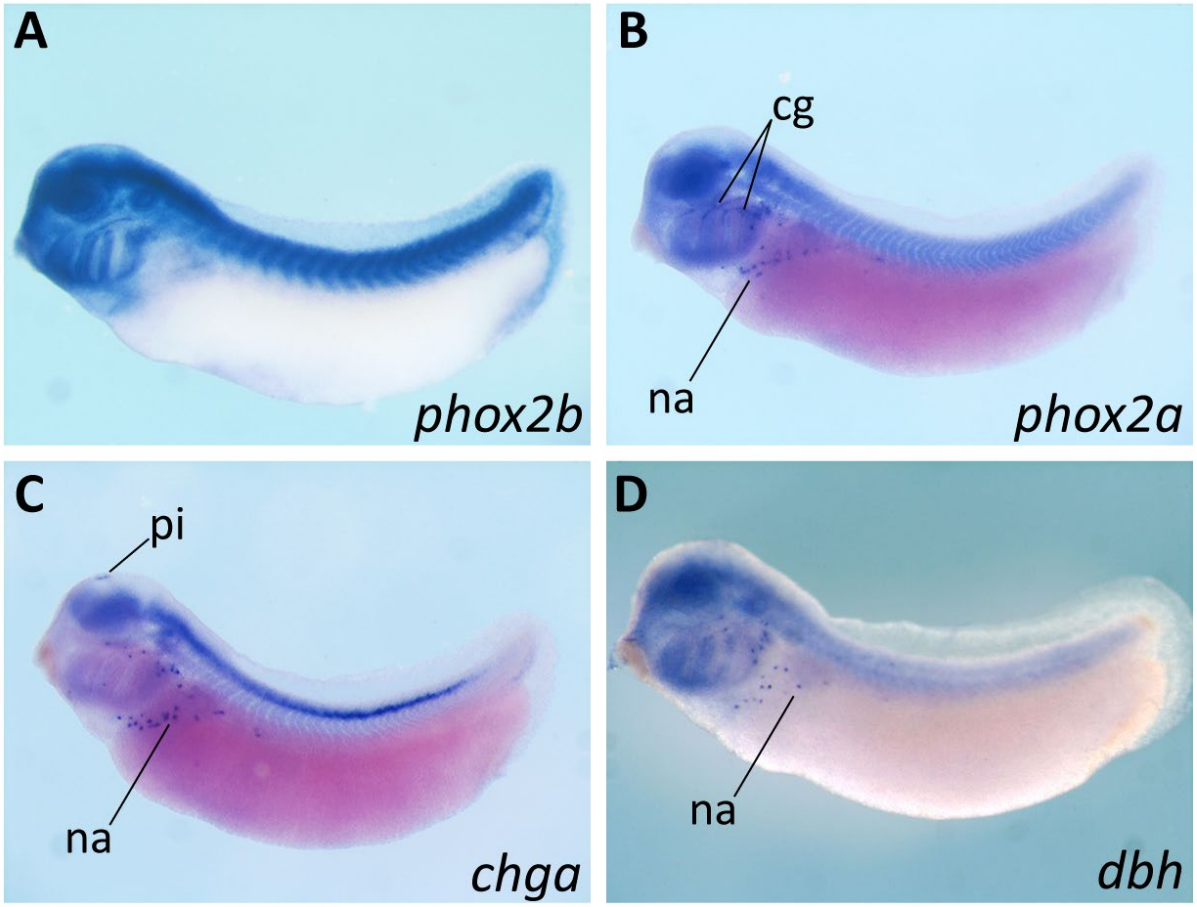

Figure 77: Previously determined marker genes of chromaffin cell development of X.laevis validated in X.tropicalis embryos at NF stage 32-33.

*WISH probes developed for use in X.laevis were evaluated in X. tropicalis tailbud stage embryos NF 33. Embryos are viewed laterally, with the head anterior and tail posterior. No expression was obtained with the X.laevis phox2b probe in X.tropicalis (**A**). Phox2a was expressed in numerous individual cells, previously labelled in X.laevis as noradrenergic cells (NA) likely being CCs or chromaffin-like cells (**B**). Additionally, phox2a expression is seen in some cranial ganglia (CG) and in a brain structure just behind the lens field that matches the expression of phox2a in X.laevis at this developmental stage. Expression of chga also matches the expression previously characterised in X.laevis. Expression is found in the NA cells, which are more numerous than in X.laevis at this developmental stage, as well as in the pineal gland and along the entire neural tube (**C**). Expression of dbh is also found in the NA cells along the anterior body of the embryo, again matching expression previously characterized in X.laevis (**D**). Noticeably, we can see a clear directionality of the NA cells in X.tropicalis towards the area of the pronephric kidney. Cg, cranial ganglia; na, noradrenergic; pi, pineal gland.*

To assess if, genes found to be important in adrenal cortex development, are also expressed in *X.tropicalis* we evaluated the *X.laevis* WISH probes made for *nr5a1* and *star* at developmental stage NF 32/33 (Fig. 2). These markers displayed expression patterns in *X. tropicalis* consistent with those previously characterized in *X. laevis*, particularly along the pronephric kidney (See chapter 4, Fig. 50). We can see that *nr5a1*, which is vital in initial steroidogenic tissue formation, is expressed along a greater area of the pronephric kidney, with its expression proceeding that of *star*, which is important in steroidogenesis. Additionally, we see *nr5a1* expression in the hypothalamic nucleus (HYPN) in front of the lens field (Fig. 2A), and *star* shows expression in the hindbrain (HB) (Fig. 2B) again consistent with expression patterns characterized in *X.laevis*.

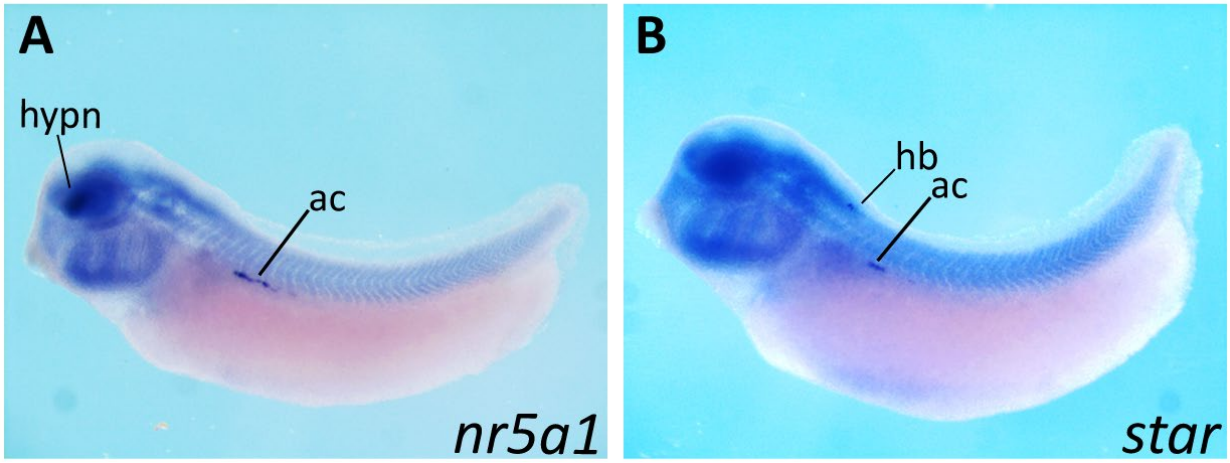

Figure 78: Previously determined marker genes of steroidogenic cells of the adrenal cortex of X.laevis validated in X.tropicalis embryos at NF stage 32-33.

WISH probes developed for use in X.laevis were assessed in X.tropicalis tailbud stage embryos. Expression of both adrenal cortex markers nr5a1 (A) and star (B) matched the expression previously characterized in X.laevis embryos at the same developmental stage. Both nr5a1 and star are expressed in the area of the pronephric kidney, just beneath the somites, presumably showing the developing adrenal cortex (AC). Additionally, nr5a1 expression is also seen in the hypothalamic nucleus (HYPN) (A). Star is also expressed in the hindbrain (HB).

The preliminary results obtained in *X.tropicalis* underscore a consistency in gene expression patterns between both *X.laevis* and *X.tropicalis*. This cross-species validation adds robustness to the identified markers and suggests that both *X. laevis* and *X. tropicalis* offer complementary insights into chromaffin cell and adrenal cortex development. Of particular

interest is the directional movement of NA cells in *X. tropicalis* towards the pronephric kidney that we expected to see in *X.laevis* but were unable to. This suggests a difference in developmental pathways or time-points that needs more investigation. Such work lays the foundation for translational applications in human neuroendocrine disorders and may reveal evolutionary insights into the regulation of chromaffin and steroidogenic cell development across vertebrates.

9.2 Additional Figures

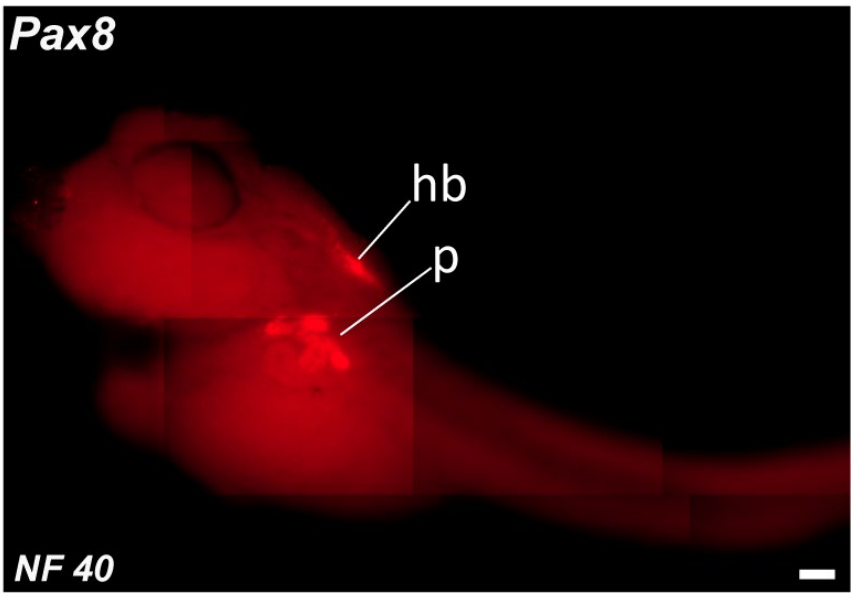

Appendix Figure 1:HCR expressio of pronephric kidney marker pax8 in Xenopus laevis embryo NF stage 40
HCR of pax8 with Alexa Fluor 647 shows expression in the pronephros (P) and in the hindbrain (HB), matching the expression pattern obtained with the pax8 WISH probe.

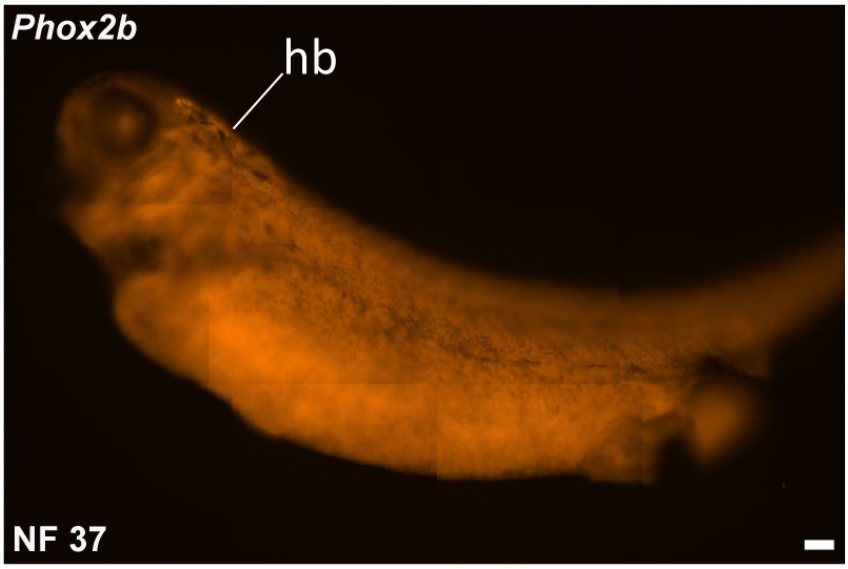

Appendix Figure 2: HCR expression of SA marker phox2b in Xenopus laevis embryo NF stage 37

HCR of phox2b with Alexa Flour 546 showing weak expression in the hindbrain (HB) but not much else. Performing HCR with Alexa Fluor 546 generally resulted in weak expression visualization of probes in X. laevis, therefore beig excluded from further use.

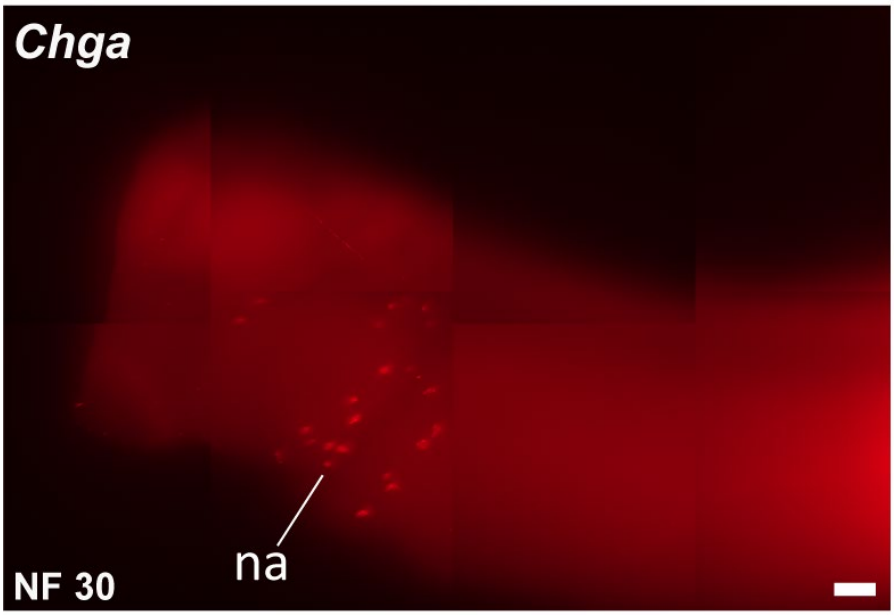

Appendix Figure 3: HCR expression of chga in Xenopus laevis embryo at NF stage 30.

Expression of chga by HCR with Alexa Fluor 647 shows strong expression of NA precursors/ putative CCs, matching the expression pattern obtained with the chga WISH probe.

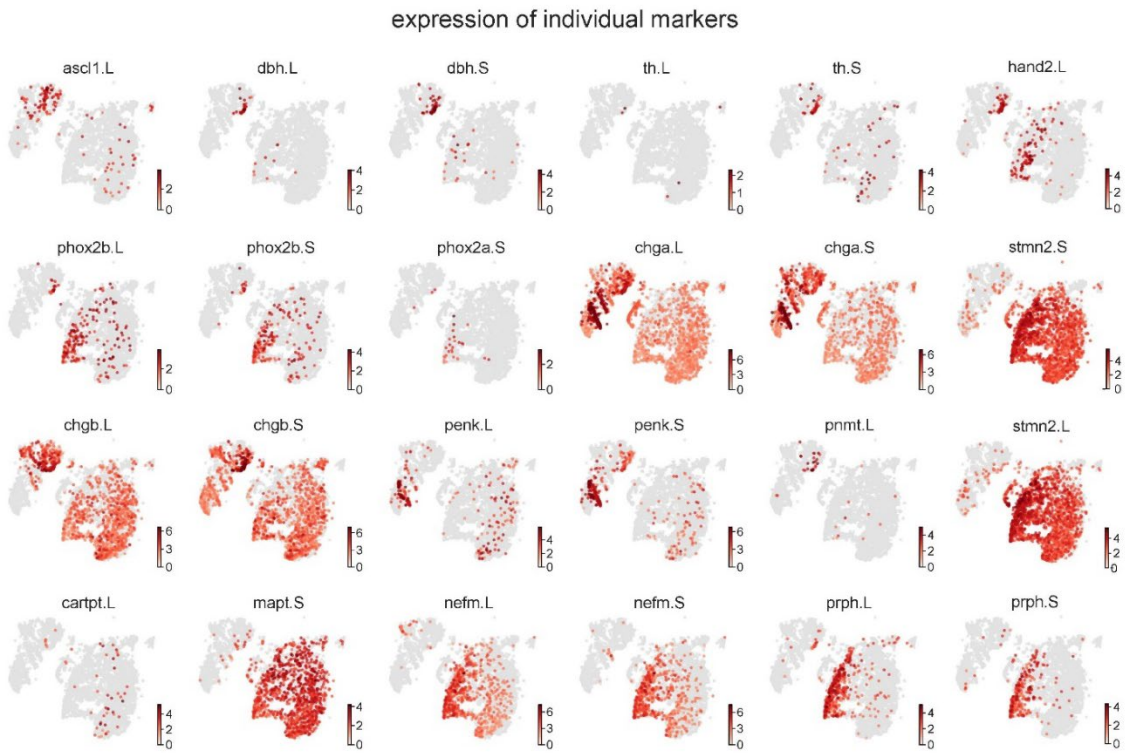

Appendix Figure 4: Expression of individual genes from SA signature.